The Function of Retinol Dehydrogenase 1 in Retinoic Acid Synthesis and Metabolic Regulation

by

Charles Robert Krois

A dissertation submitted in partial satisfaction of the
requirements for the degree of
Doctor of Philosophy
in
Comparative Biochemistry
in the
Graduate Division
of the
University of California, Berkeley

Committee in charge:
Professor Joseph L. Napoli, Chair
Professor Hei Sook Sul
Professor Jen-Chywan Wang

Fall 2011

Abstract

The Function of Retinol Dehydrogenase 1 in

Retinoic Acid Synthesis and Metabolic Regulation

by

Charles Robert Krois

Doctor of Philosophy in Comparative Biochemistry

University of California, Berkeley

Professor Joseph L. Napoli, Chair

Retinol dehydrogenases (RDH) convert retinol into retinal, the intermediate in the biosynthesis of retinoic acid. All-*trans*-retinoic acid (atRA) regulates gene transcription and/or translation through retinoic acid receptors (RARs) and PPARδ (1). To test function of *Rdh1*, an efficient (V_{max}/K_m) and widely distributed RDH (2), our lab created *Rdh1* knockout (KO) mice (3). Initial study of *Rdh1*-KO mice determined that when fed a low or vitamin A-deficient (VAD) diet, *Rdh1*-KO mice gain 33% more weight than wild-type (WT). However, when fed a chow diet (22+ IU vitamin A/g diet—i.e. copious), KO mice appeared identical to WT.

Our continued work on the *Rdh1*-KO mouse reveals additional insight into the role of *Rdh1* in both retinoic acid synthesis and energy regulation. Both a 10% increase in length and 33% increase in adiposity contribute to weight gain in VAD-fed KO animals. Based on measurements of adipocyte size, increased adiposity results from hyperplasia of white adipose tissue. *Rdh1*-KO mice, fed a diet with the recommended amount of vitamin A (4 IU/g), also increase in weight and adiposity, but not length. Interestingly, high fat diet feeding fails to exacerbate weight or adiposity. Increased weight contributes to a decline in *Rdh1*-KO mouse health. Whereas young animals respond normally to tests of glucose and insulin tolerance, older *Rdh1*-KO mice become insulin resistant and glucose intolerant, with 2.5-fold higher insulin levels. These changes in *Rdh1*-KO glucose metabolism cannot be attributed to changes in pancreatic 9-*cis*-retinoic acid (9cRA) (4). As expected in heavier animals, leptin levels also increase 1.8-fold in *Rdh1*-KO mice. In addition, loss of *Rdh1* reduces circulating thyroid hormones T4 and T3 by 12% and 17%, respectively, though TSH levels remain unchanged. These data demonstrate that atRA, generated by *Rdh1*, contributes to control of body weight, and does so to a physiologically relevant extent.

Increased weight results from either increased caloric intake or decreased energy expenditure. Overall, *Rdh1*-KO mice move just as much as WT, and their food intake increases only in proportion to body weight. Normalized to body weight, we observe no change to energy expenditure by indirect calorimetry. Thermogenesis, the generation of heat for body temperature maintenance, also contributes to energy expenditure. *Rdh1*-KO mice respond normally to cold challenge and β_3-adrenergic stimulation, but appear reduced in body temperature, especially when stressed by fasting. Consistent with these observations, the brown adipose tissue (BAT) of *Rdh1*-KO mice expresses normal levels of the β_2- and β_3-adrenergic receptors and lower levels of

Gbpar1, a bile acid receptor also involved in thermogenesis (5). *Ucp1* expression increases when KO mice are fasted and returns to WT levels upon refeeding, suggesting UCP1 compensates for, rather than causes, reduced thermogenesis.

We used stable isotopes to measure *de novo* lipogenesis and triglyceride turnover in *Rdh1*-KO animals. Long term studies reveal reduced *de novo* lipogenesis, with less newly synthesized palmitate accumulating in white adipose tissue. In short term studies, brown adipose accumulated less new palmitate during 5 hours of refeeding. Comparable levels of total palmitate per gram tissue suggest increased storage of dietary lipid. Reduced rates of *de novo* lipogenesis, however, cannot explain increased adiposity in *Rdh1*-KO mice.

In samples of liver, white and brown adipose, we measured the relative levels of the most common fatty acids. In animals refed after fasting, the relative contribution of stearate is less in the brown adipose and liver of *Rdh1*-KO mice. In *ad lib* fed animals, white and brown adipose have reduced relative stearate levels. These changes to lipid composition are likely due to reduced expression of elongase *Elovl6* in *Rdh1*-KO livers.

Loss of *Rdh1* does not affect atRA, retinal, retinol or retinyl ester levels in *ad lib* fed mice in any tissue studied. However, studies of atRA during fasting and refeeding proved insightful to atRA function in WT and KO animals. In WT animals, atRA levels increase 1.3-1.5-fold in brown adipose tissue when refed 2-4 hours after a fast. In liver, atRA levels decline 30% after 5 hours of refeeding. Furthermore, reductions in hepatic retinol and retinyl ester during refeeding coincide with transient increases to serum levels, suggesting export of retinoid in the transition from fasting. Cold exposure had a similar impact on liver retinoids, but did not affect levels in brown adipose tissue. During refeeding, *Rdh1*-KO animals fail to maintain normal atRA levels in BAT and appear delayed in the export of retinol and esters from liver to serum.

Gene expression of retinoid synthesis genes also suggests coordination or retinoid metabolism with fasting and refeeding. In brown adipose tissue, *Rdh1*, *Aldh1a1*, *Rbp1*, *Rbp4* and *Rbp7* expression decrease between fasting and 6.5 hours of refeeding. Increased atRA, despite decreased gene expression, suggests additional regulatory mechanisms of atRA synthesis in BAT. In liver, multiple Rdh (*Rdh1*, *Dhrs9*, *Rdh10*), retinal dehydrogenases (*Aldh1a1*, *Aldh1a2*, *Aldh1a3*), retinol binding proteins (*Rbp1*, *Rbp4*) and *Cyp2c39* decrease expression during refeeding. Alternately, *Cyp26a1* expression increases with refeeding. Hepatic gene expression changes during refeeding are generally consistent with decreased atRA. Additional work on retinoid gene expression suggests some of these expression changes occur within 2.5 hours of refeeding and that high retinol diet disrupts the regulation of some retinoid metabolism genes.

To better understand the molecular mechanisms underlying the *Rdh1*-KO phenotype, we performed global gene expression analysis in liver, epididymal white adipose tissue (EWAT), testes and brown adipose tissue. Despite little to no *Rdh1* expression in EWAT, we found nearly 3,000 gene changes in *Rdh1*-KO. We suspect many of these changes are secondary to weight gain. Microarray of liver, EWAT and BAT identified the gene *Gbp1* upregulated in *Rdh1*-KO mice. Using qPCR, we found increases of 3-fold, 40-fold, and over 500-fold, respectively. Many inflammatory cytokines regulate the expression of *Gbp1*, yet serum levels of TNFα and IL-6 appear normal in KO mice. Based on our microarray study, we identified increased expression of *Cap1*, *Klf2*, *Rbp4* and *Gmpr* and decreased expression of *Adh1*, *Car5b* and *Orm2*. Interestingly, increased *Rbp4* expression does not lead to increased BAT expression of *Pparg* or *Socs3*, gene expression targets of RBP-STRA6 signaling (6). We have yet to determine which gene changes in BAT are direct retinoic acid targets or which lead to the weight and adiposity increases in *Rdh1*-KO mice.

Rdh1-KO mice differ in phenotype from *Rdh16*- and *Rbp1*-KO mice and mice heterozygous for an *Rdh10* point mutation (*Rdh10* Mut Het). Physiologically, *Rbp1*-KO mice move less and expend less energy. *Rbp1*- and *Rdh16*-KO mice have increased pancreatic 9cRA. *Rdh16*-KO mice also show changes to androgen synthesis genes in liver. *Rdh10* Mut Het mice have reduced atRA in cortex and cerebellum.

All in all, this work suggests that RDH1 biosynthesizes atRA to regulate energy metabolism, and also supports the hypothesis that individual RDH generate distinct pools of cellular atRA to support specific retinoid functions. Perhaps, predisposition to weight gain in the human population can be attributed to abnormal *Rdh1* activity.

To my mom and dad.

Table of Contents

List of Figures

List of Tables

Symbols and Abbreviations

3-adiol(-G): 5α-androstane-3α, 17β-diol (glucuronide)
9cRA: 9-*cis*-retinoic acid
9,13dcRA: 9,13-di-*cis*-retinoic acid
13cRA: 13-*cis*-retinoic acid
93G: AIN 93G diet (4 IU/g of vitamin A)
ADD: α-adducin
ADH: Alcohol dehydrogenase
ALDH: Aldehyde dehydrogenase
ANOVA: Analysis of variance
apo-CRBP: Cellular retinol binding protein without retinol (see also: holo-CRBP)
atRA: all-*trans*-retinoic acid
at-Retinal: all-*trans*-retinal
at-Retinol: all-*trans*-retinol
BAT: brown adipose tissue
cDNA: Complementary DNA
CLAMS: Comprehensive Lab Animal Monitoring System
CMO: carotenoid monooxygenases
CRABP: Cellular retinoic acid binding protein
CRAD: *Cis*-retinol/androgen dehydrogenase
CRBP: Cellular retinol binding protein.
C/REBP: CCAAT/enhancer binding protein
CYP: Cytochrome P450
DEXA: Dual energy X-ray absorptiometry
DHT: Dihydrotestosterone
DMSO: dimethylsulfoxide
DNA: Deoxyribonucleic acid
EDTA: Ethylenediaminetetraacetic acid
ELISA: Enzyme-linked immunosorbent assay
EWAT: Epididymal white adipose tissue. Comparable to female PMWAT.
F: Fasted
FABP: Fatty-acid binding protein
FOXC: Forkhead box c
FWAT: Femoral white adipose tissue
GPCR: G-protein coupled receptor
H&E: Hematoxylin and eosin (staining)
HEPES: (4-(2-Hydroxyethyl)-1-piperazineeethanesulfonic acid
Het: Heterozygous
HFD: High fat diet. Content varies in other references. Here it contains 50% fat-derived calories.
holo-CRBP: Retinol bound to cellular retinol binding protein (see also apo-CRBP)
HPLC: High performance liquid chromatography
HT: Hypothalamus
IBMX: 3-isobutyl-1-methylxanthine
IFN: Interferon
IL: Interleukin

IU: International units
IWAT: Inguinal white adipose tissue
JAK: Janus kinase
KO: Knockout, unless otherwise specified *Rdh1*-KO
LDL: Low-density lipoprotein
LRAT: Lecithin retinol acyltransferase
MCP: Monocyte chemoattractive protein
mRNA: Messenger ribonucleic acid
MS/MS: Tandem mass spectrometry
MWAT: Mesentery white adipose tissue
n.d.: Not determined
NPY: Neuropeptide Y
PCR: Polymerase chain reaction
PEPCK: Phosphoenolpyruvate carboxykinase
PMWAT: Perimetrial white adipose tissue. Comparable to male EWAT.
PPAR: Peroxisome proliferator activated receptor
qPCR: Quantitative polymerase chain reaction
R: Refed
RALDH: Retinal dehydrogenase
RAR: Retinoic acid receptor
RARE: Retinoic acid response element
RBP: retinol binding protein, serum
RDH: Retinol dehydrogenase, sometimes RODH in the literature
Rdh10 Mut Het: Mice heterozygous for a hypomorphic mutation in *Rdh10*, described in (7)
RE: Retinyl esters
RNA: ribonucleic acid
RRD: Retinal reductase
RT-PCR: Reverse transcriptase polymerase chain reaction
RWAT: Retroperitoneal white adipose tissue
RXR: Retinoid X receptor
SDR: Short-chain dehydrogenase/reductase
SOCS: Suppression of cytokine signaling
STAT: Signal transducer and activator of transcription
STRA6: Stimulated by retinoic acid 6
T3: Triiodothyronine
T4: Thyroxine
TNF: Tumor necrosis factor
Tris: Tris(hydroxymethyl)-aminomethane
TSH: Thyroid stimulating hormone
TTR: Transthyretin
UCP: Uncoupling protein
Und.: Undetectable under conditions used.
Unk.: Unknown
UV: Ultraviolet
VAD: Vitamin A deficient
WAT: white adipose tissue

WT: Wild-type

Acknowledgements

First and foremost, I'd like to thank Professor Joseph Napoli. Without his stalwart support, thoughtful advice and colorful collection of idioms ("Hindsight is 20/20," "I think what we have is the elephant's trunk," "Go for the low hanging fruit," "This isn't a bank," etc.), this work wouldn't have been possible.

I'd also like to thank the rest of my dissertation committee, Professors Hei Sook Sul and Wally Wang, for their guidance and support.

When I got tired of weighing mice and food every week, I received help from Lilyana Chandra, Audrey Kim, Jane Kim, Nicholas Bonniot and Delphine Foucault, undergraduate, post-graduate and visiting scholar volunteers who helped out in the lab.

Priscilla Huang, an undergraduate research assistant for nearly 3 years, has been a second set of hands in the lab. She's been extremely helpful in everything from weighing mice to gene expression, carrying out some of the gene expression experiments that appear later.

Graduate student Daniel Benjamin also contributed to some of the gene expression work during his rotation in the lab.

Visiting scholar Mariarita Perri helped carry out the fatty acid and glycerol measurements. Hua Tran helped with the testis, EWAT and liver microarrays and provided some preliminary data that guided and influenced other parts of this work.

James Chithalen, Maureen Kane and Peirong Hu, all post-doctoral fellows in the Napoli lab, taught me a great deal about research and provided a lot of guidance during their time in lab. James patiently answered a lot of my questions, Maureen helped significantly in the measurement and analysis of retinoid data and Peirong got me started on the RDH1 project during my first year of graduate school.

I don’t know if I could find a better labmate than Kristin Obrochta. Her help in collecting tissues, analyzing samples, evaluating data and keeping the lab running, not to mention her friendship over the last 5 1/2 years, has been invaluable.

Professor Dale Leitman organized the brown adipose tissue microarray study. His graduate student Candice Herber helped prepare the samples and his collaborators Terry Speed and Moshe Olshansky carried out the statistical analysis.

Lab post-docs Nan Li and Sunny Wang helped with some of the retinoid measurements.

Stable isotope studies were carried out in lab of Professor Marc Hellerstein with the help of graduate students Matt Bruss and Airlia Thompson and technician Simply FlorCruz.

Sally Chiu from Craig Warden’s UC Davis laboratory taught which adipose depot was which. The labs of Craig Warden and Judy Stern carried out the body composition analysis.

Thanks to Lindsey Jennings, Kelly Jensen and Jay Seville from the Office of Laboratory Animal Care. Lindsey taught me more than a few techniques, Kelly helped me identify mouse thyroid and Jay maintained the lab's animal room.

Thanks to Professors Hei Sook Sul, Irving Zucker, Len Bjeldanes, Andreas Stahl, Marc Hellerstein, Barry Shane, Wally Wang and their laboratories for use of equipment.

Thanks to Marta Vuckovic, Napoli Lab post-doc, for her review of this dissertation.

Finally, thanks to all of my friends and classmates in the Comparative Biochemistry program and the Nutritional Sciences and Toxicology Department for their ideas, support and oft-needed morale boosts. *I get by with a little help from my friends*.

The Function of Retinol Dehydrogenase 1 in Retinoic Acid Synthesis and Metabolic Regulation

Introduction

Retinoid Metabolism Overview

Vitamin A or retinol is a small, lipid soluble nutrient essential for normal function in both vertebrates and invertebrates (8). First described in 1913 by McCollum (9) as "lipid soluble A," nearly 100 years of research have shed light onto the roles of retinol in humans and other mammals. However, many questions remain about the metabolism of retinol, its regulation and its impact on physiology, especially that of energy metabolism.

Dietary retinol derives from one of two sources: esters, such as retinyl palmitate, or carotenoids, such as β-carotene. β-carotene and other carotenoids are cleaved primarily in the intestine by carotenoid monooxygenases (CMO). Cleavage of β-carotene results in two molecules of all-*trans*-retinal (at-retinal). Alternately, humans can store carotenoids in adipose tissue as a pro-vitamin source of retinol. Such storage, however, is rarely seen in mice (10). At-retinal from cleavage of carotenoids can be converted into all-*trans*-retinol (at-retinol) by retinoid reductases (RRDs) or all-*trans*-retinoic acid (atRA) by retinaldehyde dehydrogenases (RALDHs). Lecithin retinol acyltransferase (LRAT) then converts retinol into retinyl esters (RE), which are packaged, along with lipids, into chylomicrons. RE are stored and formed in many tissues, with the liver and adipose tissues acting as the primary storage depots. Liver and adipose tissue can mobilize RE stores, hydrolyzing esters into at-retinol and exporting vitamin A into the blood bound to retinol-binding protein (RBP). To avoid renal excretion, RBP circulates bound to transthyretin (TTR) (1, 11, 12). Various tissues take up retinol from RBP from serum through the receptor STRA6 (stimulated by retinoic acid 6) (13). Intracellularly, cellular-retinol binding proteins (CRBPs) bind at-retinol. CRBP-bound retinol (holo-CRBP) is recognized as a substrate for LRAT, whereas apo-CRBP (CRBP without retinol) inhibits LRAT (14, 15). Thus, the balance of holo- and apo-CRBP regulates the amount of retinol stored as ester. In non-vision pathways, unesterified at-retinol is converted reversibly into at-retinal via retinol dehydrogenase (RDH) activity. Two gene families, the alcohol dehydrogenase (ADH) family and the short-chain dehydrogenase/reductase family (SDR), have members with RDH activity *in vitro* (1). The ADHs are cytosolic proteins, with some members recognizing free at-retinol, but not holo-CRBP, as a substrate. Single or combined ADH knockouts do not exhibit phenotypes related to lack of atRA. Furthermore no compensatory gene expression changes have been reported in ADH knockouts (16-20). SDRs, on the other hand, occur in both cytosol and the endoplasmic reticulum. Microsomal RDHs are active with not only free at-retinol, but also holo-CRBP (21-24).

Whereas CRBP also binds at-retinal, different binding proteins, cellular retinoic acid binding proteins (CRABPs), bind atRA. CRABPII directs atRA to RARs (retinoic acid receptors). Translocation to the nucleus occurs via sumolyation of the CRABPII protein (25, 26). Separate genes encode RAR-α, -β and -γ and each binds atRA with a K_d in the sub-nanomolar range (27-29). Binding of atRA to an RAR mediates gene expression changes primarily through heterodimerization with an RXR (retinoid X receptor) and subsequent recruitment of co-activators and co-repressors (30). Another binding protein, fatty acid binding protein 5 (FABP5), can alternately direct atRA toward peroxisome proliferator activated receptor β/δ (PPARδ). PPARδ, also through heterodimerization with RXRs, mediates additional and overlapping gene

expression regulation (31-34). CRABPI, on the other hand, directs atRA to the endoplasmic reticulum, where cytochrome P450s (CYPs) catabolize atRA into 4-hydroxy- and 4-oxo-polar metabolites for excretion (35, 36). Of the CYPs, members of family 26 (A1, B1 and C1) along with CYP2C39 show preferential activity towards RA (37-40).

Retinoic Acid and Metabolism

Whereas liver has the largest store of retinyl esters, the adipose tissue, taken as a whole, is the second largest store, accounting for 15-20% of total retinyl ester storage (41). Like the liver, white adipose tissue (WAT) can mobilize its retinoid stores, exporting retinol bound to RBP4, the serum retinol binding protein. Both brown adipose tissue (BAT) and WAT express RAR and RXR nuclear receptors (41). Presence of these nuclear receptors suggests retinoid signaling takes place in both types of adipose tissue (42). This signaling likely contributes to both adipocyte differentiation and normal function. *In vitro*, high amounts of atRA inhibit both brown and white adipocyte differentiation by blocking CCAAT/enhancer binding protein (C/REBP) β induction of PPARγ and C/REBPα in an RARα-dependent process (41-43). Conversely, low atRA levels are associated with stimulation of adipogenesis (41). High retinoic acid levels also induce apoptosis in primary WAT cells, as well as 3T3-L1 cells.

In vivo, pharmacological doses (100 mg/kg) of atRA reduce adiposity and body weight in mice, possibly through the reduction of PPARγ expression observed in both WAT and BAT, and the reduction of C/REBPα and α-adducin (ADD) 1 expression observed in WAT (44, 45). A high retinol diet (430 IU/g) also decreases adiposity without a change in body weight in F334 x BN rats (46), whereas in the WNIN/ob rat model, the same diet reduced both weight and adiposity, whereas increasing the apoptotic index of adipose tissue (47, 48). In the latter model, no changes in food intake were observed. In mice, however, another high retinol diet (581 IU/g) caused no detectable change to weight or adiposity (49). Pharmacological doses of atRA (10-100 mg/kg) in mice also lowered expression of both leptin and resistin mRNA in BAT and WAT. Circulating levels of both adipokines were also reduced. Treatment with atRA induced similar effects on leptin and resistin mRNA in BAT and WAT cell culture (49, 50). A high retinol (430 IU/g) diet also lowered serum leptin levels in rats (46). Conversely, adult mice fed a VAD diet exhibit increased adiposity, a very small increase in body weight, increased PPARγ expression in WAT, and decreased PPARγ expression in BAT (42, 45). Interestingly, rats fed a VAD diet exhibit reduced serum triglyceride and cholesterol, but increased triglycerides, phospholipid and cholesterol in the aortic tissue. Treatment with atRA reversed these effects (51).

RA also affects the expression of uncoupling proteins (UCP) in adipose tissue. UCP1 occurs predominately in BAT, where it functions critically in thermogenesis and regulation of body temperature. UCP2 and UCP3 occur in both in BAT and in additional tissues. The extra-BAT expression of these proteins suggests a function other than thermogenesis, such as facilitation of β-oxidation (52). RA upregulates *Ucp1* by 30%-80% *in vitro* in brown adipose cells (53), *in vivo* in the BAT of rats fed high levels of retinol in the diet (430 IU/g) (46) and also in mice dosed with 100 mg/kg atRA (44). Conversely, a VAD diet reduced UCP1 expression in mice (44). UCP2 expression levels are reduced in mouse BAT and WAT under VAD diet and increased under RA treatment (44). UCP3 mRNA and protein levels in skeletal muscle are increased under a high retinol diet (581 IU/g) and with atRA treatment (54). AtRA induction of *Ucp3* occurs in myotubules (43). AtRA acts through both a non-canonical RARE and PPRE in the *Ucp1* promoter and a canonical RARE in *Ucp3* (32, 55). RA's mechanism of action in *Ucp2* induction is not yet known, though the *Ucp2* promoter contains no known RAREs (43).

RA regulates expression of phosphoenolpyruvate carboxykinase (PEPCK, from gene *Pck1* in mice), a gluconeogenic enzyme that catalyzes conversion of oxaloacetate into phosphoenolpyruvate. The only known regulatory mechanism of PEPCK is mRNA expression, making regulation of synthesis an important contributor to overall protein activity. This effect occurs *in vitro* in adipocyte-derived and liver-derived cell lines (56, 57), as well as *in vivo*, as mice fed VAD diet have decreased hepatic *Pck1* expression, and RA treatment restores expression levels (58). The *Pck1* promoter has not one, but two retinoic acid response elements (59, 60). Specifically, atRA affects the cadre of coactivators present on the *Pck1* promoter, thus altering acetylation of histones, and therefore gene expression (58). Interestingly, vitamin A deficiency reduces the amount of PPARα bound to the promoter, but not the amount of RXRα or RARα bound (61).

Binding Proteins in Retinoid and Energy Metabolism

Movement of vitamin A in circulation or within the aqueous milieu of the cell requires solvation, typically mediated by binding proteins. For non-vision functions of retinol, there are three known cellular retinol binding proteins. CRBPI (from gene *Rbp1*) has a wide tissue disruption, suggesting a general function throughout the animal. On the other hand, CRBPII (*Rbp2*) and CRBPIII (*Rbp7*) are expressed primarily in intestine and mammary, respectively (62-64). CRBPs also differ in their relative binding affinities for various retinoids. CRBPI preferentially binds at-retinol over at-retinal, whereas CRBPII binds at-retinal over at-retinol (65). Additional work shows that CRBPII binds 9-*cis*-retinol preferentially over all-*trans*-retinol (66). Based on estimates of CRBP expression, retinol levels in various tissues, and the K_d of retinol for CRBP, holo-CRBP is likely the most commonly found form of retinol in the cell under non-pathological conditions (1). Interestingly, CRBPs bind retinol with the hydroxyl end deep inside the protein, suggesting conformational change and release of retinol from CBRP prior to esterification or dehydrogenation (67).

With its wide tissue distribution, CRBPI is the most well-studied of the CRBPs. CRBPI interacts with RDH and LRAT, and holo-CRBPI acts as a substrate for each (15, 68, 69). Apo-CRBPI inhibits LRAT activity, which acts to feedback inhibit the esterification of retinol during periods of low abundance. Not surprising given its wide tissue distribution, *Rbp1* knockout (KO) affects diverse tissues' function. As expected from *in vitro* studies, lack of CRBPI prevents proper esterification of retinol (70). The liver of *Rbp1*-KO mice accumulates far less RE than WT, making them much more susceptible to vitamin A deficiency. *Rbp1*-KO mice also show compromised pancreatic function (71). The pancreas of CRBPI-KO mice overexpresses CRBPII. CRBPII's preference for 9-*cis*-retinol contributes to increased 9-*cis*-retinoic acid (9cRA) production. This renders 9cRA levels unresponsive to feeding, subsequently leading to increased serum glucagon, decreased serum insulin and a low insulin-to-glucagon ratio. Thus, CRBPI-KO mice, while sensitive to insulin, become glucose intolerant. *Rbp1* has also been implicated in adipose tissue function (72). Expressed only in pre-adipocytes, CRBPI prevents differentiation by affecting levels of peroxisome proliferator γ expression. Thus, when fed a high fat diet (HFD) CRBPI KO mice increase in adiposity. Interestingly, this increased adiposity is not associated with weight gain, with others reporting a resistance to HFD-induced obesity (71). These differing reports on HFD-induced obesity have yet to be reconciled.

CRBPII is primarily expressed in the intestine. There, carotenoid monooxygenases (CMOs) cleave dietary carotenoids, yielding retinal from pro-retinol carotenoids (73). With its affinity for retinal, CRBPII thereby binds these cleavage products and directs retinal to retinal

reductases (RRD) that catalyze the conversion of retinal into retinol (74, 75). Like CRBPI, CRBPII can also direct retinol to LRAT, leading to the production of RE. Work with *Rbp2*-KO animals revealed an additional role for CRBPII in the placenta. Reduction of vitamin A in the maternal diet lead to high mortality rates in post-natal CRBPII-KO mice, suggesting a requirement for CRBPII in the transfer of retinol from dam to pup and therefore post-natal retinol in offspring (76). Although no other physiological roles of CRBPII have been described, the pathological condition observed in CRBPI-KO animals suggests CRBPII may be involved in 9cRA synthesis in certain physiological contexts.

Like CRBPII, CRBPIII shows restricted tissue expression. Most work involving CRBPIII has focused on its role in mammary gland. There, secretion of retinol into milk, and thus normal post-natal nutrition, requires expression of *Rbp7* (77). Interestingly, KO of CRBPIII also revealed a metabolic role for the binding protein (78). CRBPIII KO mice resist HFD-induced obesity. This resistance is attributed to increased expression of lipid oxidation genes, including master regulator PPARα, in brown adipose tissue (BAT).

Whereas CRBPs bind retinol and retinal, another group of binding proteins chaperone retinoic acid. Two different KO mouse lines have been generated for CRABPI, with neither presenting an obvious phenotype (79, 80), leading some to label CRBPI as "dispensable." However, developmental studies show overlapping expression of CRABPI with areas of retinoid action (81-84). Cultured mouse stem cells with knocked down levels of CRABPI show reduced atRA levels and decreased polar metabolite products, suggesting a role in atRA catabolism (85). With recent work in FABP5 expanding the number of RA binding proteins, other members of the lipocalin family may compensate for CRABPI knockout.

With the exception of polydactyly, CRABPII-KO animals appear normal compared to WT animals (86, 87), though no metabolic studies have as of yet been reported (86, 87). In humans, however, polymorphisms in *Crabp2* associates with increased cholesterol, especially in LDL (88). *Crabp2* also mediates atRA action in preventing adipocyte differentiation (89). Preadipocytes express higher levels of *Crabp2* than mature adipocytes, allowing activation of RAR by atRA. Treatment with differentiation signals insulin, 3-isobutyl-1-methylxanthine (IBMX) and dexamethasone repress *Crabp2* expression through cyclic-AMP and glucocorticoid response elements. Reduced *Crabp2* expression thereby shifts signaling of atRA to PPARδ via FABP5. This predicts increased adipogenesis in *Crabp2*-KO animals.

Identification of FABP5 (from *Fabp5*, also called E-FABP and *Mal1*) as an atRA binding protein (90) adds a new facet to atRA function. Both *in vivo* and *in vitro*, atRA induces glucose and lipid metabolism genes in white adipocytes, acting through both PPARδ and RAR signaling pathways (32). During differentiation, levels of FABP5 increase (as CRABP2 decreases), thus shifting retinoic acid signaling though PPARδ rather than RAR. The CRABP2-to-FABP5 ratio also regulates atRA function in additional cell types. In ketatinocytes, atRA treatment leads to either apoptosis or cell survival depending on the relative expression of CRABP2 to FABP5 (34).

To support RA synthesis in other tissues, liver and WAT hydrolyze stores of RE, exporting newly available retinol on the binding protein RBP (*Rbp4*) (1, 91). Circulating levels of RBP, derived from increased *Rbp4* expression in WAT, are found in a variety of insulin resistance and obesity models (92). In fact, either overexpression of *Rbp4* or the injection of recombinant RBP induces insulin resistance in mice. Conversely, *Rbp4*-KO mice maintain insulin sensitivity during HFD feeding. Subsequent research determined that binding of retinol-RBP to STRA6 triggers a signaling cascade (6). Upon binding of retinol-RBP, STRA6 becomes

phosphorylated, leading to activation of janus kinase (JAK) 2 and signal transducer and activator of transcription (STAT) 5. Activation of STAT5 triggers expression of target genes such as *Socs3* (Suppressor of cytokine signaling 3, SOCS3) and *Pparg*. SOCS3 antagonizes insulin signaling, thereby connecting elevation of RBP to insulin resistance.

Clearly, retinoid binding proteins represent important points of regulation in both atRA synthesis and downstream effects. Shifts in ratios of binding proteins can cause a variety of changes in gene expression depending on the tissue, physiological context and presence of other retinoid binding proteins.

Retinal Dehydrogenases in Retinoid and Energy Metabolism

Three genes from the Aldh1a family (93) and one from the Aldh8a family (94) convert retinal to retinoic acid *in vitro.* The least studied of the four, RALDH4 (*Aldh8a1)* recognizes 9- and 13-*cis*-retinal isomers as substrate (94, 95), suggesting a possible role in pancreatic 9cRA synthesis (4)

KO of RALDH2 (*Aldh1a2*) results in embryonic lethality (96). Consistent with loss of atRA production, *Aldh1a2*-KO embryos show defects in body patterning, limb formation and organogenesis of the heart, forebrain and pancreas (97, 98). Hypomorphic mutants of RALDH2 survive past embryogenesis, but die perinatally, with defects of the neck and chest similar to the human DiGeorge syndrome (99). Similarly, RALDH3 (*Aldh1a3)* KO animals die at birth of respiratory stress (100). Amongst other craniofacial defects, *Aldh1a3*-KO mice are born with persistent nasal fins that prevent proper respiration. The effects of *Aldh1a2* or *Aldh1a3* loss to adult tissue have yet to be determined. In regards to metabolic regulation, diabetic *db/db* (leptin receptor deficient) mice overexpress *Aldh1a3* in pancreas (101). In an alpha cell line, manipulation of *Raldh3* expression levels correlates to changes to in glucagon secretion. *Aldh1a3* expression levels may also distinguish different white adipose tissue depots (102).

Under standard conditions, *Aldh1a1*-KO mice survive to adulthood without a striking phenotype (103). However, when challenged with HFD feeding, RALDH1-KO mice resist weight gain and adiposity, in part through increased UCP1 in brown adipose (104). Additional work identified reduced PPARγ and zinc-finer 423 expression as contributors to the RALDH1-KO phenotype (102).

Retinol Dehydrogenases in Retinoid and Energy Metabolism

Two enzyme families show *in vitro* RDH activity: the alcohol dehydrogenase (ADH) family and the short-chain dehydrogenase/reductase (SDR) family. *In vitro* members of both families recognize a variety of substrates (ADH: various alcohols; SDR: different retinol isomers, steroids), though only members of the SDR family recognize holo-CRBP as substrate (1). Furthermore, knockouts of ADH1, ADH3 and ADH4 have not been shown to affect endogenous atRA levels under physiological conditions nor have they been shown to induce compensatory gene changes in other retinoid metabolism genes (17, 19, 20).

Though not yet knocked out in mice, evidence supports SDR *Dhrs9* as an important retinol dehydrogenase. Induction of *Dhrs9* in carcinoma cells with low endogenous expression increased retinoic acid synthesis (105). Expression of *Dhrs9* responds to retinoic acid, though whether expression increases or decreases expression may be context dependent (106, 107). Work in astrocytes revealed coordinated regulation of *Dhrs9* and *Aldh1a1* expression (108). Furthermore, microsomal fractions from cells transfected with *Dhrs9* recognize holo-CRBP as substrate for retinal synthesis (107).

First identified in bovine retinal pigment epithelium, the pattern of *Rdh10* expression includes many other adult tissues and embryonic regions (109, 110). Two different groups identified *Rdh10* in ENU screens of embryonic defects, one group focusing on defects in the meninges and the other on a broad characterization of limb, craniofacial and organogenic defects (7, 111, 112). In the developing forebrain, *Foxc1* (Forkhead box c 1) regulates *Rdh10* expression. Maternal treatment with atRA rescues defects in one of the *Rdh10* hypomorphic mutants and in *Foxc1* hypomorphic mutants. Knockout of *Rdh10* by homologous recombination affirms its role in proper embryogenesis (113). Maternal retinal treatment rescues defects in *Rdh10*-KO mice, allowing survival into adulthood (113). As of yet, no metabolic phenotype in *Rdh10*- KO or mutant mice has been reported, though Rdh10-KO mice display abnormal motor function (113).

Mice uniquely express three *Rdh1* paralogs: *Rdh9, Rdh7* and *Rdh16* (114, 115, 115). On a whole, these *cis*-retinol/androgen dehydrogenase (CRAD) enzymes prefer 9-*cis*-retinol, 11-*cis*-retinol and/or hydroxysteroids over all-*trans*-retinol as substrates. CRAD3 (*Rdh9*)-KO mice present no striking phenotype, though hepatic xenobiotic and steroid metabolism genes are induced and widespread *Rdh1* expression is decreased (116).

In humans, loss of RDH5 function leads to night blindness. However, *Rdh5*-KO mice show only mild defects in ocular 11-*cis*-retinol metabolism (117, 118) suggesting additional SDRs contribute to or compensate in 11-*cis*-retinal formation.

RDH1 and the *Rdh1*-KO Mouse

The mouse gene *Rdh1* was cloned during the search for a mouse ortholog to rat *Rdh2* (RDH2 or RODH2) (2). Rat RDH2, a member of the SDR family of enzymes, is the most efficient retinol dehydrogenase in the rat. Furthermore, RDH2 recognizes holo-CRBP as well as free at-retinol as a substrate (23). RDH1 and rat RDH2 share 88% amino acid sequence similarity and 84% amino acid identity. The closest human homolog to both genes is *RDH16*, with which RDH1 shares 83% sequence similarity and 74% sequence identity. By comparison, CRAD1 and CRAD2 enzymes share about 90% amino acid identity with RDH1 (2, 119).

Among the known mouse RDH2 orthologs, RDH1 shows the highest efficiency (V_{max}/K_m) with at-retinol in cell extract assays (120). RDH1 shows activity towards 9-*cis*-retinol, although at half the efficiency it has with at-retinol. *In vitro*, RDH1 can also act as a 3-α- or 17-β-dehydrogenase, converting 3-α -diol into dihydrotestosterone (DHT) and DHT into androstanedione. In addition to activity in cell extract, RDH1 can generate atRA in intact cells when co-transfected with any one of three different RALDH enzymes (2). Like rat RDH2, RDH1 targets to the endoplasmic reticulum. A 22 amino acid N-terminal sequence, consisting of a hydrophobic helix ending with a net positive charge, orients RDH1 with its catalytic domain toward the cytoplasm (121). Because CRBP is a cytoplasmic protein, the orientation of RDH1 allows holo-CRBP to be a possible substrate for RDH1.

Expression of RDH1 begins as early as e7.5 in the mouse. In fact, from e7.5 to e10.5, RDH1 is widely expressed throughout the embryo. By e14.5, expression matches that of the adult, where northern and dot blot assays have shown expression in liver, kidney, testis, heart, brain, pancreas, skeletal muscle, submaxillary gland, lung, smooth muscle, thyroid, thymus, ovary, prostate, epididymis and uterus—nearly every tissue probed. With such high efficiency with at-retinol and such widespread expression in both adult mice and embryos, RDH1 became a good knockout candidate to probe the role of RDHs in the mouse.

As such, an *Rdh1*-KO mouse was created and initially characterized by Zhang, Hu and others from our lab (3). Gene targeting was used to remove the proximal promoter and exon 1 of

Rdh1 in mouse 129SVJ embryonic stem cells. The first exon includes the N-terminal membrane-targeting domain, the ATG start codon and the co-factor binding region of RDH1, three regions important to function. Male chimeras were bred with C57BL/6 females to generate heterozygous *Rdh1*-KO mice with a mixed genetic background, which were backcrossed with C57BL/6 mice for five generations generating heterozygous *Rdh1*-KO mice on a ~98% C57BL/6 background. Mating of heterozygous mice results in homozygous *Rdh1* KO mice appearing in the expected Mendelian frequency, regardless of parental diet (0.6, 4 or 30+ IU of vitamin A/g). KO mice are initially indistinguishable in appearance from WT. Hematoxylin and eosin (H&E) staining of testis, kidney and liver revealed no morphological differences. Breeding male and female homozygous knockout mice yields healthy progeny.

Quantification of retinyl ester, retinol and atRA levels in wild-type (WT) and KO mice fed 0.6, 4 and 22+ IU/g diets were also performed. When fed a high retinol (22+ IU/g) chow diet (Purina chow), KO and WT mice showed no differences in any retinoids assayed. When fed a vitamin A sufficient diet (AIN 93G (93G) diet, with 4 IU/g), liver retinol levels in the KO mice were about twice as high as WT. Finally, when fed a marginal (0.6 IU/g) diet, retinol levels were higher in both the liver (2-fold) and the kidney (~1.4 fold). RE levels in the KO mouse liver were higher as well (~1.4 fold). In all tissues assessed (liver, kidney, brain and testis), there were no differences in atRA between KO and WT mice, regardless of diet.

Initial screens of retinoid-related gene expression in *Rdh1*-KO mice revealed hepatic *Cyp26a1* levels were decreased compared to WT mice fed a 93G and 0.6 IU/g, but not a Purina chow diet. Results from reverse transcriptase-polymerase chain reaction (RT-PCR) were confirmed using quantitative PCR (qPCR), showing a 2.5 fold decrease in KO versus WT expression in mice fed a 93G and 0.6 IU/g diets. Both WT and KO mice showed 8-fold decreased expression when fed a 0.6 IU/g diet compared to 93G diet. When fed a Purina chow diet, *Cyp26a1* expression levels were 60 and 160 fold higher than those in 93G-dieted WT and KO mice, respectively. Western blotting revealed that protein levels of CYP26A1 in 93G-fed mice were also decreased in KO mice compared to WT.

The sparing of liver retinol and/or retinyl esters along with the decreased *Cyp26a1* expression and protein levels on sufficient and marginal diets suggests decreased atRA synthesis in the *Rdh1*-KO mouse. When fed a Purina chow diet, it appears that hepatic retinol concentrations are such that other, less efficient, RDH enzymes (DHRS9/RDH15 (106), RDH10 (109, 122, 123)) generate sufficient retinal, and thus maintain atRA levels. On lower diets, however, hepatic retinol levels are reduced, reducing the ability of less-efficient enzymes to generate retinal. To compensate, CYP26A1 levels decline, lowering the rate of RA degradation in the KO livers and thus allowing maintenance of atRA.

KO mice fed a VAD diet showed a surprising phenotype. One week after weaning (4 weeks of age), both male and female mice started to become significantly heavier than WT. This weight difference gradually increased during the entire course of observation (33 weeks). Both male and female KO mice fed a 0.1 IU/g diet also grew significantly larger than WT by 8 weeks of age (males) and 1 week of age (females), however, no difference between KO and WT weight was apparent when mice were fed a Purina chow diet.

Through additional study of *Rdh1*-KO mice we hope to provide insight into the regulation of metabolism by atRA and uncover physiological processes and potential molecular targets of atRA connecting *Rdh1* to weight regulation. Furthermore, continued study will help clarify the roles of multiple RDH in the post-natal animal and the contribution of each to atRA synthesis.

Materials and Methods

Animals and Diets:

Rdh1-KO mice (3) were backcrossed a sixth time onto a C57BL/6 background and resulting *Rdh1* WT and KO progeny were interbred and used for genotype comparisons. For other experiments, C57BL/6 mice purchased from Jackson Laboratories were either used after 1-2 weeks of acclimation or were maintained on an AIN 93G (93G) diet and interbred for at least two generations. *Rdh16*-KO (Zhang, Hu and Napoli, unpublished) and *Rdh9*-KO (116) were backcrossed a sixth time onto a C57BL/6 background and resulting WT and KO progeny were interbred, with resulting *Rdh16*-WT mice used as controls. Mixed-strain *Rbp1*-KO mice (70) were interbred and compared to C57BL/6 controls (Jackson Laboratories). FVB strain mice heterozygous for a hypomorphic *Rdh10* mutant allele (7) were maintained on a 93G diet for two generations of breeding with WT FVB mice (Jackson Laboratories), maintaining heterozygous mice and generating WT controls. Rats were purchased from Charles River and allowed to acclimate at least 1 week before study.

All mice were group housed, 2-5 mice per cage. Rats were housed in pairs. Feeding was *ad libitum* unless otherwise noted. Aside from diet, animals were housed under standard conditions for our facility: 21º C, 12-hour light-dark cycle (07:00-19:00) and ventilated cages (Tecniplast) with an air circulation system (Tecniplast TouchSLIM Line) unless otherwise indicated.

Specific diet regimes using AIN 93G (Dyets, Inc. cat. #110700) (124), Purina chow diet (Purina Lab Diet 5001, Purina), Harlan chow diet (Teklad 2018 Rodent Diet, Harlan), modified AIN 93G without vitamin A (vitamin A deficient/VAD) diet (Dyets, Inc. cat. #119178) and modified AIN 93G diet with 50% fat-derived calories (HFD). Additional diets referred to, but not used include modified AIN 93G diets with 0.1 IU/g vitamin A (Dyets) and 0.6 IU/g vitamin A (Dyets, Inc. cat. #11974). Purina chow diet contains 22 IU/g of vitamin A plus 4.5 ppm carotene. Harlan chow diet contains 15.4 IU/g vitamin A plus 2.5 mg/kg β-carotene. The AIN 93G diet contains 4 IU/g vitamin A, 1.6 IU/g more than required for rodents (124, 125). When switching animals between a 93G diet and a HFD, animals were fasted overnight to entice quick acclimation.

For reference and organizational purpose and to match electronic data records, cohorts of *Rdh1*-WT and KO animals are given two numbers separated by a "w." Groups sharing the same first number come from the same set of mating pairs, with the second number indicating the number of times the pairs have been mated. For instance, "3w2" comes from the third group of mating pairs and represents pups from the second mating. In certain instances, age-matched mice from two cohorts were combined, whereas other cohorts were sub-divided into "a" and "b" by age. See Table 1 for diet information for each group. When possible, figure legends include the experimental cohort studied.

All animal experiments were approved by University of California Berkeley Animal Care and Use Committee.

Genotyping:

For PCR genotyping of mice, primers GGT TTA CAC AGC TGC TTT CAG GAC A and GAG TCA TTA GGC TTA GAC GAT CTC generate a ~300 bp amplicon used to identify *Rdh1*-WT mice (3). Primers TGT ATG CTA TAC GAA GTT ATG AAT TC and CCT CTG GGT TCT AAG TCC A generate a ~1.7 kbp amplicon used to identify *Rdh1*-KO mice. For

For *Rdh16* genotyping, primers CTC TAA GCT GTG TGT TCT TAG CC and ATA

AGA ACT TCT ATG ACT GGG AC make a ~1 kbp amplicon that identifies WT mice and primers TTT TGA TTC TGT TCA AAA GG and ATA AGA ACT TCT ATG ACT GGG AC (note: same reverse) create a ~1 kbp amplicon demarking *Rdh16*-KO mice.

Rdh9-WT and KO animals were identified using forward primer CCC TCT TGA AGT AAG AAG GTA with reverse primer ACT CCC AGA GTA GAT ATG AG (WT) or CAT TGT TGA TGG GAT TGC AAG C (KO), that yield ~1.25 kbp and 0.5 kbp amplicons, respectively.

To amplify the above primers, we used the following thermal cycle: 3 minutes at 93º C followed by 35 cycles of 30 seconds at 93º C, 30 seconds at 55º C and 1.5 minutes at 72º C, then 15 minutes at 72º C.

To identify *Rdh10* hypomorphic mutants, primers TTA CGG CGC AGA GAC TGT TCT and TGA GAA CTG TGCT GTC CTG TGT were used with the PCR conditions above to amplify genomic DNA. The 318 bp amplicon was electrophoresed on an agarose gel, excised and extracted using a commercial kit (QiaQuick Gel Extraction Kit, Qiagen # 28704). The extracted amplicon was then sequenced by the UC Berkeley DNA Sequencing Facility starting from either PCR primer. Mutant alleles contain a C to T point mutation that changes alanine 195 to valine (7, 126).

Using reverse primer GCA CTT GCG GTC GTC TAT GC with forward primer AAA AAT GGA AAG GCA AGG CAC AGA C yields a 339 bp amplicon in from the *Rbp1*-WT allele. Using the same reverse primer with forward primer GCC TTC TAT CGC CTT CTT GAC GAG TTC TTC produces a 593 bp amplicon of the *Rbp1*-KO allele. *Rbp1* genotyping primer pairs were amplified by 94º C for 5 minutes, followed by 33 cycles of 94º C for 40 seconds, 61º C for 40 seconds and 72º C for 1 minute, then 72º C for 10 minutes.

Genotyping PCR template was generated by treating small tail snips (1-2 mm) in 0.5 mL of 0.05 M sodium hydroxide for 15-20 minutes at 95º C in a 1.5 mL microcentrifuge tube. The solution was then mixed and neutralized with 50 µL of a 1 mM tris(hydroxymethyl)-aminomethane (Tris), 10 mM ethylenediaminetetraacetic acid (EDTA) solution with pH 8 before use in PCR.

PCR was carried out in 20 µL total volume of a 1.5 mM magnesium chloride, 0.2 mM nucleotide triphosphate mix, 0.4 µM forward and reverse primer, 1X PCR buffer (Invitrogen), and 1 unit Taq polymerase (Platinum Taq, Invitrogen) solution in water using 1.2 µL of DNA template.

Chemicals and Solvents:

Chemicals and solvents were purchased from Fisher Scientific or Sigma Aldrich unless otherwise indicated.

Mouse Weight and Long Term Food Intake

Rdh1-WT and KO mice were weighed to the nearest 0.1 gram using a digital scale. Long term food intake was monitored by weighing food once or twice weekly. For some measures, weekly intake was normalized to the number of mice per cage. For others, weekly intake was normalized to number of mice and average mouse weight. AIN 93G diet contains 3.766 kcal per gram (124).

Mass difference between genotypes of mice was calculated using Graphpad Prism 5.02.

Breeding Studies:

Combinations of virgin 8-10 week old male and female *Rdh16*-WT, heterozygous (Het), and KO mice were paired until obvious pregnancy or 28 days. For each pair, the number of days until birth (used here as a proxy for gestation length) was recorded for each successful pregnancy. Litter size and percentage of male pups were recorded for litters surviving until weaning. The number of unsuccessful births and infertile pairs were also recorded.

Serum and Tissue Preparation:

At ages and conditions indicated in text, mice were euthanized and tissues were harvested, weighed and flash frozen in liquid nitrogen for use in retinoid and/or gene expression determinations. Tissues used for retinoid determinations were harvested under yellow light. In some experiments, post-mortem body mass and body length (nose to anus) were also determined. Blood was collected via post-mortem cardiac puncture, kept on ice for 30 minutes and centrifuged (10 min x 10,000x g) to make serum. For thyroid stimulating hormone measures, blood was refrigerated (4º C) overnight (~16 hours) then centrifuged for 20 minutes at 1000 x g. Additionally, blood was collected via tail artery or retro-orbital bleed from anesthetized mice and processed as above to make serum. Serum samples and tissues were stored at -80° C until time of analysis.

"Fasted" indicates that tissues or serum were taken from mice fasted overnight for ~16 hours prior to collection. "Refed" indicates that tissues or serum were taken from mice fasted overnight, then refed (for length of time noted) prior to collection. "*Ad lib* fed" refers to mice sacrificed during the light half of the light-dark cycle without consideration of food intake status.

Adipocyte Size Determination:

Epididymal white adipose tissue (EWAT) from 35 week old *Rdh1*-WT and KO animals were dehydrated by successively increasing ethanol concentrations. Tissues were then embedded in paraffin, sectioned and stained with H&E. Cell diameter was estimated by counting the number of cells across a transect of the visual field for 10 fields per sample at 400X magnification.

Body Composition:

Fat, water and ash components of animals were determined as in (127).

Retinoid Determinations:

Retinol, retinal, retinyl esters and all-*trans*-retinoic acid (atRA) were measured as in (128). For small tissues (for instance, hypothalamus), tissues from several animals were pooled. Retinoid levels were normalized to tissue wet weight and/or protein content of homogenates.

Protein Measures:

Protein concentrations were determined using Bio-Rad Protein Assay reagent (cat. #500-0006) diluted 1 to 5 with water. An aliquot of 40 μL of protein solution was added to 2 mL of diluted assay reagent, mixed and absorbance at 595 nm measured using a spectrophotometer (DU 640, Beckman). A 40 uL aliquot of protein diluent was used as a "blank." Referencing known concentrations of bovine serum albumin standards, absorbances were converted to protein concentrations from a standard curve.

Glucose Metabolism:

For glucose tolerance tests, animals were fasted 16 hours overnight. The next morning animals were weighed to the nearest 0.1 g using a digital scale. Mice were then anesthetized with isoflourane (Phoenix Pharmaceutical, Inc.) via precision vaporizer, and a small nick in the tail was made with a sterile, sharp blade.

Mice were treated using an insulin syringe (28 ½ G ½ cc LO-Dose (Becton Dickinson)), 20% d-glucose solution was delivered intraperitoneally such that each mouse received a dose of 2 g glucose/kg of body weight. For rats, we administered the same glucose dose via an oral gavage of 5 μL/g body weight of a 40% d-glucose solution. Blood glucose was measured via blood from the tail nick using an Accu-chek glucometer (Roche) and Accu-chek Comfort Curve test strips (Roche) at time points 0 (pre-injection), 15, 30, 60, 90 and 120 minutes. The glucose solution was prepared no more than one day before use and was filter sterilized via 20 μm filter (25 mm Fisherbrand).

For experiments on the impact of 9cRA, mice were administered a 0.5 mg/kg dose of 9cRA in 60 μL of DMSO or 60 μL of DMSO alone intraperitoneally 15 minutes prior to a glucose dose of 0.5 g/kg.

For insulin tolerance tests, mice were fasted for 5 hours, beginning ~1 hour after the start of the light cycle. Mice were weighed to the nearest 0.1 g using a digital scale. Mice were then anesthetized with isoflourane via precision vaporizer and a small nick in the tail was made with a sterile, sharp blade. Using an insulin syringe, a dose of 0.5 U insulin/kg of body weight was administered intraperitoneally. Blood glucose was measured via blood from the tail nick using an Accu-chek glucometer and Accu-chek Comfort Curve test strips at time points 0 (pre-injection), 15, 30, 60, 90 and 120 minutes. For injections, 10 μL of 100 IU/mL Humulin (Eli Lilly) insulin was diluted as in (129) immediately before use.

For pyruvate tolerance tests, *ad lib* fed mice were weighed to the nearest 0.1 gram using a digital scale. Mice were then anesthetized with isoflourane via precision vaporizer and a small nick in the tail was made with a sterile, sharp blade. Using an insulin syringe, a dose of 2 g sodium pyruvate/kg of body weight was administered intraperitoneally. Blood glucose was measured via blood from the tail nick using an Accu-chek glucometer and Accu-chek Comfort Curve test strips at time points 0 (pre-injection), 15, 30, 60, 90 and 120 minutes. The sodium pyruvate solution was prepared no more than one day before use and was filter sterilized via 20 μm filter (25 mm Fisherbrand).

Serum Lipids and Hormones:

Serum free-fatty acid and glycerol levels were determined using the same commercially available kit (Zen Bio, cat. # GFA-1). Serum triglycerides were determined using a separate commercially available kit (Cayman Chemical Company, cat. # 10010303).

Serum insulin, leptin, resistin, tumor necrosis factor (TNF) α, monocyte chemoattractive protein (MCP) 1 and interleukin (IL) 6 levels were determined using the Milliplex Map Mouse Serum Adipokine Panel (Millipore, cat. #MADPK-71K). Additional insulin measures were made using an ultra-sensitive enzyme-linked immunosorbent assay (ELISA) (Crystal Chem, cat. # 90080).

Thyroxine (T4), triiodothyronine (T3), thyroid stimulating hormone (TSH) and growth hormone were measured using commercially available ELISAs (T3, Calbiotech, cat. #T3043T-100; T4, Calbiotech, cat. # T4044T-100; TSH, Kamiya Biomedical Company, cat. #KT-29922; growth hormone, Millipore , cat. #EZRMGH-45).

Serum neuropeptide Y (NPY) levels were measured by radioimmunoassay (Phoenix Pharmaceuticals, Inc. cat. #RK-049-03)

Serum testosterone and dihydrotestosterone (DHT) measures in *Rdh1*-KO and WT animals were determined by ELISA (Alpha Diagnostic International, cat. #1880 and 1940).

All samples above were analyzed per manufacturer's instructions.

For measures of testosterone and 5α-androstane-3α, 17β-diol glucuronide (3-adiol-G), 50 μL serum samples were extracted twice with 1 mL of ethyl ether, dried and resuspended in 60 μL of phosphate buffered saline-gelatin (0.137 mM sodium chloride, 2.68 mM potassium chloride, 7.81 mM dibasic sodium phosphate, 1.47 mM monobasic potassium phosphate and 1 g/L gelatin). Samples were then analyzed by ELISA following manufacturer's instructions (Alpco Diagnostics, cat. #11-TESHU-E01 and cat. #11-ANDHU-E01).

Metabolic Parameters:

Mice of ages and genotypes indicated were housed individually in metabolic cages (Comprehensive Lab Animal Monitoring System (CLAMS), Columbus Instruments) with an air flow rate of 0.5 L/min. Respiration (oxygen consumption, carbon dioxide production) were recorded using the packaged software (Oxymax) and normalized to an effective body mass ($mass^{0.75}$). Individual cages were monitored for movement and gas composition 2 of every 10 minutes during the study; food and water intake totals were recorded every 10 minutes. Heat was calculated by the packaged software using the equations: Heat (kcal/hr) = Calorific Value x volume oxygen consumed, where Calorific Value= 3.815+1.232 x volume carbon dioxide produced/volume oxygen consumed. During metabolic study, mice were maintained at standard housing temperature and light/dark cycle conditions.

For β_3-adregenergic studies, mice were allowed to acclimate to the metabolic cages overnight (~16 hours) at 09:00, food was removed and at 12:00, 1mg/kg of CL 316,243 (CL) (Sigma) delivered in sterile saline was administered via intraperitoneal injection in a volume equal to 10 μL/g body weight using an insulin syringe (28 ½ G ½ cc Lo-Dose (Becton Dickinson)). Metabolic data was collected for 3 hours post injection. Solutions of CL were made on day of use from frozen stock. In some studies, the procedure was repeated using saline-only injections of an equivalent volume. β_3-adregenergic induction was calculated by averaging metabolic parameters during low activity periods (total horizontal movement counts<100) for each mouse after CL injection and either normalizing to low activity averages after saline injection or to low activity periods prior to injection.

For additional metabolic data, mice were housed for 24-25 hours under *ad lib* fed, fasted or refed conditions. Data from the first hour was discarded to allow acclimation to the chambers. For hourly food consumption measures, pellets of diet were ground using a food processor before use. Food “Hourly” averages reflect the mean total food eaten for a given hour of the day. Movement was quantified based on total breaks of infrared beams in the x-axis (“Total Horizontal”), breaks of two or more beams in the x-axis (“Ambulatory”) and breaks in the z-axis (“Rearing”) per 2-minute recording interval. Hourly means were determined by first averaging 6 readings from an individual mouse and next averaging the means from individual mice. For overall means, 24-hour means from individual mice were averaged.

Stable Isotope Studies:

Stable isotope studies were carried out for lengths and conditions indicated as in (130-133). In study 1, biopsies of inguinal white adipose (IWAT) were taken from animals under

anesthesia. In studies 2 and 3, tissues samples were collected following euthanasia. In studies 1 and 2, body water enrichment was estimated based on the proportion of singly- and doubly-labeled palmitate species. In study 3, body water enrichment was determined empirically.

Temperature Studies:

Male mice at ages indicated were individually housed at 4±1° C for 24 hours under fasting conditions. Core body temperatures were taken rectally using a probe (Physitemp RET-3) attached to a digital thermometer (Physitemp BAT-12). Institutional guidelines required mice to be removed from study if body temperature fell below 28° C.

In other experiments, individually cages animals were fasted 10 hours at normal housing temperature and then fasted an additional 6 hours at either 4±1° C or normal housing temperature before tissue collection.

For "Average Daytime Body Temperature," mouse temperatures were taken 3 times during light hours (at ~10:00, 13:00 and 16:00 hours) rectally, as above, at ages indicated. Mean temperatures from individual mice were then averaged and compared.

Additional temperature data represents means calculated from single individual measures.

Gene Expression:

Total RNA was isolated either via phenol-chloroform extraction using Trizol Reagent (Invitrogen) or spin kit (Aurum Total RNA fatty and fibrous Tissue Pack, Bio-Rad, cat. #732-6870; RNeasy Mini Kit, Qiagen, cat. #74104; RNeasy Micro Kit, Qiagen, cat. #74004; RNeasy Lipid Tissue Mini Kit, Qiagen, cat. #74804) according to manufacturer's instructions.

For quantitative PCR (qPCR) and microarray of brown adipose, RNA was either DNAse treated on-column (Aurum kit) or following isolation (Turbo DNA-free, Ambion, cat. #AM1907).

For microarray of EWAT, liver and testis, RNA (isolated by Trizol) pooled from 5 *Rdh1*-WT and KO animals was cleaned-up using a spin kit (Qiagen RNeasy Micro Kit). RNA was then submitted to Phalanx Biotech for analysis. There, RNA was labeled with Cy5 and hybridized to the microarray (Phalanx Mouse Whole Genome OneArray). Pools were analyzed as technical triplicates. Samples were scanned, raw data was normalized, and fold changes with p-values were calculated using proprietary software.

For brown adipose tissue microarray, RNA isolated from 3 individual *Rdh1*-WT and KO animals was isolated and DNAse treated via spin kit (Aurum Kit, Bio-Rad). RNA was quantified using capillary electrophoresis (Experion, Bio-Rad). Samples were then labeled (Illumina TotalPrep RNA Amplification Kit, Ambion, cat. #1791) per manufacturer's instructions and biotin-labeled samples were evaluated once again by capillary electrophoresis. Labeled RNA was submitted to the University of California, San Francisco Genomics Core Facility where it was hybridized overnight to microarrays (Mouse WG-6 v2.0, Illumina, cat. #BD-201-0202) and scanned. The raw intensities data was converted into text files by Illumina BeadStudio software and then analyzed using the BioConductor limma package. The data was background corrected by Normal+Exponential model using negative controls and then quantile normalized. A linear model was fit by limma and p-values were computed based on moderated t-test and adjusted for multiple testing by applying Benjamini-Hochberg correction.

For all semi-quantitative PCR and some qPCR, reverse transcriptase (Superscript II, Invitrogen) in the presence of RNAse Inhibitors (RNAse Out, Invitrogen) and poly-thymine primer, followed by RNAse treatment (RNAse H, Invitrogen) were used to make complementary

DNA (cDNA). For additional qPCR, a reverse transcriptase with intact RNAse activity (iScript, Bio-Rad) in the presence of both random hexamer and poly-thymine primers was used. The cDNA from cell culture experiments was generated by a third reverse transcriptase to optimize detection of low transcripts (iScript Advanced, Bio-Rad). All reverse transcriptase reactions were carried out following their respective manufacturer's instructions.

Quantitative PCR reactions were carried out in 96-well plates on the ABI 7000HT (Applied Biosystems) system. Reactions were carried out in 20 μL total reaction volumes using 1 μL of cDNA solution, 1 μL TaqMan primer/probe mix (Applied Biosystems), 10 μL master mix (TaqMan Gene Expression Mix, Applied Biosystems) and 8 μL RNase and DNAse free water. For some low abundance transcripts, 4 μL of primer/probe mix were used. Dilution curves using both primer concentrations resulted in parallel curves within the linear amplification range (data not shown). A list of primer and probe sets used can be found in Table 2. Samples were run as technical duplicates or triplicates. Mean "Ct" for β-actin (*Actb*) was subtracted from mean "Ct" for genes of interest. Linear fold change was calculated using the formula $2^{\Delta Ct}$. Linear values for control group (WT or as noted) were then averaged, and individual values normalized to the control group mean to create a fold change. For comparisons between genes, linear fold change values of all genes were normalized to the average linear fold change of an arbitrarily chosen gene. Unless otherwise indicated, all gene expression studies were carried out via qPCR.

For semi-quantitative PCR, 1.2 μL of cDNA template was added to the same reaction mixture used for genotyping. Primer pairs can be found in Table 3. For all tissues, β-actin (*Actb)* was amplified for 25 cycles and used for reference. In liver, *Rdh7, Rdh9, Rdh16* and *Srd5a1* were amplified for 32 cycles. All other genes were amplified 35 cycles. To amplify, 1 minute at 93º C followed by repeated cycles (as indicated above) of 30 seconds at 93º C, 30 seconds at 55º C and 1 minute at 72º C, then 5 minutes at 72º C were used. For semi-quantitation, samples were run on a 1% agarose gel. Spot and background density was determined using packaged software (ChemiImager 4400 and software, AlphaInnotech). Background density was subtracted from spot density, normalized to β-actin then normalized once more to mean control levels.

Cell Culture:

Undifferentiated HIB-1B cells (134) were grown in 10 cm plates using 10 mL DMEM media (High Glucose, Invitrogen, cat. #10313-039) with 10% fetal bovine serum (Invitrogen, cat. #10082-147) and 1% of a 100 units/mL penicillin, 100 μg/mL streptomycin, 29.2 mg/mL L-glutamine, 10 mM citrate solution (Invitrogen, cat. #10378-016) (DMS media). Cells were split at confluence using a trypsin-EDTA solution (Invitrogen, cat. # 25200), every 2-3 days using a 1:10-1:20 dilution.

To differentiate, cells were split at a 1:20 dilution into 10 mL of adipocyte media (DMS media plus 20 mM insulin and 1 nM thyroxine). Adipocyte media was changed every 2 days until cells became confluent (about 3-4 days). Cells were then changed to 10 mL of induction media (Adipocyte media plus 0.5 mM 3-isobutyl-1-methylxanthine (IBMX), 0.5 μM hydrocortisone and 0.125 mM indomethacin). Induction media was changed daily for 3 days, upon which cells became round by visual inspection with a microscope. Cells were then maintained in 25 mL of adipocyte media, changed daily, for an additional 2-4 days.

For glucose experiments, plates of either undifferentiated cells 1 day after passage or differentiated cells 3 days after induction media treatment were changed to media made from low glucose DMEM (Invitrogen, cat. #11054) for 1 day before collection.

Statistical Measures:

In studies other than microarray, Student’s two-tailed t-test was carried out using either Microsoft Excel or GraphPad Prism. Two-way analysis of variance (ANOVA) was carried out using GraphPad Prism. In some studies, Grubb's test was used to identify outliers in the data.

Results

Dietary Vitamin A and the *Rdh1*-KO Phenotype

In initial studies, *Rdh1*-KO mice presented no phenotype when fed a chow diet containing 22+ IU/g of vitamin A (Purina chow). *Rdh1*-KO mice gained weight only when maintained on VAD or low retinol diet after being born to dams fed such diets at mating. Subsequent studies followed two different methodologies. The first was to continuously maintain mice fed an AIN 93G diet (93G), which contains 4 IU/g of vitamin A. The second was to maintain mice on a chow diet, then switch dams and their pups to a vitamin A deficient diet.

Mice maintained on Purina chow, or diets with similar amounts of vitamin A, become highly resistant to vitamin A deficiency. In order to get vitamin A deficient animals, one has to maintain mice on a vitamin A deficient diet for two generations before overt symptoms and growth defects occur (16, 17). As such, mice are believed to be highly resistant to vitamin A deficiency. In attempt to recapitulate the initial weight gain observations, dams fed a 93G diet were switched to a VAD diet at mating. Instead of weight gain in KO animals, we instead observed vitamin A deficiency in VAD-fed progeny. Both WT and KO animals showed growth defects at age 5 weeks (Figure 1A), but we ended the study when animals began dying around age 10-12 weeks. Thus, dams fed a 4 IU/g diet cannot pass on sufficient retinoid for pups to survive on a VAD diet. Attributing the VAD symptoms to the level of vitamin A in the 93G diet, we next switched chow-fed dams to a VAD diet. Once again, VAD-fed progeny from chow-fed dams gained little weight beginning at age 5 weeks (Figure 1B) and, once more, mice began to die around age 10 weeks. We rescued surviving mice by switching to a 93G diet at age 11 weeks (Figure 1B). Although no formal diagnosis of vitamin A deficiency was performed, the timing of these growth defects is consistent with those observed in other vitamin A deficient mice. Believing our chow diet to contain 22+ IU/g of vitamin A, and therefore able to pass on stores sufficient for pups to resist vitamin A deficiency, we traced our results to a change in chow diets. With little notification, our animal facility had switched diet suppliers, from a Purina chow diet to a Harlan chow diet containing 15+ IU/g of vitamin A. Though still well above recommended levels, our data suggests that resistance to VAD in mice comes from high levels of vitamin A in the diet and that even a modest reduction in vitamin A content allows for observation of VAD symptoms within a single generation of VAD diet feeding. We successfully prevented VAD symptoms, and observed modest weight gain in KO progeny switched to a 93G diet at age 5 weeks (Figure 1C). Overall, the risk of vitamin A deficiency made study under these conditions difficult. The use of VAD diet regimes and effects of vitamin A deficiency noted above likely confound early work in the *Rdh1*-KO mouse. Furthermore, switching diets at different ages made direct comparisons between cohorts and previous studies impossible.

At the same time, we began to observe the weight gain phenotype in mice fed the 93G diet (Figure 2A). This diet regimen proved easier to maintain, and yielded more consistent, though still variable, results. Due to biological variability and variable numbers of mice per group, individual cohorts do not always present the model phenotype (Figure 2C), however, pooling animals from multiple studies (Figure 2B) clearly shows *Rdh1*-KO mice fed a 4 IU/g vitamin A diet weigh more than WT, even at a young age.

Weight, Adiposity and Length in the *Rdh1*-KO Mouse

During previous studies, Zhang and Hu observed increased weight when mice were bred and maintained on low or vitamin A deficient diets (3). Because vitamin A has known effects on

growth, it was important to determine whether the increased weight was due to increased body size or increased adiposity. We assessed adiposity using two different methods. By weighing the fat depots and tissues of the (original) VAD-fed animals, the absolute mass (Figure 3A), mass relative to body weight and an adiposity index were determined (Figure 3B). Compared to WT animals, the fat pads and tissues measured were larger in *Rdh1*-KO mice, except for testes. Reduced testicular mass is a symptom of vitamin A deficiency, suggests a role for *Rdh1* in testes retinoic acid synthesis, a phenotype we have not fully explored. When normalized to body weight, three fat pads and overall adiposity were increased in KO animals. Along with this increase in tissue size, KO animals were increased in length (Figure 3C). Together, this early data suggested that both increased growth and increased adiposity contributed to overall mass increases in KO animals. However, subsequent study of length in 93G fed animals (Table 4), suggests the increased length phenotype has low penetrance or is merely a stochastic event.

In our initial group of VAD fed animals, rigorous body composition analysis (Figure 4A) confirmed higher adiposity. In later studies of adiposity (Figure 4B), we used only inguinal and epididymal fat depots for our adiposity index. Although not as thorough, measuring fewer tissues allows for study of larger groups and minimizes degradation of retinoids and RNA during sample collection. Whereas we observe variable results in individual cohorts of animals (data not shown), pooling data by age shows increased adiposity to be fairly consistent amongst KO animals. We therefore attribute the increased body mass of *Rdh1*-KO mice to changes in adiposity rather than increases in overall body size. Dual energy X-ray absorptiometry (DEXA) studies would allow multiple measures of adiposity throughout the life of the same animal. Unfortunately, this method was unavailable to us and we have only assessed adiposity post-mortem.

To determine if increased white adipose mass occurs due to hyperplasia (more cells) or hypertrophy (bigger cells), epididymal white adipose tissue (EWAT) from VAD-fed WT and KO male mice, age 35 weeks, were preserved and stained with H&E (Figure 5A-G). In these samples, we estimated cell diameter (Figure 5H). In these animals, we observed no difference in WT and KO adipocyte diameter, despite a 78% increase in EWAT size (data not shown). Lack of hypertrophy suggests that, under conditions assessed, increased adipose mass can be attributed to white adipose hyperplasia. Whether younger animals (fed a 93G diet) display hyperplasia or hypertrophy has yet to be determined.

In attempt to exacerbate the *Rdh1*-KO phenotype, we tried two feeding regimes of high fat diet (HFD; here, 50% fat derived calories). In the first, (Figure 6A) we switched mice from a 93G diet to HFD at 7 weeks of age. Although this particular cohort showed no weight difference at 7 weeks, the following 3 weeks of HFD feeding caused *Rdh1*-KO animals to quickly gain weight beyond that of WT. Although WT and KO animals fed HFD were heavier overall than 93G fed animals, the weight difference between WT and KO was the same as that commonly observed in animals fed 93G diet (Figure 6B). Interestingly, this group of KO animals did not have an increased adiposity index (Figure 6D). Because differences in tissue weight were not statistically significant (Figure 6C), other, unmeasured, tissues and fat depots must account for the weight difference.

In a second group of animals, we weaned mice from 93G-fed dams directly onto a HFD (Figure 7A). Under this regime, KO mice did not increase in weight compared to WT. However, this group showed an increase in both absolute and relative epididymal fat mass, along with a 25% increased adiposity at age 29 weeks (Figure 7B and 7C). Increased adiposity 93G-fed KO

animals (Figure 4B) ranges from ~0-50% increased. As with weight gain, HFD diet feeding failed to exacerbate adiposity in *Rdh1*-KO mice.

In *Rdh1*-KO mice, increased weight is typically accompanied by increased adiposity, although these two components of the phenotype are not completely linked (at least by simple measures of adiposity). However, because increased length is rarely observed, we believe increased adiposity to be the primary cause of weight gain in KO animals. Though our studies, we found that increases in weight and adiposity develop often early in life and these increases are independent of HFD feeding.

Energy Balance in *Rdh1*-KO

Increased weight and adiposity occurs when animals increase energy intake or decrease energy use. Because *Rdh1*-KO mice gain both weight and adiposity, we conducted a set of experiments to determine the cause of energy imbalance. In their initial studies, Zhang and Hu carried out study of energy intake in VAD fed animals (3). Since then, we have continued to monitor food intake during the lifespan of *Rdh1*-KO mice. Pooling cumulative intake data from many groups of 93G-fed animals shows *Rdh1*-KO animals consume about 25 kcal more than WT animals by 18 weeks of age (~1.7 kcal or 0.44 g of diet more per week)(Figure 8A). Because heavier animals require more calories to maintain body weight, we subsequently normalized intake to the body mass (Figure 8B). Using this metric, the difference between WT and KO mice disappears. KO mice only consume more food because of their increased body mass. Cumulative measurements of food intake average the intake of group housed animals. We also measured food intake from individual animals using CLAMS (Comprehensive Lab Animal Monitoring System) metabolic cages. Under these conditions, KO animals at various ages ate no more (nor less) than WT during a 24-hour period (Table 5). Food intake can also be monitored continuously during CLAMS. As shown in Figure 9, neither younger nor older animals substantially differ in their food intake patterns, as both WT and KO animals consume more food during the dark half of the light/dark cycle. Although ANOVA analysis suggests an interaction between genotype and time of day in young animals (Figure 9A), comparisons with other CLAMS studies (Figure 9B and data not shown) highly suggests that the subtle difference seen in these younger mice reflect biological variability rather than a reproducible trend.

Further evidence against hyperphagia in *Rdh1*-KO animals comes from the HFD diet studies. One would expect hyperphagia to have a greater impact on animals fed a calorically dense diet. HFD feeding failed to produce a more pronounced phenotype than 93G diet, therefore corroborating our food intake observations. In all, it appears that food intake is only increased in KO animals as they gain weight, and therefore hyperphagia is not the underlying cause of increased weight in *Rdh1*-KO animals.

CLAMS studies also allowed us to measure the activity of WT and KO animals. Looking across many studies under fasting, *ad lib* fed and refed conditions, loss of *Rdh1* did not consistently decrease total movement, ambulatory movement (movements over longer distances) or rearing (vertical movement) (Table 6). Like food intake, activity can be monitored continuously throughout the light/dark cycle. Neither young nor old *Rdh1*-KO mice differ in activity pattern from that of age-matched WT (Figure 10). In all, we do not believe *Rdh1*-KO animals gain weight do to decreased physical activity.

CLAMS can also measure energy expenditure using indirect calorimetry. Sensors monitor the amount of oxygen consumed and carbon dioxide produced by the animals housed inside. Because the size of the animal makes a difference in respiration (all things being equal,

larger animals respire more than smaller ones), oxygen consumption and carbon dioxide measure are adjusted based on body weight. For our measures, we used the adjustment of mass$^{0.75}$, a commonly used adjustment that estimates lean body mass (135). Because *Rdh1*-KO animals have higher adiposity (Even 4-9 week old mice have an up to ~50% higher adiposity index, Figure 4B), this may not be the most ideal adjustment. Ideally, a DEXA scan would determine the lean body mass of animals right before CLAMS, allowing for optimal adjustments. Without access to DEXA, we used the less than ideal, but common, body weight adjustment.

Looking at a variety of different ages, under different diet regimes and during fasting, *ad lib* feeding or refeeding, oxygen consumption and carbon dioxide production do not consistently differ between KO and WT animals (Table 7). Aerobic respiration requires oxygen, thus oxygen consumption rates are an indirect proxy for metabolic rate. On the other hand, carbon dioxide is the byproduct of respiration and the ratio of carbon dioxide to oxygen varies based on whether the carbon source is carbohydrate, protein or fat. Ignoring the contribution of protein, the ratio of carbon dioxide production to oxygen consumption (respiratory exchange ratio, or RER) indicates whether fat or carbohydrates provide fuel for respiration. Accounting for protein during CLAMS analysis requires collection of urine samples and additional assays. Because the relative contribution of protein to metabolism is typically small, most metabolic cage studies ignore the contribution of protein (135). Ignoring the contribution of protein, an RER of 1.0 indicates 100% of energy comes from carbohydrate oxidation, whereas an RER of 0.7 indicates 100% fat oxidation (plus or minus any calibration errors). Given the weight and adiposity increases in *Rdh1*-KO mice, we hoped to detect either increased fat production (RER greater than 1.0) or decreased fat oxidation (higher RER). However, young or old, fasted or refed, *Rdh1*-KO animals show no consistent difference in RER from WT animals (Table 7).

Oxygen consumption indirectly indicates energy expenditure, but can also be combined with RER to generate a separate estimate called Heat. For our experiments, we used to packaged software to determine heat (see Materials and Methods for how Heat is calculated). Because Heat does not account for differences in body mass, average Heat rates are often higher in *Rdh1*-KO animals (Table 7). One expects larger animals to expend more energy, and normalizing Heat measures to body weight yields results quite similar to oxygen consumption (data not shown). Regardless, *increased* energy expenditure would not explain increased weight and adiposity.

Although CLAMS measures energy expenditure with sensitivity and accuracy, biological variability and individual mouse behavior make it very difficult to detect subtle differences. Mice are very sensitivity to their environment and CLAMS study requires many changes to a mouse's typical environment: individual housing, lack of bedding, different cage size, etc. Although data from the first hour of study was discarded to allow mice to acclimate, the environmental changes required by CLAMS introduces a degree of artifice into its measures. Furthermore, without a background in statistics, it becomes difficult to untangle the impact of one metabolic parameter on the next. For instance, mouse movement impacts its energy expenditure and food intake affects RER. Although clear outliers have been excluded form the data, more active or hungrier mice complicate analysis. Therefore, our work indicates that although there are no large or robust changes in KO mice, we cannot rule out subtle changes.

With no observable changes to activity and changes to caloric intake and energy expenditure accounted for by increased body mass, we surmised *Rdh1* must play a role in thermogenesis. To challenge the animals' ability to maintain body temperature, we housed them at 4^{o} C and monitored body temperature for 24 hours under both fasted and *ad lib* fed conditions. Initially, mice rely on shivering to maintain body temperature during cold exposure. Within a

few hours, a process called non-shivering adaptive thermogenesis takes over temperature maintenance (136). Although the initial cohort studied suggested a defect in *Rdh1*-KO cold response, repeated studies determined that nearly an equal percentage of WT and KO animals fail to defend their normal body temperature over 24 hours (Table 8). Similarly, we detected no overall trends in final body temperature, weight loss or food intake at the end of 24 hours of cold exposure (Table 8). Representative temperature data for fasted (Figure 11A) and fed (Figure 11B) mice over the entire 24 hours shows, if anything, a slight protective effect of KO during fasted cold exposure. KO animals near the end of the fasted study fare perhaps slightly better than WT. This is consistent with heavier, fatter animals having more lipid stores available for thermogenesis. Comparing body fat percentage in older animals (Figure 4A) with the percent weight lost during fasted cold exposures (Table 8), it is likely that the animals removed from study (both WT and KO) merely exhausted their energy stores. In fact, nearly all mice that failed to maintain body temperature were removed at least 16 hours into the study. Also note that animals defend their body temperatures well during the first few hours of cold study. This suggests shivering remains normal in *Rdh1*-KO animals.

Because we could not rule out compensatory activity changes or enhanced shivering responses in *Rdh1*-KO animals during cold exposure, we also tested thermogenic potential pharmacologically. In these studies, animals housed in CLAMS were injected with β_3-adrenergic agonist CL 316,243 (CL). Because β_3-receptors are located primarily on adipose tissue (137), the metabolic induction following CL treatment can be attributed primarily to stimulation of brown and white adipose. Again, animals at multiple ages and various dietary regimes were monitored (Table 9). Only once, with HFD feeding, did *Rdh1*-KO animals show decreased response to CL treatment. However, a re-test of the same group of animals showed no impairment. Representative data from young 93G-fed animals (Figure 11C) shows no discernable difference between WT and KO β_3-adrenergic response.

Despite normal response to both cold and β_3-adrenergic stimulation, we continued to suspect thermogenic impairment. We began to measure core body temperature before and after metabolic cage studies (Table 10). Though not all experiments showed differences in body temperature, in every experiment with a statistically significant difference, *Rdh1*-KO animals had either a lower body temperature or greater decrease in body temperature during a fast. To follow up on this preliminary data, we challenged mice with fasting and refeeding and monitored body temperature at either 5 or 6.4 weeks of age (Figure 12A and B.). In both experiments, body temperature of WT and KO depressed during fasting, rose above *ad lib* temperature during refeeding and returned back to *ad lib* temperature. Whether due to differences in age or handling, the exact response differed between experiments, with 2 hours post refeeding in the first experiment more similar to 1 hour post refeeding in the second. These differences highlight the variability in mouse body temperature. One way to reduce variability is to pool results from both experiments (Figure 12C). The important observation, however, is that whenever a difference between WT and KO is statistically significant, KO animals that have lower body temperatures than WT.

In order to get a clearer picture of body temperature, and perhaps reduce variability to better detect subtle differences, we took three temperature measures during the day and averaged these for a given mouse. We also followed body temperature in the same cohort of animals at different ages (Figure 13A and B). Although averaging multiple measures from a single mouse reduced some variability, week-to-week, mice vary 0.5-1.0 degrees in body temperature in both WT and KO animals. It is unclear how much variability can be attributed to true physiological

changes and how much is due to behavioral variability (food intake, activity, huddling) or handling differences (cage cleaning, noise, earthquake, experimenter error). However, looking at both cohorts individually, as well as pooled (Figure 13C), *Rdh1*-KO animals at times maintain a body temperature ~0.5 degrees lower than WT.

Based on multiple observations under various conditions, we conclude that *Rdh1*-KO eat no more than expected for their body weight and move no less. We also detect no changes to metabolic rate or metabolic substrate (carbohydrate vs. fat) preference and see energy expenditure increases consistent with increased body mass. Therefore, only the reduced body temperature explains the weight gain observed in *Rdh1*-KO animals. Though not easily observed, nor concluded from a single experiment, the sum of temperature observations strongly suggests a defect in normal body temperature maintenance in *Rdh1*-KO animals. From cold and β-adrenergic agonist work, it appears that β-adrenergic activation of thermogenesis remains intact and can overcome the thermogenic defect. Interestingly, normal housing rodent housing temperature (21º C) lies well below thermoneutrality for mice (30º C), and represents a degree of thermal stress (And therefore β_3-adrenergic stimulation?). This suggests that only high levels of β-adrenergic stimulation can overcome impaired thermogenesis. Later, we will address possible hormonal and molecular mechanisms that impact both β-adrenergic dependent and independent thermogenesis.

Metabolic Consequences of *Rdh1*-KO

Weight gain and obesity belong to a cluster of symptoms known as "metabolic syndrome" or "syndrome X." Other symptoms include insulin resistance, dyslipidemia and high blood pressure. In humans, these symptoms lead to increased risk of heart disease and diabetes. The symptoms of metabolic syndrome are highly interrelated, with dysfunction in one parameter contributing to dysfunction in others. Thus, determining other aspects or consequences of weight gain in *Rdh1*-KO animals may relate the phenotype to human health as well as provide insight as to which tissue(s) are affected by *Rdh1* loss.

In *Rbp1*-KO animals, loss of CRBP1 leads to increased pancreatic 9cRA, which in turn affects insulin and glucagon secretion and therefore glucose tolerance (71). Retinoid homeostasis can also affect glucose metabolism through RBP. The RBP-retinol complex signals through STRA6, activating a JAK-STAT pathway that induces expression of *Socs3*, an antagonist of insulin signaling (6). Given both the connections between obesity and insulin resistance as well as those between retinoid metabolism and insulin resistance, we tested whether *Rdh1*-KO animals develop insulin resistance and glucose intolerance either primarily or secondarily to increased weight and adiposity.

Older KO animals, age 24-25 weeks, fed a 93G diet, show impaired glucose and insulin metabolism when challenged by a glucose and insulin tolerance tests (GTT and ITT, respectively). During GTT, KO animals fail to efficiently clear glucose from blood, suggesting either defects in glucose uptake or an impaired insulin response (Figure 14A). GTT also revealed increased fasting glucose levels in KO animals (Figure 14A, time 0). Elevated fasting glucose is an additional indicator of impaired glucose tolerance. During ITT, KO animals appear to clear glucose as well as WT (Figure 14B from 0-15 minutes) but have elevated glucose levels during the later half of the study (Figure 14B from 60 minutes on). Such results suggest normal glucose uptake by peripheral tissues, but failure of insulin to prevent hepatic gluconeogensis (129). ITT results were reproducible in a second cohort of 24-25 week old animals (10w1b, data not shown), consistent with insulin resistance preceding glucose tolerance (138). Impaired response

to insulin can be overcome by increasing insulin levels. One cohort of 8-week old KO animals indeed showed elevated insulin (Figure 15A). As shown by pyruvate tolerance test (Figure 15B), 8-week old *ad lib* fed WT and KO animals synthesize similar amounts of glucose from a bolus of pyruvate, suggesting sufficient control of gluconeogensis in such mice.

To determine whether insulin resistance and impaired glucose tolerance developed primary to loss of *Rdh1*, we performed GTT and ITT in younger animals. In multiple cohorts of mice from ages 4 to 10 weeks, we find *Rdh1* KO mice respond normally during both GTT and ITT (Figure 15C and D (4-5 weeks); Figure 16E and F (9-10 weeks); and 3w1 (8-9 weeks, data not shown)). Furthermore, in 3.5 week old fasted animals and 5 week old refed animals insulin levels appear the same as WT (Figure 14A). In one cohort of animals, fed a VAD diet until age 5 weeks, KO mice appeared more insulin sensitive than WT at both 9 and 24 weeks (Figure 16A, B, C, and D). However, these results were not reproducible in a second set of animals fed the same diet regiment (Figure 16E and F), suggesting insulin sensitivity to be the anomalous result. Together, these results suggest changes to insulin sensitivity and glucose tolerance occur secondarily in *Rdh1*-KO mice, likely the consequence of increased weight and adiposity rather than from a direct effect of retinoid metabolism.

Dyslipidemia is associated with obesity and metabolic syndrome. In humans, treatment with 13cRA (trade name Accutane) can lead to dyslipidemia (139), suggesting a primary effect of retinoids on serum lipid levels. To determine if *Rdh1*-KO affected serum lipid metabolism, we measured serum triglyceride (TG), free fatty acid (FFA) and glycerol levels in 8-week old WT and KO animals (Table 11). During fasting, adipose tissue mobilizes fatty acids into serum. Inability to mobilize lipid from adipose could potentially lead to increased adiposity. *Rdh1*-KO mice, however, show normal FFA levels during both the fasted and *ad lib* fed state. During feeding, fatty acids from diet and *de novo* synthesis are esterified to glycerol forming triglycerides. In peripheral tissues, uptake of fatty acids from triglyceride requires localized lipolysis, which releases free glycerol into serum. *Ad lib* fed levels of both glycerol and triglyceride appear normal in KO animals, suggesting normal rates of triglyceride synthesis in intestine and liver and normal uptake by adipose and other peripheral tissues. Thus, increased triglyceride synthesis does account for increased adiposity in *Rdh1*-KO animals. During fasting, glycerol liberated by lipolysis can be converted into glucose by gluconeogensis. Fasting glycerol levels are unchanged in KO animals, once again suggesting that lipolysis and gluconeogenic rates are normal in 8 week old KO animals. In young *Rdh1*- KO mice, serum lipids appear normal and thus a primary change to lipid transport or mobilization does not contribute to increased adiposity. We have not determined whether serum lipid metabolism becomes disrupted later in life as a consequence of increased adiposity, nor have we looked at lipoprotein composition in either young or old mice.

Obesity can lead to increased levels of inflammation, due, in part, to increased macrophage infiltration of adipose tissue (140). Such inflammation contributes to the development of insulin resistance (141). Increased inflammation can also be a sign of infection, which can lead to both hyper- and hypo-thermic responses (142). Thus, as a part of a hormone/cytokine panel we measured serum levels of three inflammatory markers: TNFα, MCP-1 and IL-6 (Table 12). Healthy, young animals typically have very low levels of these markers. Thus, most animals had undetectable levels of two or more cytokines (TNFα levels in all animals were undetectable). No KO animals had detectable levels of MCP-1, whereas four WT animals had detectable levels. For IL-6, only two WT and three KO animals had detectable levels, and amongst those animals the difference between WT and KO was not statistically

significant. Thus, at a systemic level and in relatively young (age 8 weeks) animals, *Rdh1*-KO animals show similar, if not lower levels of inflammation. As with serum lipids, we might expect changes to these markers as animals age, but have not yet measured levels in older mice. Furthermore, these studies do not rule out local inflammation or changes in other inflammatory markers.

Tissue Expression Pattern of Multiple Rdh, Raldh and Crabp2

Previous study of *Rdh1* looked for expression in common retinoid target tissues, but had not explored expression in tissues like white and brown adipose tissue. To better understand retinoid signaling in these tissues, we used quantitative polymerase chain reaction (qPCR) to compare expression of *Rdh1, Dhrs9, Rdh10, Raldh1, Raldh2, Raldh3 and Crabp2* in 27 tissues or distinct parts of tissues from 4-week old fasted animals (Figure 17). We also explored whether knockout of *Rdh1*, age and/or dietary retinol affected *Rdh1, Dhrs9 or Rdh10* expression in liver, EWAT or BAT (Figure 18).

While performing these assays, we determined the commercially available primers for *Rdh1* are not completely specific. We routinely get very low signal from *Rdh1*-KO animals (Figure 18A and B), perhaps due to noise from similar genes (*Rdh7, Rdh9* and *Rdh16*). To confirm expression in the low expressing tissues, it would be prudent to compare levels between WT and KO animals. For instance, though WT animals may have detectable levels of *Rdh1* in EWAT, these levels are often comparable to those observed in KO animals (Figure 18C).

Where levels were detectable, *Rdh10* and *Dhrs9* expression dwarfed that of *Rdh1*, differing by at least one order of magnitude (Figure 17A). Except for skin and pancreas, where *Dhrs9* expression predominates, *Rdh10* is the mostly highly expressed of the three RDH. Interestingly, most tissues express all three RDH, although each RDH has a unique pattern of relative expression. The presence of multiple RDH with the same tissue suggests either unique functions and/or unique locations within the cell and/or tissue. The *Rdh1*-KO phenotype suggests that even though other, more highly expressed RDHs are present, they cannot fully compensate for *Rdh1* loss.

This new *Rdh1* expression pattern is fairly consistent with previous reports (2), though here we were not able to detect *Rdh1* in pancreas or skeletal muscle. Of note, BAT shows the fourth highest expression level of *Rdh1*. By comparison, skeletal muscle has expression levels below the limit of detection. The expression pattern predicts that loss of *Rdh1* has greater effect on brown adipose tissue than skeletal muscle, and is consistent with changes to non-shivering thermogenesis rather than movement or shivering. Expression of *Rdh1* throughout the brain was low or undetectable. In this study, hypothalamus, an important central regulator of metabolism shows low levels of *Rdh1* expression. However, hypothalamic temperature regulation occurs largely via β-adrenergic stimulation of brown and white adipose (136, 143). Physiological studies with the *Rdh1*-KO mice show this pathway remains intact. Hypothalamus also regulates food intake, which also appears normal in KO animals. Thus, we do not believe temperature changes in the *Rdh1*-KO animals derive from hypothalamic dysfunction. High expression of *Rdh1* in skin suggests a functional role we have not yet explored.

Preliminary data (H. Tran and J. Napoli, unpublished) suggested decline of *Rdh1* expression with age and diet. We also predicted that loss of *Rdh1* would lead to upregulation of other RDH. Looking in three key metabolic tissues under *ad lib* fed conditions, *Rdh1* expression levels are maintained between ages 10 and 20 weeks (Figure 18). Feeding a high retinol diet for 5 weeks also fails in to change BAT *Rdh1* expression. On the other hand, age decreases *Rdh10* and *Dhrs9* expression in brown adipose, suggesting changes to retinoid signaling in BAT with age. High retinol in the diet has a similar effect on Dhrs9 and *Rdh10* expression in BAT. Liver *Rdh10* levels are affected by age, and no effect of age is seen on EWAT RDH expression. Interestingly, *Rdh1*-KO if anything decreases *Dhrs9* and *Rdh10* expression.

Much like RDH expression, RALDH expression varies from tissue to tissue and all tissues assayed appear to express multiple, if not all three RALDH (Figure 17B). *Raldh1* expression predominates in all tissues except for pituitary and thyroid glands, with median levels ~10 fold greater than *Raldh2* and ~25 fold greater than *Raldh3*. Liver shows the highest *Raldh1* expression levels, and expression levels vary by two orders of magnitude. *Raldh2* expression predominates in the pituitary gland, though highest overall expression appears in testes. Expression of *Raldh2* ranges four orders of magnitude, with lowest expression in intestinal mucosal cells. Thyroid gland represents the highest levels of *Raldh3* expression, with levels spanning three orders of magnitude down to intestinal mucosal cells. With continued interest in the role of RALDH in retinoid synthesis, detailed knowledge of relative expression greatly informs future work.

Expression of retinoic acid binding protein *Crabp2* covers at least three orders of magnitude, with highest expression in skin and olfactory bulb, and undetectable levels in skeletal muscle, pancreas and smooth muscle of the intestine (Figure 17C). Because the ratio between CRABP2 and FABP5 determines the amount of signaling through RARs or PPARδ, it would be interesting and informative for future work to compare expression patterns.

While looking at RDH, RALDH and *Crabp2* tissue distribution, we originally included inguinal white adipose tissue, but discarded expression results when it appeared IWAT samples had been contaminated by skin (data not shown). To address this concern, we did a preliminary study of RDH and RALDH expression in multiple fat depots from the same animal with liver as a reference (Figure 19). Interestingly, different white adipose depots appear to express different levels of RDH and RALDH. More interestingly, RDH appear more highly expressed in brown adipose and WAT with higher *Ucp1* expression (Figures 19A and C). On the other hand, RALDH appear more highly expressed in white adipose, with expression generally decreasing with *Ucp1* expression (Figures 19B and C). *Ucp1* expression in white adipose derives from pockets of brown (or at least *Ucp1* expressing brown-like) adipocytes within white adipose (143). With more thorough study, and by looking at protein expression, these trends may provide interesting insight into how retinoic acid synthesis differs between white and brown adipose.

Lipid Flux in *Rdh1*-KO Mice using Stable Isotope Labeling

Using isotopic tracers, the relative synthesis rates of various *in vivo* compounds can be measured. Applying one such technique, we used deuterium oxide (heavy water) to measure rates of fatty acid synthesis and triglyceride turnover. Newly synthesized fatty acids, as well as glycerol freed by lipolysis, incorporate deuterium atoms in place of hydrogen, allowing for detection of labeled molecules by differences in mass (130, 131).

In the first such experiment, mice age 9 weeks were labeled for 4 days of *ad lib* feeding and IWAT was collected via biopsy (Figure 20A). During this study, newly synthesized

palmitate accounted for only 10% of the KO animal palmitate pool, whereas WT animals accumulated 25%. The simplest interpretation of the data is that KO animals have lower rates of *de novo* lipogenesis. Alternately, KO animals may have more fat overall, and thus newly synthesized fatty acids comprise a smaller fraction of the overall pool. Two additional time points were collected in this experiment, though results from these timepoints were atypical, suggesting error in biopsy collection or experimental conditions.

To better understand the size of lipid pool, we repeated our study in a second group of mice. In this experiment, we studied both inguinal and epididymal white adipose depots. In this cohort of animals, no statistically significant differences occurred in *de novo* palmitate synthesis, although IWAT accumulation in KO trends toward a decrease (Figure 20B). Using flame ionization detection (FID), the total amounts of several fatty acids, including palmitate, were measured, allowing for measures of absolute palmitate synthesis (Figure 20C). Again, differences in IWAT trended toward statistical significance. Comparable changes to both fractional and absolute differences suggest differences arise due to difference in lipogenic rates rather than pool size. Finally, we looked at triglyceride turnover by measuring the fraction of labeled glycerol, and found no difference between WT and KO animals in either white adipose depot (Figure 20D). Previous reports have noted differences in newly synthesized palmitate rates between different fat depots, but importantly, dietary or genetic intervention tend to affect all fat depots similarly (133, 144).

Lipids in brown adipose turn over much more rapidly than those in white adipose tissues. Thus, to assess lipid flux in brown adipose, we labeled 6-8 week old mice during a 5-6 hour refeeding period. Similar to the second study, the fraction of newly synthesized palmitate and triglyceride turnover were unchanged between WT and KO in EWAT (Figure 21A and C). In BAT, however, KO animals accumulated only 75-80% of WT fractional or absolute new palmitate levels (Figure 21A and B), though TG turnover rate in brown adipose tissue was unchanged (Figure 21C). Despite reduced levels of newly synthesized palmitate, overall levels of palmitate as well as other common fatty acids are comparable between WT and KO (Figure 21D). Increased dietary palmitate must account for difference. Newly synthesized fatty acids found in brown adipose likely originate either from local synthesis or from synthesis in liver via circulation. In liver, KO and WT animals had similar fractions of new palmitate (Figure 21A). Because KO and WT animals maintain similar levels of circulating fatty acid and triglyceride levels, the newly synthesized lipid from liver is available to BAT. Thus, brown adipose must either be synthesizing less fatty acid *in situ* or taking up fewer fatty acids from circulating LDL particles. Either of these options supports a change in brown adipose physiology, though additional work is needed to determine which of these hypotheses is correct.

Using FID data from study 3, we were able to measure relative levels of several fatty acids in EWAT, BAT and liver (Figure 22A-C). In both liver and BAT, KO animals had a lower percentage of stearate (Figure 22A and B), suggesting defects in elongation of palmitate to stearate. In brown adipose, we observe increases in palmitate and palmitoleate consistent with decreased elongation (Figure 22A). *Ad lib* fed animals from study 2 showed decreased percentages of stearate in all KO adipose depots (Figure 22D). Liver, however, shows comparable stearate percentages. Study length cannot account for differences between liver results in the two studies, because fatty acid composition reflects total fatty acid, not just newly synthesized fatty acid. Liver differences most likely reflect the different collection conditions (*ad lib* fed vs. 5-6 hr. refed after a fast). Importantly, both studies indicate a similar defect in stearate synthesis. Elongase *Elovl6* recognizes fatty acids sixteen carbons or shorter, and therefore

converts palmitate synthesized by fatty acid synthase into stearate (145). In brown adipose, gene expression levels of *Elovl6* are comparable between WT and KO animals during both fasting and refeeding (Figure 22 E). However in liver, KO levels of *Elovl6* are about 60% of WT during refeeding (Figure 22E). Decreased liver elongation therefore accounts for differences in stearate throughout the animal. In study 3, an increased percentage of linoleate is present in EWAT (Figure 22C). As an essential fatty acid, increased linoleate suggests that more fatty acid in EWAT derives from diet rather than *de novo* synthesis.

Rdh1-KO mice accumulate more fat. The results of our stable isotope studies suggest this accumulation comes not from increased *de novo* lipogenesis, but from increased storage of dietary lipids. In some cases *de novo* lipogenic rates decrease in KO animals. In KO BAT, decreased newly-synthesized palmitate levels indicate dysfunction in either local synthesis or uptake. Interestingly, changes to *Elovl6* in liver leads to changes in the relative percent of stearate. We have yet to determine how these changes to BAT lipid dynamics and overall changes in fatty acid composition connect to weight gain in *Rdh1*-KO animals.

Hormones and Adipokines in *Rdh1*-KO Mice

Rdh1 expression spans tissues with endocrine function such as testis, thyroid, pituitary, adrenal glands and ovary (Figure 17A and (2)). In addition, RDH1 recognizes 3-adiol and DHT as substrates *in vitro* (2), suggesting a possible role in androgen metabolism. Furthermore, adipose tissue has also been identified as an endocrine organ, sending factors dubbed "adipokines" into circulation that signal metabolic information between tissues. With the broad tissue distribution of *Rdh1* and metabolic phenotype observed in the *Rdh1*-KO mouse, we measured a variety of endocrine factors to better define the role of *Rdh1 in vivo*.

Much like atRA, testosterone and DHT bind a nuclear hormone receptor, the androgen receptor (146). Like RAR, androgen receptor regulates gene transcription through heterodimerization with RXR and DNA binding. The more active androgen, androgen target tissues generate DHT from circulating testosterone. As fans of major league baseball know, androgens help regulate muscle mass and body composition. Based on *in vitro* studies, RDH1 can either generate DHT from 3-adiol or metabolize DHT to androstanedione (2). To determine if *Rdh1* plays an *in vivo* role in androgen metabolism, we measured circulating levels of testosterone and DHT in male animals under various dietary regimes (Table 13). Fed a chow, 93G or VAD diet, *Rdh1*-KO animals showed no statistically significant differences in either circulating DHT or testosterone. Furthermore, if *Rdh1* were affecting body composition through androgen pathways, we would not expect dietary retinoid to have an impact on phenotype. Because circulating androgens do not change and chow-fed *Rdh1*-KO animals do not increase in weight and adiposity, we do not believe *Rdh1* plays a major role in global androgen metabolism.

Initial observations suggested *Rdh1*-KO mice were longer and therefore larger in size (3). We therefore wondered if *Rdh1*-KO affected pituitary function. The pituitary gland regulates a myriad of endocrine pathways and secretes, amongst other hormones, thyroid stimulating hormone (TSH) and growth hormone. Growth hormone, amongst other functions, impacts body size and insulin sensitivity (147, 148). To determine if loss of *Rdh1* affected growth hormone levels, we measured circulating levels in *ad lib* fed animals 8 weeks of age (Table 13). Rather than higher predicted by increased length, growth hormone levels trended toward decreased in *Rdh1*-KO mice. Animals lacking growth hormone receptor (and therefore with decreased growth hormone signaling) do become overweight, but are also smaller in overall size (148). Thus, the *Rdh1*-KO phenotype cannot be attributed to changes in growth hormone levels.

Thyroid hormone also plays an important role in regulation of energy expenditure, body temperature and therefore weight and body composition (149). Hypothalamus detects circulating levels of thyroxine (T4), and responds by adjusting secretion of thyroid releasing hormone (TRH). TRH acts on the pituitary gland, signaling release of TSH. TSH, in turn, stimulates secretion of T4 by the thyroid gland. Target tissues take up T4, where it is converted into triiodothyronine (T3) by the action of deiodinases DIO1 and DIO2. T3 binds to the thyroid hormone receptor, which heterodimerizes with RXR, signaling a variety of gene changes. Hypothyroidism, or low T4/T3 levels, is associated with decreased temperature, energy expenditure and weight gain (136, 149).

To understand the role thyroid hormone plays in the *Rdh1*-KO phenotype, we measured circulating levels of total T4 and T3 in 6-week old male WT and KO mice under both fasting and refed conditions. When fasted, both WT and KO animals maintain similar T3 and T4 levels. However, during refeeding T4 and T3 are decreased by 12% and 16%, respectively, in KO animals (Table 13). Low T4 levels arise due to either low TSH signal from pituitary or from impaired T4 production/secretion by thyroid hormone. Defects in T4 production/secretion are often accompanied by increased TSH levels, because hypothalamus and pituitary attempt to compensate for thyroid dysfunction. Thus, we next measured TSH levels in refed *Rdh1*-KO and WT animals at two different ages (Table 13). We chose age 5.5 weeks, of age with mice in T3 and T4 studies, and age 18 weeks, older animals to allow for possible TSH compensation. At both ages, KO animals showed no significant difference from WT. Without lower TSH levels, we can infer that T4 and subsequent T3 changes are due to a primary effect of *Rdh1* loss on thyroid. However, because TSH is not increased in KO, we can reason that the changes to T4 and T3 are only mild. Measurement of thyroid gene changes, especially those of genes involved in thyroid hormone synthesis, would provide further evidence of a tissue autonomous role for *Rdh1* in thyroid.

Since the discovery of leptin, a growing number of adipose secreted hormones have been discovered (150). These adipokines serve as endocrine/paracrine signals and help to coordinate energy metabolism. Mice missing leptin (*ob/ob*) or leptin receptor (*db/db*) gain weight through a multiple mechanisms including hyperphagia, reduced body temperature and decreased energy expenditure (151-154). In normal animals, leptin levels increase with increased adiposity and act as a satiety signal to the hypothalamus (150). Although *Rdh1*-KO mice are not hyperphagic (Figure 8 and Table 5), we asked whether changes to leptin levels contributed to the *Rdh1*-KO phenotype. In 8-week old ad lib fed animals, leptin levels are increased nearly 2-fold in KO mice. Clearly, leptin deficiency does not contribute to the *Rdh1*-KO phenotype. Van Heek and colleagues correlated leptin and body weight in mice with diet induced obesity, finding that circulating leptin increases 1100 pg/mL in circulation for every gram of body weight (155). In the leptin study, KO mice weighed 2.1 g more than WT. This weight difference predicts an increase of 2300 pg/mL from WT to 4000 pg/mL, a level higher than measured KO levels. Thus, elevated leptin levels are most likely a symptom of increased weight rather than a primary defect in *Rdh1*-KO animals.

Adipose tissue also secretes the protein resistin. Resistin levels increase with adiposity and contribute to insulin resistance (156, 157). Furthermore, WAT resistin expression increases with increased dietary vitamin A and pharmacological doses of atRA (50). To determine whether resistin levels contribute to the *Rdh1*-KO phenotype, we measured serum resistin levels in 8 week old *ad lib* fed male mice (Table 13). Although KO animals studied were 2.1 g heavier, we

found so significant difference between WT and KO resistin levels. At least in young animals, changes in serum resistin do not contribute to insulin resistance in *Rdh1*-KO mice.

Secreted by both liver and adipose tissue, RBP links retinoid metabolism to insulin resistance and allows for retinoic acid-independent effects on metabolism (6, 92). In *ad lib* fed, fasted or refed animals we found no change to *Rbp4* expression in EWAT of *Rdh1*-KO mice (Figure 23). In liver, we observed no differences between WT and KO animals, but found that hepatic *Rbp4* expression in both genotypes declines 60-70% upon refeeding (Figure 24). Because fasting animals must rely on stored vitamin A, we might expect increased retinol mobilization during a fast and suppression in refeeding. In addition, increased RBP may be an important suppressor of insulin signaling during a fast. Future work will need to determine if hepatic secretion or circulating levels of RBP correlate with changes to hepatic expression.

In brown adipose tissue, *Rbp4* expression is 2.5-4 fold increased in KO animals *ad lib* fed (Figure 25A), fasted or refed (Figure 25B). As in the liver, BAT expression of *Rbp4* decreases ~50% with refeeding. To assess whether elevated RBP levels were having a local (autocrine/paracrine) effect in KO mice, we measured expression levels of *Pparg* and *Socs3* during both fasting and refeeding (Figure 25B). Despite increased *Rbp4* expression, *Socs3* and *Pparg* expression levels were unchanged in KO animals. To confirm these results, we measured gene expression again in a comparable cohort of animals (Figure 25C). Signal transduction pathways exponentially amplify signals, therefore we expect readily detectable expression changes if RBP signaled locally in BAT.

To provide additional insight, we measured *Stra6* expression in brown adipose during both fasting and refeeding. Interestingly, *Stra6* levels in both WT and KO animals are nigh undetectable in fasted animals (not clearly shown with the scale used) and rise with refeeding (Figure 25B). No difference was detected between WT and KO expression. In BAT, RBP and STRA6 appear oppositely regulated with fasting and refeeding. This opposite regulation may prevent autocrine/paracrine signaling of RBP-retinol in brown adipose. Such a role may explain why *Rdh1*-KO animals do not have the expected increases in *Pparg* and *Socs3* expression. In BAT, the role of RBP and the amount contributed to circulation have yet to be determined.

Retinoid Measurements

Initial studies of *Rdh1*-KO mice focused on traditional targets of retinoid function, such as liver, testes and kidney. Theses tissues, in *ad lib* fed animals, showed no difference in atRA levels under any dietary regime (3). As dietary retinol was lowered, liver and later kidney showed increased retinyl ester and retinol, suggesting a sparing of retinol in the absence of *Rdh1*.

To explore the impact of *Rdh1*-KO on additional tissues, we subsequently began to included EWAT/PMWAT (perimetrial WAT), IWAT, BAT, pancreas, skeletal muscle, hippocampus and hypothalamus in our retinoid studies. Furthermore, we often included retinal and pancreatic 9cRA to the array of retinoids measured. Fearing the diet, age, retinoid or tissue selection incorrect in any given study, we subsequently measured retinoids in ten cohorts of WT and *Rdh1*-KO mice at a variety of ages and fed either a dietary regime including VAD diet (Tables 14-17) or 93G diet (Tables 18-23). Throughout all of these studies, few, if any, consistent changes in retinoids appear. Comparing the three most similar groups studied (Tables 18-20; 8-9 week old, male, 93G-fed animals), no statistically significant changes observed in one group of animals was reproducible in a second. Thus, we conclude that under *ad lib* fed conditions retinoid levels in liver, EWAT/PMWAT, BAT, pancreas and most likely serum, skeletal muscle, IWAT, intestinal mucosal cells, hippocampus, whole brain and hypothalamus

remain unchanged. With little to no *Rdh1* expression in tissues such as EWAT, pancreas and hypothalamus, these results are not unexpected. However, *Rdh1* shows relatively high expression in liver and brown adipose tissue, yet we observed no consistent changes to retinoids in these tissues.

Surprisingly, we no longer observe the 2-fold increased retinol in KO livers. One possible explanation may be maternal diet. Other studies in the lab indicate it takes at least two if not three generations of 93G diet feeding before tissue retinoid levels reflect those in the diet (Obrochta and Napoli, unpublished). All mice reported here come from at least two (and often more) generations of 93G diet feeding. The retinoid studies of Zhang, Hu and Kane took place before we knew the full impact of maternal diet on tissue retinoids. Thus, their work may reflect an interaction between genotype and acclimation to the diet rather than genotype *per se*.

Increased (presumably) *ad lib* fed retinal levels have been reported in the WAT of *Raldh1*-KO animals, leading some to link increased retinal to resistance to obesity (104). Here, we observe no change to retinal in EWAT, IWAT or BAT of *ad lib* fed *Rdh1*-KO animals. Pancreatic 9cRA levels change with fasting and refeeding (4) and knockout of *Rbp1* elevates 9cRA levels, affecting the insulin to glucagon ratio in *Rbp1*-KO mice (71). Though they develop elevated insulin levels, insulin resistance and glucose intolerance, *Rdh1*-KO animals show no changes to pancreatic 9cRA levels under *ad lib* fed conditions. Thus, changes to glucose metabolism in KO animals cannot be attributed to changes in 9cRA.

We also looked at the impact of HFD on retinoids in *Rdh1*-KO and WT mice, age 29 weeks (Figures 26 and 27). In this study, KO lowered atRA in both EWAT and IWAT, regardless of 93G or HFD. Compared to the studies above, however, this result does not appear reproducible. Also in this study, *Rdh1*-KO lowers hepatic retinal levels, though in other studies (Table 19), retinal levels were elevated in KO liver. Compared to loss of *Rdh1*, HFD feeding had a more widespread effect on tissue retinoids. HFD feeding increased hepatic atRA levels, likely at the expense of RE. In IWAT, HFD reduced atRA and retinal levels. Retinal and retinyl esters lowered in pancreas. In BAT, only retinal levels decreased with HFD feeding. In retrospect, normalizing tissue retinoids to tissue weight may not be appropriate when comparing normal to HFD diet. In this cohort of animals, HFD feeding increased the overall size of liver, IWAT and BAT (data not shown) due to increased lipid storage. Because of increased lipid storage, the same mass of tissue from HFD fed mice likely contains fewer cells than that of 93G fed mice. Thus, retinoid differences between HFD and 93G fed mice may reflect changes in tissue composition rather than changes to cellular retinoid levels. In future HFD studies, tissue retinoids should be normalized to either tissue protein or DNA content to rule out effects of tissue composition.

Given the metabolic phenotype of the *Rdh1*-KO mouse, and the knowledge that fasting and feeding alters 9cRA levels in pancreas, we wondered whether fasting and refeeding impacts atRA levels in other metabolic tissues. In our initial inquiry, wild-type animals were either fasted 16 hours, refed 2 hours or *ad lib* fed (Figure 28). Surprisingly, atRA levels in BAT uniquely increased 1.3 fold during refeeding, compared to fasted or *ad lib* fed animals. Given this unique and unexpected result, we repeated the study in a second group of animals. This time, mice were either fasted 16 hours or refed for 4 hours (Figure 29). Once again, atRA levels were increased in the BAT of refed animals, here about ~1.5 fold. This time, RE in BAT trended toward a significant increase, with levels ~1.8 fold higher than fasted animals. Unlike the previous study, atRA also increased in EWAT ~1.5 fold.

Mice defend a lower body temperature during fasting and return to normal upon refeeding (Table 10, Figure 12 and (158)). In this context, refeeding can be seen as an activator of thermogenesis, perhaps similar to cold exposure. Thus, we asked whether cold exposure also upregulates atRA synthesis in BAT. Fasted wild-type animals, age 8-12 weeks, were housed at either 4º C or maintained at normal housing temperature (21º C) for the last 6 hours of a 16 hour fast (Figure 30). In BAT, serum and EWAT, retinoid levels were unchanged by cold exposure. In liver, atRA levels decreased ~30%, but RE and retinol levels did not change. Because cold exposure failed to induce BAT atRA levels, atRA increases cannot be a general activation signal or response in BAT. This also means that β-adrenergic stimulation, increased during cold exposure, does not modulate atRA in BAT. Instead, induction of atRA may be part of the shift from fatty acid metabolism to carbohydrate metabolism. This hypothesis implies that fasted, cold exposed animals do not require increased atRA signaling, because fasted animals already depend on fatty acids for energy.

Rdh1-KO mice fail to maintain a normal body temperature, a phenotype consistent with changes to atRA in brown adipose. However, under *ad lib* conditions, no consistent change arose. We therefore asked if atRA in BAT of *Rdh1*-KO mice in responds to refeeding. In the first study with KO animals, we measured retinoids in BAT, EWAT, IWAT and liver in male animals fasted or refed for 4 hours (Figure 31). As expected, atRA levels in WT BAT increased by ~1.5 fold. However, KO animals fail to induce atRA in BAT. In liver, IWAT and EWAT, WT and KO animals respond similarly to refeeding with atRA levels decreasing during refeeding in EWAT of both genotypes. In previous refeeding experiments, WT EWAT atRA either did not change (Figure 28A) or increased (Figure 29A), suggesting handling differences, biological variability or a confounding variable. Contrary to other work in the lab (4, 71), refeeding increased pancreatic atRA but did not change 9cRA in WT animals. However, previous studies used either *ad lib* fed conditions or time points within two hours of glucose injection rather than refeeding, which may explain these differences. In addition, KO animals show increased 9cRA during refeeding, though we see no changes to 9cRA in *ad lib* fed animals. Pancreatic retinol increased in these KO animals, and in comparably aged *ad lib* fed animals, increased pancreatic retinol occurred in one of two experiments (Table 19, but not Table 20). Young *Rdh1*-KO animals maintain glucose tolerance, leading us to conclude that results with 9cRA are atypical. However, changes in pancreatic retinol may reflect a larger trend and be worth additional follow-up.

To confirm and extend results seen in refed KO animals, we next measured fasted, 1.5 hour and 5 hour refed retinoid levels in liver, serum and BAT from WT and KO females, age 10-12 weeks (Figure 32). In this study, WT atRA in BAT did not significantly increase, however, KO atRA levels decline with refeeding and differ from WT at 5 hours refed (Figure 32A). Whether this reflects a sex difference in WT animals or biological or instrumental variability is as of yet unknown. Regardless, *Rdh1*-KO animals once again fail to maintain atRA levels during refeeding. In liver, a refeeding time course reveals trends not previously observed. Here, KO animals showed atRA elevated ~20% from WT (differing from previous observations), but more interestingly, both WT and KO animals showed a steady decrease in atRA with refeeding. Retinol levels showed the same trend, as did WT RE. In the serum, WT animals showed transient increases in atRA, retinol and RE at 1.5 hours refeeding, whereas KO animals appeared delayed in this response. Liver and serum data present two interesting insights. First, liver reduces atRA levels during refeeding and exports retinol and RE to serum. The serum then transports retinol and RE to the periphery. If we suppose livers of ~1 g and ~1 mL of blood

(given the sex, age and body weight of mice studied, these are reasonable assumptions), the increased serum retinol and RE can be completely attributed to reduction in liver retinoids. Because *Rbp4* expression decreases with refeeding, perhaps LDL distributes hepatic retinoids during refeeding (an idea proposed by Folias, Kane and Napoli, unpublished). In BAT, increased uptake of serum retinol/RE during refeeding may drive increased atRA synthesis. Second, KO animals may have defects in this response, failing to mobilize retinol and RE properly through serum. This may contribute to decreased refed atRA in BAT. In previous studies, WT liver retinol trended toward a decrease at 4 hours refeeding (Figure 31B) or showed no significant change at 2 hours refeeding (Figure 28B). RE esters were previously unchanged at 4 hours refeeding (Figure 31C) or increased at 2 hours refeeding (Figure 28C). Further work, once again using a refeeding time course, will be needed to confirm or refute results in liver. However, this study suggests that changes to retinoid in response to refeeding may be more general than just BAT.

In a group of 45 week old male WT and KO animals, refeeding failed to change BAT retinoids in response to refeeding or *Rdh1*-KO (Figure 33). Because these mice were fed a VAD diet until age 5 weeks, it is unclear whether differences between this study and others reflect changes to RDH expression with age (Figure 18A) or impact of early VAD diet feeding.

Comparable to mouse refed data, atRA levels increased ~1.3-fold above fasted levels in rats given an oral gavage of glucose, though this change only trended toward statistical significance (Figure 34A). Retinol and RE levels were unchanged (Figure 34B and C). For such a rapid change to occur, post-translational modifications to enzymes or binding proteins must change in response to feeding. This data also suggests that regulation of atRA in BAT is common between rat and mouse.

Gene Expression in the *Rdh1*-KO Mouse

Uncoupling protein 1, a protein expressed exclusively in brown adipose tissue, uses the mitochondrial proton gradient to generate heat rather than ATP (136, 143). β-adrenergic stimulation induces *Ucp1* indirectly by inducing expression of the co-activator *Ppargc1* (PGC1α) and deiodinase 2 (*Dio2*/DIO2). DIO2 converts T4 to T3, generating ligand for thyroid hormone receptor, whereas PGC1α recruits transcriptional machinery to ligand bound nuclear hormone receptors. The *Ucp1* promoter contains PPAR, retinoic acid and thyroid hormone response elements. Through both retinoic acid and PPAR response elements, atRA can regulate *Ucp1* expression (32). β-adrenergic stimulation also induces UCP1 activity via induction of hormone sensitive lipase activity and increased free-fatty acid levels. Nucleotide binding, especially that of GTP/GDP, inhibits UCP1 activity. Like β-adrenergic stimulation, the activation of G-protein coupled receptor TGR5 (*Gpbar1*) by bile acids also induces *Ucp1* expression through induction of *Dio2* and *Ppargc1* (5).

Given the reduced body temperature, reduced thyroid hormone levels and changes to BAT atRA levels in *Rdh1*-KO mice, *Ucp1* and its regulatory pathways represented a promising molecular link between loss of *Rdh1* and weight gain in the *Rdh1*-KO mouse. In 10 week old, *ad lib* fed mice, we initially saw decreased *Gpbar1*, *Ppargc1* and *Dio2* expression, however *Ucp1* expression levels remained unchanged (Figure 35A). This suggested a possible decline in TGR5 signaling, although without changes to *Ucp1* this decline may not be enough to affect UCP1-dependent thermogenesis. We next tried to confirm these results in 28 week old *ad lib fed* animals. In this study, we once again found a decline in *Gpbar1* expression, but no changes to *Ppargc1* and *Dio2* (Figure 35B). In addition, the thyroid hormone-responsive gene *Thrsp*

(thyroid hormone responsive SPOT14 homolog) showed reduced expression that trended toward statistical significance.

Because loss of *Rdh1* had the most striking effect on BAT atRA during fasting and refeeding (rather than *ad lib* fed), we went on to measure *Ucp1* and its regulators in both fasted and refed mice, ages 6 and 7.5 weeks. In fasted animals, *Ucp1* levels in *Rdh1*-KO BAT increase 1.6-fold compared to WT, although after 6-7 hours of refeeding *Ucp1* expression returns to WT levels (Figure 36A). KO *Ucp2* and *Ucp3* levels were unchanged in both fasting and refeeding. In addition, KOs show normal levels of *Ucp1* expression in *ad lib* fed EWAT (Figure 37A). Thus, reduced body temperature in *Rdh1*-KO mice cannot be explained by reduced *Ucp1* expression nor reduced expression of *Ucp1* homologs. Increased fasting *Ucp1* expression likely compensates for reduced body temperature in *Rdh1*-KO mice.

Regulation of UCP1 also includes non-transcriptional changes to activity. Thus, we once again looked at expression of *Gpbar1* along with *Adrb2* (β_2-adrengic receptor) and *Adrb3* (β_3-adrengic receptor), G-protein coupled receptors (GPCRs) that impact both *Ucp1* expression and UCP1 activity (Figure 36B). Similar to *ad lib* experiments, levels of *Gbpar1* are reduced in KO animals under fasting conditions. Levels of the two β-adrenergic receptors, however, were unchanged between WT and KO in both fasting and refeeding. To see if reduced *Gpbar1* expression impacted downstream targets, we once again looked at *Ppargc1* and *Dio2* expression levels (Figure 36C). Here, as with the 28 week old *ad lib* fed mice, we see no impact of *Rdh1* loss on expression. We repeated *Gbpar1* and *Ppargc1* expression studies in a second set of fasted and refed animals, and found no impact on either gene's expression (Figure 36F). Intact β-adrenergic signaling is consistent with normal response to both cold and β_3-adrengic stimulation. *Gbpar1* levels often appear reduced in *Rdh1*-KO mice, though a ~50% reduced expression only inconsistently affects downstream targets *Dio2* and *Ppargc1* and fails to decrease *Ucp1* expression.

We next asked whether *Rdh1* loss impacted local thyroid hormone levels during both fasting and refeeding. Because *Rdh1*-KO mice have reduced T3 and T4 levels during refeeding (Table 13), we measured expression of thyroid hormone gene target *Thrsp*, thyroid hormone and atRA target *Pck1* (PEPCK**)** and atRA target and thyroid hormone transporter *Slc16a2* (Monocarboxylate transporter 8, MCT8) (Figure 36D). Of the three, only fasted levels of *Thrsp* appear reduced by loss of *Rdh1,* similar to *ad lib* fed results (Figure 35B). A second set of animals confirms unchanged *Slc16a2* expression, and showed increased *Thrsp* expression in fasted KO animals (Figure 36F). Overall, loss of Rdh1 does not appear to impact thyroid hormone signaling in brown adipose tissue.

The three PPAR nuclear hormone receptors (α, γ, and β/δ) together regulate adipogenesis, fatty acid synthesis, fatty acid oxidation and myriad of other cellular functions (159). Aside from metabolic regulation, the PPARs have been connected to atRA metabolism. For instance, atRA can bind to and affect gene expression through PPARδ (160), PPARγ regulates *Rbp7* expression (78), PPARα induces RRD (74), atRA reduces *Pparg* (45), and loss of *Rbp7* induces *Ppara* and PPARα target genes (78). Thus, we determined if loss of *Rdh1* and *Rdh1*-dependent atRA impacts the expression of any PPAR in BAT. In both fasted and refed animals, we observe no effect of genotype on *Pparg* (Figure 25B), *Ppara* or *Ppard* expression (Figure 36E).

Early in our work with *Rdh1*-KO mice, we took an unbiased look at global gene expression of EWAT, testis and liver from 10 week old, fasted WT and KO mice. In EWAT, we observed statistically significant changes to 2957 genes (Table 24 and 25 show select gene changes). Considering the low or absent expression of *Rdh1* in EWAT (Figures 17, 18 and 19),

this result is surprising. One explanation for the abundance of gene changes maybe be technical. To minimize variability, we pooled RNA from WT and KO animals and analyzed technical rather than biological triplicates. Furthermore, it may be that many of these changes occur secondarily weight gain, rather than from *Rdh1* loss directly.

Broadly, EWAT microarray revealed changes to retinoid metabolism, adipokines and cellular or metabolic regulation (Table 24) as well as intermediary metabolism, transporters or carriers and immune response (Table 25). Despite so many promising targets, our follow-up on the EWAT microarray has been relatively limited and marred by negative results. For instance, microarray revealed a 40% decline in expression of *Retn* (Resistin), yet serum resistin levels are unchanged in *Rdh1*-KO mice (Table 13). Similarly, serum neuropeptide Y (NPY) levels are unchanged in KO mice, despite a 7.6-fold increase in *Npy* expression in microarray (Figure 37C). Lipocalin 2 (*Lcn2*), 23-fold induced in the microarray study, appeared unchanged in EWAT from 10 week old *ad lib* fed animals (Figure 37A). We also detect no change to *Rbp1* or *Aldh1a1* expression in PMWAT during either fasting or refeeding (Figure 42), though microarray suggested 1.5 and 2 fold inductions, respectively. In our follow up of EWAT microarray, only increased *Gbp1* expression, up 6.4 fold in microarray and 40-60 fold during fasting or refeeding by qPCR, has been confirmed (for additional *Gbp1* discussion, see below). Though β-defensins are markedly induced in EWAT microarray, recall that inflammatory markers TNFα, IL-6 and MCP-1 are normal in *Rdh1*-KO mice (Table 12).

In microarray of testis, we observed 1308 gene changes (Table 26 shows select changes), once again by technical replicates of RNA pools. We have not done qPCR follow up of testis data, though interesting gene changes to transcriptions factors (*Tieg1*, *Hoxc12*), genes that arise in other microarrays (*Pla2g12a, Cap1, Npy*) and a *Rdh1* paralog (CRAD-L) are amongst the 1308 gene changes. Testes present an interesting tissue in which to study retinoic acid synthesis, because the blood-testes barrier requires all RA to be synthesized *in situ* (161).

In liver microarray, we found 535 significant gene changes (Table 27 shows select changes). Again, follow-up on liver results has been minimal. However, changes liver are more likely than changes in EWAT to be primary to *Rdh1* loss, considering the relatively high level of *Rdh1* expression in liver (Figure 17) and possible impact of *Rdh1*-KO on hepatic retinol and retinyl ester dynamics (Figure 32). Amongst the changes in liver, one finds transcription factors (*Foxq1*), immune responses (*Gbp1* and *Gbp4*), metabolic genes (*Gck* and *Ppargc1b*), genes found in other microarrays (*Gbp1* and *Cap1*), retinoid metabolism genes (*Cyp2c39*) and *Rdh1* paralogs (*Rdh9*). Decreased *Rdh9* expression was previously observed in *Rdh1*-KO animals (Zhang, Hu and Napoli, unpublished) (3), a promising sign for assessing the microarray's data quality.

Without consistent changes to liver atRA, it is unclear how much direct impact loss of *Rdh1* has on liver function. With its important role in gluconeogenesis and regulation by thyroid hormone and atRA, we looked at hepatic *Pck1* expression under *ad lib* fed (Figure 38A), fasted and refed conditions (Figure 38B). In *ad lib* fed animals, *Pck1* expression in KO appears reduced 50%. However, fasted animals show a 3-fold induction and refed animals no change. Although promising, further work will be required to sort out which, if any, change(s) in *Pck1* occurs. Because *Gbpar1* levels are reduced in BAT, we determined *Gbpar1* expression levels in the livers of *ad lib* fed animals (Figure 38A). Unfortunately, expression in both WT and KO mice was highly variable, obscuring the possible impact of *Rdh1* loss on expression. However, any possible change to *Gbpar1* expression does not appear sufficient to effect hepatic *Ppargc1* expression levels (Figure 38A). Like in EWAT, we also see increased *Gbp1* expression in both

microarray (Table 27) and qPCR (Figure 38B), with expression about 3-fold higher in KO mice compared to WT.

The changes to body temperature, BAT refed atRA and BAT fatty acid dynamics all point to dysfunction in brown adipose. However, expression of the most obvious molecular targets (*Ucp1*, its paralogs and regulatory network, PPARs) provided little insight into the underlying molecular mechanism. Thus, we used microarray to assess global gene expression changes in 6 week old, fasted WT and *Rdh1*-KO animals. In this study, biological triplicates were used and, perhaps because of study design, we identified only 3 statistically significantly changes (*Pla2g12a, Adh6b* and LOC675899-the NCBI record of which has since been discontinued). However, a modest list of 34 genes showed a 2+-fold increase or decrease in expression (Table 28).

Given the additional evidence pointing to BAT dysfunction, follow-up by qPCR in BAT has been much more extensive. By qPCR, the most robust gene change occurs in *Gbp1,* with KO expression induced by over 1000 fold in one set of fasted and refed animals (Figure 39A) and 200-460 fold induced in a second set (Figure 39D). Regulation of *Gbp1,* part of a family of large GTPases, has been best characterized in inflammation and immune response (162-164). Specifically, IFN-γ, IL-1α, IL-1β and TNFα induce *Gbp1* expression, whereas growth factors bFGF and VEGF reduce *Gbp1* expression. With no change to circulating TNFα levels (Table 12), we looked for signs of local inflammation in BAT (Figure 39E). Expression of macrophage marker *Itgam* (MAC-1) was unchanged in KO, as was expression of *Ifng* (IFNγ) and *Irf4* (Interferon regulatory factor 4), an interferon-related transcription factor also identified in the microarray. Although not an exhaustive study of inflammation, this suggests a role for *Gbp1* outside of immune context.

Two other genes, *Cap1* and *Adh1* were identified in microarray, and found to be dysregulated in both fasting and refeeding by qPCR (Figure 39A). *Cap1*, upregulated 2.3-fold in fasting and 3.5-fold in refeeding, contributes to actin filament formation and apoptosis (165, 166), but no direction connection between *Cap1* and energy metabolism or thermogenesis has been identified. *Adh1*, down 80% in fasting and 90% in refeeding, oxidizes ethanol to acetalaldehyde, though *Adh1* can operate on a broad range of substrates (167). Like with *Gbp1* and *Cap1*, how *Adh1* may connect loss to *Rdh1* to reduced body temperature remains unclear.

Transcription factor *Klf2* and guanosine monophosphate reductase *Gmpr*, both identified in microarray, are upregulated only in fasted KO BAT (Figure 39B). *Klf2* inhibits preadipocyte differentiation (168) and down-regulates *Fabp5* expression (168). Perhaps *Klf2* modulates the CRABP2 to FABP5 ratio in BAT. Future work will test this hypothesis. Cold exposure induces *Gmpr* expression, which may activate UCP1 by reducing GTP levels (169). Like increased *Ucp1*, increased Gmpr may compensate for reduced thermogenesis in *Rdh1*-KO.

In one cohort of animals, *Elovl3* expression decreased in KO BAT, in line with microarray data (Figure 39B). However, in a second set of animals, *Elovl3* expression increased (Figure 39D). *Elovl3* elongates fatty acids in support of thermogenesis (170), making it either an attractive connection between expression changes and thermogenesis or another form of compensation. The opposite expression patterns thus far observed call into question whether *Elovl3* truly changes, and in which direction.

Car5b and *Orm2* expression decreased in fasted KO BAT, in line with microarray data (Figure 39B). Found in the mitochondria, changes to carbonic anhydrase *Car5b* expression may affect bicarbonate availability for pyruvate carboxylase in gluconeogensis and carbamoyl phosphate synthetase 1 in the urea cycle (171). *Orm2* (orosomucoid 2), a member of lipocalin

family, is induced in acute phase immune response (172), though little is known about its exact function.

Microarray also implicated changes to *Pla2g12a, Acot11* and *Per2,* though qPCR confirmation yielded no significant changes in these genes between WT and KO animals (Figure 39C and D). Upregulation of *Rbp4* in BAT, identified by microarray, was discussed above (see also Figures 23-25).

Retinoid Metabolism Genes in Fasting and Refeeding

Changes to atRA in BAT, and possibly liver, in response to refeeding suggest broad coordination between retinoid and energy metabolism. As such, we sought to identify gene expression changes between fasting and refeeding in retinoid metabolism genes. We also looked for differences between WT and KO animals, in hopes of identifying compensatory gene changes or signs of additional retinoid dysregulation.

In brown adipose tissue, we found that 6-7 hours of refeeding reduces expression of *Rdh1* (Figure 40A and 41A) and possibly *Rdh10* (Figure 41A, but not 40A). In KO animals, *Rdh1* levels are, as expected, decreased (Figure 40B and 41B). It is not yet clear whether expression of *Dhrs9* or *Rdh10* decreases with feeding (Figure 41A and B) or not (Figure 40A and B). Interestingly, decreased *Rdh1* expression during refeeding predicts a decrease in refed atRA, not the observed increase.

Amongst the Raldh, *Aldh1a1* reproducibly changes with fasting and refeeding in BAT (Figures 40C and 41C) and in one set of mice *Aldh1a2* and *Aldh1a3* also changed with refeeding (Figure 41C, but not 40C). Like with *Rdh1* (and *Rdh10*?), we would not predict increased atRA from gene expression data. Because *Rdh1*-KO mice also down-regulate *Aldh1a1* in refeeding (Figure 40D and implied by ANOVA in 41D), we can infer that regulation of *Aldh1a1* is not feedback regulation from increased atRA. In KO animals we observe no consistent change to Raldh expression between WT and KO animals (Figures 40D and 41D).

Adding further complexity, levels of *Rbp1* (Figure 40E and 41E) and *Rbp7* (Figure 40E) are also downregulated in BAT by refeeding. As with Rdh and Raldh, loss of *Rdh1* does not appear to affect overall expression levels or metabolic regulation of either Crbp (Figure 40F and 41E). Because BAT retinol at the least remains constant during refeeding, decreased Crbp levels predict increased holo-CRBP, and again reduced atRA synthesis.

Changes in Cyp-mediated catabolism could also explain changes to atRA levels. We failed to detect *Cyp26a1, Cyp2c39* or *Cyp26c1* expression in brown adipose tissue (data not shown). *Cyp26b1* is expressed in BAT, though two cohorts of animals showed different responses to refeeding and varied differences between WT and KO animals (Figure 40G and 41F). In all, reconciling gene expression and atRA data during fasting and refeeding requires additional information, such as protein levels and post-translational modification. However, both show coordinated response of retinoid metabolism in response to metabolic state.

With clear, reproducible changes to gene expression in BAT, we expanded our study to other tissues. Interestingly, in PMWAT, we observed no statistically significant changes to *Aldh1a1, Aldh1a2, Aldh1a3* or *Rbp1* gene expression upon refeeding (Figure 42). Additionally, and consistent *Rdh1* expression levels in EWAT, KO and WT mice show similar levels of gene expression.

In liver, we observe a more dramatic set of gene changes. Here, all Rdh assayed are downregulated by refeeding and only *Rdh1* expression differs between WT and KO (Figure 43A and B). Two-way ANOVA reveals all Raldh assessed are downregulated by refeeding, again

with no difference between WT and KO mice (Figure 43C and D). Like BAT, *Rbp1* levels also decline with refeeding in both WT and KO animals (Figure 43E). Such changes appear consistent with a decline in hepatic atRA (Figure 32A).

Liver expresses a variety of Cyps capable of catabolizing atRA. Initial work in *Rdh1*-KO mice found decreased *Cyp26a1* at both gene and protein expression levels (3). During fasting and refeeding, the picture becomes a little more muddled (Figure 44). In both studies, fasted *Cyp26a1* levels are similar between WT and KO animals. Upon refeeding, WT levels of *Cyp26a1* are induced in both studies; however, whether KO levels are also induced upon refeeding is unclear. Expression in 10 week old female mice shows no *Cyp26a1* induction in KO liver, but expression in 7.5 week old male mice shows induction of *Cyp26a1* to the same level as WT. Whether this reflects a an actual sex difference remains unclear, especially considering the original work, that more closely resembles data from female mice, used male mice under presumably *ad lib* fed conditions.

Initial work with *Rdh1*-KO animals found no change in *Cyp26b1* between WT and KO; however, here observe decreased *Cyp26b1* levels in KO animals (Figure 44B and D). In liver, *Cyp26b1* does not appear responsive to refeeding.

Further complicating the picture is *Cyp2c39.* Expression of this gene decreases with refeeding, but is surprisingly induced over 50-fold and as much as 126-fold in KO mice (Figure 44, though microarray (Table 27) indicated downregulation). It was initially believed that reduced *Cyp26a1* levels compensated for loss of *Rdh1* in liver. The opposing changes to *Cyp26a1* (or instead *26b1?*) and *Cyp239* are difficult to interpret by gene expression data alone. Clearly, additional regulatory measures in liver (and BAT) must help to reconcile gene expression data with atRA synthesis.

We have also undertaken a few preliminary studies to better understand regulation of retinoid metabolism during fasting and refeeding. In the first such study, we looked at how quickly gene expression changes take place. In a group of WT animals, we looked at mice 2.5 hours after refeeding, rather than the usual 6-7 (Figure 45). In these mice, BAT expression of *Raldh1* and *Rbp1* were already decreased (or trending toward a decrease). Because chow fed *Rdh1*-KO mice do not gain weight relative to WT, we wondered whether a diet with 15+ IU/g vitamin A (Harlan chow) impacted fasting and refeeding gene regulation. In this preliminary study, we found that some gene changes still occur, such as BAT *Rdh1* expression (Figure 46A) and liver *Cyp26a1*, *Rdh1* and *Ald1a3* (Figure 46C and D), while others do not, such as BAT *Aldh1a1* (Figure 46B) and liver *Ald1a1* and *Aldh1a2* (Figure 46D).

To better isolate possible refeeding signals, we also began work in a cell culture BAT model, mouse HIB-1B cells (134). Work in a pancreatic β-cell line suggested that glucose may regulate 9cRA synthesis (Obrochta and Napoli, unpublished). As such, we tested whether changes to glucose levels affected HIB-1B retinoid metabolism gene expression. In both undifferentiated (Figure 47 A and C) and differentiated (Figure 47B and D) HIB-1B cells, glucose levels did not appear to change expression of *Rdh1*, *Dhrs9*, *Rdh10*, *Aldh1a1* or *Rbp1*. Interestingly, differentiation increased *Rdh1* expression ~3.5 fold, *Aldh1a1* ~1.5 fold and *Rbp1* 5-8 fold, but decreased *Rdh10* expression 30-40%. This predicts that brown adipocytes *in vivo* express higher levels of *Rdh1*, *Aldh1a1* and *Rbp1* than precursor cells.

The Physiological Role of 9-*cis*-Retinoic Acid

To better understand the interplay between retinoids and metabolism, and as a comparison point for the phenotype observed in *Rdh1*-KO mice, we also undertook study to

better characterize the physiological impact of 9cRA. Others had described fasting-to-refeeding fluctuations in pancreatic 9cRA and found super-physiological 9cRA in pancreas of *Rbp1*-KO mice (4, 71). However, the impact of pharmacological treatment with exogenous 9cRA remained unclear levels. As such, we treated adult C57BL/6 male mice with either 5 mg/kg of 9cRA or vehicle (dimethylsulfoxide, DMSO) control 15 minutes prior to a low dose (0.5 g/kg) glucose tolerance test. In 9cRA treated mice, we found that blood glucose levels rose higher than that of vehicle alone (Figure 48A). In such animals, we also found reduced serum insulin levels relative to vehicle-treated animals (Figure 48B). Combined with work in cell culture, this study suggests that high pancreatic 9cRA impairs the secretion of insulin.

The *Rbp1*-KO (CRBP1-KO) mouse represents a mouse model with high endogenous 9cRA in the pancreas. To better understand the impact of *Rbp1* loss on mouse energy metabolism, we studies WT and *Rbp1*-KO mice in CLAMS metabolic cages. *Rbp1*-KO mice respired less than their WT counterparts (Figure 49A), with lower rates of oxygen consumption and carbon dioxide production. Reduced movement in *Rbp1*-KO mice likely contributes to lower respiration (Figure 49C). Even though *Rbp1*-KO mice ate similar amounts of food (Figure 49D), their RER was lower than that of WT (Figure 49B), meaning *Rbp1*-KO mice burn more fat than WT. A low insulin to glucagon ratio would prevent normal carbohydrate uptake and oxidation and may explain the low RER. Furthermore, the high blood glucose levels of *Rbp1*-KO may contribute the sluggish behavior observed, though the exact cause of reduced movement has not been determined.

Contributions of *Rdh1* Paralogs to Retinoid and Steroid Metabolism

A mutation screen for defects in cortical development (126) identified an *Rdh10* hypomorphic mutation (*Rdh10* Mut) where mice homozygous for the mutation only survive until E 16.5 (7). In casual observation, heterozygous (Het) adults for the mutation survive, breed and appear normal (unpublished personal observation). To determine whether such adults have impaired retinoid metabolism, we measured atRA, retinol and retinyl esters of WT and *Rdh10* Mut Het mice in tissues and tissue regions previously reported to have the highest *Rdh10* expression (109, 122). Consistent with reports in embryonic homozygous mutants (7), adult heterozygotes showed decreased atRA levels in the cerebellum and cortex, compared to WT (Figure 50A). *Rdh10* Mut Hets also displayed higher atRA levels in the spleen (Figure 50A). Of three tissues with altered atRA, only cerebellum, with low levels of retinyl ester, showed disruption of another retinoid (Figure 50C). Kidney retinol levels also differed from WT (Figure 50B).

Unique to mice are three enzymatic *Rdh1* paralogs: *Rdh16* (*cis*-retinol/3α-hydroxysterol short-chain dehydrogenase 1 or CRAD1), *Rdh7* (CRAD2) and *Rdh9* (CRAD3) (114, 115, 173). Compared to *Rdh1*, these enzymes show greater activity toward *cis*-retinol isomers and steroids as substrates. To better understand the *in vivo* role of the enzymes our lab generated knockouts of both *Rdh16* (Zhang, Hu and Napoli, unpublished) and *Rdh9* (116). Given the *in vitro* activity of these enzymes toward *cis*-retinol isomers, we asked whether CRAD1 or CRAD3 KO mice have disrupted retinoid homeostasis in pancreas. Interestingly, CRAD1-KO mice show elevated 9cRA in pancreas (Figure 51A), though levels fall within the normal range observed in WT (4, 71). CRAD1-KO mice also present reduced retinal and retinyl ester levels in pancreas (Figure 51B). By contrast, 9,13-di-*cis*-RA (9,13dcRA) is elevated in the CRAD3-KO pancreas. With low affinity for RAR (174-176), 9,13dcRA may represent an inactivated form of 9cRA (174-176). Retinal and retinol levels are also reduced compared to WT in the CRAD3-KO pancreas. We

have yet to determine whether these changes affect glucose tolerance, insulin sensitivity or energy metabolism in either CRAD1- or CRAD3-KO mice.

Casual observation of the CRAD1-KO line suggested reduced litter size and a skewed male-to-female ratio amongst *Rdh16*-KO litters. In addition, we repeatedly observed a parturition defect where CRAD1-KO dams died in the process of giving birth, with such births seemingly occurring later relative to pairing than WT. In attempt to quantify these observations, we mated 8-10 week old virgin male and female mice of WT, *Rdh16*-KO and heterozygous phenotypes. After 65 crosses, we found no effect of *Rdh16* male or female gene dosage on gestational length (estimated by the time from first pairing until birth) (Table 29), fecundity (Table 30), percent male per litter (calculated as average percent per litter, not overall percentage) (Table 31), parturition defect (Table 32) or fertility (Table 33). In casual observations since, there have been no other deaths during parturition in the *Rdh16*-KO line. One explanation may be *Pasteurella pneumotropica* infection, a pathogen found in our animal facility (Nina Hahn, head veterinarian, personal communication) and common cause of intrauterine infection in mice (177). We have not determined if CRAD1-KO affects immune response or function nor have we tested CRAD1-KO animals for *Pasteurella pneumotropica* infection.

With *in vitro* activity toward 3-adiol and 5α -androstan-3 α -ol-17-one, we asked whether *Rdh16* loss affects steroid metabolism. We therefore measured both serum testosterone and serum 3-adiol glucuronide (3-adiol-G), an inactivated steroid metabolite (and proxy for 3-adiol levels) (Figure 52). Neither analyte changed in the serum of *Rdh16*-KO male animals. In livers of CRAD1-KO mice, semi-quantitative gene expression analysis revealed changes to 3β-hydroxysteroid dehydrogenases 1, 2 and 3, which may compensate for *Rdh16* loss to maintain proper androgen levels (Figure 53A). However, none of these gene changes were observed in kidney or testis (Figure 53B and C).

Conclusions and Discussion:

Original studies of the *Rdh1*-KO mouse mice observed increased weight and/or adiposity in mice fed diets low or deficient in vitamin A. In our studies since, we find that KO animals become overweight and higher in adiposity when fed an AIN 93G diet. This diet contains 4 IU/g of vitamin A, a level of vitamin A recommended for mice and comparable to the 2.6 IU/g necessary for normal mouse growth. *Rdh1*-KO mice also gain weight independent of HFD feeding. In the literature, most obesity and overweight models require HFD feeding for weight gain. Together, these observations show that *Rdh1* plays a physiological, rather than pathological, role in the maintenance of energy metabolism. The implication is that even with recommended levels of vitamin A nutrition and caloric intake, defects in retinoid metabolism can have an effect on energy metabolism.

Weight gain in the *Rdh1*-KO mouse is not without consequence. Either compounded by, or as a result of, weight gain, KO animals become insulin resistant, with elevated fasting glucose and high serum insulin levels that eventually lead them to become glucose intolerant. Changes to insulin levels, glucose tolerance and insulin sensitivity cannot be attributed to changes to pancreatic 9cRA, as in the *Rbp1*-KO mouse. Interestingly, *Rdh1* paralogs CRAD1 and CRAD3 may affect pancreatic 9cRA metabolism. When placed in metabolic cages, the *Rbp1*-KO and *Rdh1*-KO mice also show distinctly different phenotypes. *Rbp1*-KO mice move and respire less than WT, while burning more fat than WT animals, whereas *Rdh1*-KO mice move, respire and burn fat comparable to WT mice. Differences between the two phenotypes highlight the complexity of retinoid homeostasis and its interactions with metabolic regulation.

Rdh1 loss also impacts serum T3, T4 and leptin levels. Increased in leptin can most likely be explained by increased adiposity in *Rdh1*-KO mice. With no changes to TSH levels, reductions to thyroid hormone levels can be attributed to thyroid dysfunction. Overall, the change to thyroid hormones appears minor. Circulating TSH does not rise to compensate for low thyroid hormones nor do we see consistent changes to thyroid responsive genes. Gene expression studies in thyroid would provide additional insight into the both the molecular cause and degree of thyroid dysfunction.

Physiologically, we have ruled out hyperphagia and inactivity as underlying causes of weight gain. In short term studies, KO animals do not eat any more than WT and in long term studies, KO mice eat more, but only as expected from mice with increased mass.

Decreased body temperature represents our best explanation for weight gain. With high variation of body temperature in both WT and KO animals, this change is not always apparent. However, a pattern of reduced body temperature emerges from accumulated data. Surprisingly, stressors to thermogenesis such as β-adrenergic agonist stimulation or cold exposure fail to reveal thermogenic dysfunction, yet fasting and refeeding provides a useful stress for revealing the phenotype. Consistent with physiology results, we see no change to BAT gene expression of β-adrenergic receptors, which respond to cold and agonist stimulation, but do see changes to *Gbpar1*, a bile acid responsive receptor. However, both of these signaling pathways induce *Dio2*, *Ppargc1* and *Ucp1* expression and changes to these genes are inconsistent between studies or inconsistent with decreased signal.

From the literature, we expected a direct effect of *Rdh1*-KO on *Ucp1* expression. The *Ucp1* promoter contains both an RARE and PPRE that respond to atRA in a variety of contexts and *Rdh1*-KO animals are deficient in BAT atRA during refeeding. However, gene expression of *Ucp1*, and its paralogs *Ucp2* and *Ucp3*, remain unchanged in refed *Rdh1*-KO BAT. During fast, increased *Ucp1* expression in BAT may even compensate for *Rdh1* loss. *Ucp1*-KO mice only gain weight during HFD feeding at thermoneutrality (178), whereas *Rdh1*-KO mice gain weight fed a low fat diet at normal housing temperature. From a physiological standpoint, *Rdh1*-KO does not phenocopy *Ucp1*-KO. Because the physiological phenotype differs, this predicts *Ucp1*-independent defects in the *Rdh1*-KO mouse. The literature also supports a growing link between retinoic acid signaling and the PPAR nuclear hormone receptors. Here again, we find no change to expression of any PPAR in the BAT of *Rdh1*-KO mice.

Results such as these made us look to white adipose tissue as the source of defect, and through microarray we identified a wide variety of gene changes. However, gene changes to *Lcn2*, *Rbp1* and *Aldh1a1* could not be confirmed by qPCR and predicted changes to circulating resistin and neuropeptide Y failed to materialize. Thus, we revisited *Rdh1* gene expression, and found little to no expression in EWAT. Interestingly, *Rdh1* expression in various white adipose depots correlates with *Ucp1* expression, once again pointing to defects in brown adipose.

We expected stable isotope studies to show increased *de novo* lipogenesis rates, and thereby explain weight gain in *Rdh1*-KO mice. Instead, we found less newly-synthesized palmitate in both long-term studies of white adipose tissue and short-term studies of brown adipose tissue. Because palmitate levels per gram adipose were similar between WT and KO, a greater amount of dietary palmitate must be present in KO fat. Stable isotope studies also revealed either a defect in either local fatty acid synthesis or reduced uptake of LDL in BAT. We suspect a lower rate of fatty acid oxidation inhibits synthesis and/or uptake of new fatty acid. Future studies will test this hypothesis.

Loss of *Rdh1* also affects overall fatty acid composition. Most likely through changes in hepatic *Elovl6* expression during refeeding, *Rdh1*-KO mice have a reduced percentage of stearate in liver and adipose. In the near future, we hope to use heavy isotope studies to confirm that pool composition changes are due to decreased elongation of palmitate rather than changes to stearate uptake or oxidation. *Elovl6*-KO animals gain a normal amount of weight and are protected from insulin resistance during HFD feeding (179), presenting a different phenotype than that of *Rdh1*-KO. As such, changes to hepatic *Elovl6* do not readily explain the *Rdh1*-KO phenotype. However, the impact of decreased *Elovl6* on tissue stearate concentrations suggests we may have overlooked the liver and its contribution to the *Rdh1*-KO phenotype.

Reduced expression of hepatic *Elovl6* underscores the importance of *Rdh* to normal liver homeostasis. Although we observe no consistent changes to hepatic atRA levels in KO mice, we find divergent gene changes to Cyp enzymes that catabolize atRA. In our hands, we found both a reduction in *Cyp26b1* (but not *Cyp26a1*) expression and a dramatic increase in *Cyp2c39* expression. Clearly, hepatic retinoid metabolism is complex and the maintenance of retinoid homeostasis is integral to liver function. In the future, enzyme activity assays may prove insightful and help to reconcile the interaction between *Rdh1* and Cyps. Imaging of cellular Rdh suggests unique localizations of each isozyme within the endoplasmic reticulum (Jiang and Napoli, unpublished). Perhaps, knowledge of Cyp intracellular location will inform understanding of *in vivo* interactions.

After repeated measures of retinoids in *ad lib* fed animals at different ages with different diets, we saw no consistent changes between WT and *Rdh1*-KO animals. This stands in stark contrast to *Rbp1*-KO animals, with elevated 9cRA in pancreas and decreased RE levels in liver (70, 71), and *Rdh10* mutant heterozygotes, with changes to atRA in brain regions and spleen. This led us to the surprising conclusion that atRA levels change with metabolism. In BAT, we found that refeeding induces atRA in young male WT animals, and that in both sexes, *Rdh1*-KO mice fail to maintain atRA during refeeding. We investigated further, finding that gene expression of various retinoid synthesis enzymes, including *Rdh1, Rbp1, Rbp4, Rbp7* and *Aldh1a1* (all genes whose loss causes a metabolic phenotype), decrease in BAT with refeeding. We also have evidence of decreased atRA, retinol and retinyl ester in the refed liver. Our study in female refed mice showed reductions in liver atRA, retinol and retinyl ester coincident with increases to serum levels. Gene expression of many retinoid metabolism genes responds to refeeding in the liver and appears much more diverse than in BAT.

Though not directly addressed, our work here provides some insight to the regulation of atRA synthesis in response to metabolism. In BAT, reduced refed expression of atRA synthesis enzymes suggests post-transcriptional regulation mediates atRA increase. We also determined that cold affects BAT atRA different than refeeding, though cold and refeeding appear to have similar effects on liver atRA. In at least some cases, these expression changes appear to occur as soon 2.5 hours after refeeding and high retinol diets appear to override some normal regulation. In a cell culture experiment, we ruled out glucose levels *per se* as the regulator of gene expression. Though spatially and temporally regulated during development, few have considered dynamic atRA synthesis in adult animals, and confirming and expanding on these studies would be game changing in the retinoid field.

Failure of *Rdh1*-KO mice to maintain refed atRA levels renewed our interest in BAT gene changes. We therefore used microarray to assess global gene expression in fasted animals in hopes of identifying important basal changes. In hindsight, it may have been more informative to look in refed animals, but microarray, and qPCR follow-up, revealed upregulation of *Rbp4*,

Gbp1, *Cap1*, *Klf2* and *Gmpr* and down regulation of *Adh1*, *Elovl3* (maybe?), *Car5b* and *Orm2* in the fasted and/or fed state.

Upregulation of *Rbp4* in brown adipose does not affect expression of *Pparg* or *Socs3*, two downstream targets of RBP-STRA6 signaling. *Rbp4* levels in EWAT and liver do not change in KO mice, so effects on *Rbp4* expression appear specific to BAT. In future studies, it may informative to measure serum RBP levels. This will help determine the relative contribution of BAT-derived RBP to both circulating levels of WT animals and insulin resistance in *Rdh1*-KO mice.

Based on the literature, upregulation of *Gbp1* suggests increased inflammation in *Rdh1*-KO mice. However, both systemic TNFα levels and local *Ifng* expression are normal in *Rdh1*-KO animals. Interestingly, EWAT and liver also present increased *Gbp1* levels, suggesting either a systemic signal or multiple local effects. With little to no *Rdh1* expression in white adipose, systemic signaling seems most likely. Measurement of circulating inflammatory cytokines IL-1α, IL-β and IFNγ and growth factors bFGF and VEGF would provide additional insight into the cause *Gbp1* overexpression and its connection to the *Rdh1*-KO phenotype.

Of the gene changes in BAT, it has been difficult to determine which leads to weight gain in *Rdh1*-KO animals. Thus far, pathway mapping of BAT gene changes failed to yield any satisfactory results (data not shown, because no pathways appeared enriched beyond one gene change). We plan to carry out further pathway analysis using an expanded gene list. Other future plans include using metabolomics and microarray in refed animals, in hopes of finding clear molecular links between thermogenesis and *Rdh1*. We could also take a genetic approach with some of the more robust changes. For instance, *Rdh1*-KO mice could be crossed with *Gbp1*-KO mice, to see if weight gain, temperature regulation and other gene changes return to normal. Chromatin immunoprecipitation could also be used to identify which genes are direct atRA targets.

Though we have not found the exact molecular cause of weight gain in *Rdh1*-KO animals, we have made important insights into the mostly likely physiological cause (body temperature) and have identified potential gene targets (*Elovl6*, *Gbp1*) upon which to base future work. We have also discovered physiological regulation of atRA levels in brown adipose tissue and perhaps liver. These changes may have much broader implications beyond that of *Rdh1*-KO.

Table 1) Mouse Diet by *Rdh1*-KO Cohort

Cohort	Born (Month/Year)	Diet(s) (Also maternal diet at mating.)	Maternal Diet
1w1	7/2005	VAD	Purina Chow
1.5w1	3/2007	AIN 93G	AIN 93G
2w1	07/2007	VAD or AIN 93G	AIN 93G
2w2	09/2007	AIN 93G	AIN 93G
3w1	06/2008	Harlan Chow or VAD then AIN 93G at 11 weeks	Harlan Chow
3w2	08/2008	AIN 93G or VAD then AIN 93G at 5 weeks	Harlan Chow
4w1	10/2008	Harlan Chow or VAD then AIN 93G at 5 weeks	Harlan Chow or AIN 93G
4w2	12/2008	AIN 93G	AIN 93G
5w1	12/2008	AIN 93G or AIN 93G then HFD at 7 weeks	AIN 93G
5w2	02/2009	AIN 93G or HFD at Weaning	AIN 93G
6w1	04/2009	AIN 93G	AIN 93G
6w2	05/2009	AIN 93G	AIN 93G
7w1	07/2009	AIN 93G	AIN 93G
7w2	09/2009	AIN 93G	AIN 93G
8w1	11/2009	AIN 93G	AIN 93G
8w2	12/2009	AIN 93G	AIN 93G
9w1	12/2009	AIN 93G	AIN 93G
9w2	02/2010	AIN 93G	AIN 93G
10w1a	02/2010	AIN 93G	AIN 93G
10w1b	02/2010	AIN 93G	AIN 93G
10w2a	04/2010	AIN 93G	AIN 93G
10w2b	05/2010	AIN 93G	AIN 93G
11w1	05/2010	AIN 93G	AIN 93G
11w2	07/2010	AIN 93G	AIN 93G
12w1	10/2010	AIN 93G	AIN 93G
12w2	12/2010	AIN 93G	AIN 93G
13w1	03/2011	AIN 93G	AIN 93G
13w2	05/2011	AIN 93G	AIN 93G
13w3	06/2011	AIN 93G	AIN 93G
14w1	09/2011	AIN 93G	AIN 93G

Legend: Cohorts sharing the same first number come from the same set of mating pairs. The second number indicates the number of times the pairs have been mated. See Materials and Methods for additional diet information.

Table 2) List of qPCR Primers/Probe Sets

Gene Symbol	Gene Name	Assay ID
Acot11	Acyl-CoA thioesterase 11	Mm00452633_m1
Actb	Actin, beta	Mm00607939_s1
Adrb2	Adrenergic receptor, beta 2	Mm02524224_s1
Adrb3	Adrenergic receptor, beta 3	Mm02601819_g1
Adh1	Alcohol dehydrogenase 1 (class I)	Mm00507711_m1
Aldh1a1	Aldehyde dehydrogenase family 1, subfamily A1	Mm00657317_m1
Aldh1a2	Aldehyde dehydrogenase family 1, subfamily A2	Mm00501306_m1
Aldh1a3	Aldehyde dehydrogenase family 1, subfamily A3	Mm00474049_m1
Cap1	CAP, adenylate cyclase-associated protein 1 (yeast)	Mm00482950_m1
Car5b	Carbonic anhydrase 5b, mitochondrial	Mm00490359_m1
Crabp2	Cellular retinoic acid binding protein II	Mm00801693_g1
Cyp2c39	Cytochrome P450, family 2, subfamily c, polypeptide 39	Mm00656110_gH, Mm04207909_g1^
Cyp26a1	Cytochrome P450, family 26, subfamily a, polypeptide 1	Mm00514486_m1
Cyp26b1	Cytochrome P450, family 26, subfamily b, polypeptide 1	Mm00558507_m1
Cyp26c1	Cytochrome P450, family 26, subfamily c, polypeptide 1	Mm03412453_m1
Dhrs9	Dehydrogenase/reductase (SDR family) member 9	Mm00615706_m1
Dio2	Deiodinase, iodothyronine, type II	Mm00515664_m1
Elovl3	Elongation of very long chain fatty acids-like 3	Mm00468164_m1
Elovl6	ELOVL family member 6, elongation of long chain fatty acids (yeast)	Mm04209852_g1
Gmpr	Guanosine monophosphate reductase	Mm00499395_m1
Gbp1	Guanylate binding protein 1	Mm00657086_m1
Itgam	Integrin alpha M	Mm00434455_m1
Ifng	Interferon gamma	Mm01168134_m1
Irf4	Interferon regulatory factor 4	Mm00516431_m1
Klf2	Kruppel-like factor 2 (lung)	Mm01244979_g1
Orm2	Orosomucoid 2	Mm00440570_g1
Per2	Period homolog 2 (Drosophila)	Mm00478113_m1
Ppargc1	Peroxisome proliferator activated receptor, gamma, coactivator 1 alpha	Mm01208835_m1
Ppara	Peroxisome proliferator activated receptor alpha	Mm00440939_m1
Pparg	Peroxisome proliferator activated receptor gamma	Mm01184322_m1
Ppard	Peroxisome proliferator activator receptor delta	Mm00803184_m1
Pck1	Phosphoenolpyruvate carboxykinase 1, cytosolic	Mm01247058_m1
Pla2g12a	Phospholipase A2, group XIIA	Mm01321734_m1
Rbp1	Retinol binding protein 1, cellular	Mm00441119_m1
Rbp4	Retinol binding protein 4, plasma	Mm00803266_m1
Rbp7	Retinol binding protein 7, cellular	Mm00458145_m1
Rdh1	Retinol dehydrogenase 1 (all trans)	Mm00650636_m1
Rdh10	Retinol dehydrogenase 10 (all-trans)	Mm00467150_m1
Stra6	Stimulated by retinoic acid gene 6	Mm00486457_m1
Socs3	Suppressor of cytokine signaling 3	Mm00545913_s1
Thrsp	Thyroid hormone responsive SPOT14 homolog (Rattus)	Mm01273967_m1
Ucp1	Uncoupling protein 1 (mitochondrial, proton carrier)	Mm01244861_m1
Ucp2	Uncoupling protein 2 (mitochondrial, proton carrier)	Mm00627597_m1
Ucp3	Uncoupling protein 2 (mitochondrial, proton carrier	Mm00494077_m1

Legend: See Materials and Methods for additional information. ^ *Cyp2C39* (Mm00656110_gH), used in some experiments, amplifies some off-target transcripts. However, direct comparisons of both primer/probe sets in the same samples yielded comparable results.

Table 3) Semi-quantitative PCR Primers

Symbol	Gene or Protein Name	Primer Pair
Actb	β-Actin	F-TTC GTT GCC GGT CCA CAC CCG R- TAG GAG TCC TTC TGA CCC ATT C
Akr1c6	17β-hydroxysteroid dehydrogenase 1	F-AGG GAA GAT ATA TTT TAC ACA TCA AAG GT R-TCG TAC GGG TCT GCT TGG A
Hsd3b1	3β-hydroxysteroid dehydrogenase 1	F-TGG TGC AGG AGA AAG AAC TG R-ACT GCC TTC TCA GCC ATC TT
Hsd3b2	3β-hydroxysteroid dehydrogenase 2	F-CCA GTT TGG GAC TGC TGA CA R-AGT GAG GTT AAC TTA ATG TAC GTG ACA CT
Hsd3b3	3β-hydroxysteroid dehydrogenase 3	F-CCA GAA CTT ATT GGA GGC CTG TA R-GGC CCT GCA ACG TCA ACT
Hsd3b4	3β-hydroxysteroid dehydrogenase 4	F-CTT CCA GAC AGA CCA TCC TAG ATG T R-TGG CAC GTT GGC TTC CA
Hsd3b5	3β-hydroxysteroid dehydrogenase 5	F-GTC GAA AAC ATG AAG AGG AAT TGT C R-TCC AGA ATG TCT CCC TTC AGT ACT C
Hsd17b2	17β-hydroxysteroid dehydrogenase 2	F-GCT CAC AGC AAA GTC ACA GAG AA R-GAA GAC CCC GGC ATT GTT AA
Hsd17b3	17β-hydroxysteroid dehydrogenase 3	F-TCA CGA TCG GAG CTG AAT CC R-GAT CCG GTT CAG AAT TAT TGC AA
Rdh1	Retinol dehydrogenase 1	F-AGC AGG ATT AAA GGA AAG AAA AGC R-CCT TGT CCC AGA TCA TCT TGG TG
Rdh7	CRAD2	F-CGG AGG TCA AGG AGG TCT ATG A R-CTG AGC ATG TGT CTG TCA ATG ACT
Rdh9	CRAD3	F-CTA CAA ACT ATG TGG CTC TTT CTA R-CAG TAG TGT CAT AGG AGA ATT AAT G
Rdh16	CRAD1	F-GTG TCA TGG GTC GAG TGT CTC TC R-GAG TAG TGT CAT AGG AGA ATT AAC A
Srd5a1	5α-reductase 1	F-AGC CGA TAC TTG AGC CAG TT R-CGA GGT ACC ACT GAT GAT GC
Srd5a2	5α-reductase 2	F-CTG CGC CAG CTC AGG AA R-GAC ACA TAC GTA AAC AAG CCA CCT T

Legend: For PCR conditions see Materials and Methods. F: forward primer. R: reverse primer.

Figure 1) Vitamin A Deficiency in Mice

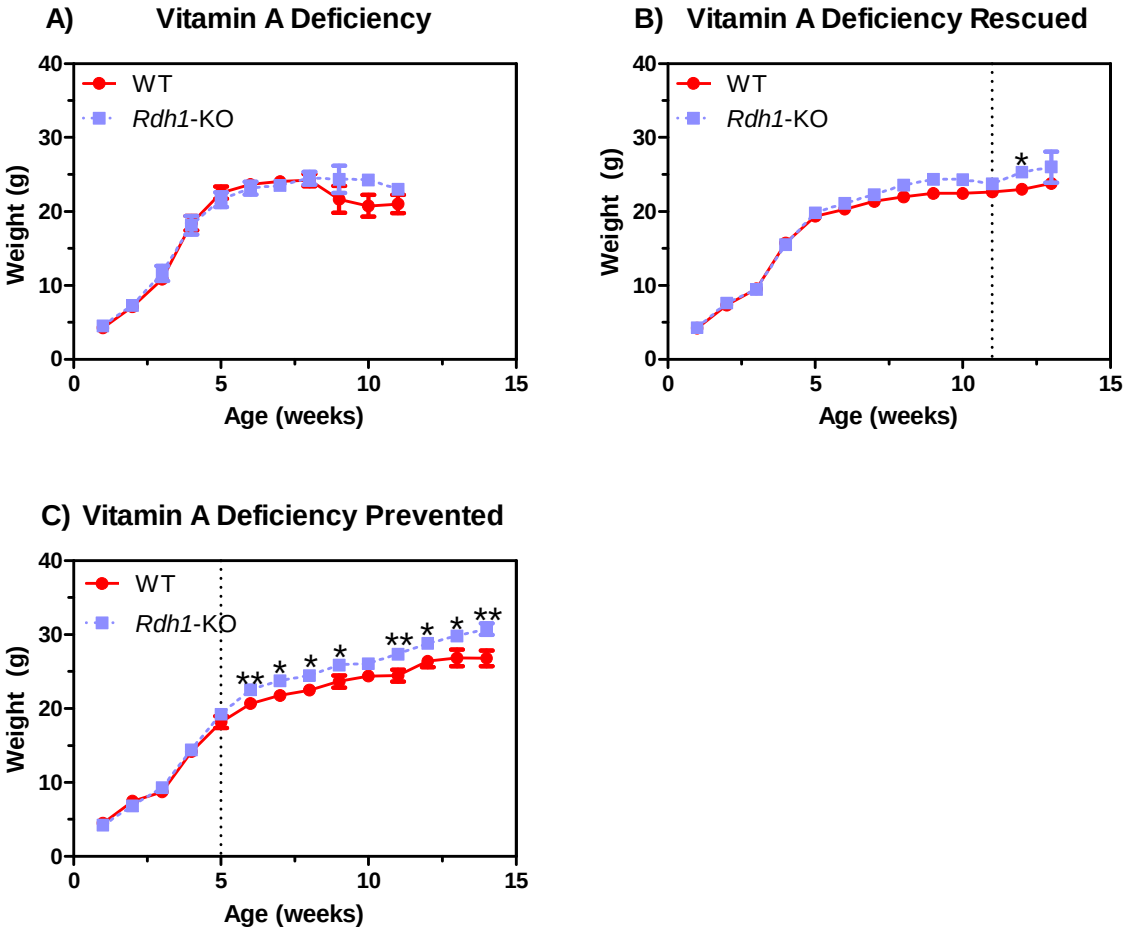

Legend: (A) Body weights from male WT (n=5) and *Rdh1*-KO (n=2) mice. Mice were fed a VAD diet and born to dams switched from a 93G diet to a VAD diet at mating (cohort 2w1). By two-way ANOVA, effect of age ($p \leq 0.001$). (B) Body weight of male WT (n=11-12) and *Rdh1*-KO (n=3-7) mice. Mice were fed a VAD diet until age 11 weeks (dotted line), and then switched to a 93G diet to rescue vitamin A deficiency. The dams of mice shown were switched from a Harlan chow diet to a VAD diet at mating (cohort 3w1). By two-way ANOVA, effects of age ($p \leq 0.0001$) and genotype ($p \leq 0.0001$). (C) Body weight of male WT (n=9) and *Rdh1*-KO (n=13-18) mice. At age 5 weeks (dotted line), mice were switched from VAD to a 93G diet to prevent vitamin A deficiency. The dams of mice shown were switched from a Harlan chow diet to a VAD diet at mating (cohort 3w2). By two-way ANOVA, effects of interaction between genotype and age ($p \leq 0.01$), age ($p \leq 0.0001$) and genotype ($p \leq 0.0001$). WT: red circle with solid line. *Rdh1*-KO: blue square with dashed line. **$p \leq 0.01$, *$p \leq 0.05$ vs. WT by Student's two-tailed t-test. All values Mean $\pm$ SEM.

Figure 2) Increased Weight in *Rdh1*-KO Mice Fed a 4 IU/g Vitamin A Diet

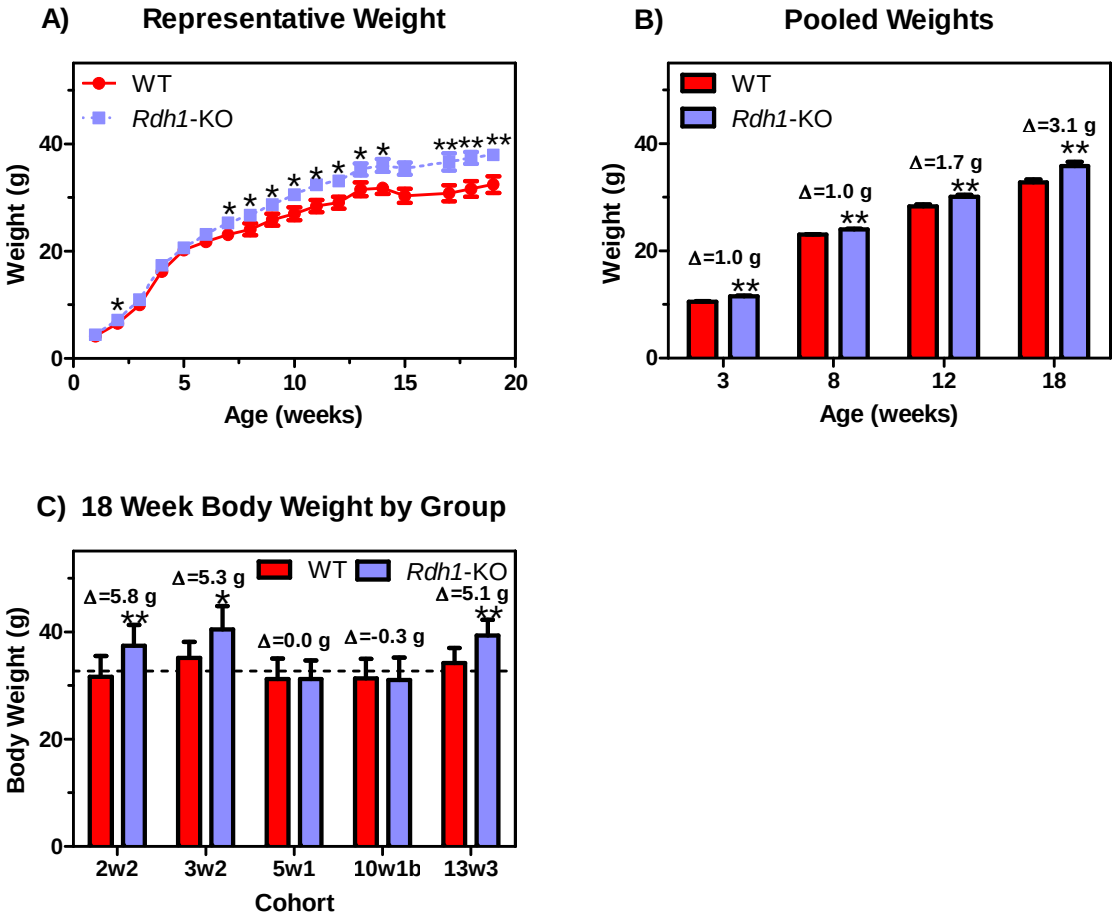

Legend: (A) Body weights from male WT (n=7-8) and *Rdh1*-KO (n=9-12) mice. Mice were both fed and born to dams fed a 93G diet (cohort 2w2). By two-way ANOVA, effects of interaction between age and genotype ($p \leq 0.05$), age ($p \leq 0.0001$) and genotype ($p \leq 0.0001$). (B) Body weight of male, 93G diet-fed mice from multiple studies at age 3 weeks (n=307 WT, 348 *Rdh1*-KO), 8 weeks (n=234 WT, 259 *Rdh1*-KO), 12 weeks (n=74 WT, 88 *Rdh1*-KO) and 18 weeks (n=40 WT, 49 *Rdh1*-KO) (cohorts 2w2-12w1). By two-way ANOVA, effects of interaction between genotype and age ($p \leq 0.0001$), age ($p \leq 0.0001$) and genotype ($p \leq 0.0001$). Δ indicates the weight difference between WT and *Rdh1*-KO for a given age. (C) Body weight data for 93G diet-fed male mice at age 18 weeks by cohort (2w2, n= 7 WT, 12 *Rdh1*-KO; 3w2, n=7 WT, 6 *Rdh1*-KO; 5w1, n=6 WT, 4 *Rdh1*-KO; 10w1b, n=10 WT, 9 *Rdh1*-KO; 13w3, n=10 WT, 13 *Rdh1*-KO). Δ indicates the weight difference between WT and *Rdh1*-KO for a given group. Dashed lines indicate the average weight of 18 week old WT mice from (B). WT: red circle with solid line or red bar. *Rdh1*-KO: blue square with dotted line or blue bar. **$p \leq 0.01$, *$p \leq 0.05$ vs. WT by Student's two-tailed t-test. All values Mean $\pm$ SEM.

Figure 3) Tissue Weight, Adiposity and Length in VAD Diet-fed *Rdh1*-KO Mice

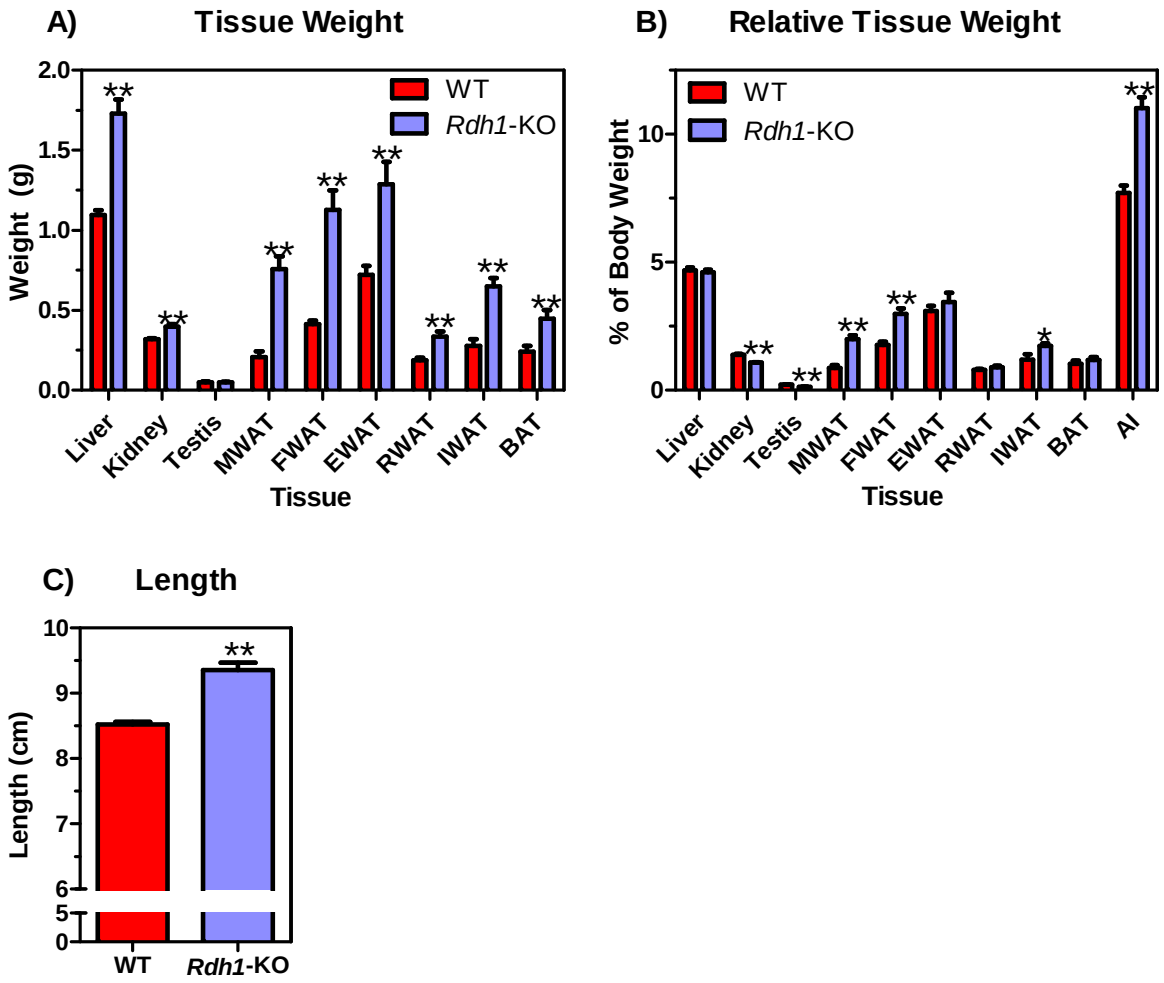

Legend: (A) Tissue weights from male, VAD-fed mice, age 35 weeks of age (n=5 WT, 6 *Rdh1*-KO). Mice were born to dams fed a Purina chow diet and switched to VAD diet at mating (cohort 1w1). (B) Tissue weights from (A) as a percent of overall body weight and AI (Adiposity Index), the sum all white adipose tissue depots. (C) Length (nose to anus) of mice from (A). MWAT, mesentery white adipose tissue. FWAT, femoral white adipose tissue. EWAT, epididymal white adipose tissue. RWAT, retroperitoneal white adipose tissue. IWAT, inguinal white adipose tissue. BAT, brown adipose tissue. WT: red bar. *Rdh1*-KO: blue bar. **p≤0.001, *p≤0.05 vs. WT by Student's two-tailed t-test. All values Mean ± SEM. Figure adapted from (3).

Table 4) *Rdh1*-KO Length

Cohort	Age (wks)	WT Length (cm)	*Rdh1*-KO Length (cm)
VAD Diet			
3w1	1	4.2 ± 0.3 (12)	4.1 ± 0.5 (7)
3w1	3	6.8 ± 0.3 (9)	6.7 ± 0.9 (6)
3w1	8-9	9.0 ± 0.5 (12)	9.4 ± 0.5 (7)
AIN 93G Diet			
7w1	5	8.4 ± 0.1 (6)	8.5 ± 0.3 (8)
6w1	8	9.2 ± 0.2 (11)	9.5 ± 0.2 (12)**
10w1	9	9.1 ± 0.2 (4)	9.2 ± 0.2 (4)
9w1 +G8w2	10-11	9.0 ± 0.3 (27)	9.0 ± 0.3 (21)
9w2	10-11	8.9 ± 0.3 (15)	9.0 ± 0.3 (19)
5w2	28	10.3 ± 0.2 (11)	10.4 ± 0.4 (10)

Legend: Length of male mice, diets and ages noted. **$p \leq 0.01$ vs. WT by Student's two-tailed t-test. All values Mean ± SEM (number).

Figure 4) Adiposity and Body Composition of *Rdh1*-KO Mice

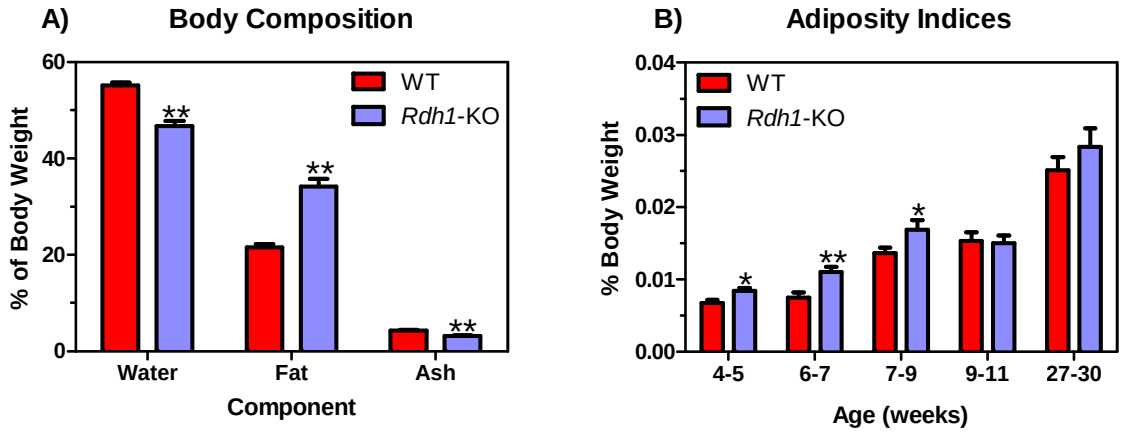

Legend: (A) Body composition of VAD diet-fed mice (n=5 WT, 6 *Rdh1*-KO) at age 33 weeks. Dams of mice shown were fed Purina chow then switched to a VAD diet at mating (cohort 1w1). (B) Adiposity index, here the sum of IWAT and EWAT relative to body weight, of 93G Diet-fed male mice at ages 4-5 weeks (n=12 WT, 11 *Rdh1*-KO), 6-7 weeks (n=6 WT, 12 *Rdh1*-KO), 7-9 weeks (n=11 WT, 12 *Rdh1*-KO), 9-11 weeks (n=29 WT and *Rdh1*-KO) and 27-30 weeks (n=19 WT, 12 *Rdh1*-KO). Data pooled from either *ad lib* fed or refed mice in cohorts 5w1, 5w2, 6w1, 6w2, 7w1, 8w2, 9w1, 9w2, 10w1a, 10w1b, 11w1, 12w1, 12w2 and 14w1. By two-way ANOVA, effects of age ($p \leq 0.001$) and genotype ($p \leq 0.05$). WT: red bar. *Rdh1*-KO: blue bar. **$p \leq 0.01$, *$p \leq 0.05$ vs. WT by Student's two-tailed t-test. All values Mean $\pm$ SEM. (A) Adapted from (3).

Figure 5) Adipocyte Size in *Rdh1*-KO Mice

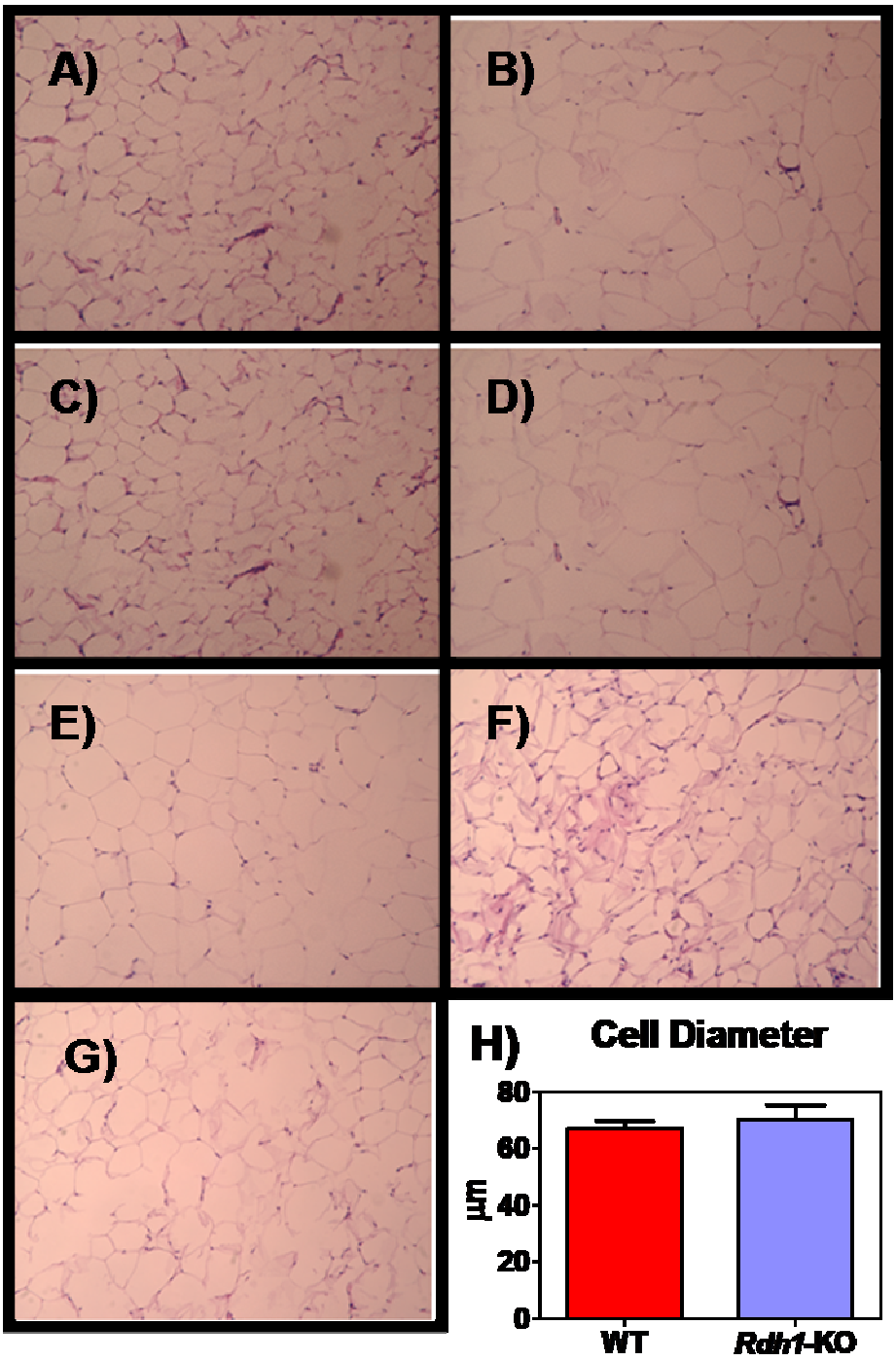

Legend: (A-D) Representative pictures of H&E stained EWAT from WT male, VAD Diet-fed mice, age 35 weeks (cohort 1w1). (E-G) Representative pictures of H&E stained EWAT from *Rdh1*-KO male, VAD Diet-fed mice, age 35 weeks (cohort 1w1). (H) Quantification of cell diameter in EWAT of mice in (A-G). WT: red bar. *Rdh1*-KO: blue bar. All values Mean ± SEM.

Figure 6) High Fat Diet-fed *Rdh1*-KO Mice, Study 1

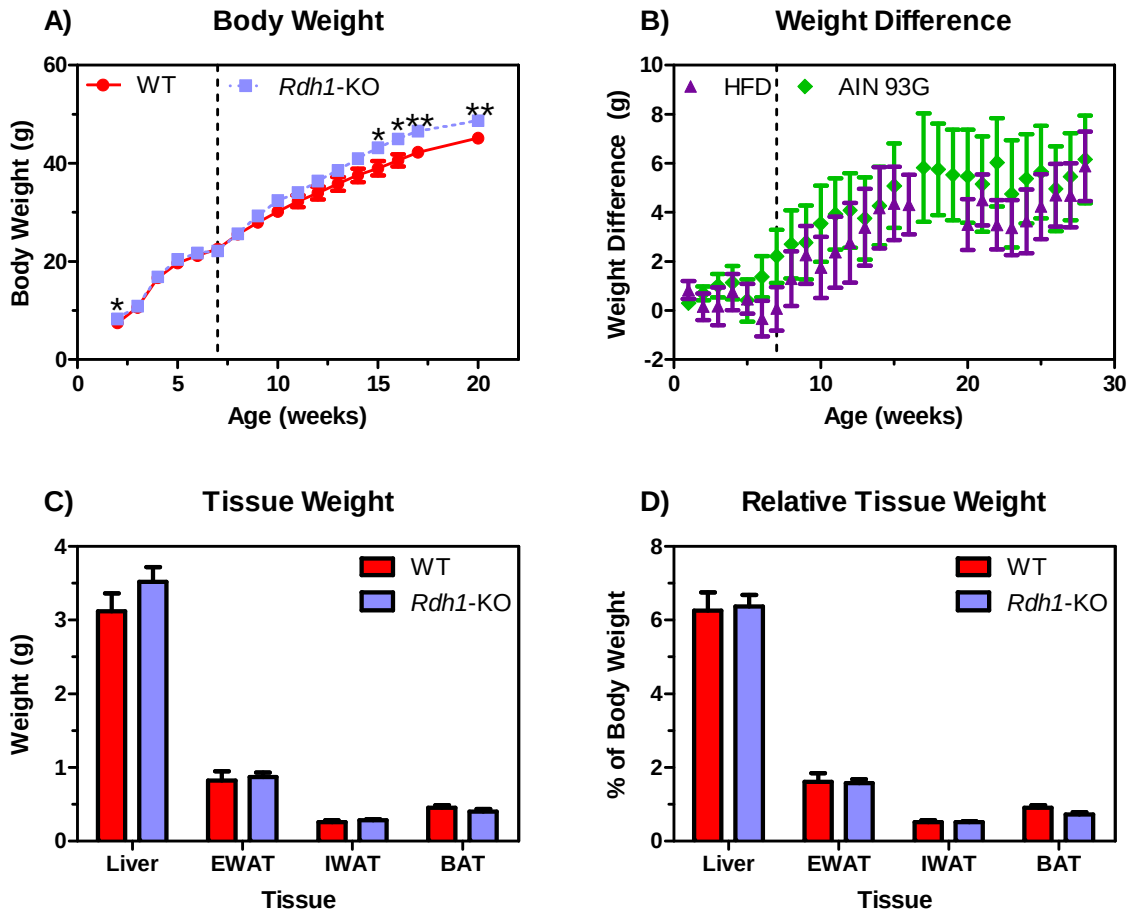

Legend: (A) Body weight of male WT (n=7-10) and *Rdh1*-KO (n=7-8) mice switched from a 93G diet to a high fat diet (HFD, here 50% fat derived calories) beginning at age 7 weeks (dotted line) (cohort 5w1). By two-way ANOVA, effects of interaction between age and genotype ($p \leq 0.05$), age ($p \leq 0.0001$) and genotype ($p \leq 0.0001$). (B) Body weight difference between *Rdh1*-KO and WT mice fed either HFD (mice from (A)) or 93G diet (mice from Figure 2A). (C) Tissue weights of mice from (A) at age 29 weeks (n=9 WT, 7 *Rdh1*-KO). (D) Tissue weights from (C) and adiposity index (EWAT+IWAT) normalized to body weight. WT: red circle with solid line or red bar. *Rdh1*-KO: blue square with dotted line or blue bar. 93G-fed mice: green diamond. HFD-fed mice: purple triangle. **$p \leq 0.01$, *$p \leq 0.05$ vs. WT by Student's two-tailed t-test. All values Mean $\pm$ SEM.

Figure 7) High Fat Diet-fed *Rdh1*-KO Mice, Study 2

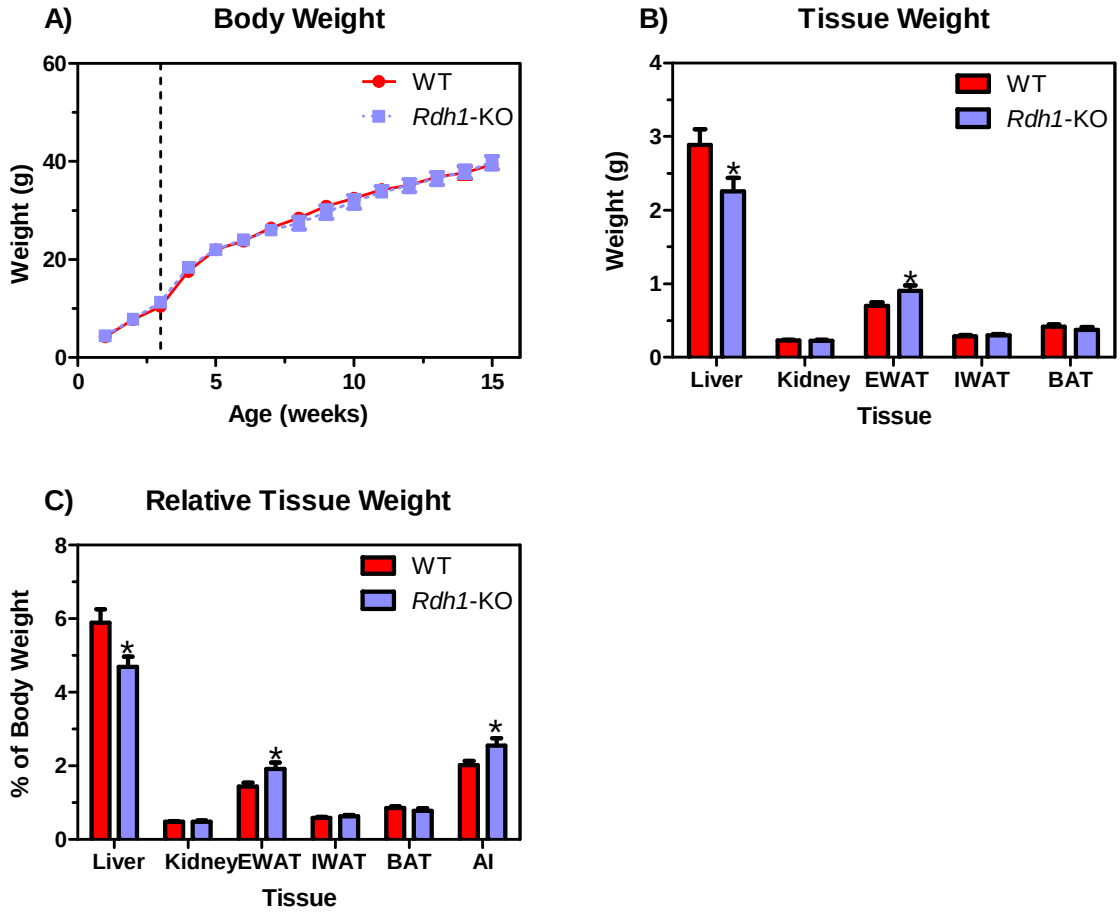

Legend: (A) Body weight of male mice (n=11-14 WT, 9-12 *Rdh1*-KO) fed a HFD beginning at age 3 weeks (dotted line) (cohort 5w2). By two-way ANOVA, effect of age ($p \leq 0.0001$). (B) Tissue weights of mice in (A) at age 29 weeks (n=11 WT, 10 *Rdh1*-KO). (C) Tissue weights from (B) and adiposity index (EWAT+IWAT) normalized to body weight. WT: red circle with solid line or red bar. *Rdh1*-KO: blue square with dotted line or blue bar.*$p \leq 0.05$, vs. WT by Student's two-tailed t-test. All values Mean $\pm$ SEM.

Figure 8) Food Intake of *Rdh1*-KO Mice

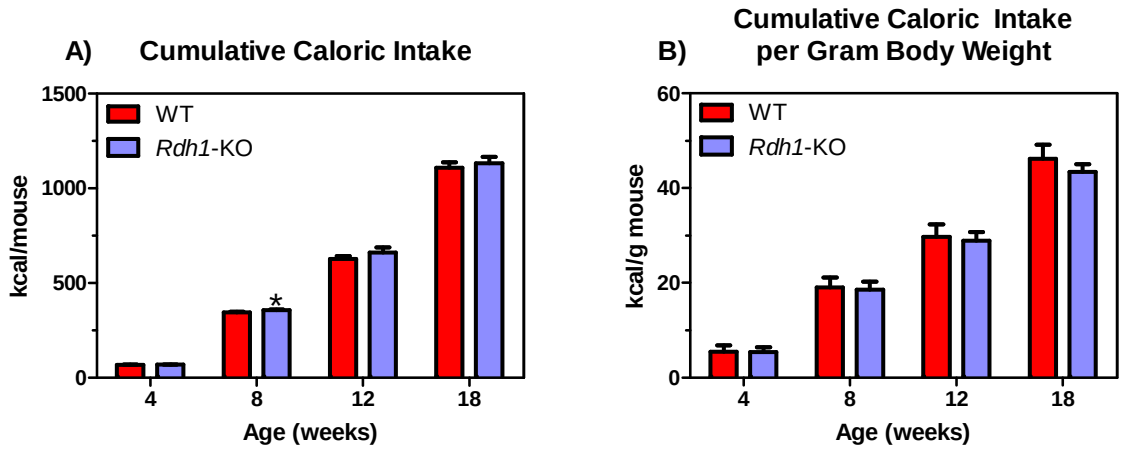

Legend: (A) Pooled cumulative caloric intake per mouse from multiple 93G-fed cohorts (2w2-11w2) at age 4 weeks (n=68 WT cages, 66 *Rdh1*-KO cages), 8 weeks (n=54 WT, 45 *Rdh1*-KO), 12 weeks (n=9 WT, 7 *Rdh1*-KO) and 18 weeks (n=8 WT, 7 *Rdh1*-KO). By two-way ANOVA, effects of age ($p \leq 0.0001$) and genotype ($p \leq 0.01$). (B) Pooled cumulative caloric intake normalized to mouse body weight from multiple 93G-fed cohorts (8w1-11w2) at ages 4 weeks (n=46 WT cages, 48 *Rdh1*-KO cages), 8 weeks (n=40 WT, 45 *Rdh1*-KO), 12 weeks (n=11 WT, 11 *Rdh1*-KO) and 18 weeks (n=6 WT, 4 *Rdh1*-KO). By two-way ANOVA, effect of age ($p \leq 0.0001$). WT: red bar. *Rdh1*-KO: blue bar. *$p \leq 0.05$ vs. WT by Student's two-tailed t-test. All values Mean $\pm$ SEM.

Table 5) Food Intake of *Rdh1*-KO Mice During CLAMS

Cohort	Age (wks)	WT (kcal/day)	*Rdh1*-KO (kcal/day)	Condition
VAD Diet Switched to 93G Diet at 11 Weeks				
3w1	4-5	19.3 ± 1.9 (6)	17.1 ± 0.6 (6)	*Ad lib* fed
3w1	9-10.5	21.9 ± 1.0 (6)	22.3 ± 1.9 (6)	*Ad lib* fed
3w1	12	15.9 ± 0.5 (2)	14.5 ± 0.4 (2)	*Ad lib* fed
VAD Diet Switched to 93G Diet at 5 Weeks				
3w2	8-9	20.8 ± 0.8 (5)	20.4 ± 1.1 (6)	*Ad lib* fed
4w1	15	12.8 ± 1.2 (6)	14.7 ± 0.6 (6)	*Ad lib* fed
AIN 93G Diet				
6w1	4	20.4 ± 0.8 (6)	19.5 ± 0.7 (6)	*Ad lib* fed
7w2	8	18.9 ± 1.4 (6)	16.5 ± 1.1 (9)	Refed
2w2	36-37	17.2 ± 1.1 (7)	18.4 ± 1.3 (8)	*Ad lib* fed

Legend: Food intake of male mice in metabolic cage studies at ages noted. Diets as in (Table 1). All values Mean ± SEM (number).

Figure 9) Hourly Food Intake of *Rdh1*-KO Mice

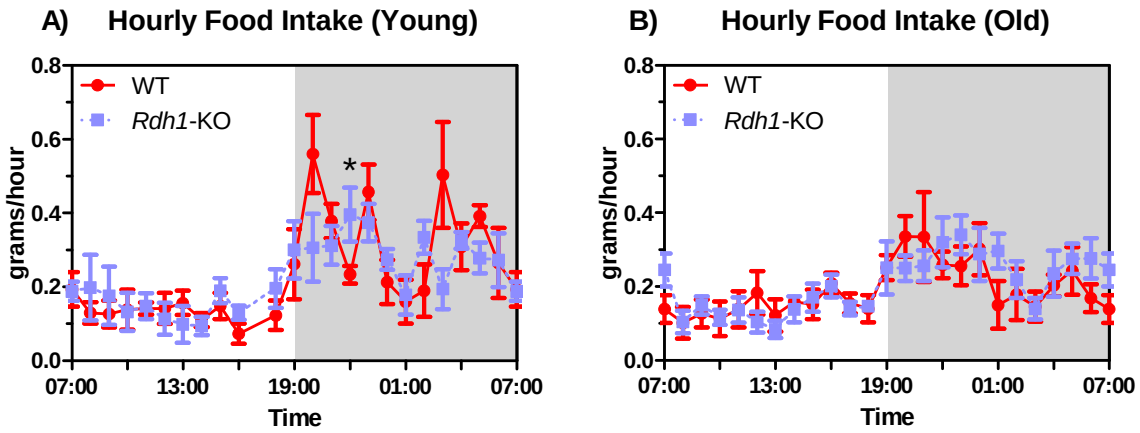

Legend: (A) Hourly food intake for male WT (n=6) and *Rdh1*-KO (n=6) mice age 4 weeks fed a 93G diet (cohort 6w1). By two-way ANOVA, effects of interaction between time and genotype ($p \leq 0.05$) and time ($p \leq 0.0001$). (B) Hourly food intake for male WT (n=7) and *Rdh1*-KO (n=8) mice age 36-37 weeks fed a 93G diet (cohort 2w2). By two-way ANOVA, effect of time ($p \leq 0.0001$). WT: red circle with solid line. *Rdh1*-KO: blue square with dotted line. Shaded area: dark period of light/dark cycle. *$p \leq 0.05$ vs. WT by Student's two-tailed t-test. All values Mean $\pm$ SEM

Table 6) Movement of *Rdh1*-KO mice During CLAMS

Cohort	Age (wks)	WT (avg. counts)	*Rdh1*-KO (avg. counts)	Number (WT, *Rdh1*-KO)	Condition
VAD Diet Switched to 93G Diet at 11 Weeks					
3w1	4-5	XM: 394 ± 61 AM: 198 ± 39 ZM: 58 ± 13	XM: 337 ± 47 AM: 161 ± 33 ZM: 51 ± 15	6, 6	*Ad lib* fed
3w1	9-10.5	XM: 364 ± 57 AM: 180 ± 34 ZM: 56 ± 14	XM: 394 ± 41 AM: 192 ± 30 ZM: 77 ± 22	6, 6	*Ad lib* fed
3w1	12	XM: 405 ± 37 AM: 203 ± 29 ZM: 73 ± 5	XM: 330 ± 137 AM: 170 ± 91 ZM: 60 ± 48	2, 2	*Ad lib* fed
VAD Diet Switched to 93G Diet at 5 Weeks					
3w2	8-9	XM: 336 ± 48 AM: 154 ± 34 ZM: 38 ± 15	XM: 360 ± 74 AM: 178 ± 48 ZM: 56 ± 19	5, 6	*Ad lib* fed
4w1	15	XM: 474 ± 96 AM: 269 ± 75 ZM: 130 ± 41	XM: 378 ± 61 AM: 200 ± 46 ZM: 100 ± 28	6, 6	*Ad lib* fed
3w2	18	XM: 312 ± 69 AM: 154 ± 46 ZM: 66 ± 22	XM: 496 ± 65 AM: 291 ± 53 ZM: 153 ± 18*	6, 6	Fasted
AIN 93G Diet					
6w1	4	XM: 308 ± 38 AM: 130 ± 21 ZM: 52 ± 18	XM: 286 ± 21 AM: 114 ± 11 ZM: 25 ± 18	6, 6	*Ad lib* fed
6w1	4	XM: 366 ± 38 AM: 178 ± 25 ZM: 100 ± 16	XM: 365 ± 45 AM: 187 ± 34 ZM: 86 ± 15	6, 6	Fasted
7w2	8	XM: 407 ± 45 AM: 223 ± 32 ZM: 79 ± 21	XM: 377 ± 28 AM: 197 ± 19 ZM: 96 ± 10	6, 8	Refed
7w2	8	XM: 492 ± 74 AM: 288 ± 56 ZM: 120 ± 33	XM: 419 ± 62 AM: 228 ± 42 ZM: 121 ± 31	6, 8	Fasted
11w2	9	XM: 339 ± 46 AM: 169 ± 32 ZM: 77 ± 22	XM: 561 ± 69 * AM: 326 ± 46 * ZM: 159 ± 21 *	5, 5	Fasted (16 hrs)
2w2	36-37	XM: 360 ± 28 AM: 172 ± 18 ZM: 177 ± 15	XM: 342 ± 24 AM: 171 ± 19 ZM: 190 ± 20	7, 8	*Ad lib* fed
2w2	36-37	XM: 592 ± 51 AM: 340 ± 40 ZM: 316 ± 40	XM: 369 ± 31* AM: 193 ± 20** ZM: 205 ± 20*	7, 9	Fasted

Legend: Movement of male mice, ages and diets as noted. XM: Total horizontal movement. AM: Ambulatory movement. ZM: Total vertical movement (rearing). **$p \leq 0.01$, *$p \leq 0.05$ vs. WT by Student's two-tailed t-test. All values Mean ± SEM.

Figure 10) Hourly Ambulatory Activity in *Rdh1*-KO Mice

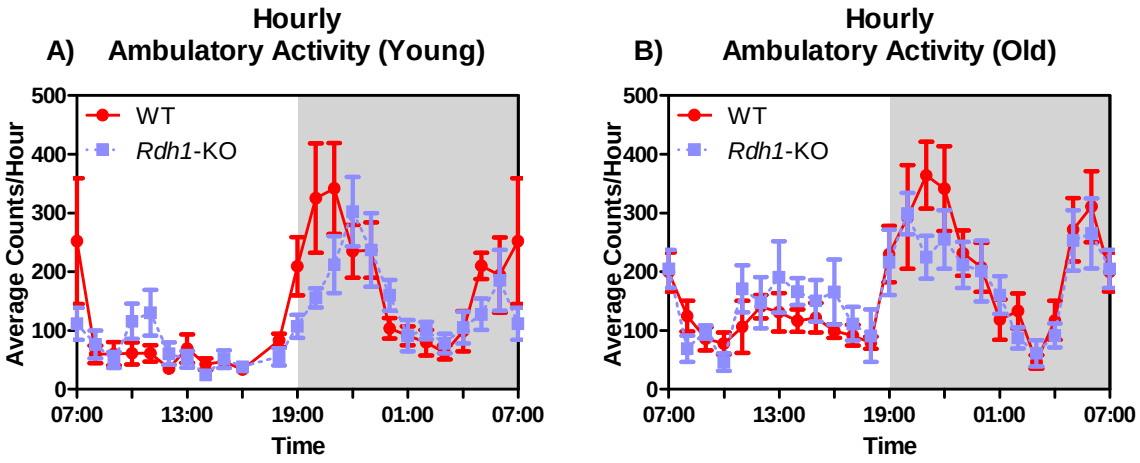

Legend: (A) Average hourly ambulatory activity for male WT (n=6) and *Rdh1*-KO (n=6) mice age 4 weeks fed a 93G diet (cohort 6w1). By two-way ANOVA, effect of time ($p \leq 0.0001$). (B) Average hourly ambulatory activity for male WT (n=7) and *Rdh1*-KO (n=8) mice age 36-37 weeks fed a 93G diet (cohort 2w2). By two-way ANOVA, effect of time ($p \leq 0.0001$). WT: red circle with solid line. *Rdh1*-KO: blue square with dotted line. Shaded area: dark period of light/dark cycle. All values Mean $\pm$ SEM

Table 7) Metabolic Parameters of *Rdh1*-KO Mice During CLAMS

Cohort	Age (wks)	WT	*Rdh1*-KO	Number (WT, KO)	Condition
VAD Diet Switched to 93G Diet at 11 Weeks					
3w1	4-5	O_2: 1937 ± 38 mL/kg/hr CO_2: 1790 ± 36 mL/kg/hr Heat: 0.499 ± 0.011 kcal/hr RER: 0.923 ± 0.012	O_2: 2017 ± 42 mL/kg/hr CO_2: 1877 ± 36 mL/kg/hr Heat: 0.508 ± 0.004 kcal/hr RER: 0.929 ± 0.005	6, 6	*Ad lib* fed
3w1	9-10.5	O_2: 1645 ± 23 mL/kg/hr CO_2: 1635 ± 31 mL/kg/hr Heat: 0.486 ± 0.008 kcal/hr RER: 0.993 ± 0.011	O_2: 1647 ± 20 mL/kg/hr CO_2: 1579 ± 28 mL/kg/hr Heat: 0.500 ± 0.010 kcal/hr RER: 0.955 ± 0.010	6, 6	*Ad lib* fed
3w1	12	O_2: 1752 ± 41 mL/kg/hr CO_2: 1564 ± 46 mL/kg/hr Heat: 0.523 ± 0.035 kcal/hr RER: 0.894 ± 0.004	O_2: 1658 ± 39 mL/kg/hr CO_2: 1441 ± 19 mL/kg/hr Heat: 0.570 ± 0.010 kcal/hr RER: 0.870 ± 0.007	2, 2	*Ad lib* fed
VAD Diet Switched to 93G Diet at 5 Weeks					
3w2	8-9	O_2: 1706 ± 17 mL/kg/hr CO_2: 1579 ± 20 mL/kg/hr Heat: 0.489 ± 0.009 kcal/hr RER: 0.924 ± 0.008	O_2: 1777 ± 56 mL/kg/hr CO_2: 1632 ± 46 mL/kg/hr Heat: 0.534 ± 0.011 kcal/hr* RER: 0.916 ± 0.013	5, 6	*Ad lib* fed
4w1	15	O_2: 1576 ± 32 mL/kg/hr CO_2:1363 ± 10 mL/kg/hr Heat: 0.519 ± 0.010 kcal/hr RER: 0.866 ± 0.019	O_2: 1539 ± 17mL/kg/hr CO_2: 1421 ± 10mL/kg/hr Heat: 0.513 ± 0.011 kcal/hr RER: 0.926 ± 0.009*	6, 6	*Ad lib* fed
3w2	18	O_2: 1342 ± 36 mL/kg/hr CO_2: 936 ± 18 mL/kg/hr** Heat: 0.441 ± 0.016 kcal/hr RER: 0.697 ± 0.007	O_2: 1534 ± 41 mL/kg/hr** CO_2: 1070 ± 23 mL/kg/hr** Heat: 0.532 ± 0.014 kcal/hr** RER: 0.6961 ± 0.004	6, 6	Fasted
AIN 93G Diet					
6w1	4	O_2: 1918 ± 55 mL/kg/hr CO_2: 1938 ± 68 mL/kg/hr Heat: 0.439 ± 0.011 kcal/hr RER: 1.012 ± 0.138	O_2: 1855 ± 33 mL/kg/hr CO_2: 1875 ± 48 mL/kg/hr Heat: 0.477 ± 0.008 kcal/hr * RER: 1.011 ± 0.015	6, 6	*Ad lib* fed
6w1	4	O_2: 1700 ± 27 mL/kg/hr CO_2: 1272 ± 20 mL/kg/hr Heat: 0.364 ± 0.007 RER: 0.745 ± 0.003	O_2: 1603 ± 26 mL/kg/hr* CO_2: 1199 ± 17 mL/kg/hr* Heat: 0.386 ± 0.007 kcal/hr RER: 0.747 ± 0.004	6, 6	Fasted
7w2	8	O_2: 1621 ± 33 mL/kg/hr CO_2: 1625 ± 46 mL/kg/hr Heat: 0.502 ± 0.031 kcal/hr RER: 1.000 ± 0.013	O_2: 1570 ± 32 mL/kg/hr CO_2: 1541 ± 25 mL/kg/hr Heat: 0.490 ± 0.016 kcal/hr RER: 0.983 ± 0.011	6, 8	Refed
7w2	8	O_2: 1502 ± 31 mL/kg/hr CO_2: 1098 ± 19 mL/kg/hr Heat: 0.433 ± 0.018 kcal/hr RER: 0.728 ± 0.003	O_2: 1468 ± 34 mL/kg/hr CO_2: 1071 ± 24 mL/kg/hr Heat: 0.429 ± 0.015 kcal/hr RER: 0.729 ± 0.002	6, 8	Fasted
11w2	9	O_2: 1547 ± 18 mL/kg/hr CO_2: 1104 ± 14 mL/kg/hr Heat: 0.437 ± 0.006 kcal/hr RER: 0.711 ±0.002	O_2: 1629 ± 52 mL/kg/hr CO_2: 1161 ± 37 mL/kg/hr Heat: 0.478 ± 0.015kcal/hr* RER: 0.711 ± 0.001	8, 8	Fasted (16 hrs)
2w2	36-37	O_2: 1380 ± 26 mL/kg/hr CO_2: 1208 ± 33 mL/kg/hr Heat: 0.616 ± 0.011 kcal/hr RER: 0.875 ± 0.013	O_2: 1341 ± 19 mL/kg/hr CO_2: 1162 ± 21 mL/kg/hr Heat: 0.641 ± 0.014 kcal/hr RER: 0.866 ± 0.014	7, 8	*Ad lib* fed
2w2	36-37	O_2: 1295 ± 26 mL/kg/hr CO_2: 925 ± 16 mL/kg/hr Heat: 0.560 ± 0.013 kcal/hr RER: 0.715 ± 0.008	O_2: 1248 ± 29 mL/kg/hr CO_2: 889 ± 20mL/kg/hr Heat: 0.584 ± 0.014 kcal/hr RER: 0.713 ± 0.007	7, 9	Fasted

Legend: (See next page.)

Legend: Metabolic parameters measured via indirect calorimetry in male mice at ages and diets as noted. O_2: Oxygen consumed. CO_2: Carbon dioxide produced. Heat: Energy expended. RER: Respiratory exchange ratio. **$p \leq 0.01$,*$p \leq 0.05$ vs. WT by Student's two-tailed t-test. All values Mean $\pm$ SEM.

Table 8) Summary of Cold Challenges of *Rdh1*-KO Mice

Cohort	Age (wks)	Sex	Final Temperature (ºC, change from initial)	Weight Change (grams, relative)	Food Intake (g)	# Removed from Study/Total (time removed)
2w2	57	Male	WT: 33.9 ± 1.4 -2.9 ± 1.1 KO: 35.2 ± 0.4 -1.3 ± 1.2	WT: -4.3 ± 0.4 -9.0 ± 0.6% KO: -4.9 ± 0.2 -8.9 ± 0.5%	Fasted	WT: 2/6 (9, 21 hrs) KO: 1/6 (24 hrs)
2w2	57	Female^	WT: 36.1 ± 0.3 -1.4 ± 0.3 KO: 36.4 ± 0.3 -0.8 ± 0.5	WT: -3.4 ± 0.3 -10.3 ± 1.1% KO: -3.5 ± 0.2 -8.6 ± 0.4%	Fasted	WT: 1/6 (16.5 hrs) KO: 0/6
3w2 (5 wks VAD)	11	Male	WT: 34.6 ± 0.4 -2.5 ± 0.4 KO: 34.6 ± 0.8 -2.9 ± 1.0	WT: -3.7 ± 0.1 -14.6 ± 0.5% KO: -5.4 ± 0.3* -18.9 ± 0.6%**	Fasted	WT: 0/6 KO: 2/6 (18,19 hrs)
3w2 (5 wks VAD)	16	Female	WT: 33.9 ± 0.6 -3.6 ± 0.8 KO: 34.6 ± 0.3 -2.7 ± 1.3	WT: -3.9 ± 0.2 -16.8 ± 0.8% KO: -4.0 ± 0.1 -16.48 ± 0.01%	Fasted	WT: 2/6 (18, 24 hrs) KO: 4/6 (16, 16, 16, 24 hrs)
3w2 (5 wks VAD)	19	Male	WT: 36.8 ± 0.3 -0.1 ± 0.6 KO: 37.8 ± 0.8* -1.4 ± 0.5	WT: -1.3 ± 0.3 -4.3 ± 0.9% KO: -0.3 ± 0.3* -2.1 ± 1.2%	WT: 3.0 ± 0.6 KO: 4.6 ± 0.1*	WT: 0/4 KO: 0/4
4w1 (5 wks VAD)	8	Male	WT: 34.1 ± 0.5 -3.3 ± 0.8 KO: 34.3 ± 0.7 -3.2 ± 0.7	WT: -3.9 ± 0.2 -17.5 ± 0.5% KO: -3.7 ± 0.1 -16.4 ± 0.6%	Fasted	WT: 1/7 (21 hrs) KO: 2/9 (22.5, 24 hrs)
6w1	6	Male	WT: 33.3 ± 0.9 -5.0 ± 1.1 KO: 35.4 ± 0.2 -3.0 ± 0.3	WT: -4.1 ± 0.1 -20.3 ± 0.5% KO: -4.4 ± 0.1 -20.3 ± 0.6%	Fasted	WT: 1/6 (21 hrs) KO: 0/5
6w1	6	Male	WT: 38.1 ± 0.2 0.2 ± 0.2 KO: 37.6 ± 0.2 -0.1 ± 0.2	WT: -0.60 ± 0.19 -3.3 ± 1.0% KO: -0.65 ± 0.17 -3.0 ± 0.8%	WT: 4.3 ± 0.2 KO: 4.5 ± 0.2	WT: 0/5 KO: 0/5
						# Removed/Total Fasted (%) **WT: 7/37 (19%)** **KO: 9/38 (24%)**

Legend: Final temperature and weight change calculated from mice, age and sex as noted, maintaining a safe body temperature for 24 hours housed at 4º C. Diets as in (Table 1). Animals were removed from study upon reaching a body temperature at or below 29º C. ^Ended at 19 hrs not 24. **p≤0.01, *p≤0.05 vs. WT by Student's two-tailed t-test. All values Mean ± SEM.

Figure 11) Representative β_3-adrenergic Challenge of *Rdh1*-KO Mice

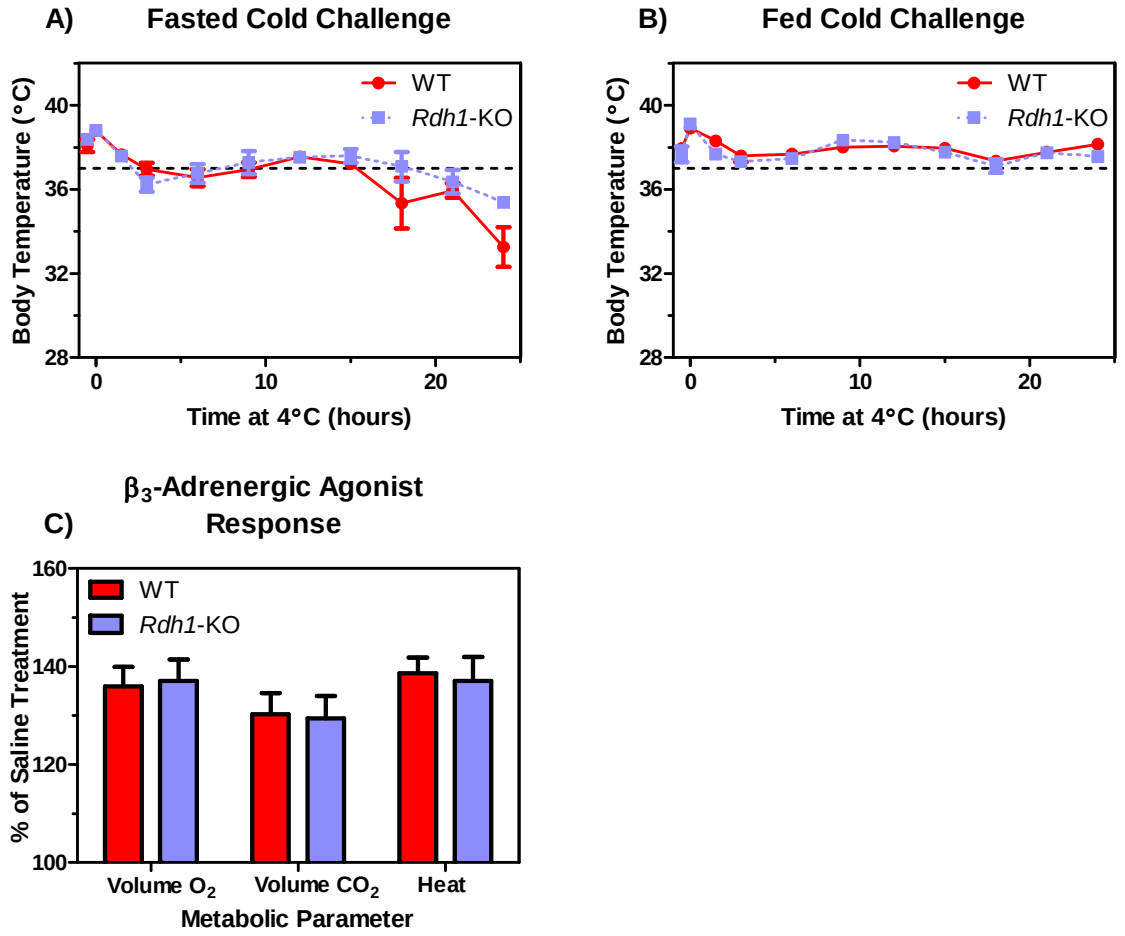

Legend: (A) Body temperatures of 6 week old, fasted male WT (n=5) and *Rdh1*-KO (n=6) mice normally fed a 93G diet (cohort 6w1). Data excludes a 6th WT mouse removed from study due to low body temperature at 21 hours of exposure. By two-way ANOVA, effects of genotype ($p \leq 0.05$) and time ($p \leq 0.0001$). (B) Body temperatures of 6 week old, male WT (n=5) and *Rdh1*-KO (n=5) mice fed a 93G diet (cohort 6w1). By two-way ANOVA, effect of time ($p \leq 0.0001$). (C) Metabolic response of 6-7 week old, 93G-fed male WT (n=9) and *Rdh1*-KO (n=7) mice to treatment with β_3-adrenergic agonist (cohort 6w1). WT: red circle with solid line or red bar. *Rdh1*-KO: blue square with dotted line or blue bar. Dotted black line indicates 37º C. All values Mean $\pm$ SEM.

Table 9) β_3-adrenergic Agonist Studies of *Rdh1*-KO Mice

Cohort	Age (wks)	WT (% pre-induction)	*Rdh1*-KO (% pre-induction)	Normalized to:	Number (WT, KO)
2w2	58	O_2: 114 ± 4% CO2: 110 ± 5% Heat: 113 ± 4%	O_2: 114 ± 11% CO_2: 114 ± 11% Heat: 114 ± 11%	Pre-injection	4, 4
3w2 (5 wks VAD)	14-15	O_2: 134 ± 4% CO2: 130 ± 4% Heat: 134 ± 4%	O_2: 130 ± 3% CO_2: 127 ± 3% Heat: 129 ± 3%	Pre-injection	6, 7
5w1 (HFD)	17	O_2: 123 ± 6% CO_2: 121 ± 6% Heat: 123 ± 6%	O_2: 103 ± 2%** CO_2: 95 ± 2%** Heat: 99 ± 3%**	Pre-injection	5, 6
5w1 (HFD)	19	O_2: 129 ± 4% CO_2: 130 ± 5% Heat: 129 ± 4%	O_2: 134 ± 3% CO_2: 132 ± 3% Heat: 133 ± 3%	Pre-injection	5,6
6w1	6-7	O_2: 136 ± 4% CO_2: 130 ± 4% Heat: 139 ± 3%	O_2: 137 ± 4% CO_2: 129 ± 5% Heat: 137 ± 5%	Saline injection	9,7

Legend: Normalized metabolic response of male mice, ages as noted, to β_3-adrenergic agonist. Diets as in (Table 1). O_2: Oxygen consumed. CO_2: Carbon dioxide produced. Heat: Energy expended. **$p \leq 0.01$ vs. WT by Student's two-tailed t-test. All values Mean ± SEM

Table 10) Body Temperature Data of *Rdh1*-KO Mice Before and After CLAMS

Cohort	Age (wks)	Initial Temperature (ºC)	Final Temperature (ºC)	Change in Temperature (ºC)	Condition	Number (WT, KO)
3w1 (11 wks VAD)	18	WT: 38.4 ± 0.1 KO: 38.5 ± 0.1	WT: 36.7 ± 0.5 KO: 35.7 ± 0.7	WT: -1.7 ± 0.5 KO: -2.8 ± 0.7*	Fasted 24 hours	4, 4
6w1	4	WT: 38.0 ± 0.4 KO: 37.6 ± 0.2	WT: 37.8 ± 0.4 KO: 37.7 ± 0.4	WT: -0.2 ± 0.4 KO: -0.1 ± 0.5	*Ad lib* fed 24 hours	6, 6
6w1	4	WT: 37.8 ± 0.4 KO: 37.7 ± 0.4	WT: 36.6 ± 0.2 KO: 36.2 ± 0.2*	WT :-1.3 ± 0.5 KO: -1.5± 0.5	Fasted 24 hours	6, 6
7w2	8	WT: 37.8 ± 0.4 KO: 37.1 ± 0.4*	WT: 35.9 ± 0.5 KO: 36.1 ± 0.5	WT: -1.8 ± 0.8 KO: -1.1± 0.6	Fasted 24 hours	6, 9
7w2	8	WT: 35.9 ± 0.5 KO: 36.1 ± 0.5	WT: 36.6 ± 0.5 KO: 36.5 ± 0.4	WT: 0.6 ± 0.6 KO: 0.4 ± 0.2	Refed 24 hours	6, 9

Legend: Average body temperature of male mice at ages and conditions noted. Diets as in (Table 1). *p≤0.05 vs. WT by Student's two-tailed t-test. All values Mean ± SEM.

Figure 12) Fasted and Refed Body Temperatures of *Rdh1*-KO Mice

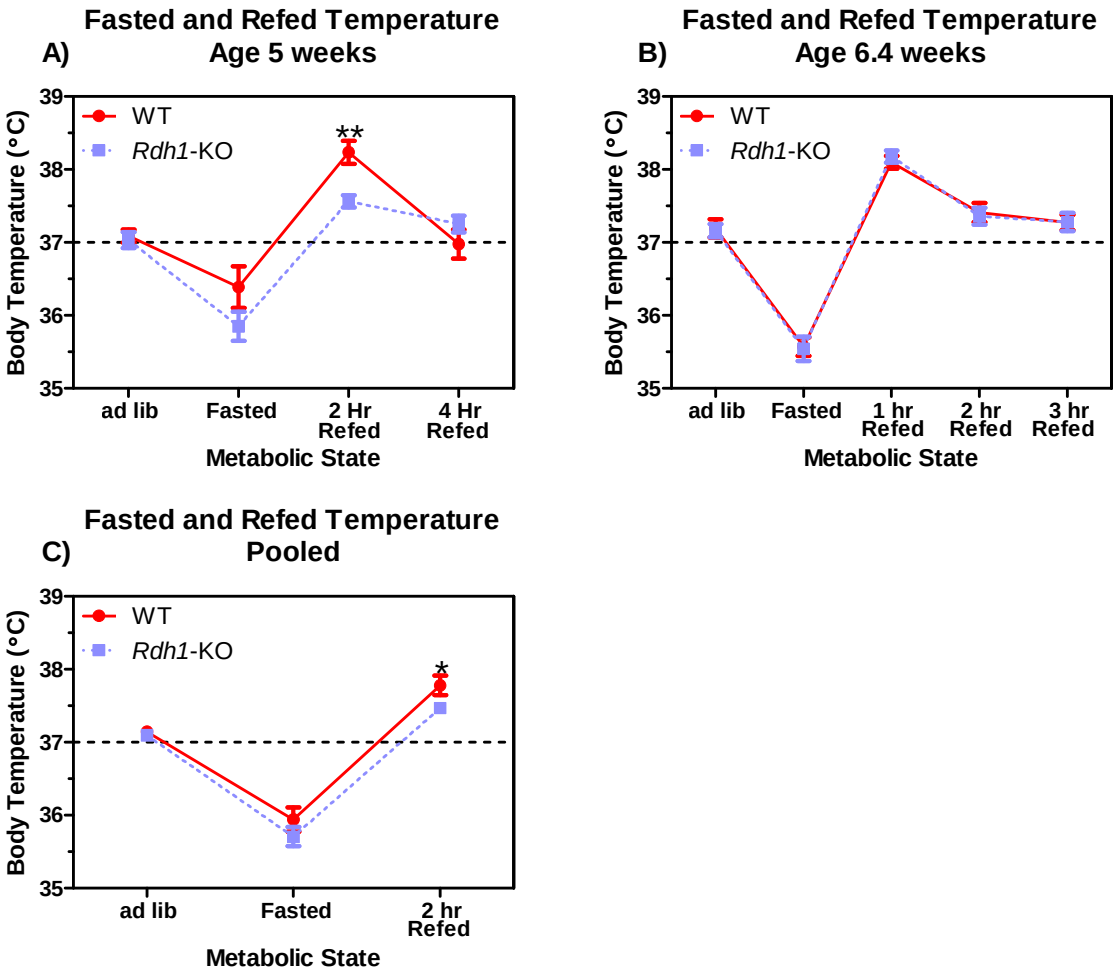

Legend: (A) Body temperatures of 5 week old male WT (n=9) and *Rdh1*-KO (n=16) mice before and after fast and at times indicated during refeeding. Mice were fed a 93G diet (cohort 6w1). By two-way ANOVA, effects of interaction between genotype and metabolic state ($p \leq 0.05$), genotype ($p \leq 0.05$) and metabolic state ($p \leq 0.0001$). (B) Body temperatures of 6.4 week old male WT (n=11) and *Rdh1*-KO (n=14) mice before and after fast, and at times indicated during refeeding. Mice were fed a 93G diet (cohort 9w1). By two-way ANOVA, effect of metabolic state ($p \leq 0.0001$). (C) Combined body temperatures from (A) and (B). By two-way ANOVA, effects of genotype ($p \leq 0.05$) and metabolic state ($p \leq 0.0001$). WT: red circle with solid line. *Rdh1*-KO: blue square with dotted line. Dotted black line indicates 37º C. **$p \leq 0.01$, *$p \leq 0.05$ vs. WT by Student's two-tailed t-test. All values Mean $\pm$ SEM.

Figure 13) Average Daytime Body Temperatures of *Rdh1*-KO Mice

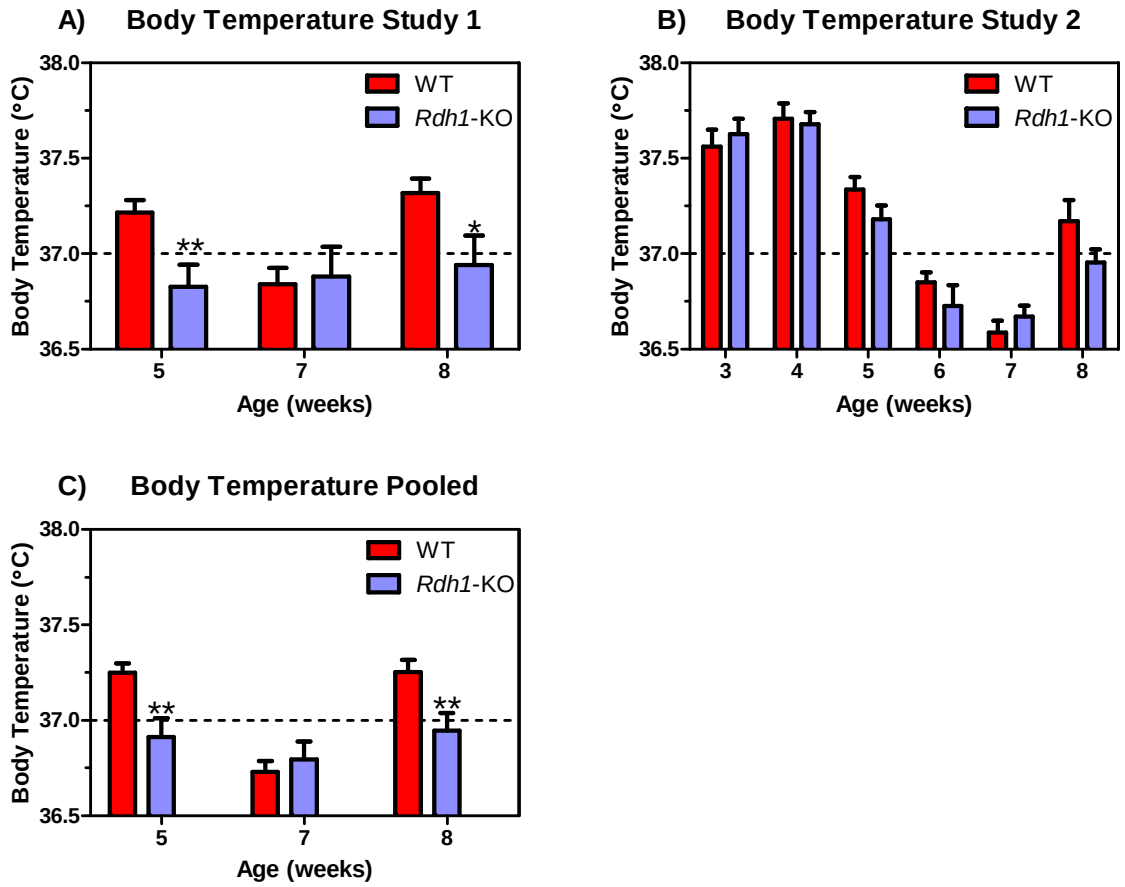

Legend: (A) Average daytime body temperatures of male WT (n=22) and *Rdh1*-KO (n=10) mice. Mice were fed a 93G diet (cohort 6w1). By two-way ANOVA, effects of genotype ($p \leq 0.01$) and age ($p \leq 0.05$). (B) Average daily body temperatures of male WT (n=14-17) and *Rdh1*-KO (n=6-7) mice. Mice were maintained on a 93G diet (cohort 6w2). By two-way ANOVA, effect of age ($p \leq 0.0001$). (C) Pooled data from (A) and (B) (n=39-40 WT, 17-18 *Rdh1*-KO). By two-way ANOVA, effects of interaction between age and genotype ($p \leq 0.05$), genotype ($p \leq 0.01$) and age ($p \leq 0.0001$). WT: red bar. *Rdh1*-KO: blue bar. Dotted black line indicates 37º C. $^{**}p \leq 0.01$, $^{*}p \leq 0.05$ vs. WT by Student's two-tailed t-test. All values Mean $\pm$ SEM.

Figure 14) Glucose and Insulin Tolerance in Aged *Rdh1*-KO Mice

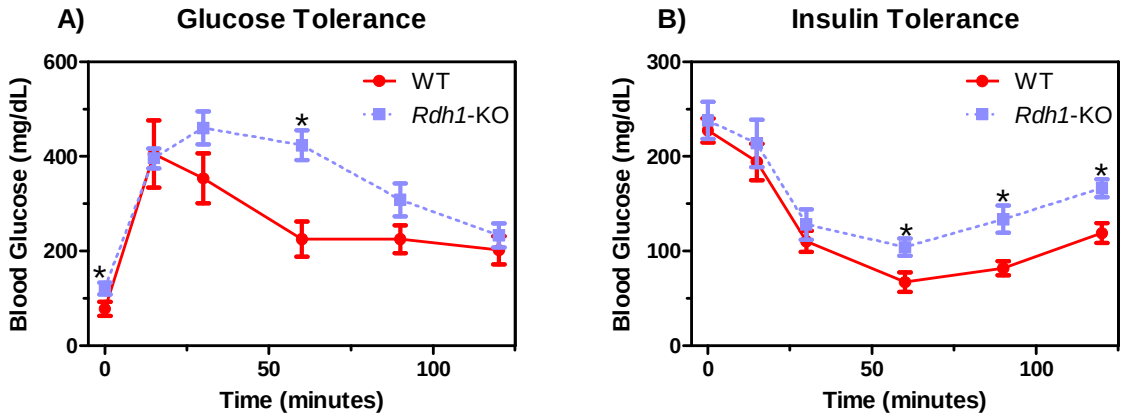

Legend: (A) Blood glucose levels of 24-25 week old male WT (n=7) and *Rdh1*-KO (n=9) mice during a glucose tolerance test. Mice were fed a 93G diet (cohort 2w2). By two-way ANOVA, effects of genotype ($p \leq 0.001$) and time ($p \leq 0.0001$). (B) Blood glucose levels of 25-26 week old male WT (n=7) and *Rdh1*-KO (n=9) mice during an insulin tolerance test. Same group as (A) (cohort 2w2). By two-way ANOVA, effects of genotype ($p \leq 0.001$) and time ($p \leq 0.0001$). WT: red circle with solid line. *Rdh1*-KO: blue square with dotted line. *$p \leq 0.05$ vs. WT by Student's two-tailed t-test. All values Mean $\pm$ SEM.

Figure 15) Serum Insulin and Pyruvate, Glucose and Insulin Tolerance in Young *Rdh1*-KO Mice

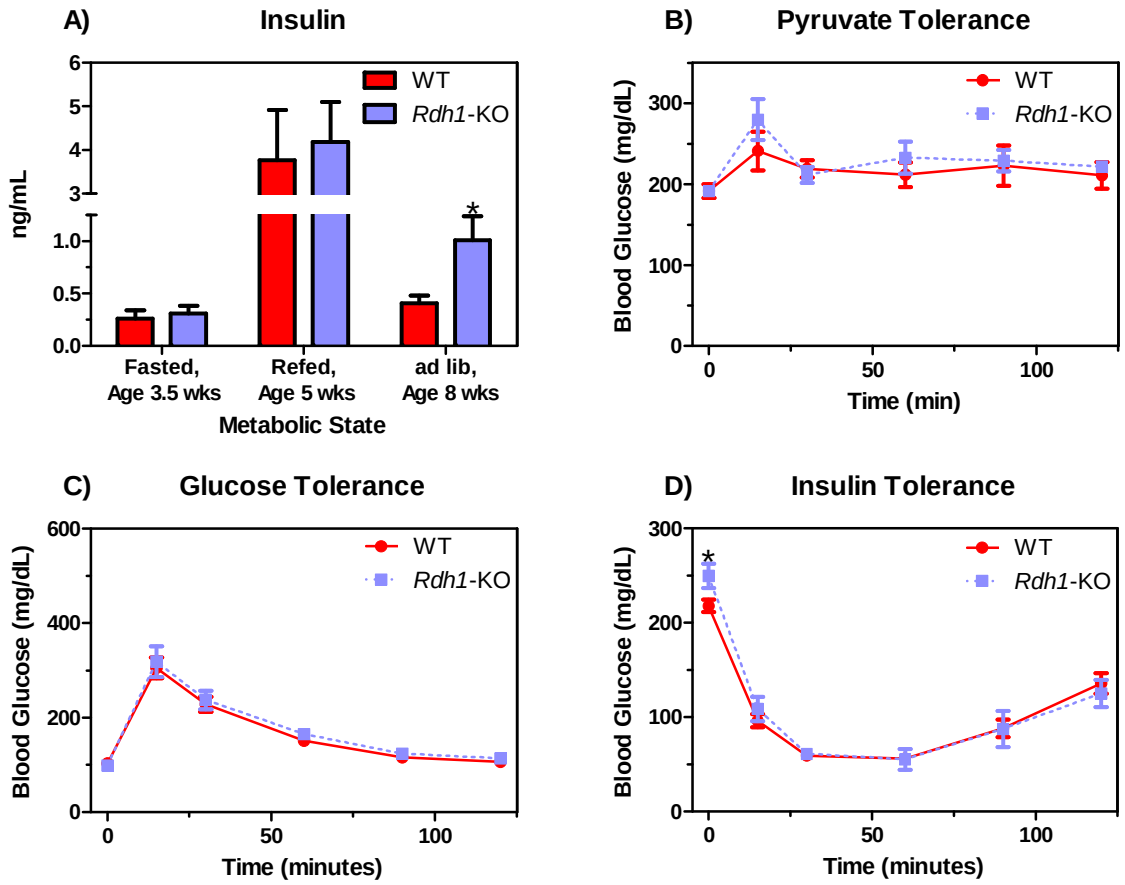

Legend: (A) Insulin levels in fasted mice age 3.5 weeks (WT, n=11; *Rdh1*-KO, n=14) (cohort 9w2), 2-3.5 hour refed mice age 5 weeks (WT, n=11; *Rdh1*-KO, n=9) (cohort 11w1) and *ad lib* fed mice age 8 weeks (WT, n=10; *Rdh1*-KO, n= 10) (cohort 6w1). All cohorts 93G fed. (B) Blood glucose levels of 8 week old male WT (n=5) and *Rdh1*-KO (n=4) mice during a pyruvate tolerance test. Mice were fed a 93G diet (cohort 6w2). By two-way ANOVA, effect of time ($p \leq 0.01$). (C) Blood glucose levels of 4-5 week old male WT (n=11) and *Rdh1*-KO (n=11) mice during a glucose tolerance test. Mice were fed a 93G diet (cohort 6w1). By two-way ANOVA, effect of time ($p \leq 0.0001$). (D) Blood glucose levels of 4-5 week old male WT (n=12) and *Rdh1*-KO (n=8) mice during an insulin tolerance test. Same group as (C) (cohort 6w1). By two-way ANOVA, effect of time ($p \leq 0.0001$). WT: red circle with solid line or red bar *Rdh1*-KO: blue square with dotted line or blue bar. **$p \leq 0.01$, *$p \leq 0.05$ vs. WT by Student's two-tailed t-test. All values Mean $\pm$ SEM.

Figure 16) Glucose and Insulin Tolerance in an Insulin Sensitive Cohort of *Rdh1*-KO Mice

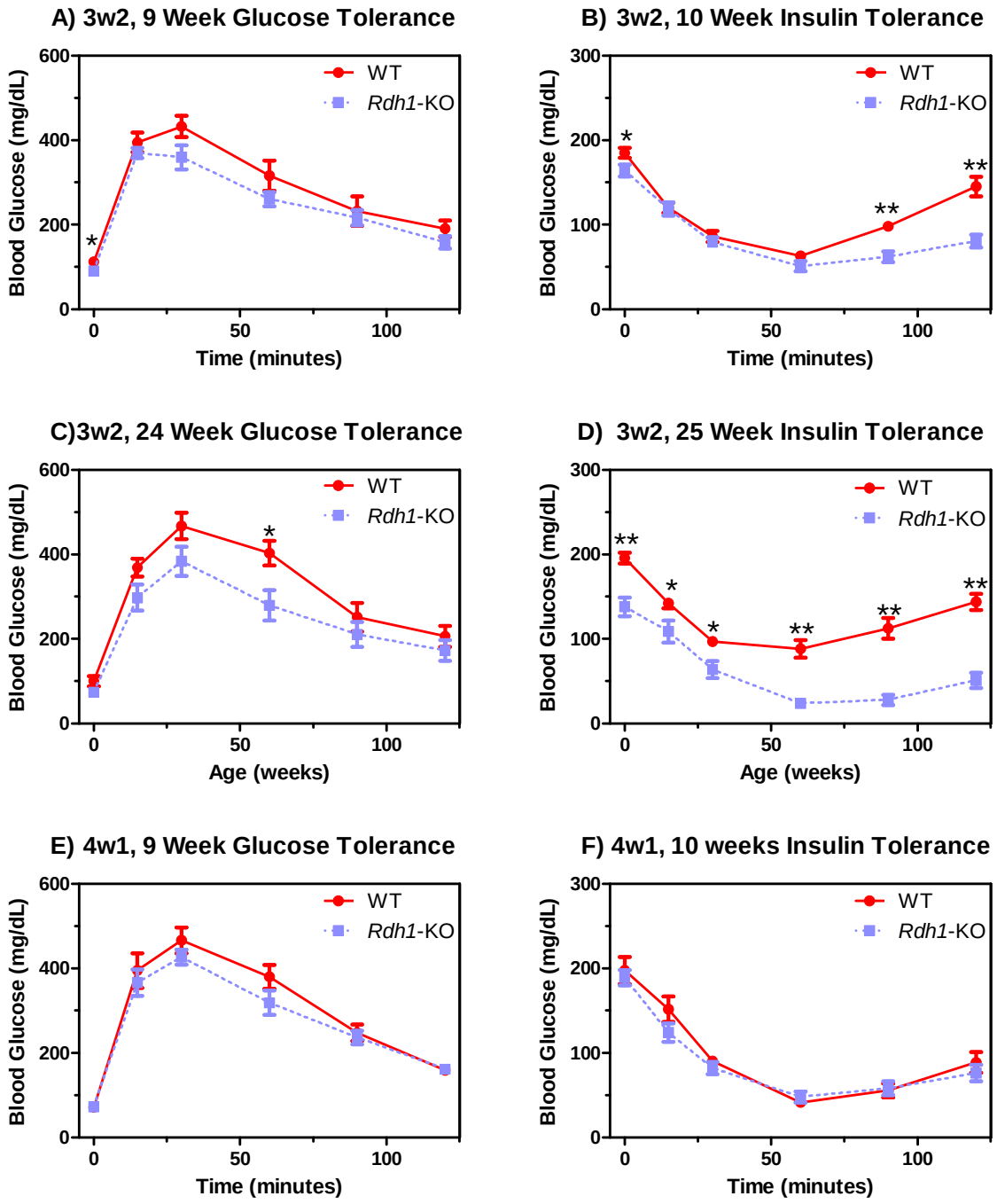

Legend: (See next page)

Legend: (A) Blood glucose levels of 9 week old male WT (n=9) and *Rdh1*-KO (n=12) mice during a glucose tolerance test. Mice were fed VAD diet until age 5 weeks, and then switched to 93G diet. Dams of mice shown were switched from Harlan chow diet to VAD diet at mating (cohort 3w2). By two-way ANOVA, effects of genotype ($p \leq 0.01$) and time ($p \leq 0.0001$). (B) Blood glucose levels of 10 week old male WT (n=10) and *Rdh1*-KO (n=12) mice during an insulin tolerance test. Same group as (A) (cohort 3w2). By two-way ANOVA, effects of interaction between time and genotype ($p \leq .0.0001$), genotype ($p \leq 0.0001$) and time ($p \leq 0.0001$). (C) Blood glucose levels of 24 week old male WT (n=9) and *Rdh1*-KO (n=10) mice during a glucose tolerance test. Same group as (A) (cohort 3w2). By two-way ANOVA, effects of genotype ($p \leq 0.0001$) and time ($p \leq 0.0001$). (D) Blood glucose levels of 10 week old male WT (n=9) and *Rdh1*-KO (n=9) mice during an insulin tolerance test. Same group as (A) (3w2). By two-way ANOVA, effects of interaction between time and genotype ($p \leq .0.01$), genotype ($p \leq 0.0001$) and time ($p \leq 0.0001$). (E) Blood glucose levels of 9 week old male WT (n=7) and *Rdh1*-KO (n=9) mice during a glucose tolerance test. Mice were fed VAD diet until age 5 weeks, and then switched to 93G diet. Dams of mice shown were switched from Harlan chow diet to VAD diet at mating (cohort 4w1). By two-way ANOVA, effect of time ($p \leq 0.0001$). (F) Blood glucose levels of 10 week old male WT (n=7) and *Rdh1*-KO (n=9) mice during an insulin tolerance test. Same group as (E) (4w1). By two-way ANOVA, effect of time ($p \leq 0.0001$). WT: red circle with solid line. *Rdh1*-KO: blue square with dotted line. **$p \leq 0.01$, *$p \leq 0.05$ vs. WT by Student's two-tailed t-test. All values Mean $\pm$ SEM.

Table 11) Serum Lipid Factors in *Rdh1*-KO Mice

Serum Factor	WT	*Rdh1*-KO	Condition
Free Fatty Acid	209.1 ± 16.5 μM (6)	219.4 ± 13.7 μM (6)	Fasted
	79.1 ± 6.7 μM (8)	79.4 ± 7.0 μM (8)	*Ad lib* fed
Glycerol	148.4 ± 5.1 μM (6)	146.0 ± 24.4 μM (6)	Fasted
	229.9 ± 18.9 μM (8)	281.2 ± 46.8 μM (8)	*Ad lib* fed
Triglyceride	115.1 ± 7.1 mg/dL (11)	123.6 ± 7.3 mg/dL (12)	*Ad lib* fed

Legend: Lipid factors from 7-8.5 week old male mice fed a 93G diet (cohort 6w1). All values Mean ± SEM (number).

Table 12) Inflammatory Markers in *Rdh1*-KO Mice

Inflammatory Marker	WT	*Rdh1*-KO
TNFα	*not detected*, (0/10)	*not detected*, (0/10)
MCP-1	19 ± 3 pg/mL, (4/10)	*not detected*, (0/10)
IL-6	15 ± 1 pg/mL, (2/10)	29 ± 16 pg/mL, (3/10)

Legend: Serum inflammation markers in 7-8.5 week old male mice fed a 93G diet (cohort 6w1). All values Mean ± SEM, (# of mice with detectable levels/ # of mice assayed). In the assay used, the limit of detection for each analyte was is 12.2 pg/mL.

Figure 17) Rdh, Raldh and *Crabp2* Gene Expression by Tissue

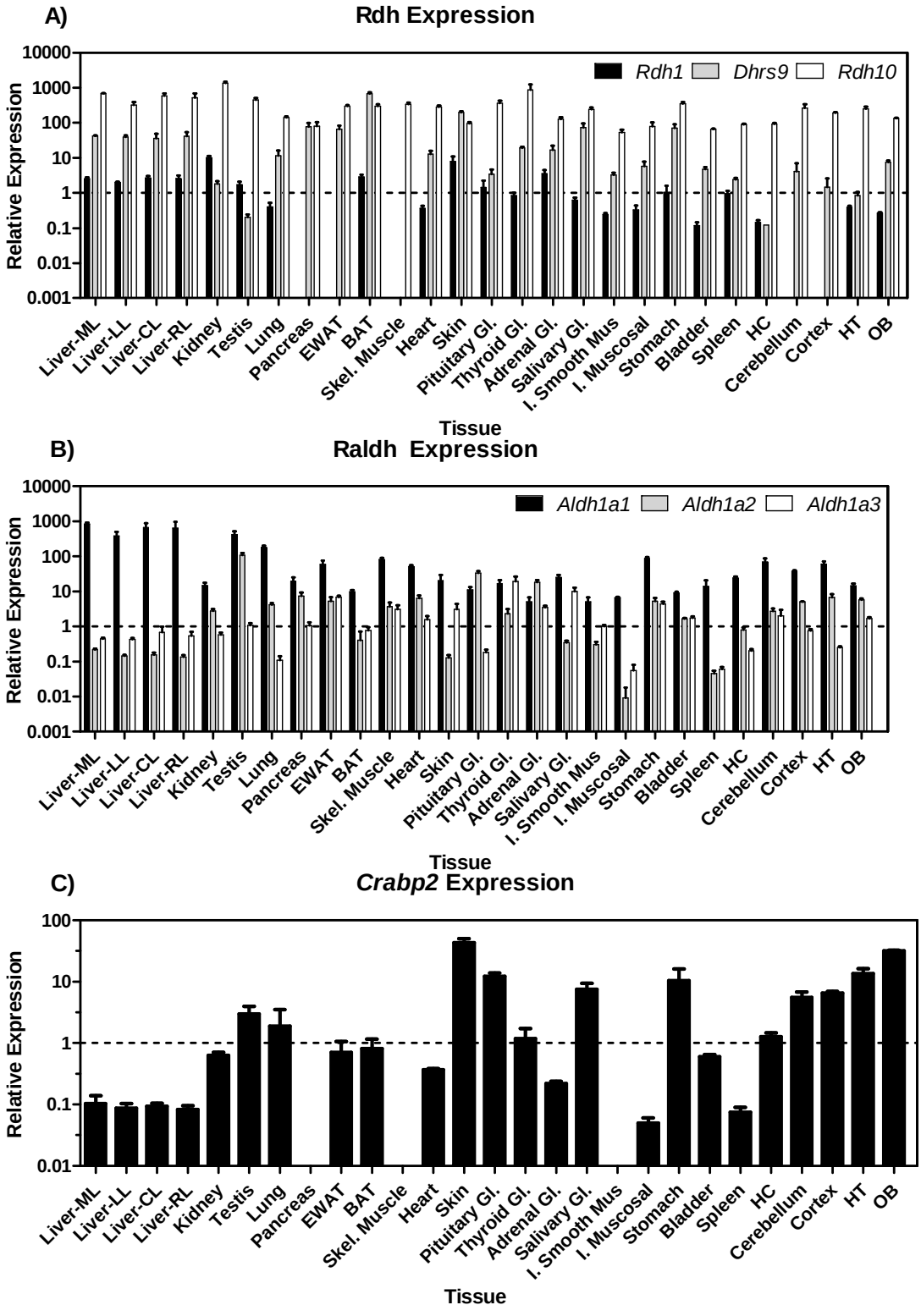

Legend: (See next page.)

Legend: (A) Relative expression of Rdh in 4 week old, fasted C57BL/6 mice fed a 93G diet (n=3). Data arbitrarily normalized to median *Rdh1* expression (dotted line). *Rdh1*: black bar. *Dhrs9*: grey bar. *Rdh10*: white bar. (B) Relative expression of Raldh in mice from (A). Data arbitrarily normalized to median *Raldh3* expression (dotted line). *Raldh1*: black bar. *Raldh2*: grey bar. *Raldh3*: white bar. (C) Relative expression of *Crabp2* in mice from (A). Data arbitrarily normalized to median expression (dotted line). ML, Median Lobe; LL, Left Lobe, CL, Caudate Lobe; RL, Right Lobe; BAT, brown adipose; EWAT, epididymal white adipose; Skel, Skeletal; I. Smooth Mus, Intestinal Smooth Muscle; Gl., Gland; HC, Hippocampus; HT, Hypothalamus; OB, Olfactory Bulb. Missing values indicate expression below the limit of detection. All values Mean $\pm$ SEM.

Figure 18) Rdh Expression with Age, Diet and Genotype

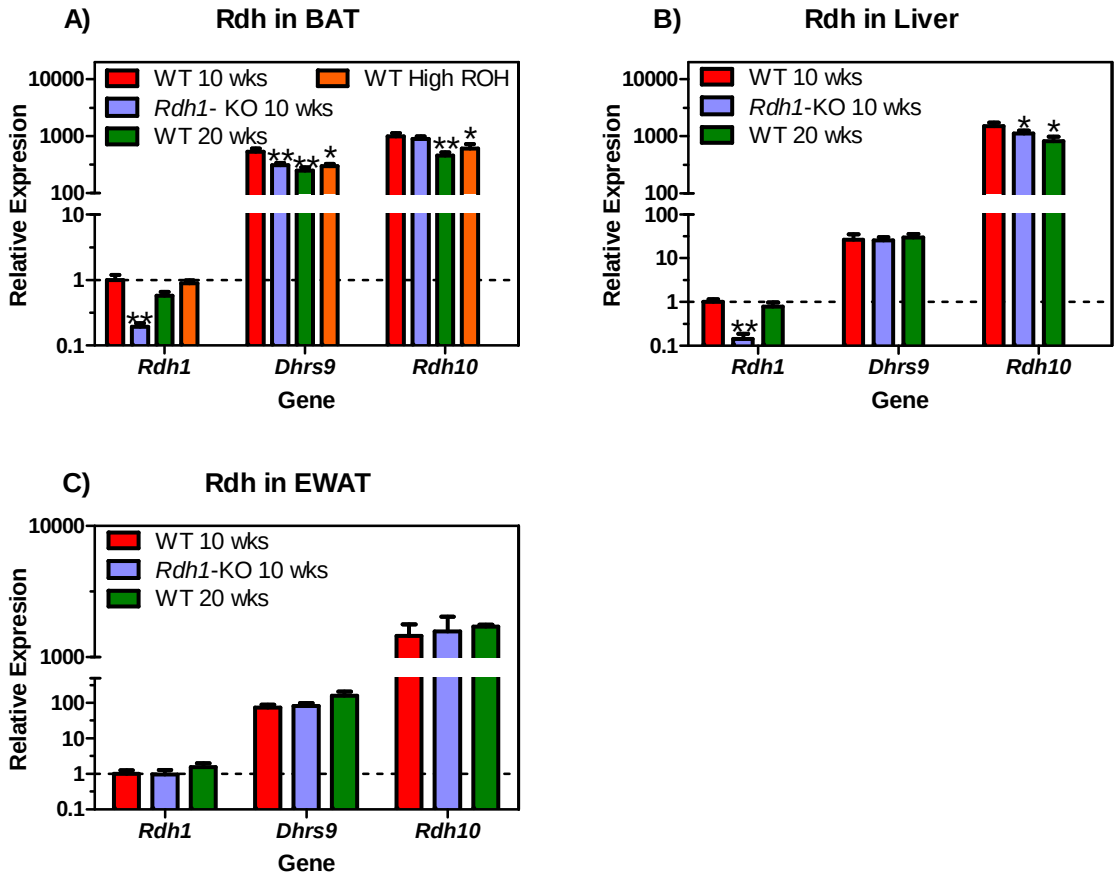

Legend: (A) Relative expression of RDH in brown adipose from 10 week old WT (n=11) (WT 10 wks), 10 week old *Rdh1*-KO (n=9-10) (*Rdh1*-KO 10 wks), 18-20 week old WT (n=7-8) (WT 20 wks) and 10 week old WT fed a high retinol diet (n=5) (WT High ROH). Mice were fed a 93G diet, except WT High ROH mice, who were fed 93G diet until age 5 weeks, then switched to a modified AIN 93G diet with 30 IU/g of vitamin A (cohort 8w2). (B) Relative expression of RDH in liver (WT 10 wks, n=9-10; *Rdh1*-KO 10 wks, n=6-9; WT 20 wks, n=4). Same mice as (A) (cohort 8w2). (B) Relative expression of RDH in EWAT (WT 10 wks, n=5-9; *Rdh1*-KO 10 wks, n=5-6; WT 20 wks, n=4). Same mice as (A) (cohort 8w2). Data for each tissue arbitrary normalized to mean WT 10 wk *Rdh1* expression (dotted lines). WT 10 wks: red bar. *Rdh1*-KO 10 wks: blue bar. WT 20 wks: green bar. WT High ROH: orange bar. **$p \leq 0.01$, *$p \leq 0.05$ vs. WT by Student's two-tailed t-test. All values Mean $\pm$ SEM.

Figure 19) Rdh and Raldh Expression across Adipose Depots

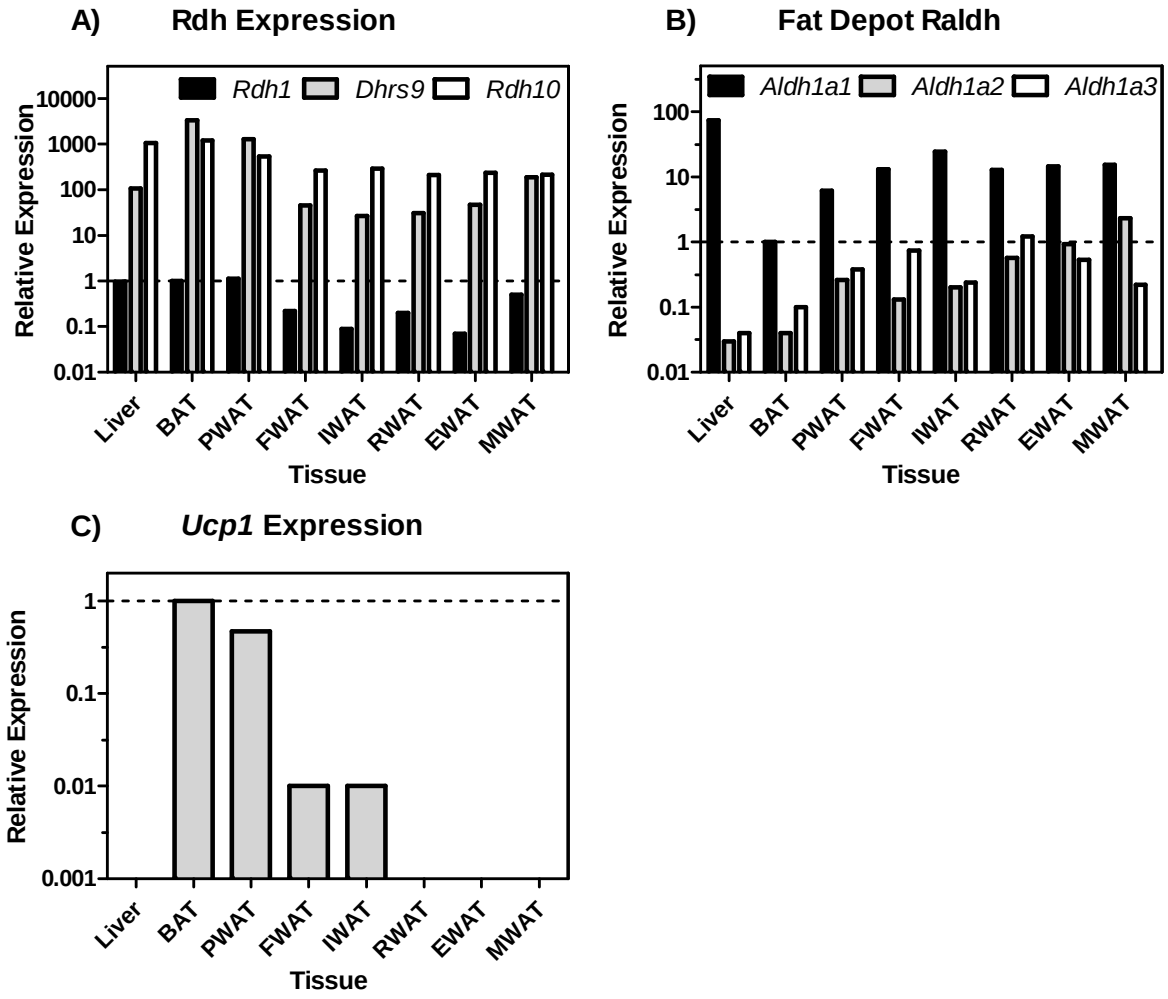

Legend: (A) Relative Rdh expression across adipose depots and liver from an 8-week old C57BL/6 mouse fed a 93G diet under *ad lib* fed conditions (n=1). Data arbitrary normalized to BAT *Rdh1* expression (dotted line). *Rdh1*: black bar. *Dhrs9*: grey bar. *Rdh10*: white bar. (B) Relative Raldh expression across adipose depots and liver from mouse in (A). Data arbitrary normalized to BAT *Raldh1* expression (dotted line). *Raldh1*: black bar. *Raldh2*: grey bar. *Raldh3*: white bar. (C) Relative *Ucp1* expression across adipose depots and liver of mouse in (A). Data arbitrary normalized to BAT expression (dotted line). BAT, brown adipose tissue; PWAT, perirenal white adipose tissue; FWAT, femoral white adipose tissue; IWAT, inguinal white adipose tissue; RWAT, retroperitoneal white adipose tissue; EWAT, epididymal white adipose tissue; MWAT, mesentery white adipose tissue.

Figure 20) *De novo* Lipogenesis and Triglyceride Turnover in *Rdh1*-KO Mice, Studies 1 and 2

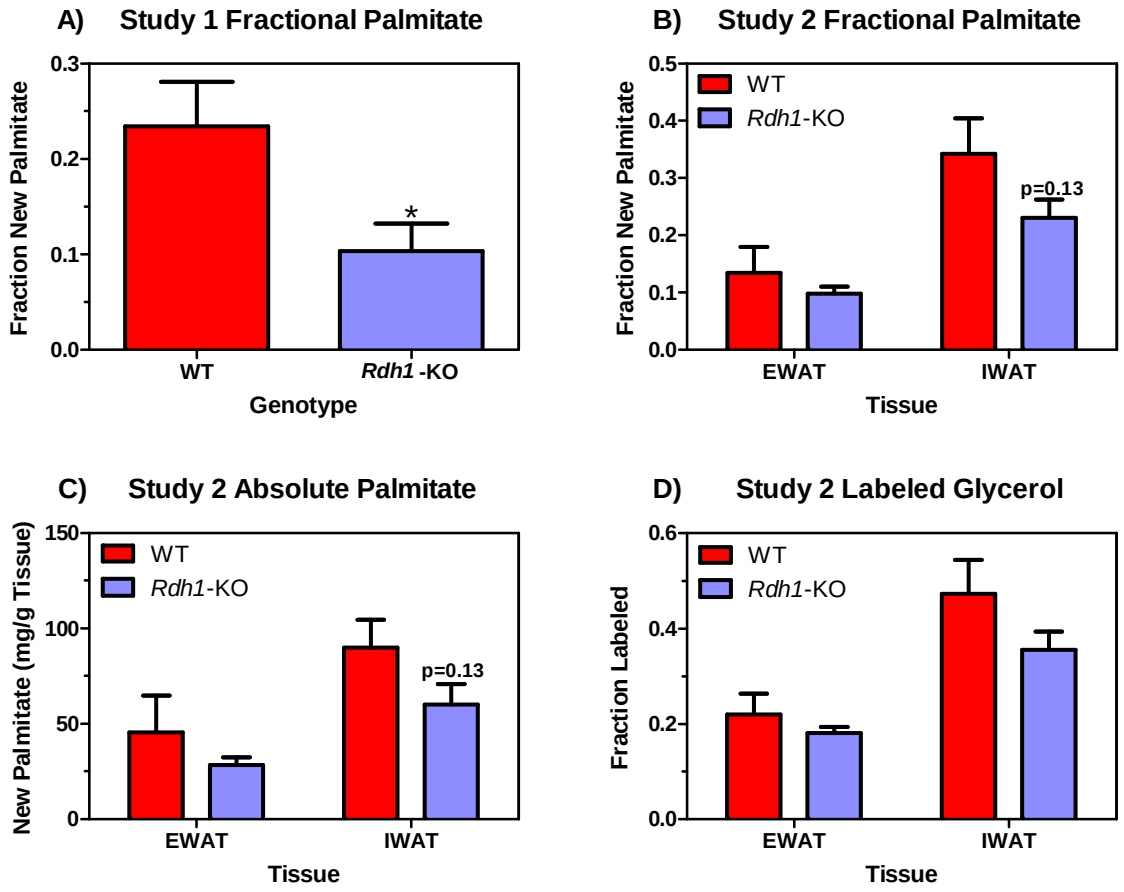

Legend: (A) Fraction of newly synthesized palmitate after 4 days of heavy water labeling from inguinal white adipose biopsies collected from WT (n=5-6) and *Rdh1*-KO (n=6-7) male mice aged 9 weeks. Mice fed a 93G diet (cohort 7w2). (B) Fraction of newly synthesized palmitate after 4 days of heavy water labeling in EWAT and IWAT collected from WT (n=5) and *Rdh1*-KO (n=6) male mice age 9-10 weeks. Mice fed a 93G diet (cohort 10w2a). (C) Milligrams of newly synthesized palmitate per gram of tissue after 4 days in EWAT and IWAT from WT (n=5) and *Rdh1*-KO (n=6) mice from (B). (D) Fraction of heavy water labeled glycerol after 4 days in EWAT and IWAT from WT (n=5) and *Rdh1*-KO (n=6) mice from (B). WT: red bar. *Rdh1*-KO: blue bar. **p≤0.01, *p≤0.05 or as indicated vs. WT by Student's two-tailed t-test. All values Mean ± SEM.

Figure 21) *De novo* Lipogenesis and Triglyceride Turnover in *Rdh1*-KO Mice, Study 3

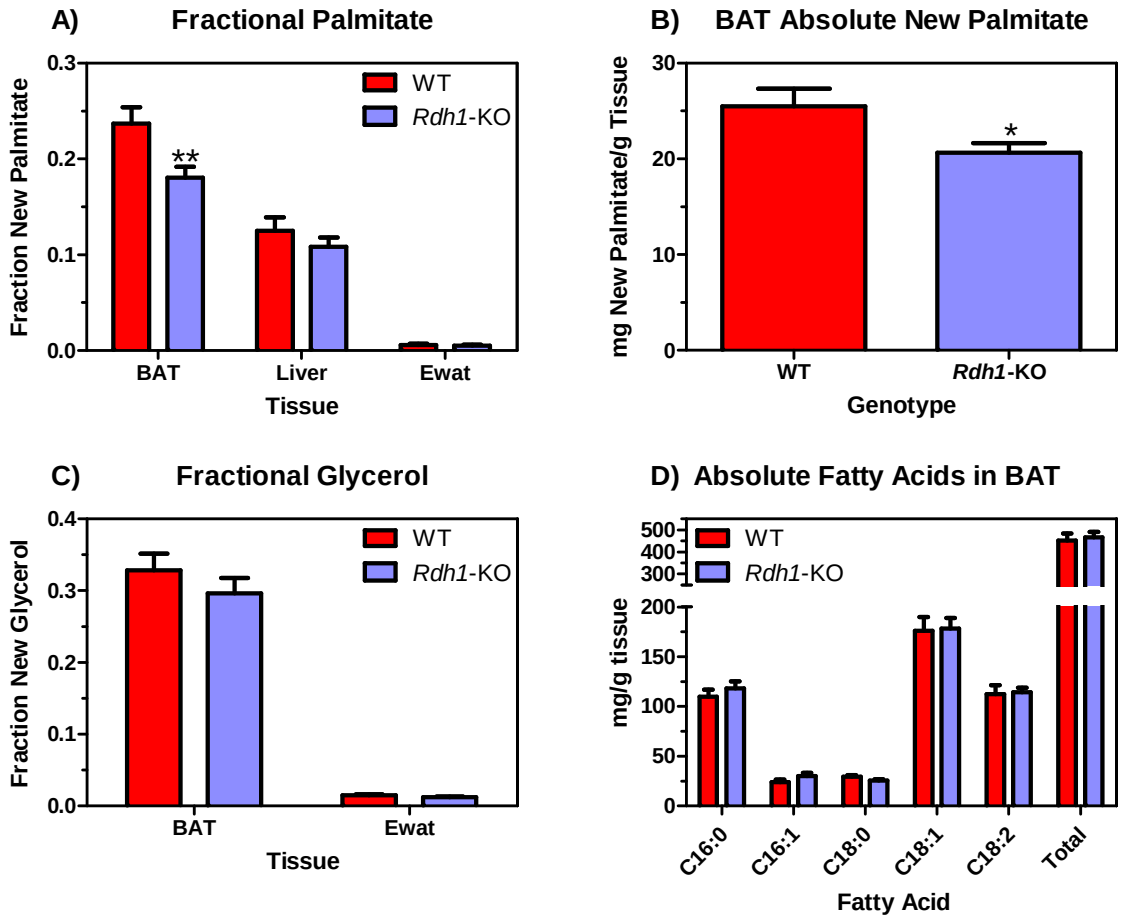

Legend: (A) Fraction of newly synthesized palmitate after 5-6 hours of refeeding in BAT, liver and EWAT collected from WT (n=10) and *Rdh1*-KO (n=12-13) male mice age 6-8 weeks. Mice fed a 93G diet (cohort 13w2). (B) Milligrams of newly synthesized palmitate per gram of tissue after 5-6 hours of refeeding in BAT from WT (n=10) and *Rdh1*-KO (n=13) mice from (A). (C) Fraction of heavy water labeled glycerol after 5-6 hours of refeeding in BAT and EWAT collected from WT (n=10) and *Rdh1*-KO (n=13) mice from (A). (D) Milligrams of fatty acid per gram of BAT from WT (n=10) and *Rdh1*-KO (n=13) mice from (A).WT: red bar. *Rdh1*-KO: blue bar. **p≤0.01, *p≤0.05 vs. WT by Student's two-tailed t-test. All values Mean ± SEM.

Figure 22) Fatty Acid Composition of Tissues from *Rdh1*-KO Mice

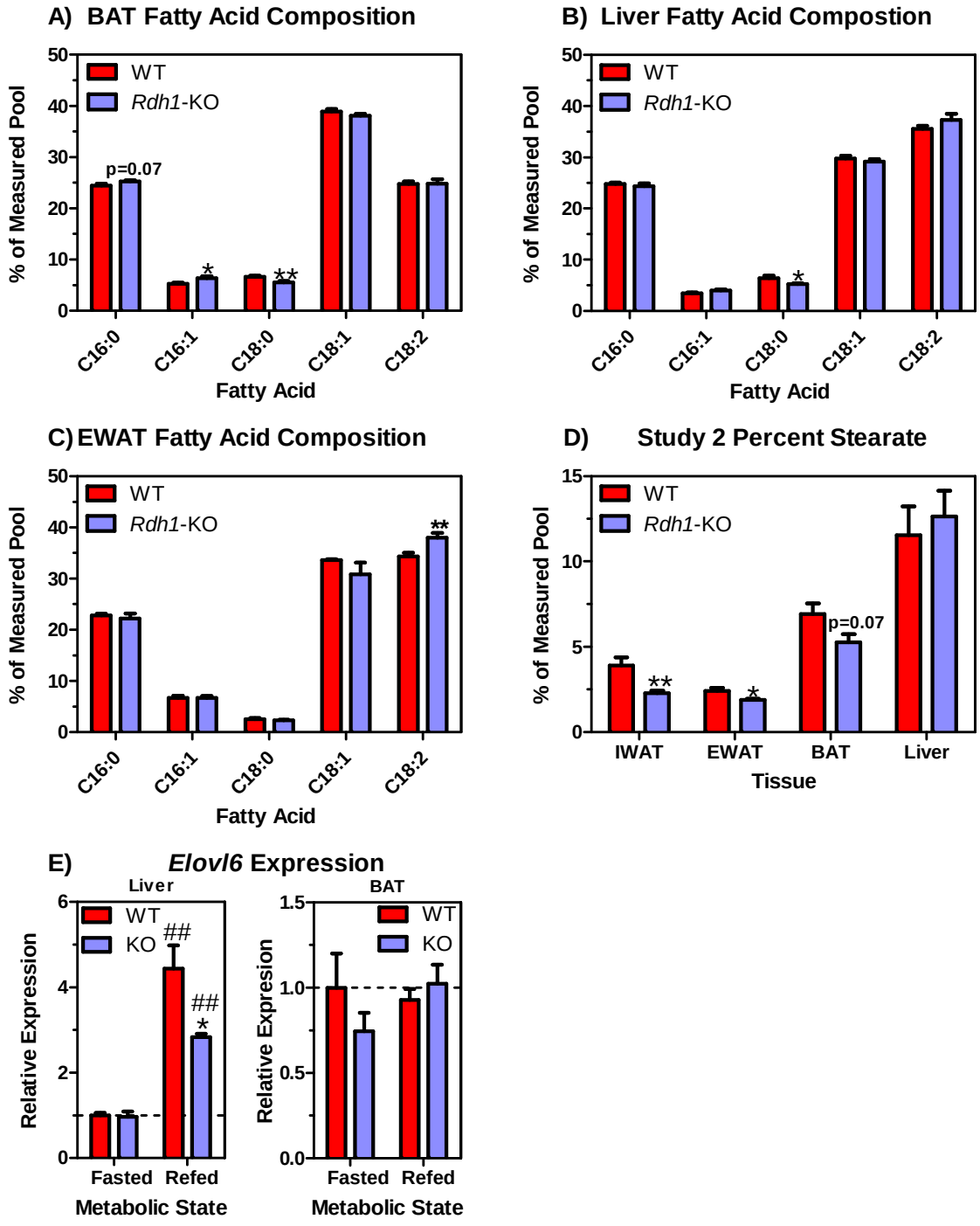

Legend: (See next page.)

Legend: (A) Relative fatty acid composition of BAT from WT (n=10) and *Rdh1*-KO (n=13) male mice aged 6-8 weeks and 5-6 hours refed. Same mice as (Figure 21) (13w2). (B) Relative fatty acid composition of liver from WT (n=10) and *Rdh1*-KO (n=13) mice from (A). (C) Relative fatty acid composition of EWAT from WT (n=10) and *Rdh1*-KO (n=13) mice from (A). (D) Relative stearate levels in IWAT, EWAT, BAT and liver from WT (n=5) and *Rdh1*-KO (n=6) male mice age 9-10 weeks fed a 93G diet *ad lib.* Same mice as (Figure 20B) (cohort 10w2a). (E) *Elovl6* expression in liver (n=5-6) and BAT (n=6-7) from fasted and 6-7 hour refed WT and *Rdh1*-KO male mice age 6-8 weeks. Mice fed a 93G diet (Liver, cohort 12w2; BAT, cohort 12w1). By two-way ANOVA, effects of interaction between genotype and refeeding ($p \leq 0.05$), genotype ($p \leq 0.01$) and refeeding ($p \leq 0.0001$) in liver. WT: red bar. KO: blue bar. $^{**}p \leq 0.01$, $^{*}p \leq 0.05$ or as indicated vs. WT and $\#\#p \leq 0.01$ vs. fasted by Student's two-tailed t-test. All values Mean $\pm$ SEM.

Table 13) Serum Hormones in *Rdh1*-KO Mice

Serum Factor	WT	*Rdh1*-KO	Condition	Age (wks)	Cohort
DHT	184 ± 68 pg/mL (12)	219 ± 71 pg/mL (13)	*Ad lib* fed	Unk.	na, Purina chow
	419 ± 260 pg/mL (7)	401 ± 147 pg/mL (8)	*Ad lib* fed	Unk	na, 93G Diet
	109 ± 29 pg/mL (4)	119 ± 51 pg/mL (3)	*Ad lib* fed	Unk	na, VAD Diet
Testosterone	2.0 ± 1.0 ng/mL (11)	4.9 ± 1.4 ng/mL (13)	*Ad lib* fed	Unk	na, Purina chow
	2.0 ± 0.7 ng/mL (8)	1.6 ± 0.5 ng/mL (9)	*Ad lib* fed	Unk	na, 93G Diet
	0.32 ± 0.02 ng/mL (3)	1.03 ± 0.36 ng/mL (3)	*Ad lib* fed	Unk	na, VAD Diet
Growth Hormone	7.6 ± 3.1 ng/mL (11)	1.9 ± 0.8 ng/mL (11)	*Ad lib* fed	8	8w2
T4	2.70 ± 0.15 µg/dL (12)	2.62 ± 0.11 µg/dL (8)	Fasted	6	12w2
	4.57 ± 0.12 µg/dL (6)	4.01 ± 0.20 µg/dL (9)*	Refed 5-6 hrs	6	12w2
T3	1.52 ± 0.06 ng/mL (9)	1.47 ± 0.07 ng/mL (9)	Fasted	6	12w2
	2.45 ± 0.13 ng/mL (11)	2.05 ± 0.09 ng/mL (9)*	Refed 5-6 hrs	6	12w2
TSH	0.98 ± 0.21 ng/mL (9)	0.76 ± 0.07 ng/mL (16)	Refed 6-8 hrs	5-6	14w1
	0.61 ± 0.07 ng/mL (11)	0.61 ± 0.05 ng/mL (12)	Refed 5-6 hrs	18	13w3
Leptin	1708 ± 199 pg/mL (10)	3094 ± 382 pg/mL (9)*	*Ad lib* fed	8	6w1
Resistin	1442 ± 293 pg/mL (10)	1241 ± 54 pg/mL (10)	*Ad lib* fed	8	6w1

Legend: Hormone levels from male mice, condition and age as noted. Diets as noted or as in (Table 1). *$p \leq 0.05$ vs. WT by Student's two-tailed t-test. Unk: Unknown. All values Mean ± SEM (number).

Figure 23) EWAT *Rbp4* Expression in *Rdh1*-KO Mice

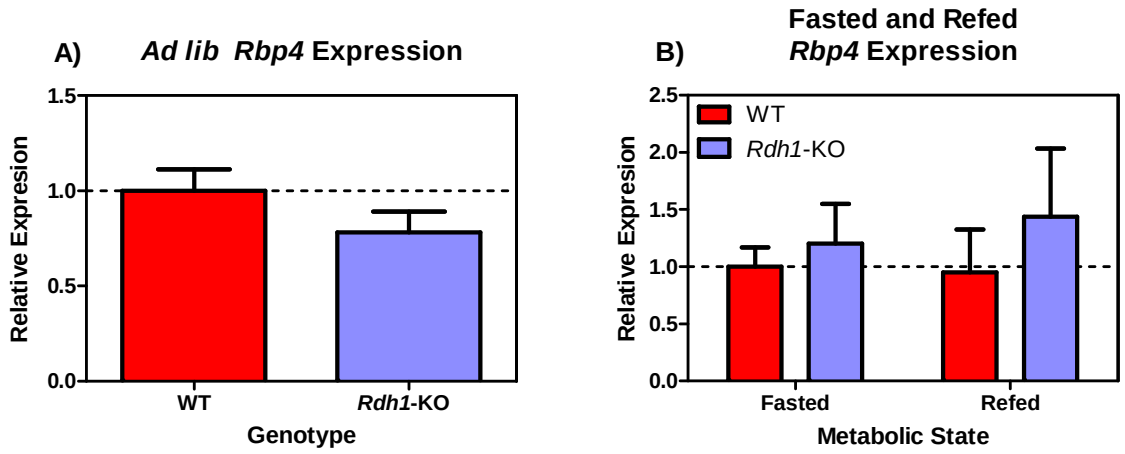

Legend: (A) Expression of *Rbp4* in EWAT from *ad lib* fed WT (n=8) and *Rdh1*-KO (n=5) male mice age 10 weeks. Mice fed a 93G diet (cohort 8w2). Data normalized to mean WT (dotted line). (B) Expression of *Rbp4* in EWAT from fasted and 6 hr refed WT (n=5) and *Rdh1*-KO (n=5) female mice age 10 weeks. Mice fed a 93G diet (cohort 12w1). Data arbitrarily normalized to mean fasted WT (dotted line). WT: red bar. *Rdh1*-KO: blue bar. All values Mean $\pm$ SEM.

Figure 24) Liver *Rbp4* Expression in *Rdh1*-KO Mice

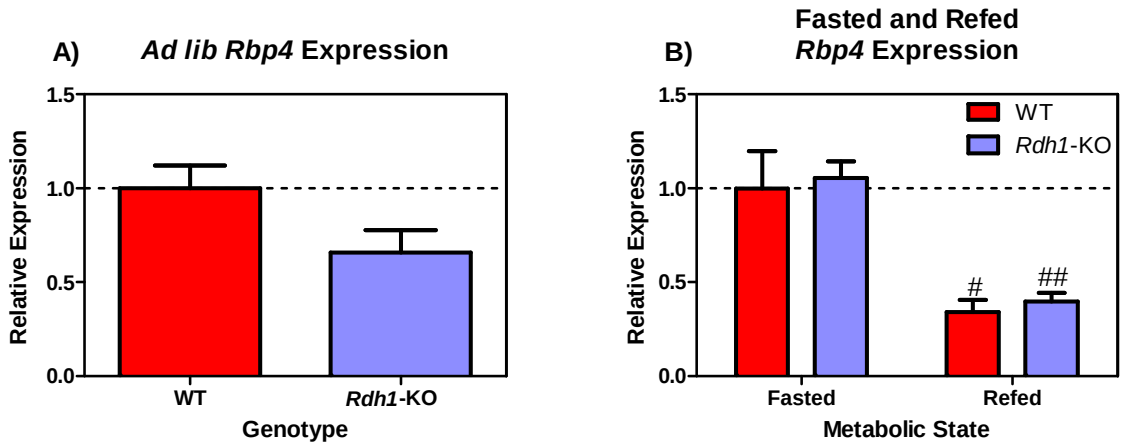

Legend: (A) Expression of *Rbp4* in liver from *ad lib* fed WT (n=7) and *Rdh1*-KO (n=6) male mice age 10 weeks. Mice fed a 93G diet (cohort 8w2). Data normalized to mean WT (dotted line). (B) Expression of *Rbp4* in liver from fasted and 7 hr refed WT (n=5) and *Rdh1*-KO (n=4-5) male mice age 7.5 weeks. Mice fed a 93G diet (cohort 12w2). By two-way ANOVA, effect of refeeding ($p \leq 0.0001$). Data arbitrarily normalized to mean fasted WT (dotted line). WT: red bar. *Rdh1*-KO: blue bar. ##$p \leq 0.01$, #$p \leq 0.05$ vs. fasted by Student's two-tailed t-test. All values Mean $\pm$ SEM.

Figure 25) RBP-STRA6 Signaling in BAT in *Rdh1*-KO Mice

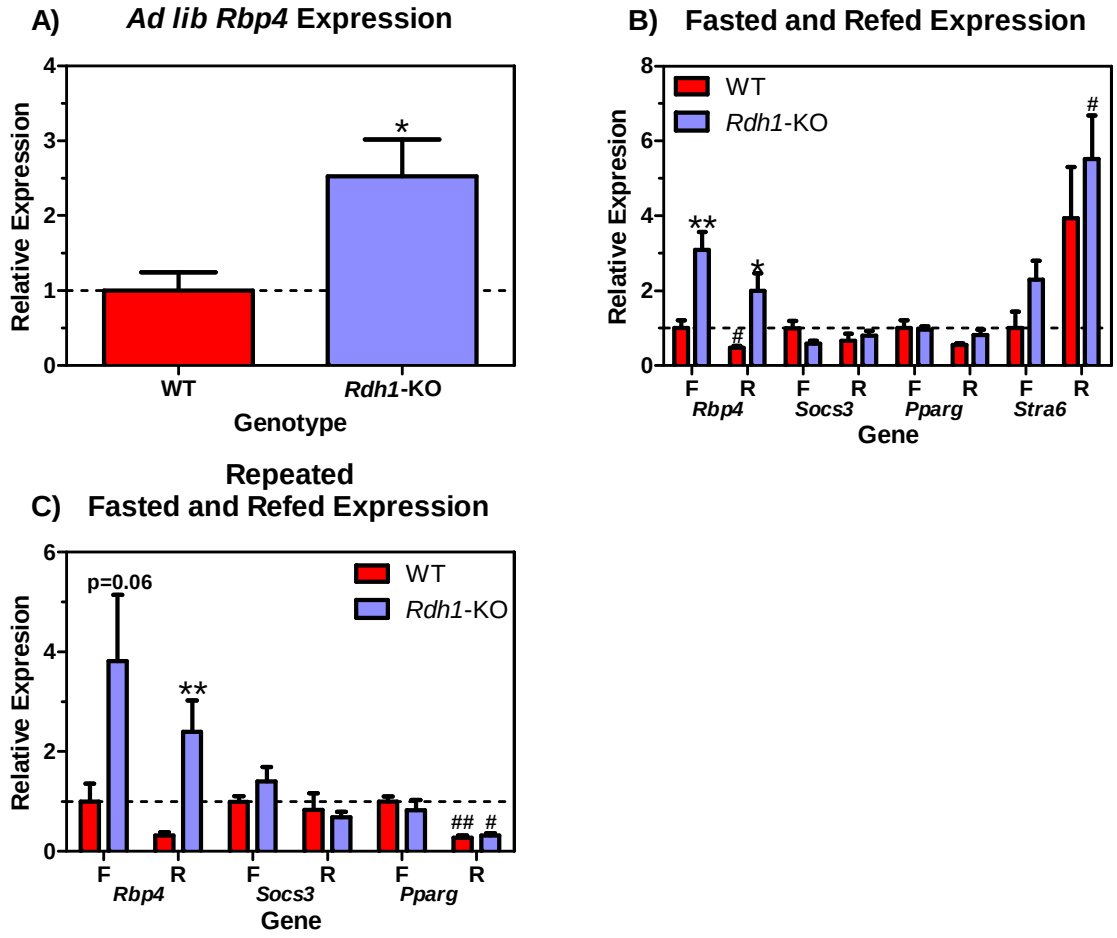

Legend: (A) *Rbp4* expression in BAT from *ad lib* fed WT (n=6) and *Rdh1*-KO (n=6) mice, age 28 weeks and fed a 93G diet (cohort 10w1b). Expression normalized to WT (dotted line). (B) Gene expression from fasted and 6.5 hr refed WT (n=5-8) and *Rdh1*-KO (n=6-7) male mice age 6 weeks. Mice fed a 93G diet (cohort 12w1). Expression of each gene arbitrarily normalized to WT fasted (dotted line).By two-way ANOVA, effect of refeeding on *Rbp4* ($p \leq 0.05$), *Pparg* ($p \leq 0.05$) and *Stra6* ($p \leq 0.01$) and genotype on *Rbp4* ($p \leq 0.0001$). (C) Gene expression from 16 hour fasted or 6-7 hour refed male WT (n=) and *Rdh1*-KO (n=) mice, age 7.5 weeks and fed a 93G diet (cohort 12w2). Expression of each gene arbitrarily normalized to WT fasted (dotted line). By two-way ANOVA, effect of refeeding on *Pparg* ($p \leq 0.0001$) and genotype on *Rbp4* ($p \leq 0.01$). WT: red bar. *Rdh1*-KO: blue bar. **$p \leq 0.01$, *$p \leq 0.05$ vs. WT and ##$p \leq 0.01$, #$p \leq 0.05$ vs. fasted by Student's two-tailed t-test. All values Mean $\pm$ SEM.

Table 14) *Ad lib* VAD Diet-fed *Rdh1*-KO Female Retinoids

Tissue	WT	*Rdh1*-KO
Serum	atRA: 4.0 ± 0.8 pmol/mL (5) ROH: 25.5 ± 6.2 nmol/mL (5) RE: 0.07 ± 0.03 nmol/mL (5)	atRA: 4.2 ± 0.7 pmol/mL (7) ROH: 27 ± 5.5 nmol/mL (7) RE: 0.05 ± 0.01 nmol/mL (7)
BAT	atRA: 6.8 ± 1.1 pmol/g (5) ROH: 43.2 ± 6.0 nmol/g (5) RE: 0.65 ± 0.08 nmol/g (5)	atRA: 11.7 ± 3.3 pmol/g (7) ROH: 34.1 ± 5.8 nmol/g (7) RE: 0.57 ± 0.07 nmol/g (7)
PMWAT	atRA: 7.1 ± 1.1 pmol/g (5) ROH: 22.3 ± 4.4 nmol/g (5) RE: 0.41 ± 0.04 nmol/g (5)	atRA: 11.4 ± 2.5 pmol/g (7) ROH: 20.2 ± 2.8 nmol/g (7) RE: 0.61 ± 0.21 nmol/g (7)
Brain	atRA: 1.9 ± 0.4 pmol/g (5) ROH: 11.7 ± 3.3 nmol/g (5) RE: 0.47 ± 0.06 nmol/g (5)	atRA: 3.5 ± 1.2 pmol/g (7) ROH: 12.5 ± 7.4 nmol/g (7) RE: 0.50 ± 0.01 nmol/g (7)
Kidney	atRA: 4.7 ± 0.2 pmol/g (5) ROH: 29.9 ± 6.2 nmol/g (5) RE: 2.15 ± 0.57 nmol/g (5)	atRA: 6.7 ± 0.7 pmol/g (7)* ROH: 33.2 ± 4.5 nmol/g (7) RE: 2.07 ± 0.32 nmol/g (7)
Liver	atRA: 32.9 ± 2.6 pmol/g (5) ROH: 93.8 ± 10.7 nmol/g (5) RE: 6.6 ± 1.0 nmol/g (5)	atRA: 34.8 ± 1.6 pmol/g (7) ROH:95.6 ± 9.4 nmol/g (7) RE: 8.7 ± 1.0 nmol/g (7)

Legend: Tissue retinoids from WT and *Rdh1*-KO female mice, age 61 weeks. Mice fed a VAD diet and born to dams switched from a Purina chow diet to a VAD diet at breeding (cohort 1w1). Tissues collected under *ad lib* fed conditions. PMWAT, perimetrial white adipose tissue. atRA: all-*trans*-retinoic acid; ROH, retinol; RE, retinyl esters. *$p \leq 0.05$ vs. WT. All values Mean ± SEM (number).

Table 15) *Ad lib* VAD Diet-fed *Rdh1*-KO Male Retinoids

Tissue	WT	*Rdh1*-KO
Kidney	atRA: 1.2 ± 0.1 pmol/g (5) ROH: 10.0 ± 0.3 nmol/g (3) RE: 3.1 ± 1.2 nmol/g (5)	atRA: 0.9 ± 0.1 pmol/g (4) ROH: 12.5 ± 0.9 nmol/g (5) RE: 1.6 ± 0.3 nmol/g (5)
Liver	atRA: 2.1 ± 0.1 pmol/g (5) ROH: 4.4 ± 0.3 nmol/g (4) RE: 0.33 ± 0.11 nmol/g (5)	atRA: 2.0 ± 0.1 pmol/g (5) ROH: 5.9 ± 0.2 nmol/g (5)* RE: 0.27 ± 0.01 nmol/g (5)
Testes	atRA: 8.2 ± 0.9 pmol/g (5) ROH: undetectable RE: 1.1 ± 0.1 nmol/g (5)	atRA: 10.5 ± 1.3 pmol/g (5) ROH: undetectable RE: 1.1 ± 0.1 nmol/g (5)

Legend: Tissue retinoids from male WT and *Rdh1*-KO mice, age 22 weeks. Mice fed a VAD diet and born to dams switched from a Purina chow diet to a VAD diet at mating (cohort 1w1). Tissues collected under *ad lib* fed conditions. atRA: all-*trans*-retinoic acid; ROH, retinol; RE, retinyl esters. *$p \leq 0.05$ vs. WT. All values Mean ± SEM (number).

Table 16) *Ad lib* Fed Retinoids from a *Rdh1*-KO Cohort with Vitamin A Deficient Mice

Tissue	WT	*Rdh1*-KO
Serum	atRA: 0.84 ± 0.25 pmol/mL (3) ROH: 0.04 ± 0.01 nmol/mL (3) RE: 0.24 ± 0.02 nmol/mL (3)	atRA: 0.76 ± 0.25 pmol/mL (2) ROH: 0.06 ± 0.01 nmol/mL (2) RE: 0.20 ± 0.05 nmol/mL (2)
Liver	atRA: 5.18 ± 1.12 pmol/g (5) ROH: 0.08 ± 0.01 nmol/g (5) RE: 4.22 ± 0.51 nmol/g (5)	atRA: 6.03 ± 1.11 pmol/g (3) ROH: 0.07 ± 0.03 nmol/g (3) RE: 3.87 ± 0.65 nmol/g (3)
Brain	atRA: 1.04 ± 0.11 pmol/g (5) ROH: 0.04 ± 0.01 nmol/g (5) RE: 0.59 ± 0.04 nmol/g (5)	atRA: 0.98 ± 0.11 pmol/g (4) ROH: 0.04 ± 0.01 nmol/g (5) RE: 0.47 ± 0.04 nmol/g (5)
Testes	atRA: 11.59 ± 5.98 pmol/g (4) ROH: 0.13 ± 0.01 nmol/g (4) RE: 1.00 ± 0.13 nmol/g (4)	No males
Kidney	atRA: 6.58 ± 0.97 pmol/g (5) ROH: 0.18 ± 0.02 nmol/g (5) RE: 9.40 ± 1.09 nmol/g (5)	atRA: 5.76 ± 1.08 pmol/g (4) ROH: 0.19 ± 0.07 nmol/g (4) RE: 9.10 ± 2.70 nmol/g (4)
BAT	atRA: 26.92 ± 6.24 pmol/g (4) ROH: 0.07 ± 0.02 nmol/g (4) RE: 0.66 ± 0.14 nmol/g (4)	atRA: 24.99 ± 3.35 pmol/g (4) ROH: 0.06 ± 0.01 nmol/g (4) RE: 0.64 ± 0.04 nmol/g (4)
EWAT/PMWAT	atRA: 19.70 ± 0.98 pmol/g (4) ROH: 0.04 ± 0.01 nmol/g (4) RE: 0.63 ± 0.12 nmol/g (4)	atRA: 16.30 ± 2.72 pmol/g (3) ROH: 0.05 ± 0.03 nmol/g (3) RE: 0.34 ± 0.16 nmol/g (3)

Legend: Tissue retinoids in 12.5 week old WT and *Rdh1*-KO mice. WT data is from 4 male mice and 1 female mouse. *Rdh1*-KO data is from only female mice. All mice fed a VAD diet and born to dams switched from a 93G diet to VAD at mating (cohort 2w1). Tissues collected under *ad lib* fed conditions. Analyzed side-by-side with mice in Table 21, allowing for direct comparisons. atRA: all-*trans*-retinoic acid; ROH, retinol; RE, retinyl esters. All values Mean ± SEM (number).

Table 17) *Ad lib* Fed Retinoids from a VAD Diet-fed *Rdh1*-KO Cohort Rescued with 93G Diet

Sex	Tissue	WT	*Rdh1*-KO
Pooled	Hypo-thalamus	atRA: 54.2 ± 12.5 pmol/g (6) ROH: 1.61 ± 0.04 nmol/g (6) RE: 0.66 ± 0.07 nmol/g (6)	atRA: 39.3 ± 4.0 pmol/g (6) ROH: 1.85 ± 0.25 nmol/g (4) RE: 0.67 ± 0.06 nmol/g (4)
Male	Serum	atRA: 2.76 ± 0.37 pmol/mL (6) ROH: 0.83 ± 0.05 nmol/mL (6) RE: 0.21 ± 0.02 nmol/mL (6)	atRA: 2.73 ± 0.02 pmol/mL (2) ROH: 0.78 ± 0.01 nmol/mL (2) RE: 0.34 ± 0.14 nmol/mL (2)
Female	Serum	atRA: 1.4 ± 0.5 pmol/mL (4) ROH: 0.45 ± 0.12 nmol/mL (5) RE: 0.29 ± 0.04 nmol/mL (5)	atRA: 3.1 ± 0.2 pmol/mL (6)** ROH: 0.49 ± 0.05 nmol/mL (6) RE: 0.36 ± 0.04 nmol/mL (6)
Male	BAT	atRA: 2.1 ± 0.3 pmol/g (6) ROH: 0.26 ± 0.04 nmol/g (6) RE: 0.22 ± 0.05 nmol/g (6)	atRA: 1.3 ± 0.2 pmol/g (2) ROH: 0.20 ± 0.01 nmol/g (2) RE: 0.18 ± 0.01 nmol/g (2)
Female	BAT	atRA: 8.9 ± 1.1 pmol/g (8) ROH: 0.50 ± 0.03 nmol/g (8) RE: 1.17 ± 0.09 nmol/g (8)	atRA: 5.7 ± 0.6 pmol/g (8)* ROH: 0.45 ± 0.05 nmol/g (8) RE: 0.81 ± 0.12 nmol/g (8)*
Male	EWAT	atRA: 4.2 ± 0.2 pmol/g (6) ROH: 0.49 ± 0.04 nmol/g (6) RE: 0.13 ± 0.01 nmol/g (6)	atRA: 5.7 ± 0.1 pmol/g (2)** ROH: 0.62 ± 0.02 nmol/g (2) RE: 0.25 ± 0.01 nmol/g (2)**
Female	PMWAT	atRA: 7.2 ± 0.9 pmol/g (8) ROH: 0.64 ± 0.16 nmol/g (8) RE: 0.57 ± 0.10 nmol/g (8)	atRA: 9.2 ± 1.1 pmol/g (8) ROH: 0.88 ± 0.17 nmol/g (8) RE: 0.70 ± 0.13 nmol/g (8)
Male	Pancreas	atRA: 14.5 ± 2.9 pmol/g (6) 9cRA: 27.9 ± 5.0 pmol/g (6) ROH: 0.45 ± 0.06 nmol/g (6) RE: 2.1 ± 0.6 nmol/g (6)	atRA: 15.9 ± 7.8 pmol/g (2) 9cRA: 30.0 ± 4.5 pmol/g (2) ROH: 0.72 ± 0.02 nmol/g (2)* RE: 1.6 ± 0.6 nmol/g (2)
Female	Pancreas	atRA: 11.9 ± 0.9 pmol/g (8) 9cRA: 24.8 ± 4.5 pmol/g (8) ROH: 0.44 ± 0.05 nmol/g (8) RE: 1.2 ± 0.2 nmol/g (8)	atRA: 18.6 ± 2.6 pmol/g (7)* 9cRA: 21.7 ± 4.2 pmol/g (7) ROH: 0.61 ± 0.12 nmol/g (8) RE: 1.5 ± 0.2 nmol/g (8)
Male	Liver	atRA: 12.5 ± 1.7 pmol/g (6) ROH: 2.5 ± 0.4 nmol/g (6) RE: 48.5 ± 4.0 nmol/g (6)	atRA: 15.0 ± 1.4 pmol/g (2) ROH: 2.7 ± 0.0 nmol/g (2) RE: 40.7 ± 3.0 nmol/g (2)
Female	Liver	atRA: 17.1 ± 2.4 pmol/g (8) ROH: 3.1 ± 0.3 nmol/g (8) RE: 95.6 ± 5.2 nmol/g (8)	atRA: 17.0 ± 0.9 pmol/g (8) ROH: 5.1 ± 0.8 nmol/g (8)* RE: 93.9 ± 14.1 nmol/g (8)
Male	Skeletal Muscle	atRA: 1.6 ± 0.2 pmol/g (6) ROH: 0.08 ± 0.01 nmol/g (6) RE: 0.12 ± 0.01 nmol/g (6)	atRA: 2.3 ± 0.3 pmol/g (2) ROH: 0.10 ± 0.03 nmol/g (2) RE: 0.14 ± 0.06 nmol/g (2)
Female	Skeletal Muscle	atRA: 2.0 ± 0.2 pmol/g (7) ROH: 0.11 ± 0.01 nmol/g (7) RE: 0.11 ± 0.01 nmol/g (7)	atRA: 2.1 ± 0.3 pmol/g (8) ROH: 0.08 ± 0.01 nmol/g (8)* RE: 0.10 ± 0.01 nmol/g (8)

Legend: Tissue retinoids from male and female WT and *Rdh1*-KO mice, age 16 weeks. Mice were switched from a VAD diet to 93G diet at age 11 weeks and were born to dams switched from a Harlan chow diet to VAD diet at mating (cohort 3w1). Tissues collected under *ad lib* fed conditions. atRA: all-*trans*-retinoic acid; 9cRA: 9-*cis*-retinoic acid; ROH, retinol; RE, retinyl esters. **$p \leq 0.01$, *$p \leq 0.05$ vs. WT by Student's two-tailed t-test. All values Mean ± SEM (number).

Table 18) *Ad lib* Fed Retinoids in 8-week Old, 93G Diet-fed, *Rdh1*-KO Male Mice

Tissue	WT	*Rdh1*-KO
BAT	atRA: 10.99 ± 0.72 pmol/g (11) RAL: 91.47 ± 3.66 pmol/g (6) ROH: 1.08 ± 0.03 nmol/g (11) RE: 0.74 ± 0.06 nmol/g (11)	atRA: 11.85 ± 0.80 pmol/g (12) RAL: 94.10 ± 21.42 pmol/g (6) ROH: 1.07 ± 0.05 nmol/g (12) RE: 0.63 ± 0.06 nmol/g (12)
EWAT	atRA: 4.28 ± 0.46 pmol/g (11) RAL: 40.55 ± 2.03 pmol/g (11) ROH: 1.20 ± 0.11 nmol/g (11) RE: 0.50 ± 0.20 nmol/g (11)	atRA: 4.03 ± 0.44 pmol/g (12) RAL: 46.61 ± 3.45 pmol/g (12) ROH: 0.90 ± 0.06 nmol/g (12)* RE: 0.38 ± 0.10 nmol/g (12)
IWAT	atRA: 3.47 ± 0.42 pmol/g (11) RAL: 77.64 ± 6.77 pmol/g (6) ROH: 0.72 ± 0.06 nmol/g (11) RE: 0.22 ± 0.04 nmol/g (11)	atRA: 3.63 ± 0.59 pmol/g (12) RAL: 101.96 ± 18.10 pmol/g (6) ROH: 0.61 ± 0.05 nmol/g (12) RE: 0.36 ± 0.18 nmol/g (12)
Liver	atRA: 8.75 ± 0.52 pmol/g (11) RAL: 56.20 ± 2.09 pmol/g (11) ROH: 10.07 ± 1.16 nmol/g (11) RE: 223.54 ± 32.56 nmol/g (11)	atRA: 11.14 ± 0.60 pmol/g (12)** RAL: 59.65 ± 5.22 pmol/g (12) ROH: 10.22 ± 1.23 nmol/g (12) RE: 192.29 ± 17.18 nmol/g (12)
Hypo-thalamus	atRA: 143.4 ± 14.8 pmol/g protein (6) ROH: 83.79 ± 13.73 nmol/g protein (6) RE: 12.75 ± 1.19 nmol/g protein (6)	atRA: 130.1 ± 5.8 pmol/g protein (6) ROH: 74.01 ± 8.61 nmol/g protein (6) RE: 12.18 ± 0.84 nmol/g protein (6)

Legend: Tissue retinoids from WT and *Rdh1*-KO male mice, age 8 weeks, fed a 93G diet with tissues collected under *ad lib* fed conditions (cohort 6w1). atRA: all-*trans*-retinoic acid; RAL: retinal; ROH, retinol; RE, retinyl esters. **$p \leq 0.01$, *$p \leq 0.05$ vs. WT by Student's two-tailed t-test. All values Mean ± SEM (number).

Table 19) *Ad lib* Fed Retinoids in 8-9 week Old, 93G Diet-fed, *Rdh1*-KO Male Mice

Tissue	WT	*Rdh1*-KO
Liver	atRA: 8.16 ± 0.81 pmol/g (12) RAL: 163.56 ± 8.72 pmol/g (11) ROH: 4.15 ± 0.46 nmol/g (12) RE: 97.32 ± 10.50 nmol/g (12)	atRA: 7.76 ± 0.60 pmol/g (7) RAL: 219.74 ± 23.30 pmol/g (8)* ROH: 4.04 ± 0.47 nmol/g (7) RE: 81.21 ± 7.89 nmol/g (7)
EWAT	atRA: 3.35 ± 0.35 pmol/g (10) RAL: 24.80 ± 1.78 pmol/g (12) ROH: 0.75 ± 0.07 nmol/g (12) RE: 0.53 ± 0.05 nmol/g (12)	atRA: 2.54 ± 0.28 pmol/g (6) RAL: 28.23 ± 2.40 pmol/g (8) ROH: 0.89 ± 0.10 nmol/g (8) RE: 0.82 ± 0.30 nmol/g (8)
Pancreas	atRA: 15.68 ± 1.97 pmol/g (12) 9cRA: 37.61 ± 5.76 pmol/g (12) ROH: 1.21 ± 0.17 nmol/g (12) RE: 2.31 ± 0. 12 nmol/g (12)	atRA: 17.17 ± 3.17 pmol/g (8) 9cRA: 23.89 ± 3.18 pmol/g (8) ROH: 3.57 ± 0.54 nmol/g (8)** RE: 3.18 ± 0.76 nmol/g (8)
BAT	RAL: 43.42 ± 3.87 pmol/g (12)	RAL: 45.21 ± 3.60 pmol/g (8)

Legend: Tissue retinoids from WT and *Rdh1*-KO male mice, age 8-9 weeks, fed a 93G diet with tissues collected under *ad lib* fed conditions (cohort 8w1). atRA: all-*trans*-retinoic acid; 9cRA: 9-*cis*-retinoic acid; RAL: retinal; ROH, retinol; RE, retinyl esters. **$p \leq 0.01$, *$p \leq 0.05$ vs. WT by Student's two-tailed t-test. All values Mean ± SEM (number).

Table 20) *Ad lib* Fed Retinoids in 9 week Old, 93G Diet-fed, *Rdh1*-KO Male Mice

Tissue	WT	*Rdh1*-KO
Liver	atRA: 18.16 ± 1.79 pmol/g (8) RAL: 28.27 ± 1.50 pmol/g (8) ROH: 3.83 ± 0.67 nmol/g (8) RE: 86.43 ± 15.04 nmol/g (8)	atRA: 17.43 ± 0.77 pmol/g (7) RAL: 31.96 ± 1.47 pmol/g (7) ROH: 5.59 ± 0.88 nmol/g (7) RE: 92.88 ± 15.21 nmol/g (7)
EWAT	atRA: 6.25 ± 1.20 pmol/g (8) RAL: 33.51 ± 3.38 pmol/g (8) ROH: 1.24 ± 0.23 nmol/g (8) RE: 0.30 ± 0.10 nmol/g (8)	atRA: 7.76 ± 0.69 pmol/g (7) RAL: 34.39 ± 2.32 pmol/g (7) ROH: 1.34 ± 0.12 nmol/g (7) RE: 0.29 ± 0.03 nmol/g (7)
BAT	atRA: 12.90 ± 1.55 pmol/g (8) RAL: 61.92 ± 3.92 pmol/g (8) ROH: 1.08 ± 0.07 nmol/g (8) RE: 0.44± 0.05 nmol/g (8)	atRA: 11.54 ± 1.40 pmol/g (6) RAL: 70.72 ± 4.90 pmol/g (7) ROH: 1.13 ± 0.07 nmol/g (6) RE: 0.41 ± 0.07 nmol/g (6)
Pancreas	atRA: 55.77 ± 6.08 pmol/g (8) 9cRA: 22.60 ± 3.00 pmol/g (8) RAL: 87.13 ± 2.80 pmol/g (8) ROH: 22.30 ± 7.64 nmol/g (8) RE: 29.87 ± 6.81 nmol/g (8)	atRA: 58.65 ± 5.77 pmol/g (7) 9cRA: 18.73 ± 1.78 pmol/g (7) RAL: 115.87 ± 15.97 pmol/g (7) ROH: 8.87 ± 3.05 nmol/g (7) RE: 44.19 ± 22.30 nmol/g (7)

Legend: Tissue retinoids from WT and *Rdh1*-KO male mice, age 9 weeks, fed a 93G diet with tissues collected under *ad lib* fed conditions (cohort 6w2). atRA: all-*trans*-retinoic acid; 9cRA: 9-*cis*-retinoic acid; RAL: retinal; ROH, retinol; RE, retinyl esters. All values Mean ± SEM (number).

Table 21) *Ad lib* Fed Retinoids in 12.5 week Old, 93G Diet-fed, *Rdh1*-KO Mice

Sex	Tissue	WT	*Rdh1*-KO
Male	Serum	atRA: 0.65 ± 0.08 pmol/g (3) ROH: 121.82 ± 64.58 nmol/g (3) RE: 14.07 ± 5.85 nmol/g (3)	atRA: 0.84 ± 0.21 pmol/g (5) ROH: 136.96 ± 32.65 nmol/g (4) RE: 28.57 ± 10.38 nmol/g (4)
Female	Serum	atRA: 0.93 ± 0.24 pmol/g (5) ROH: 75.16 ± 12.54 nmol/g (5) RE: 22.18 ± 4 .78 nmol/g (5)	atRA: 0.61 ± 0.12 pmol/g (5) ROH: 44.57 ± 12.43 nmol/g (5) RE: 28.43 ± 2.50 nmol/g (5)
Male	Liver	atRA: 10.20 ± 0.73 pmol/g (3) ROH: 1294.67 ± 326.38 nmol/g (3) RE: 1864.27 ± 531.55 nmol/g (3)	atRA: 12.41 ± 1.18 pmol/g (5) ROH: 1547.61 ± 383.75 nmol/g (5) RE: 2617.88 ± 548.70 nmol/g (3)
Female	Liver	atRA: 12.82 ± 1.66 pmol/g (5) ROH: 1430.65 ± 406.49 nmol/g (4) RE: 5543.13 ± 1803.48 nmol/g (5)	atRA: 11.46 ± 0.97 pmol/g (5) ROH: 2513.12 ± 309.90 nmol/g (5) RE: 4737.74 ± 2039.15 nmol/g (5)
Male	Brain	atRA: 8.48 ± 0.38 pmol/g (5) ROH: 69.54 ± 2.73 nmol/g (5) RE: 345.12 ± 4.42 nmol/g (3)	atRA: 9.51 ± 0.57 pmol/g (5) ROH: 67.26 ± 3 .10 nmol/g (5) RE: 416.33 ± 20.85 nmol/g (5)*
Female	Brain	atRA: 8.63 ± 0.58 pmol/g (5) ROH: 68.07 ± 2.01 nmol/g (4) RE: 421.54 ± 15.17 nmol/g (4)	atRA: 5.80 ± 0.81 pmol/g (5)* ROH: 66.47 ± 5.20 nmol/g (4) RE: 358.23 ± 23.07 nmol/g (4)
Male	Testes	atRA: 6.46 ± 0.77 pmol/g (3) ROH: 22.06 ± 5.03 nmol/g (3) RE: 45.07 ± 5 .67 nmol/g (3)	atRA: 5.70 ± 0.73 pmol/g (5) ROH: 31.61 ± 5.02 nmol/g (5) RE: 49.38 ± 10.49 nmol/g (5)
Male	Kidney	atRA: 11.93 ± 0.99 pmol/g (3) ROH: 135.50 ± 16.09 nmol/g (3) RE: 668.53 ± 26.61 nmol/g (3)	atRA: 6.66 ± 0.44 pmol/g (5)* ROH: 92.99 ± 10.34 nmol/g (5) RE: 536.18 ± 20.51 nmol/g (5)*
Female	Kidney	atRA: 6.56 ± 0.75 pmol/g (5) ROH: 97.79 ± 8.09 nmol/g (5) RE: 1130.86 ± 110.92 nmol/g (5)	atRA: 6.08 ± 0.53 pmol/g (5) ROH: 68.20 ± 4.75 nmol/g (5)* RE: 899.55 ± 118.58 nmol/g (5)
Male	Brown	atRA: 3.81 ± 1.38 pmol/g (3) ROH: 62.96 ± 8.06 nmol/g (3) RE: 52.22 ± 9.25 nmol/g (3)	atRA: 1.88 ± 0.27 pmol/g (5) ROH: 45.81 ± 6.53 nmol/g (5) RE: 83.46 ± 37.40 nmol/g (5)
Female	Brown	atRA: 4.81 ± 1.18 pmol/g (5) ROH: 48.40 ± 4.13 nmol/g (5) RE: 82.73 ± 6.71 nmol/g(5)	atRA: 1.85 ± 0.28 pmol/g (5)* ROH: 36.96 ± 2.07 nmol/g (5)* RE: 69.47 ± 14.80 nmol/g (5)
Male	EWAT	atRA: 3.26 ± 0.97 pmol/g (3) ROH: 155.46 ± 25.45 nmol/g (3) RE: 32.84 ± 8.98 nmol/g (3)	atRA: 5.91 ± 0.77 pmol/g (5) ROH: 141.58 ± 5.74 nmol/g (5) RE: 34.20 ± 2.84 nmol/g (4)
Female	PMWAT	atRA: 5.87 ± 1.70 pmol/g (5) ROH: 103.54 ± 16.18 nmol/g (5) RE: 36.37 ± 3.84 nmol/g (5)	atRA: 8.25 ± 2.38 pmol/g (4) ROH: 84.94 ± 31.20 nmol/g (5) RE: 48.85 ± 15.68 nmol/g (5)

Legend: Tissue retinoids from male and female WT and *Rdh1*-KO mice, age 12.5 weeks, fed a 93G diet with tissues collected under *ad lib* fed conditions (cohort 2w1). Analyzed side-by-side with mice in (Table 16), allowing for direct comparisons. atRA: all-*trans*-retinoic acid; ROH, retinol; RE, retinyl esters. *$p \leq 0.05$ vs. WT by Student's two-tailed test. All values Mean ± SEM (number).

Table 22) *Ad lib* Fed Retinoids in 73 week Old, 93G Diet-fed, *Rdh1*-KO Male Mice

Tissue	WT	*Rdh1*-KO
Hypothalamus	atRA: 9.5 ± 1.6 pmol/g (3) ROH: 6.0 ± 1.4 nmol/g (3) RE: 1.7 ± 0.7 nmol/g (3)	atRA: 7.0 ± 0.8 pmol/g (4) ROH: 5.6 ± 0.9 nmol/g (4) RE: 1.8 ± 0.3 nmol/g (4)
Hypothalamus	atRA: 141 ± 18 pmol/g protein (3) ROH: 89 ± 18 nmol/g protein (3) RE: 24 ± 9 nmol/g protein (3)	atRA: 135 ± 30 pmol/g protein (4) ROH: 112 ± 35 nmol/g protein (4) RE: 34 ± 5 nmol/g protein (3)
Hippocampus	atRA: 7.0 ± 0.4 pmol/g (5) ROH: 2.3 ± 0.1 nmol/g (5) RE: 2.1 ± 0.2 nmol/g (5)	atRA: 6.8 ± 0.3 pmol/g (7) ROH: 2.6 ± 0.2 nmol/g (7) RE: 1.7 ± 0.3 nmol/g (7)
BAT	atRA: 2.6 ± 0.2 pmol/g (5) RAL: 39.4 ± 1.6 pmol/g (5) ROH: 0.96 ± 0.04 nmol/g (5) RE: 0.9 ± 0.1 nmol/g (5)	atRA: 3.4 ± 0.6 pmol/g (7) RAL: 42.3 ± 2.8 pmol/g (7) ROH: 1.25 ± 0.14 nmol/g (7) RE: 1.0 ± 0.1 nmol/g (7)
EWAT	atRA: 2.5 ± 0.2 pmol/g (5) RAL: 34.1 ± 2.5 pmol/g (5) ROH: 1.1 ± 0.1 nmol/g (5) RE: 0.30 ± 0.03 nmol/g (5)	atRA: 2.9 ± 0.5 pmol/g (7) RAL: 35.0 ± 1.5 pmol/g (7) ROH: 1.5 ± 0.1 nmol/g (7)** RE: 0.63 ± 0.04 nmol/g (7)**
IWAT	atRA: 3.0 ± 0.2 pmol/g (5) RAL: 36.2 ± 2.6 pmol/g (5) ROH: 1.4 ± 0.1 nmol/g (5) RE: 0.62 ± 0.11 nmol/g (5)	atRA: 2.6 ± 0.2 pmol/g (7) RAL: 33.6 ± 1.7 pmol/g (7) ROH: 1.2 ± 0.1 nmol/g (7) RE: 0.40 ± 0.03 nmol/g (7)*
Skeletal Muscle	atRA: 1.2 ± 0.2 pmol/g (5) RAL: 70.1 ± 17.9 pmol/g (5) ROH: 0.26 ± 0.03 nmol/g (5) RE: 243 ± 29 nmol/g (5)	atRA: 2.0 ± 0.8 pmol/g (6) RAL: 55.7 ± 7.6 pmol/g (6) ROH: 0.40 ± 0.07 nmol/g (6) RE: 196 ± 18 nmol/g (7)
Liver	atRA: 8.3 ± 0.2 pmol/g (4) RAL: 44.2 ± 4.0 pmol/g (5) ROH: 9.1 ± 1.2 nmol/g (5) RE: 244 ± 29 nmol/g (5)	atRA: 7.6 ± 0.5 pmol/g (7) RAL: 46.5 ± 3.5 pmol/g (7) ROH: 8.6 ± 1.0 nmol/g (7) RE: 197 ± 18 nmol/g (7)
Pancreas	atRA: 8.8 ± 1.1 pmol/g (5) 9cRA: 11.4 ± 0.6 pmol/g (5) ROH: 0.60 ± 0.02 nmol/g (5) RE: 0.31 ± 0.01 nmol/g (5)	atRA: 8.6 ± 1.3 pmol/g (7) 9cRA: 10.7 ± 1.4 pmol/g (6) ROH: 0.79 ± 0.06 nmol/g (7)* RE: 0.35 ± 0.11 nmol/g (7)
Spleen	atRA: 4.3 ± 0.3 pmol/g (5) ROH: 0.9 ± 0.1 nmol/g (5) RE: 1.3 ± 0.1 nmol/g (5)	atRA: 4.9 ± 0.4 pmol/g (7) ROH: 1.0 ± 0.1 nmol/g (7) RE: 1.7 ± 0.3 nmol/g (7)
Mucosal Cells of the Small Intestine	atRA: 12.5 ± 1.15 pmol/g (5) ROH: 0.17 ± 0.02 nmol/g (5) RE: 0.54 ± 0.12 nmol/g (5)	atRA: 9.3 ± 1.4 pmol/g (7) ROH: 0.18 ± 0.03 nmol/g (7) RE: 0.57 ± 0.14 nmol/g (7)
Mucosal Cells of the Small Intestine	atRA: 460 ± 46 pmol/g protein (5) ROH: 6.1 ± 0.4 nmol/g protein (5) RE: 19 ± 4 nmol/g protein (5)	atRA: 453 ± 77 pmol/g protein (7) ROH: 8.5 ± 1.4 nmol/g protein (7) RE: 24 ± 4 nmol/g protein (7)
Kidney	atRA: 6.1 ± 0.5 pmol/g (5) ROH: 1.2 ± 0.1 nmol/g (5) RE: 11.2 ± 0.8 nmol/g (5)	atRA: 6.2 ± 0.5 pmol/g (5) ROH: 1.1 ± 0.1 nmol/g (5) RE: 7.7 ± 1.2 nmol/g (7)*

Legend: (See next page)

Legend: Tissue retinoids from male WT and *Rdh1*-KO mice, age 73 weeks, fed a 93G diet with tissues collected under *ad lib* fed conditions (cohort 2w2). Analyzed side-by-side with mice in (Table 23), allowing for direct comparisons. atRA: all-*trans*-retinoic acid; RAL: retinal; 9cRA: 9-*cis*-retinoic acid; ROH, retinol; RE, retinyl esters. **$p \leq 0.01$, *$p \leq 0.05$ vs. WT by Student's two-tailed t-test. All values Mean $\pm$ SEM (number).

Table 23) *Ad lib* Fed Retinoids in 73 week Old, 93G Diet-fed, *Rdh1*-KO Female Mice

Tissue	WT	*Rdh1*-KO
Hypo-thalamus	atRA: 8.6 ± 0.7 pmol/g (2) ROH: 3.9 ± 0.4 nmol/g (2) RE: 1.6 ± 0.6 nmol/g (2)	atRA: 13.9 ± 3.0 pmol/g (3) ROH: 4.7 ± 0.4 nmol/g (3) RE: 0.98 ± 0.04 nmol/g (3)
Hypo-thalamus	atRA: 136 ± 37 pmol/g protein (2) ROH: 60 ± 6 nmol/g protein (2) RE: 26 ± 14 nmol/g protein (2)	atRA: 248 ± 47 pmol/g protein (3) ROH: 89 ± 19 nmol/g protein (3) RE: 18 ± 2 nmol/g protein (3)
Hippocampus	atRA: 9.3 ± 1.0 pmol/g (5) ROH: 4.0 ± 0.5 nmol/g (5) RE: 1.2 ± 0.2 nmol/g (5)	atRA: 9.1 ± 1.1 pmol/g (7) ROH: 3.5 ± 0.4 nmol/g (7) RE: 1.1 ± 0.1 nmol/g (7)
BAT	atRA: 4.7 ± 0.6 pmol/g (5) RAL: 67.9 ± 9.0 pmol/g (5) ROH: 1.13 ± 0.07 nmol/g (5) RE: 1.4 ± 0.1 nmol/g (5)	atRA: 5.1 ± 0.7 pmol/g (5) RAL: 65.4 ± 7.1 pmol/g (7) ROH: 1.28 ± 0.13 nmol/g (7) RE: 1.4 ± 0.2 nmol/g (7)
PMWAT	atRA: 1.4 ± 0.1 pmol/g (5) RAL: 51.8 ± 1.8 pmol/g (5) ROH: 0.68 ± 0.07 pmol/g (5) RE: 0.26 ± 0.03 nmol/g (5)	atRA: 1.9 ± 0.1 pmol/g (7)* RAL: 48.3 ± 3.6 pmol/g (7) ROH: 0.84 ± 0.08 pmol/g (7) RE: 0.23 ± 0.03 nmol/g (7)
IWAT	atRA: 2.5 ± 0.4 pmol/g (5) RAL: 62.5 ± 6.0 pmol/g (5) ROH: 1.2 ± 0.1 nmol/g (5) RE: 0.28 ± 0.05 nmol/g (5)	atRA: 2.7 ± 0.6 pmol/g (7) RAL: 64.2 ± 5.3 pmol/g (7) ROH: 1.3 ± 0.2 nmol/g (6) RE: 0.29 ± 0.05 nmol/g (6)
Skeletal Muscle	atRA: 1.7 ± 0.2 pmol/g (5) RAL: 108.1 ± 20.3 pmol/g (5) ROH: 0.30 ± 0.03 nmol/g (5) RE: 473 ± 43 nmol/g (5)	atRA: 1.7 ± 0.2 pmol/g (7) RAL: 79.4 ± 9.6 pmol/g (7) ROH: 0.28 ± 0.02 nmol/g (7) RE: 545 ± 143 nmol/g (7)
Liver	atRA: 18.7 ± 2.6 pmol/g (5) RAL: 41.4 ± 4.1 pmol/g (5) ROH: 18.0 ± 1.7 nmol/g (5) RE: 473 ± 43 nmol/g (5)	atRA: 18.6 ± 1.9 pmol/g (6) RAL: 48.5 ± 2.5 pmol/g (7) ROH: 22.9 ± 6.7 nmol/g (7) RE: 545 ± 143 nmol/g (7)
Pancreas	atRA: 3.8 ± 0.4 pmol/g (5) ROH: 0.51 ± 0.03 nmol/g (5) RE: 1.6 ± 0.2 nmol/g (5)	atRA: 4.5 ± 0.4 pmol/g (6) ROH: 0.68 ± 0.07 nmol/g (6) RE: 2.2 ± 0.2 nmol/g (6)
Spleen	atRA: 4.8 ± 0.4 pmol/g (5) ROH: 1.3 ± 0.1 nmol/g (5) RE: 2.7 ± 0.5 nmol/g (5)	atRA: 4.3 ± 0.3 pmol/g (7) ROH: 0.9 ± 0.2 nmol/g (7) RE: 1.7 ± 0.3 nmol/g (7)

Legend: Tissue retinoids from female mice, age 73 weeks, fed a 93G diet with tissues collected under *ad lib* fed conditions (cohort 2w2). Analyzed side-by-side with mice in (Table 22), allowing for direct comparisons. atRA: all-*trans*-retinoic acid; RAL: retinal; 9cRA: 9-*cis*-retinoic acid; ROH, retinol; RE, retinyl esters. **p≤0.01, *p≤0.05 vs. WT by Student's two-tailed t-test. All values Mean ± SEM (number).

Figure 26) Retinoic Acid and Retinal in *Rdh1*-KO mice fed HFD

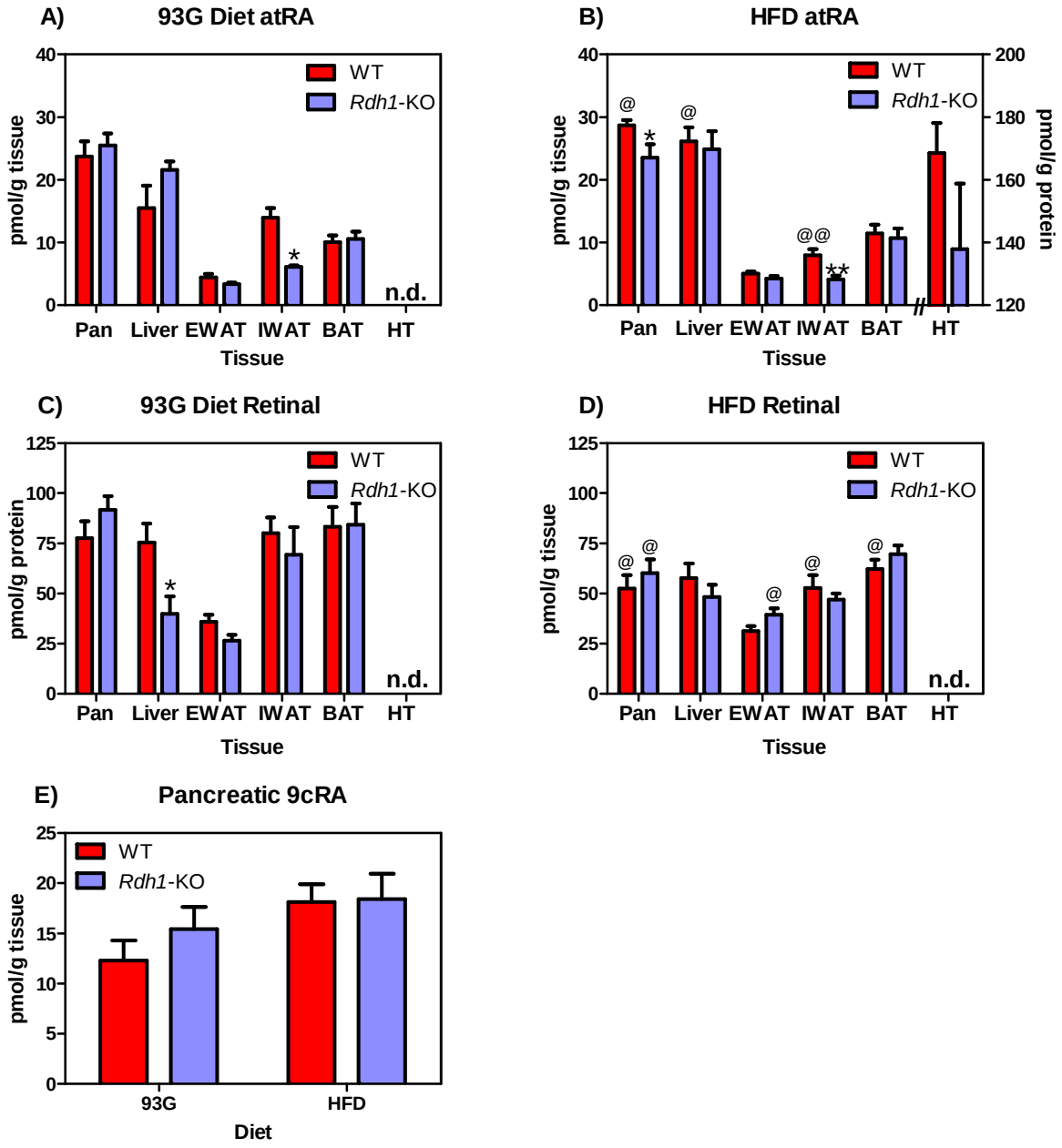

Legend: (See next page)

Legend: (A) atRA levels from WT (n=3-6) and *Rdh1*-KO (n=3-4) male mice fed a 93G diet, age 29 weeks. Tissues collected under *ad lib* fed conditions (cohort 5w1). (B) atRA levels from WT (n=4-9) and *Rdh1*-KO (n=3-7) male mice age 29 weeks, diet changed from a 93G diet to a HFD at age 7 weeks (5w1). By two way ANOVA, effect of diet in liver ($p \leq 0.05$) and IWAT ($p \leq 0.01$) and effect of genotype in IWAT ($p \leq 0.0001$) and EWAT ($p \leq 0.05$). (C) Retinal levels from mice in (A). (D) Retinal levels from mice in (B). By two-way ANOVA, effect of interaction between diet and genotype in EWAT ($p \leq 0.05$), effect of diet in pancreas ($p \leq 0.01$), IWAT ($p \leq 0.001$) and BAT ($p \leq 0.05$) and effect of genotype in liver ($p \leq 0.05$). (E) 9cRA levels from mice in (A) and (B). HFD, high fat diet; Pan, pancreas; HT, hypothalamus; n.d., not determined. WT: red bar. *Rdh1*-KO: blue bar. **$p \leq 0.01$, *$p \leq 0.05$ vs. WT, @@$p \leq 0.01$, @$p \leq 0.05$ vs. 93G diet by Student's two-tailed t-test. All values Mean $\pm$ SEM.

Figure 27) Retinol and Retinyl Esters in *Rdh1*-KO mice fed HFD

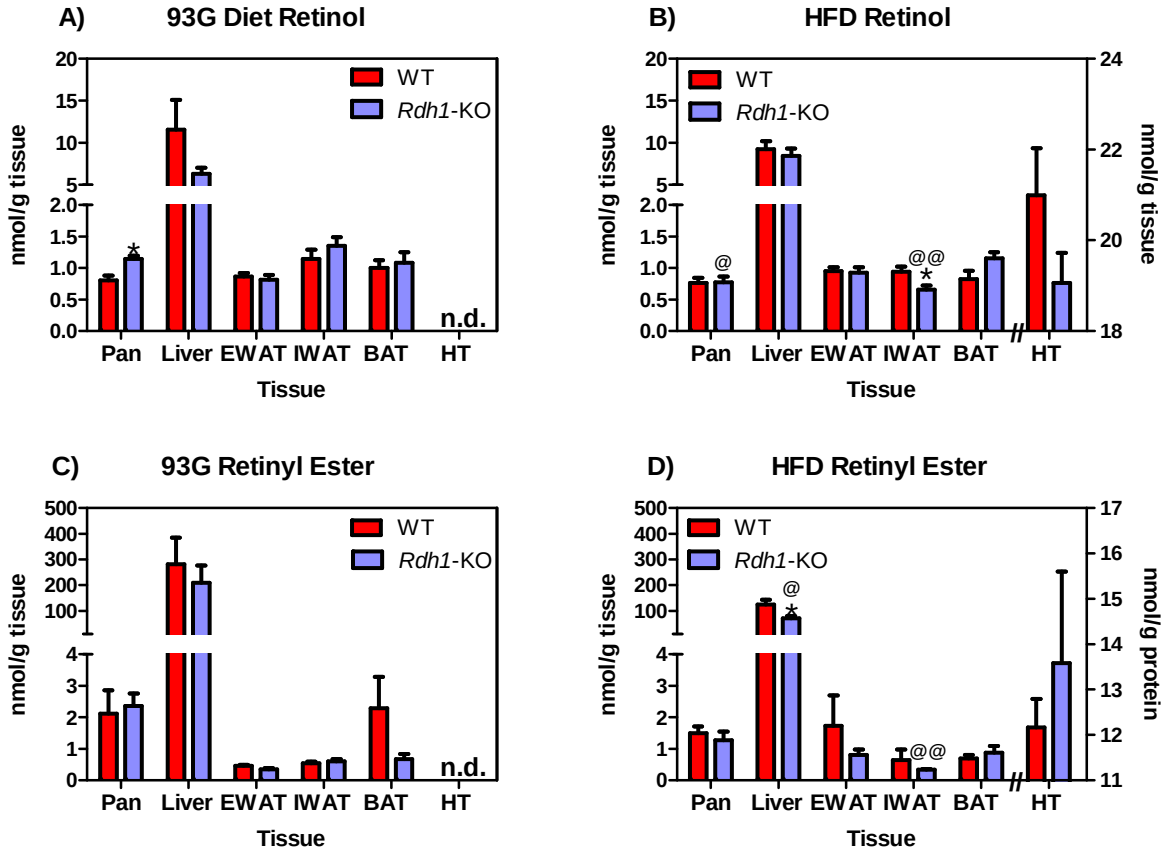

Legend: (A) Retinol levels from WT (n=3-6) and *Rdh1*-KO (n=3-4) male mice fed a 93G diet, age 29 weeks. Tissues collected under *ad lib* fed conditions (cohort 5w1). (B) Retinol levels from WT (n=4-9) and *Rdh1*-KO (n=3-7) male mice age 29 weeks, diet changed from a 93G to a HFD at age 7 weeks (5w1). By two way ANOVA, effect of interaction between diet and genotype in IWAT ($p \leq 0.05$), effect of diet in IWAT ($p \leq 0.001$) and effect of genotype in IWAT ($p \leq 0.0001$) and EWAT ($p \leq 0.05$). (C) Retinyl ester levels from mice in (A). (D) Retinyl ester levels from mice in (B). By two-way ANOVA, effect of diet in pancreas ($p \leq 0.05$) and liver ($p \leq 0.05$). HFD, high fat diet; Pan, pancreas; HT, hypothalamus. n.d., not determined. WT: red bar. *Rdh1*-KO: blue bar. **$p \leq 0.01$, *$p \leq 0.05$ vs. WT, @@$p \leq 0.01$, @$p \leq 0.05$ vs. 93G diet by Student's two-tailed t-test. All values Mean $\pm$ SEM.

Figure 28) Fasted, 2 hours Refed and *Ad Lib* Fed Retinoids in Wild-Type Mice

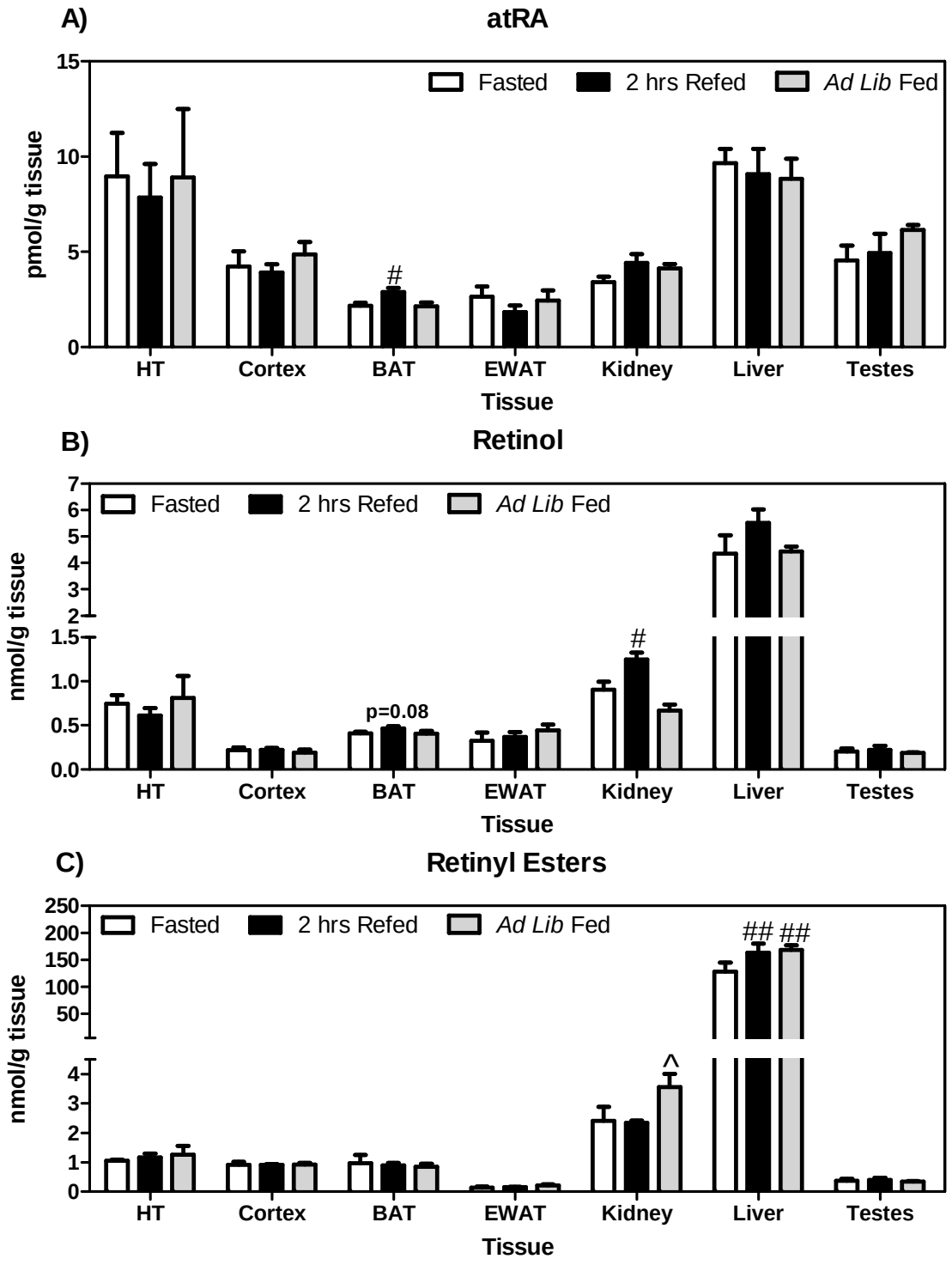

Legend: (See next page.)

Legend: (A) atRA levels in 16 hour fasted (n=4-8), 2 hours refed (n=4-8) or *ad lib* fed (n=3-6) male C57BL/6 mice, age 8-12 weeks fed a 93G diet. (B) Retinol levels from mice in (A). (C) Retinyl ester levels from mice in (A). HT, hypothalamus. Fasted: white bar. 2 hours Refed: black bar. *Ad lib* fed: grey bar. ##$p \leq 0.01$, #$p \leq 0.05$ or as indicated vs. Fasted, ^$p \leq 0.05$ vs. 2 hours Refed by Student's two-tailed t-test. All values Mean $\pm$ SEM.

Figure 29) Fasted and 4 hours Refed Retinoids in Wild-Type Mice

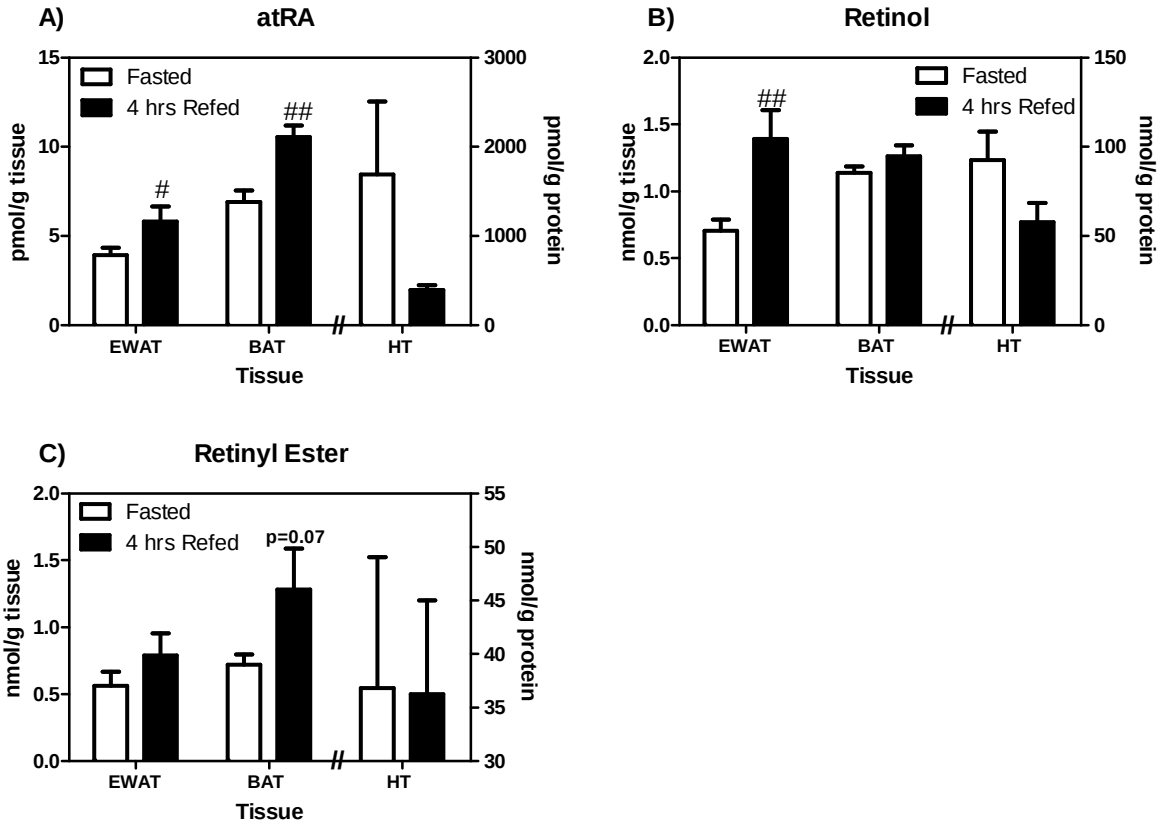

Legend: (A) atRA levels in 16 hour fasted (n=7-10) or 4 hours refed (n=6-8) male C57BL/6 mice, age 8-12 weeks, fed a 93G diet. (B) Retinol levels from mice in (A). (C) Retinyl ester levels from mice in (A). HT, hypothalamus. Fasted: white bar. 4 hours Refed: black bar. ##p≤0.01, #p≤0.05 or as indicated vs. Fasted by Student's two-tailed t-test. All values Mean ± SEM.

Figure 30) Retinoids Following Cold Exposure in Wild-Type Mice

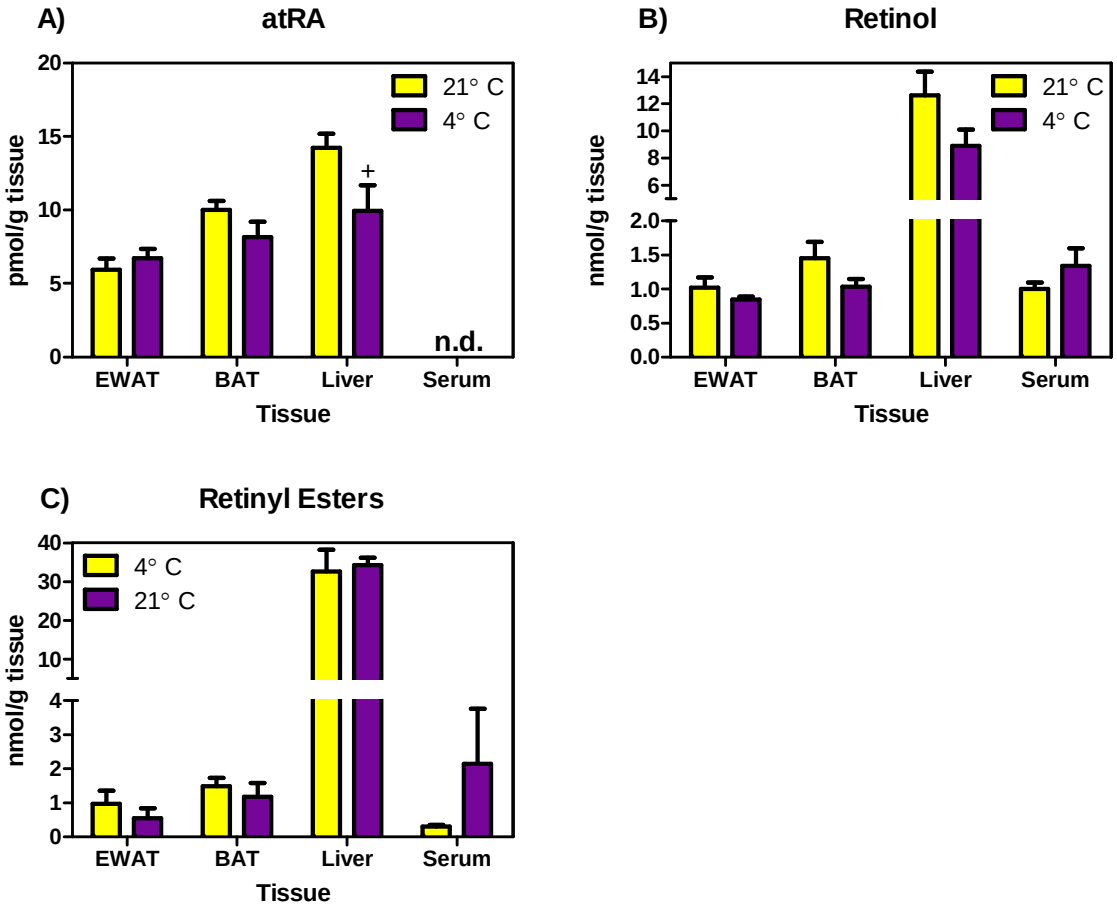

Legend: (A) atRA levels in male C7BL/6 mice, age 10-12 weeks either housed at normal housing temperature, 21º C (n=8-9), or at 4º C during the final 6 hours of a 16 hour fast. Mice fed a 93G diet. (B) Retinol levels from mice in (A). (C) Retinyl ester levels from mice in (A). n.d., not determined. 21º C: gold bar. 4º C: purple bar. +$p \leq 0.05$ vs. 21º C by Student's two-tailed t-test. All values Mean $\pm$ SEM.

Figure 31) Fasted and Refed Retinoids in Male *Rdh1*-KO Mice

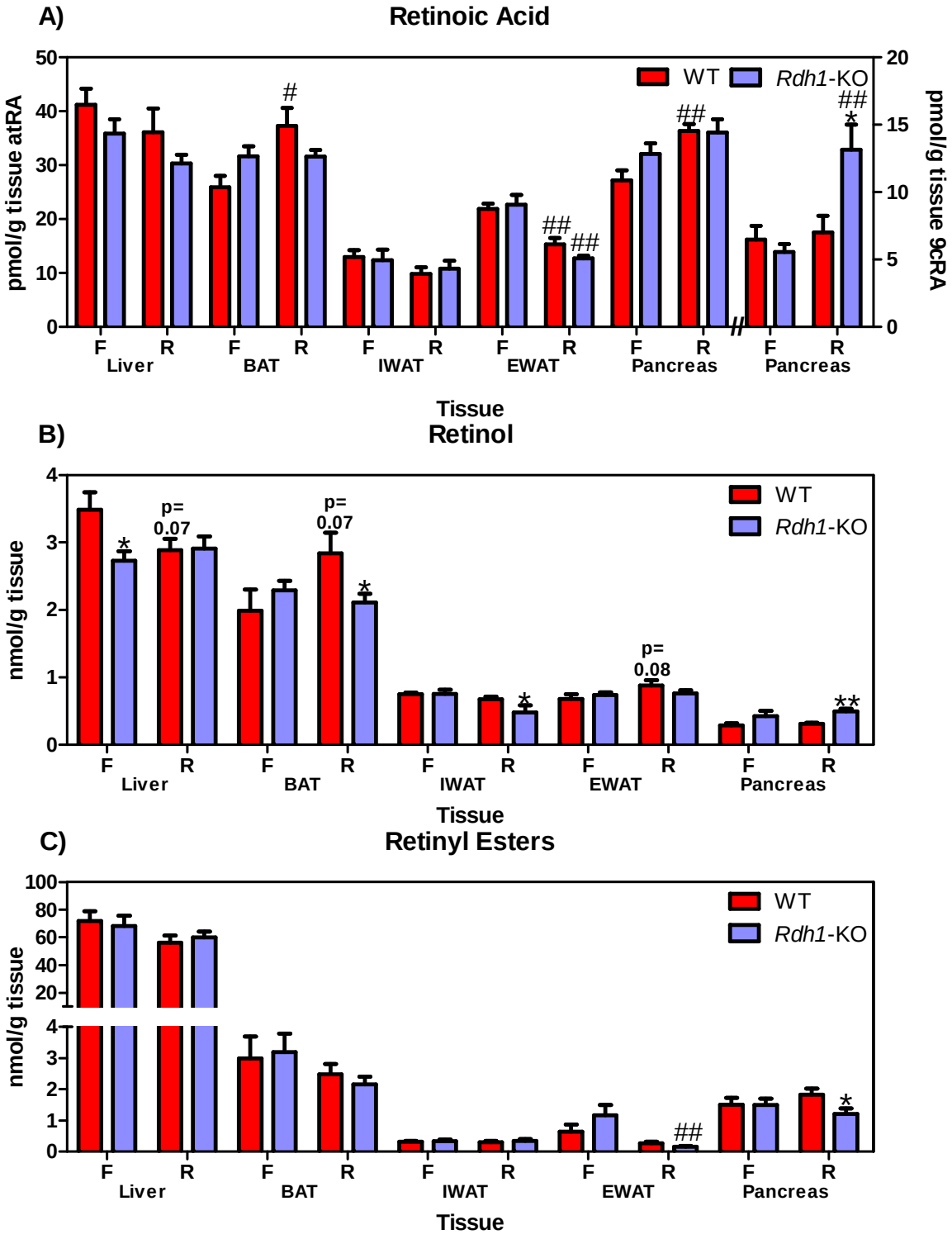

Legend: (See next page)

Legend: (A) atRA and pancreatic 9cRA levels in male WT (n=5-8) and *Rdh1*-KO (n=7-8) mice, age 9.5-11 weeks, fasted 16 hours or refed 4 hours after fast. Mice were fed a 93G diet (cohort 11w1). By two-way ANOVA, effect of interaction between refeeding and genotype in BAT ($p \leq 0.05$) and pancreatic 9cRA ($p \leq 0.01$), effect of genotype in pancreatic 9cRA ($p \leq 0.05$) and effect of refeeding in BAT ($p \leq 0.05$), EWAT ($p \leq 0.0001$), pancreatic atRA ($p \leq 0.001$) and pancreatic 9cRA ($p \leq 0.01$). (B) Retinol levels from mice in (A) (n=7-8). By two-way ANOVA, effect of interaction between refeeding and genotype in BAT ($p \leq 0.05$), effect of genotype in pancreas ($p \leq 0.01$) and effect of refeeding in IWAT ($p \leq 0.01$). (C) Retinyl ester levels from mice in (A) (n=2-8). By two-way ANOVA, effect of refeeding in EWAT ($p \leq 0.01$). F, fasted; R, refed. WT: red bar. *Rdh1*-KO: blue bar. **$p \leq 0.01$, *$p \leq 0.05$ vs. WT, ##$p \leq 0.01$, #$p \leq 0.05$ or as indicated vs. fasted by Student's two-tailed t-test. All values Mean $\pm$ SEM.

Figure 32) Fasted and Refed Retinoids in Female *Rdh1*-KO Mice

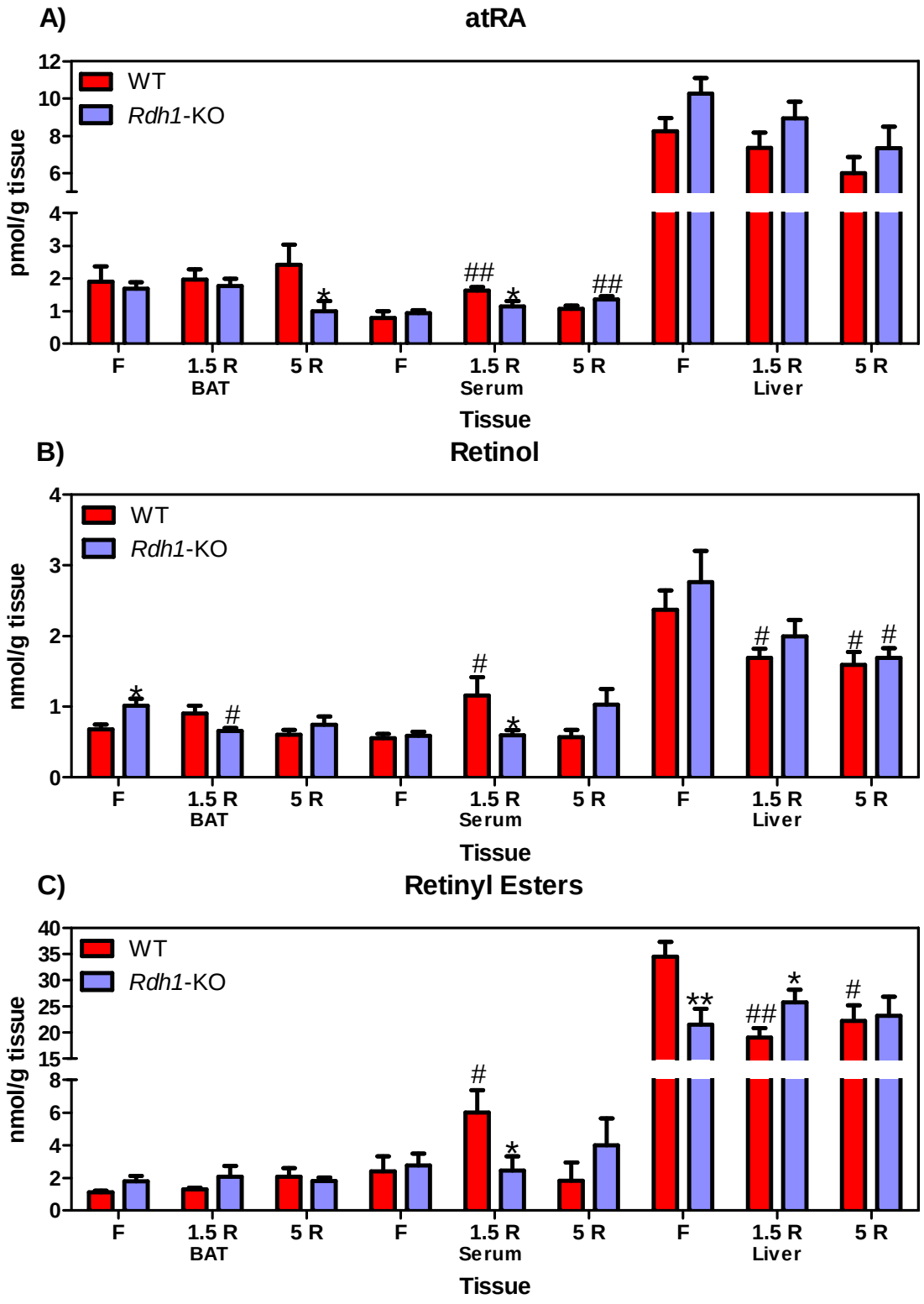

Legend: (See next page.)

Legend: (A) atRA in female WT (n=5-6) and *Rdh1*-KO (n=7-9) mice, age 10-11 weeks, fasted 16 hours or refed 1.5 or 5 hours after fast. Mice were fed a 93G diet (cohort 13w2). By two-way ANOVA, effect of interaction between refeeding and genotype in serum ($p \leq 0.05$), effect of genotype in BAT ($p \leq 0.05$) and liver ($p \leq 0.05$) and effect of refeeding in serum ($p \leq 0.01$) and liver ($p \leq 0.05$). (B) Retinol levels from mice in (A) (n=4-9). By two-way ANOVA, effect of interaction between refeeding and genotype in BAT ($p \leq 0.05$) and serum ($p \leq 0.05$) and effect of refeeding in liver ($p \leq 0.01$). (C) Retinyl ester levels from mice in (A) (n=5-9). By two-way ANOVA, effect of interaction between genotype and refeeding in liver ($p \leq 0.01$). F, fasted; R, refed. WT: red bar. *Rdh1*-KO: blue bar. **$p \leq 0.01$, *$p \leq 0.05$ vs. WT, ##$p \leq 0.01$, #$p \leq 0.05$ vs. fasted by Student's two-tailed t-test. All values Mean $\pm$ SEM.

Figure 33) Fasted and Refed Retinoids in Old *Rdh1*-KO Brown Adipose Tissue

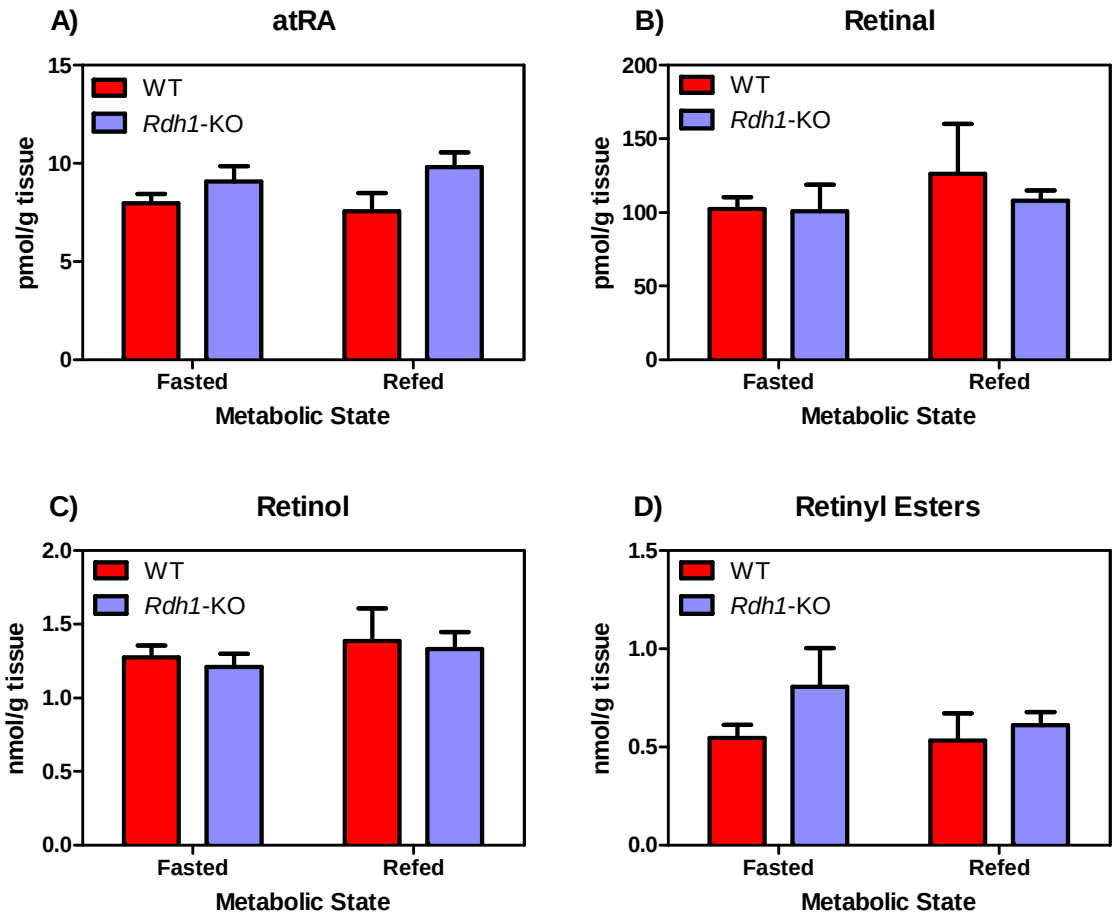

Legend: (A) atRA in male WT (n=4-5) and *Rdh1*-KO (n=7) mice, age 45 weeks, fasted 16 hours or refed 4 hours after fast. Mice were switched from a VAD diet to a 93G diet at age 5 weeks and born to dams switched from a Harlan chow diet to VAD diet at mating (cohort 3w2). (B) Retinal levels from mice in (A). (C) Retinol levels from mice in (A). (D) Retinyl ester levels from mice in (A). WT: red bars. *Rdh1*-KO: blue bars. All values Mean $\pm$ SEM.

Figure 34) Retinoids in Rat BAT following Oral Gavage

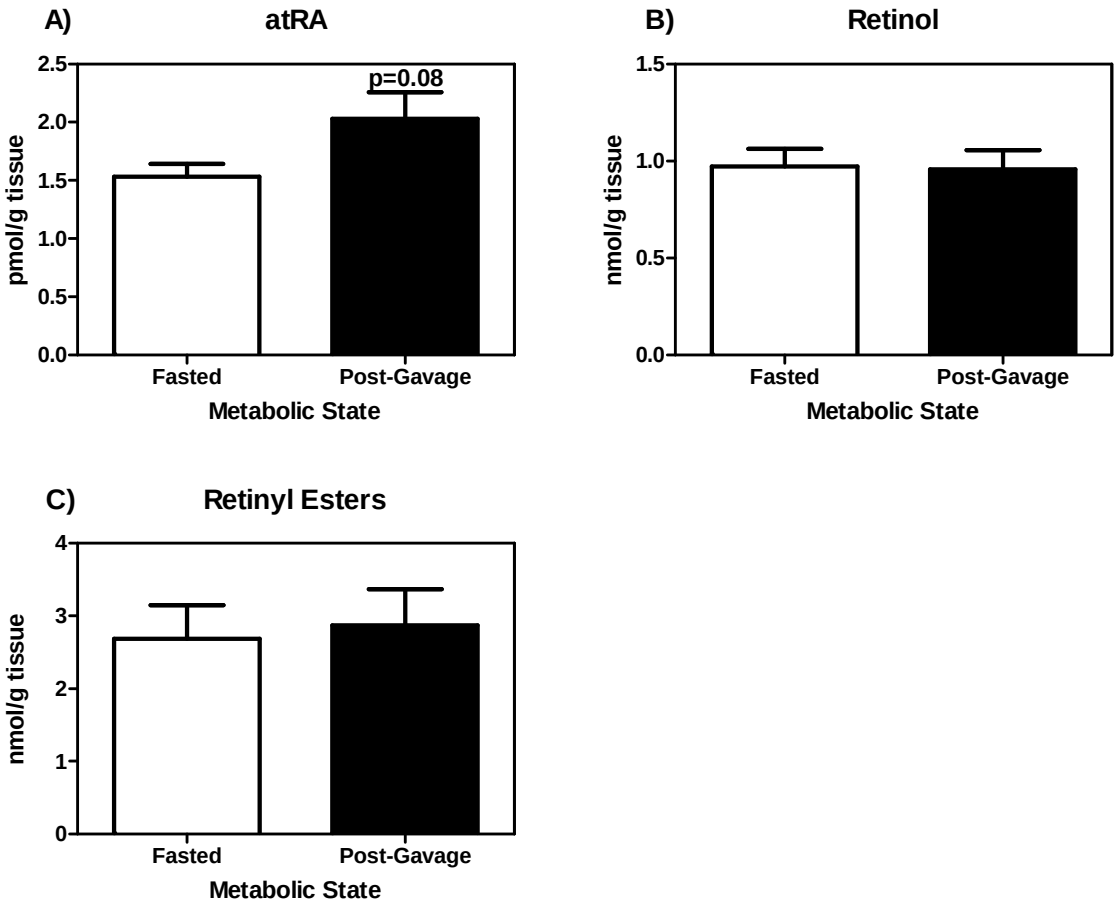

Legend: (A) atRA in brown adipose tissue from male rats age 3.5-4 months either fasted 16 hours (n=4) or 15 minutes following a oral gavage of 2 g/kg glucose. (B) Retinol levels from rats in (A) (n=5). (C) Retinyl ester levels from rats in (A) (n=5). Fasted: white bars. 15 minutes post-gavage: black bars. By Student's two tailed t-test, p as indicated. All values Mean $\pm$ SEM

Figure 35) Brown Adipose Gene Expression in *Ad Lib* fed *Rdh1*-KO Mice

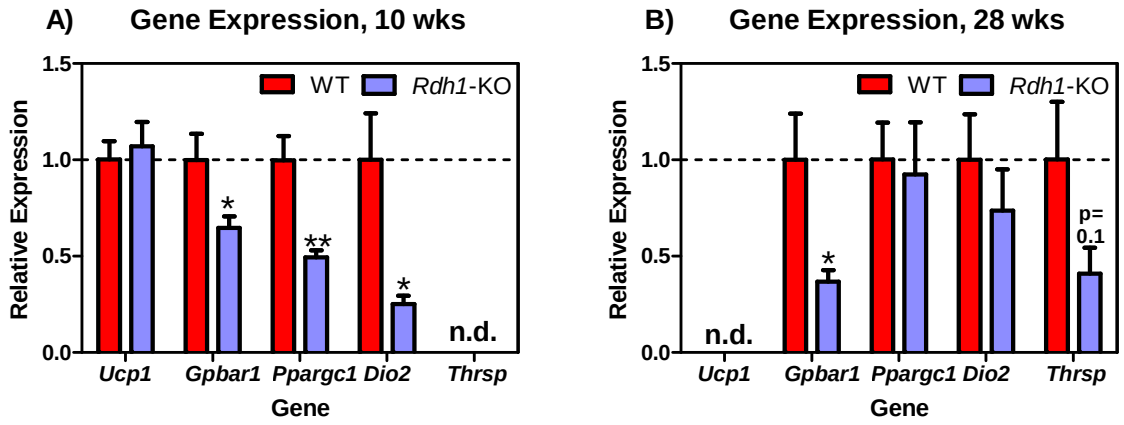

Legend: (A) Gene expression from male WT (n=6-9) and *Rdh1*-KO (n=6-9) mice, age 10 weeks and fed a 93G diet (cohort 8w1). Tissue collected under *ad lib* fed conditions. Expression of each gene normalized to WT (dotted line). (B) Gene expression from male WT (n=6-7) and *Rdh1*-KO (n=6-7) mice, age 28 weeks and fed a 93G diet (cohort 10w1b). Tissues collected under *ad lib* fed conditions. Expression of each gene normalized to WT (dotted line). WT: red bars. *Rdh1*-*Rdh1*-KO: blue bars. n.d., not determined. **$p \leq 0.01$, *$p \leq 0.05$ or as indicated vs. WT by Student's two-tailed t-test. All values Mean $\pm$ SEM.

Figure 36) Fasted and Refed BAT Gene Expression in *Rdh1*-KO Mice

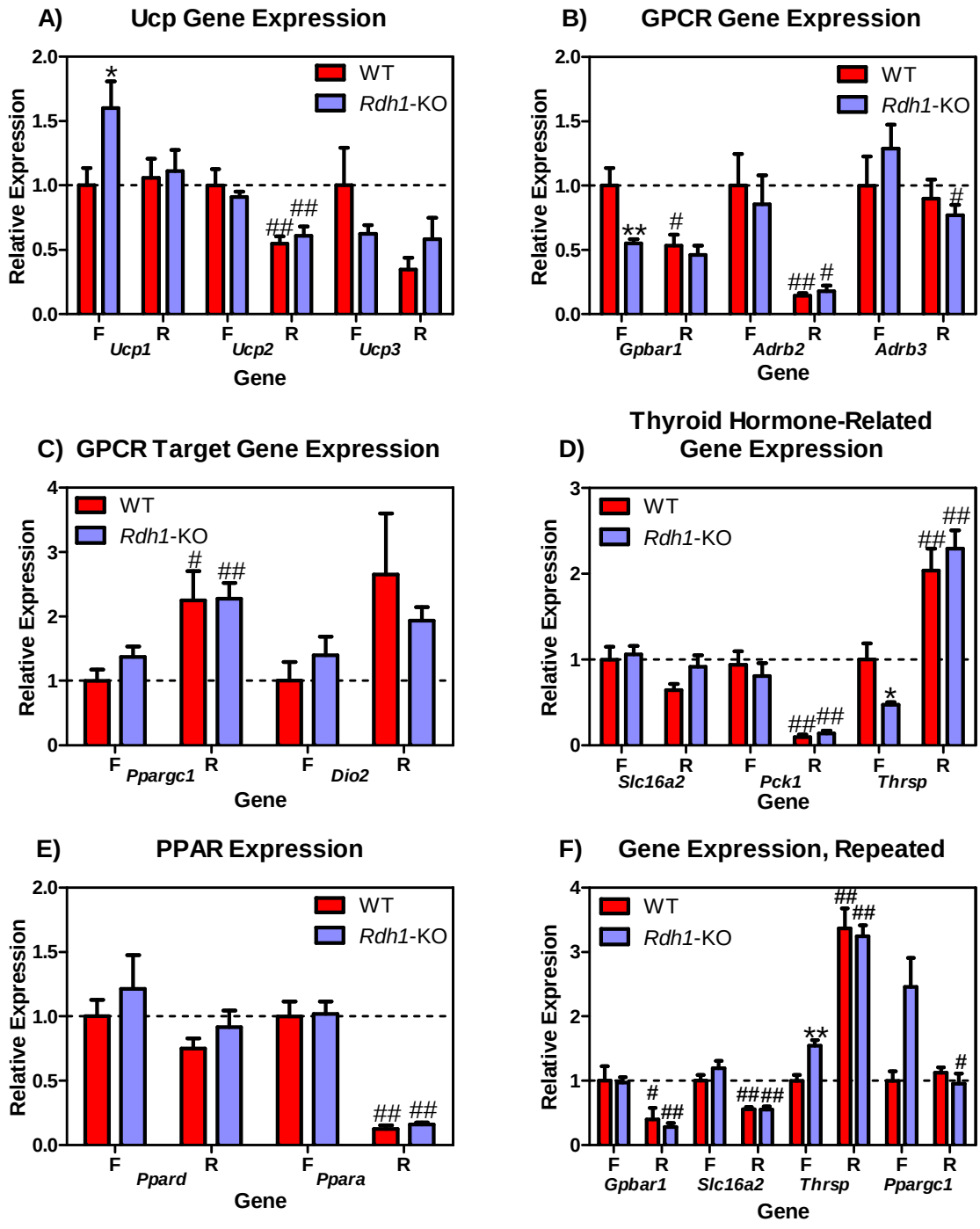

Legend: (See next page.)

Legend: (A-E) Gene expression from 16 hour fasted or 6-7 hour refed male WT (n=5-8) and *Rdh1*-KO (n=5-8) mice, age 6 weeks and fed a 93G diet (cohort 12w1). Expression of each gene arbitrarily normalized to WT fasted (dotted line). By two-way ANOVA, effect of interaction between genotype and feeding on *Thrsp* ($p \leq 0.05$), effect of feeding on *Ucp2* ($p \leq 0.0001$), *Gpbar1* ($p \leq 0.01$), *Adrb2* ($p \leq 0.001$), *Ppargc1* ($p \leq 0.001$), *Dio2* ($p \leq 0.05$), *Pck1* ($p \leq 0.0001$), *Thrsp* ($p \leq 0.0001$), *Ppara* ($p \leq 0.0001$) and effect of genotype on *Gpbar1* ($p \leq 0.05$). (F) Gene expression from 16 hour fasted or 6-7 hour refed male WT (n=4-5) and *Rdh1*-KO (n=4-5) mice, age 7.5 weeks and fed a 93G diet (cohort 12w2). Expression of each gene arbitrarily normalized to WT fasted (dotted line). By two-way ANOVA, effect of interaction between genotype and feeding on *Ppargc1* ($p \leq 0.05$) and effect of feeding on *Gpbar1* ($p \leq 0.0001$), *Slc16a2* ($p \leq 0.0001$), *Thrsp* ($p \leq 0.0001$) and *Ppargc1* ($p \leq 0.05$). F, fasted; R, refed. WT: red bars. *Rdh1*-KO: blue bars. **$p \leq 0.01$, *$p \leq 0.05$ vs. WT and ##$p \leq 0.01$, #$p \leq 0.05$ vs. Fasted by Student's two-tailed t-test. All values Mean $\pm$ SEM.

Table 24) Select Differentially-Regulated Genes from *Rdh1*-KO EWAT Microarray, Part I

Rel. Exp.	*P* (≤)	Gene	Description
Retinoid homeostasis			
2.0	0.0008	*Rbp1*	Cellular retinol binding protein 1
1.5	0.01	*Aldh1a1*	Retinal dehydrogenase 1
1.3	0.003	*Rdh11*	Retinol dehydrogenase 11
0.3	0.0005	*Ttr*	Transthyretin
Adipokines			
7.6	0.000002	*Npy*	Neuropeptide Y
0.6	0.01	*Retn*	Resistin
Cell or metabolic regulation			
10.2	0.003	*Egr2*	Early growth response 2
5.3	0.002	*Gpr64*	G protein-coupled receptor 64
4.4	0.0002	*Grb7*	Growth factor receptor binding protein 7
4.2	0.00002	*Sh3yl1*	Sh3 domain YSC-like 1
2.5	0.003	*Ace*	Angiotensin I converting enzyme 1
2.4	0.0003	*Insl6*	Insulin-like 6
2.3	0.0005	*Egf*	Epidermal growth factor
2.0	0.00009	*Sbk*	SH3-binding kinase 1
1.6	0.003	*Fgfr2*	Fibroblast GF receptor 2
1.6	0.007	*Bhlhb2*	Basic hlh domain, class B2
1.3	0.002	*Mapk14*	MAPK 14
0.8	0.03	*Med1*	PPAR Binding Protein
0.8	0.02	*Pparg*	PPARγ
0.7	0.005	*Irs1*	Insulin receptor substrate 1
0.7	0.002	*Gpr43*	Free fatty acid receptor 2
0.7	0.009	*Ucp3*	Uncoupling protein 3
0.7	0.0008	*Igfbp5*	Insulin-like growth factor binding protein 5
0.7	0.0004	*Igfbp6*	Insulin-like growth factor binding protein 6
0.6	0.002	*Flrt2*	MAPK kinase kinase kinase 5
0.6	0.0008	*Agt*	Angiotensinogen
0.5	0.0006	*Tnfrsf11b*	TNF receptor (osteoprotegerin)
0.5	0.0003	*Adcyap1r1*	Adenylate cyclase act. pp 1 receptor 1

Legend: Select genes of the 2957 differentially-regulated genes identified in *Rdh1*-KO EWAT from 10 week old, fasted male mice fed a 93G diet (cohort 1.5w1). Rel. Exp.: Expression relative to WT.

Table 25) Select Differentially-Regulated Genes from *Rdh1*-KO EWAT Microarray, Part 2

Rel. Exp.	*P* (≤)	Gene	Description
Intermediary metabolism			
3.8	0.003	*Gyk*	Glycerol kinase
3.1	0.0006	*Cds1*	CDP-diacylglycerol synthase 1
2.4	0.02	*Scd2*	Stearoyl-Coenzyme A desaturase 2
1.9	0.003	*Elovl6*	Elongation of long chain fatty acids 6
1.8	0.0009	*Acly*	ATP citrate lyase
1.6	0.009	*Acat2*	Acetyl-Coenzyme A acetyltransferase
1.5	0.008	*Ldh2*	Lactate dehydrogenase B
1.5	0.009	*Acas2l*	Acyl-CoA synthetase short-chain 1
1.4	0.03	*Pdk1*	Pyruvate dehydrogenase, isoenzyme 1
0.8	0.04	*Plin*	Perilipin
0.8	0.006	*Lipe*	Hormone sensitive lipase
0.8	0.002	*Gpd2*	Glycerol phosphate dehydrogenase 2
0.7	0.01	*Crat*	Carnitine acetyltransferase
0.7	0.003	*Sort1*	Sortilin 1
0.7	0.0008	*Dgat1*	Diacylglycerol O-acyltransferase 1
0.6	0.009	*Acacb*	Acetyl-Coenzyme A carboxylase beta
0.6	0.0001	*Mogat1*	Monoacylglycerol O-acyltransferase 1
0.5	0.00007	*Sah*	Acyl-CoA synthetase medium-chain 3
0.5	0.002	*Pte2b*	Acyl-CoA thioesterase 4
Transporters and carriers			
50.9	0.0003	*Lcn8*	Lipocalin 8
38.0	0.007	*Ap1s2*	Adaptor-related complex 1, σ2
23.1	0.003	*Lcn2*	Lipocalin 2
19.6	3.5E-11	*Lcn5*	Lipocalin 5
19.1	0.006	*Lcn10*	Lipocalin 10
10.5	0.002	*Slc1a1*	Solute carrier 1, member 1
2.9	0.004	*Slc2a5*	GLUT5
2.8	0.004	*Frag1*	FGF receptor activating protein 1
2.1	0.009	*Lcn13*	Lipocalin 13
0.8	0.002	*Apoc1*	Apolipoprotein C-I
0.8	0.004	*Slc2a4*	GLUT4
0.3	0.00004	*Apoc3*	Apolipoprotein C-III
0.3	0.009	*Apoh*	Apolipoprotein H
0.2	0.02	*Apoa2*	Apolipoprotein A-II
Immune Response			
10487.3	0.002	*Defb12*	Beta-defensin 12
5310.5	0.0000005	*Defb15*	Beta-defensin 15
4433.0	0.0004	*Defb39*	Beta-defensin 39
6.4	0.00005	*Gbp1*	Guanylate binding protein 1

Legend: Select genes of the 2957 differentially-regulated genes identified in *Rdh1*-KO EWAT from 10 week old, fasted male mice fed a 93G diet (cohort 1.5w1). Rel. Exp.: Expression relative to WT.

Figure 37) *Rdh1*-KO EWAT Microarray Follow-up

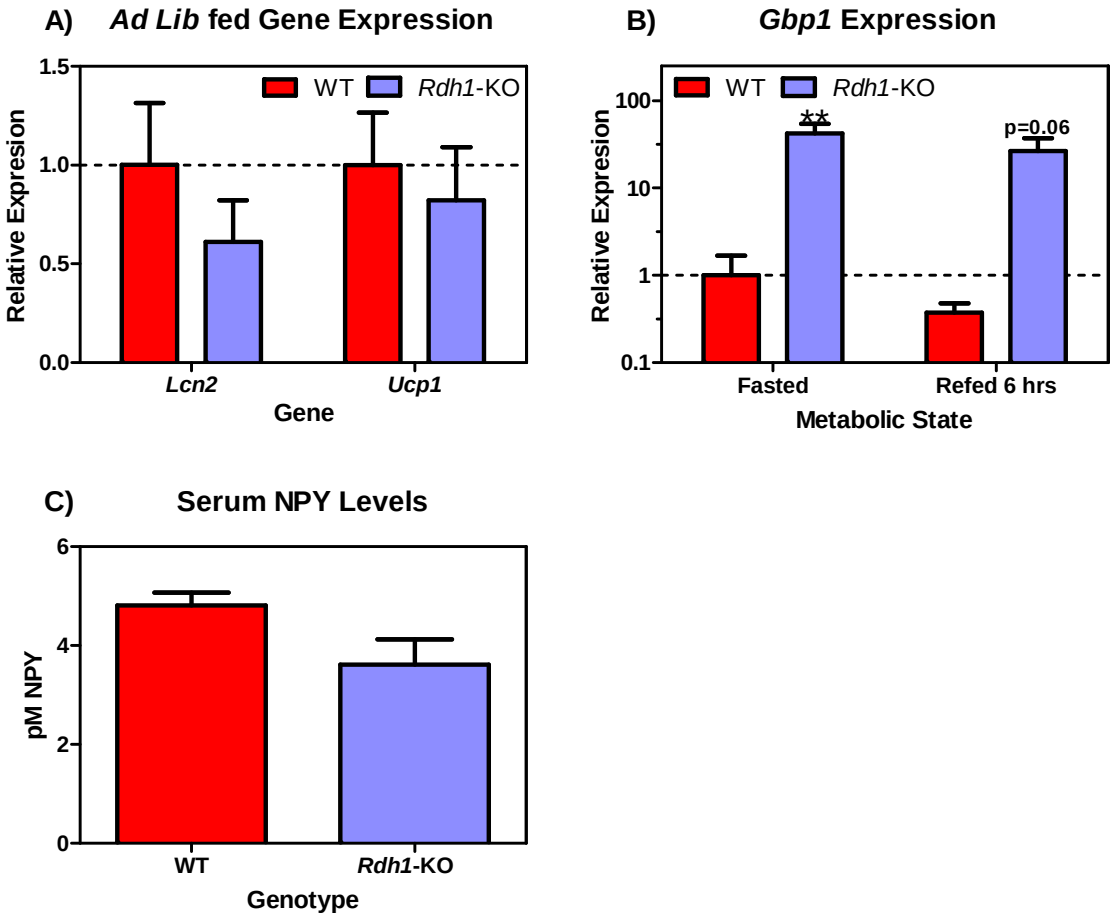

Legend: (A) EWAT Gene expression from WT (n=5-7) and *Rdh1*-KO (n=4-5) male mice, age 10 weeks and fed a 93G diet (cohort 8w2). Tissues collected under *ad lib* fed conditions. Expression of each gene normalized to WT (dotted line). (B) *Gbp1* gene expression from EWAT of 16 hour fasted or 6 hour refed WT (n=4-5) and *Rdh1*-KO (n=5) female mice, age 10 weeks and fed a 93G diet (cohort 12w1). Expression arbitrarily normalized to WT Fasted (dotted line). By two-way ANOVA, effect of genotype ($p \leq 0.001$). (C) Serum neuropeptide Y levels from 4-5 week old fasted WT (n=3) and *Rdh1*-KO (n=3) mice fed a 93G diet (cohort 6w1). WT: red bars. *Rdh1*-KO: blue bars. **$p \leq 0.01$ or as indicated vs. WT by Student's two-tailed t-test. All values Mean $\pm$ SEM.

Table 26) Select Differentially-Regulated Genes from *Rdh1*-KO Testis Microarray

Rel. Exp.	*P* (≤)	Gene	Description
1.48	0.001	CRAD-L	CRAD-like
0.59	0.001	*Pla2g12a*	Phospholipase A2, group XIIA
0.58	0.001	*Npy*	Neuropeptide Y
0.56	0.00004	*Cap1*	Adenylate cyclase-associated protein 1
0.56	0.001	*Tieg1*	Kruppel-like factor 10
0.51	0.001	*Hoxc12*	Homeobox C12

Legend: Select genes of the 1308 differentially-regulated genes identified in *Rdh1*-KO testis from 10 week old, fasted male mice fed a 93G diet (cohort 1.5w1). Rel. Exp.: Expression relative to WT.

Table 27) Select Differentially-Regulated Genes from *Rdh1*-KO Liver Microarray

Rel. Exp.	*P* (≤)	Gene	Description
3.7	0.002	*Foxq1*	Forkhead box Q1
3.24	0.01	*Gbp1*	Guanylate binding protein 1
1.98	0.03	*Gbp4*	Guanylate binding protein 4
1.95	0.05	*Gck*	Glucokinase
1.94	0.02	*Ppargc1b*	PPARγ, coactivator beta
0.71	0.03	*Cap1*	Adenylate cyclase-associated protein 1
0.46	0.003	*Rdh9*	CRAD3
0.29	0.05	*Cyp2c39*	Cytochrome P450 family 2, subfamily c, polypeptide 39

Legend: Select genes of the 535 differentially-regulated genes identified in *Rdh1*-KO liver from 10 week old, fasted male mice fed a 93G diet (cohort 1.5w1). Rel. Exp.: Expression relative to WT.

Figure 38) Gene Expression in *Rdh1*-KO Liver

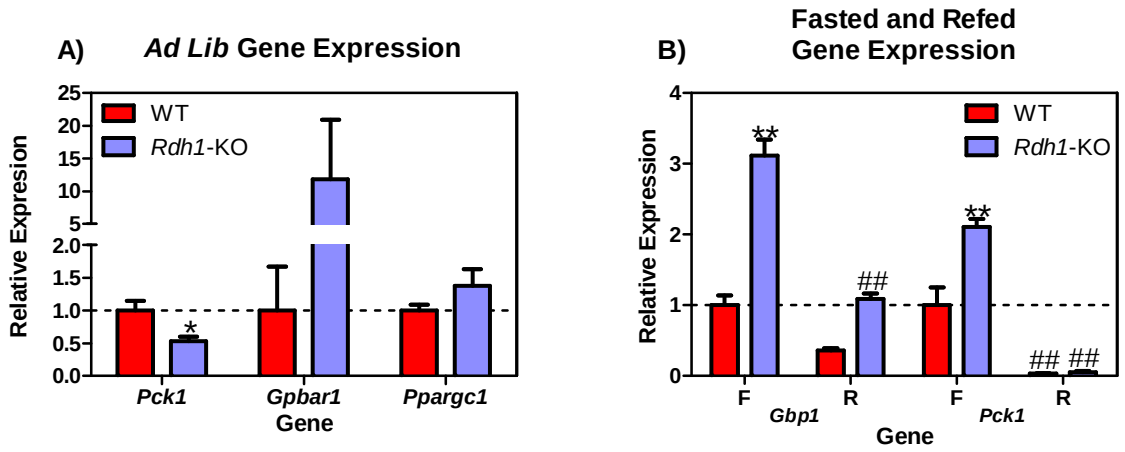

Legend: (A) Liver gene expression from WT (n=9) and *Rdh1*-KO (n=9) male mice, age 10 weeks and fed a 93G diet (cohort 8w2). Tissues collected under *ad lib* fed conditions. Expression of each gene normalized to WT (dotted line). (B) Gene expression from livers of 16 hour fasted or 6-7 hour refed WT (n=5-6) or *Rdh1*-KO (n=6) male mice, age 7.5 weeks and fed a 93G diet (cohort 12w2). Expression of each gene arbitrarily normalized to WT Fasted (dotted line). By two-way ANOVA, effect of interaction between genotype and refeeding in *Gbp1* ($p \leq 0.0001$) and *Pck1* ($p \leq 0.001$), effect of genotype in *Gbp1* ($p \leq 0.0001$) and *Pck1* ($p \leq 0.001$) and effect of refeeding for *Gbp1* ($p \leq 0.0001$) and *Pck1* ($p \leq 0.0001$). F, fasted; R, refed. WT: red bars. *Rdh1*-KO: blue bars. **$p \leq 0.01$, *$p \leq 0.05$ vs. WT and ##$p \leq 0.01$, #$p \leq 0.05$ vs. Fasted by Student's two-tailed t-test. All values Mean $\pm$ SEM.

Table 28) Genes Changes 2-Fold or Greater from *Rdh1*-KO BAT Microarray

Rel. Exp.	Adj. P (≤)	Gene	Description
0.13	0.008	*Pla2g12a*	Phospholipase A2, group XIIA
0.18	0.03	*Adh6b*	Alcohol dehydrogenase 6B (class V)
0.23	0.34	*Adh1*	Alcohol dehydrogenase 1
0.26	0.5	*Elovl3*	Elongation of very long chain fatty acids-like 3
0.37	0.6	*Ccdc28b*	Coil-coil domain containing 28b
0.40	0.8	*Arl3*	ADP-ribosylation factor-like 3
0.43	0.5	*Abcd3*	ATP-binding cassette, sub-family D, member 3
0.44	0.5	*Gsta3*	Glutathione S-transferase, alpha
0.45	0.8	*Car5b*	Carbonic anhydrase 5b, mitochondrial
0.45	0.5	*Orm2*	Orosomucoid 2
0.45	0.6	*Tmem184a*	Transmembrane protein 184a
0.47	0.6	*Lgals3bp*	Lectin, galactoside-binding, soluble, 3 binding protein
0.48	0.7	*Bsdc1*	BSD domain containing 1
0.49	0.5	*Pfkl*	Phosphofructokinase, liver, B-type
0.50	0.7	*Acot11*	Acyl-CoA thioesterase 11
2.00	0.9	*Myl2*	Myosin, light polypeptide 2, regulatory, cardiac, slow
2.09	0.9	*Klf2*	Kruppel-like factor 2 (lung)
2.09	0.7	*Gmpr*	Guanosine monophosphate reductase
2.10	0.6	*Gpcpd1*	Glycerophosphocholine phosphodiesterase GDE1 homolog
2.13	0.7	*Per2*	Period homolog 2 (Drosophila)
2.14	0.8	*Nif3l1*	Ngg1 interacting factor 3-like 1 (S. pombe)
2.21	0.7	*Car3*	Carbonic anhydrase 3
2.29	0.6	*Pisd-ps3*	Phosphatidylserine decarboxylase, pseudogene 3
2.34	0.9	*Irf4*	Interferon regulatory factor 4
2.40	0.9	*Ppp1r3g*	Protein phosphatase 1, regulatory (inhibitor) subunit 3G
2.48	0.7	*Trp53inp1*	Transformation related protein 53 inducible nuclear protein 1
2.55	0.7	*Hyi*	Hydroxypyruvate isomerase homolog (E. coli)
2.70	0.9	*Adrb2*	Adrenergic receptor, beta 2
2.72	0.6	A930005H10 RIK	RIKEN cDNA A930005H10 gene
3.02	0.2	*Col27a1*	Collagen, type XXVII, alpha 1
3.03	0.9	*Ppil3*	Peptidylprolyl isomerase (cyclophilin)-like 3
3.04	0.7	*Rbp4*	Retinol binding protein 4, plasma
3.96	0.8	*Cap1*	CAP, adenylate cyclase-associated protein 1 (yeast)
5.91	0.5	*Gbp1*	Guanylate binding protein 1

Legend: All genes with greater than 2-fold change in a microarray of BAT from 16 hour fasted, WT and *Rdh1*-KO male mice, age 6 weeks, fed a 93G diet (cohort 12w1). Rel. Exp.: Expression relative to WT. Adj. P: p-value adjusted for multiple comparisons.

Figure 39) *Rdh1*-KO BAT Gene Expression of Genes Identified in Microarray

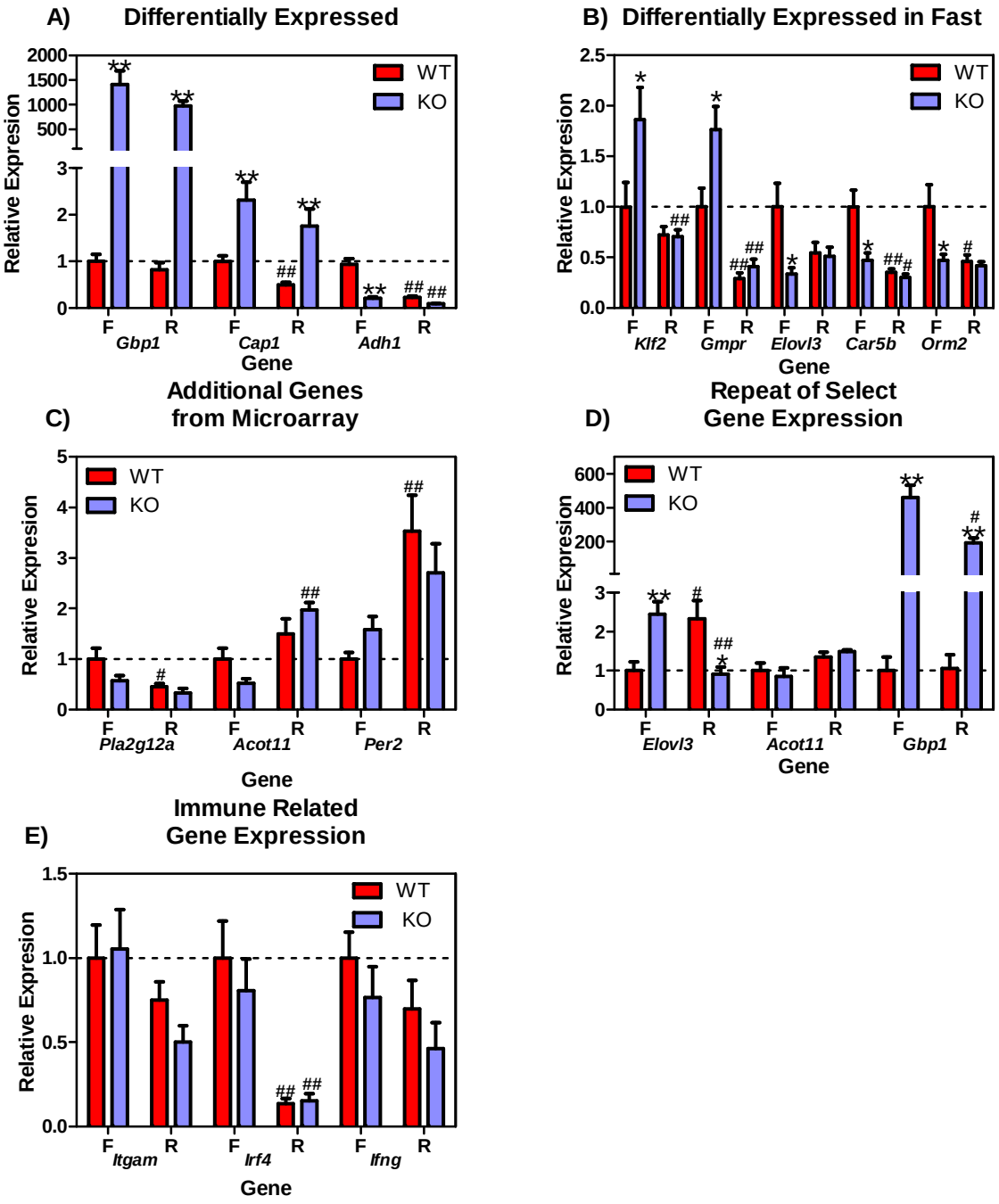

Legend: (See next page.)

Legend: (A) Microarray-identified genes (Table 25) differentially expressed in *Rdh1*-KO mice after both a 16 hour fast and 6-7 hours of refeeding. Tissues from 6 week old male WT (n=6-8) and *Rdh1*-KO (n=6-8) mice fed a 93G diet (cohort 12w1). By two-way ANOVA, effect of interaction between genotype and refeeding in *Adh1* ($p \leq 0.001$), effect of genotype in *Gbp1* ($p \leq 0.0001$), *Cap1* ($p \leq 0.0001$) and *Adh1* ($p \leq 0.0001$) and effect of refeeding in *Adh1* ($p \leq 0.0001$). Expression of each gene arbitrarily normalized to WT Fasted (dotted line). (B) Microarray-identified genes (Table 25) differentially expressed in *Rdh1*-KO mice following a 16 hour fast. Same mice as (A). By two-way ANOVA, effect of interaction between genotype and refeeding on *Elovl3* ($p \leq 0.05$) and *Car5b* ($p \leq 0.05$), effect of genotype on *Gmpr* ($p \leq 0.05$), *Elovl3* ($p \leq 0.05$), *Car5b* ($p \leq 0.01$) and *Orm2* ($p \leq 0.05$) and effect of refeeding on *Klf2* ($p \leq 0.01$), *Gmpr* ($p \leq 0.0001$), *Car5b* ($p \leq 0.001$) and *Orm2* ($p \leq 0.05$). Expression of each gene arbitrarily normalized to WT Fasted (dotted line). (C) Expression of microarray-identified genes (Table 25) after 16 hours fasting or 6-7 hours refeeding. Same mice as (A). By two-way ANOVA, effects of interaction between genotype and refeeding on *Acot11* ($p \leq 0.05$) and refeeding on *Pla2g12a* ($p \leq 0.01$) and *Acot11* ($p \leq 0.0001$). Expression of each gene arbitrarily normalized to WT Fasted (dotted line). (D) Repeated gene expression measure of select microarray-identified genes (Table 25) after 16 hours fasting or 6-7 hours refeeding. Tissues from 7.5 week old male WT (n=3-5) and *Rdh1*-KO (n=3-5) mice fed a 93G diet (cohort 12w2). By two-way ANOVA, effect of interaction between genotype and refeeding on *Gbp1* ($p \leq 0.05$) and *Elovl3* ($p \leq 0.001$), effect of genotype on *Gbp1* ($p \leq 0.001$) and effect of refeeding on *Gbp1* ($p \leq 0.05$) and *Acot11* ($p \leq 0.01$). Expression of each gene arbitrarily normalized to WT Fasted (dotted line). F, fasted; R, refed. WT: red bars. *Rdh1*-KO: blue bars. $^{**}p \leq 0.01$, $^{*}p \leq 0.05$ vs. WT and $\#\#p \leq 0.01$, $\#p \leq 0.05$ vs. Fasted by Student's two-tailed t-test. All values Mean $\pm$ SEM.

Figure 40) Expression of Retinoid Metabolism Genes in BAT during Fasting and Refeeding

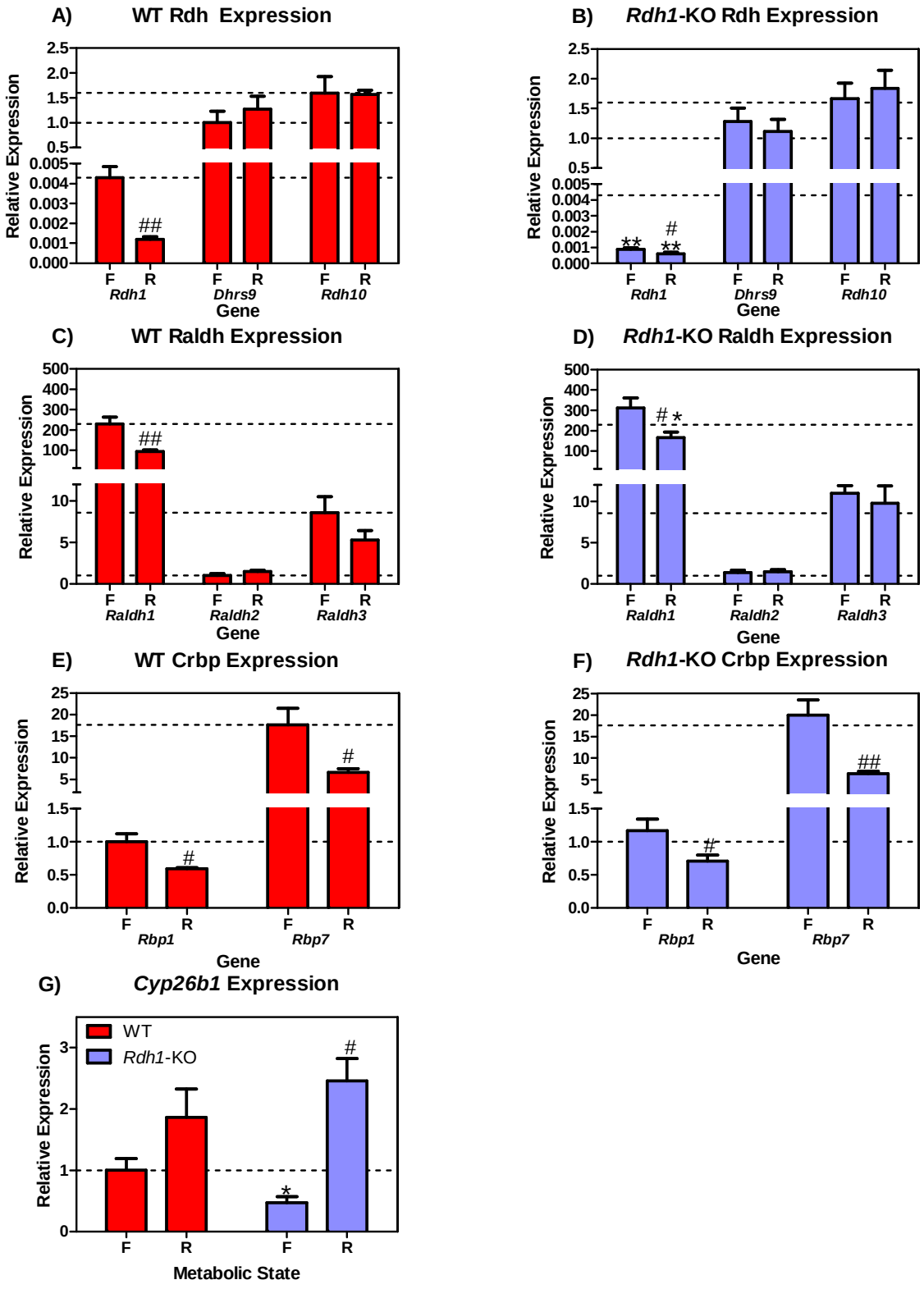

Legend: (See next page.)

Legend: (A) Expression of Rdh in WT BAT (n=6-8) after 16 hours fasting or 6-7 hours refeeding. Tissues from 6 week old male mice fed a 93G diet (cohort 12w1). Expression of all genes arbitrarily normalized to fasted *Dhrs9* levels. Dotted lines represent fasted levels of each gene. (B) Expression of Rdh in *Rdh1*-KO BAT (n=6-8) after 16 hours fasting or 6-7 hours refeeding. Tissues from 6 week old male mice fed a 93G diet (cohort 12w1). Expression of all genes arbitrarily normalized to fasted WT *Dhrs9* levels. Dotted lines represent fasted WT levels of each gene. By two-way ANOVA, effect of interaction between genotype and refeeding, effect of genotype and effect of refeeding for *Rdh1* (all $p \leq 0.001$). (C) Expression of Raldh in WT BAT (n=6-8) after 16 hours fasting or 6-7 hours refeeding. Same mice as (A). Expression of all genes arbitrarily normalized to fasted *Raldh2* levels. Dotted lines represent fasted levels of each gene. (D) Expression of Raldh in *Rdh1*-KO BAT (n=6-8) after 16 hours fasting or 6-7 hours refeeding. Same mice as (B). Expression of all genes arbitrarily normalized to fasted WT *Raldh2* levels. Dotted lines represent fasted WT levels of each gene. By two-way ANOVA, effects of genotype on *Raldh1* ($p \leq 0.05$) and *Raldh3* ($p \leq 0.05$) and effect of refeeding on *Raldh1* ($p \leq 0.0001$). (E) Expression of Crbp in WT BAT (n=6-8) after 16 hours fasting or 6-7 hours refeeding. Same mice as (A). Expression of all genes arbitrarily normalized to fasted *Rbp1* levels. Dotted lines represent fasted levels of each gene. (F) Expression of Crbp in *Rdh1*-KO BAT (n=6-8) after 16 hours fasting or 6-7 hours refeeding. Same mice as (B). Expression of all genes arbitrarily normalized to fasted WT *Rbp1* levels. Dotted lines represent fasted WT levels of each gene. By two-way ANOVA, effect of refeeding on *Rbp1* and *Rbp7* (both $p \leq 0.0001$). (G) Expression of *Cyp26b1* in WT (n=6-8) and *Rdh1*-KO (n=6-8) BAT after 16 hours fasting or 6-7 hours refeeding. Same mice as (A) and (B). Expression arbitrarily normalized to fasted WT levels (dotted line). By two-way ANOVA, effect of feeding ($p \leq 0.0001$). F, fasted; R, refed. WT: red bars. *Rdh1*-KO: blue bars. $**p \leq 0.01$, $*p \leq 0.05$ vs. WT and $\#\#p \leq 0.01$, $\#p \leq 0.05$ vs. Fasted by Student's two-tailed t-test. All values Mean $\pm$ SEM.

Figure 41) Expression of Retinoid Metabolism Genes in BAT during Fasting and Refeeding, Repeated

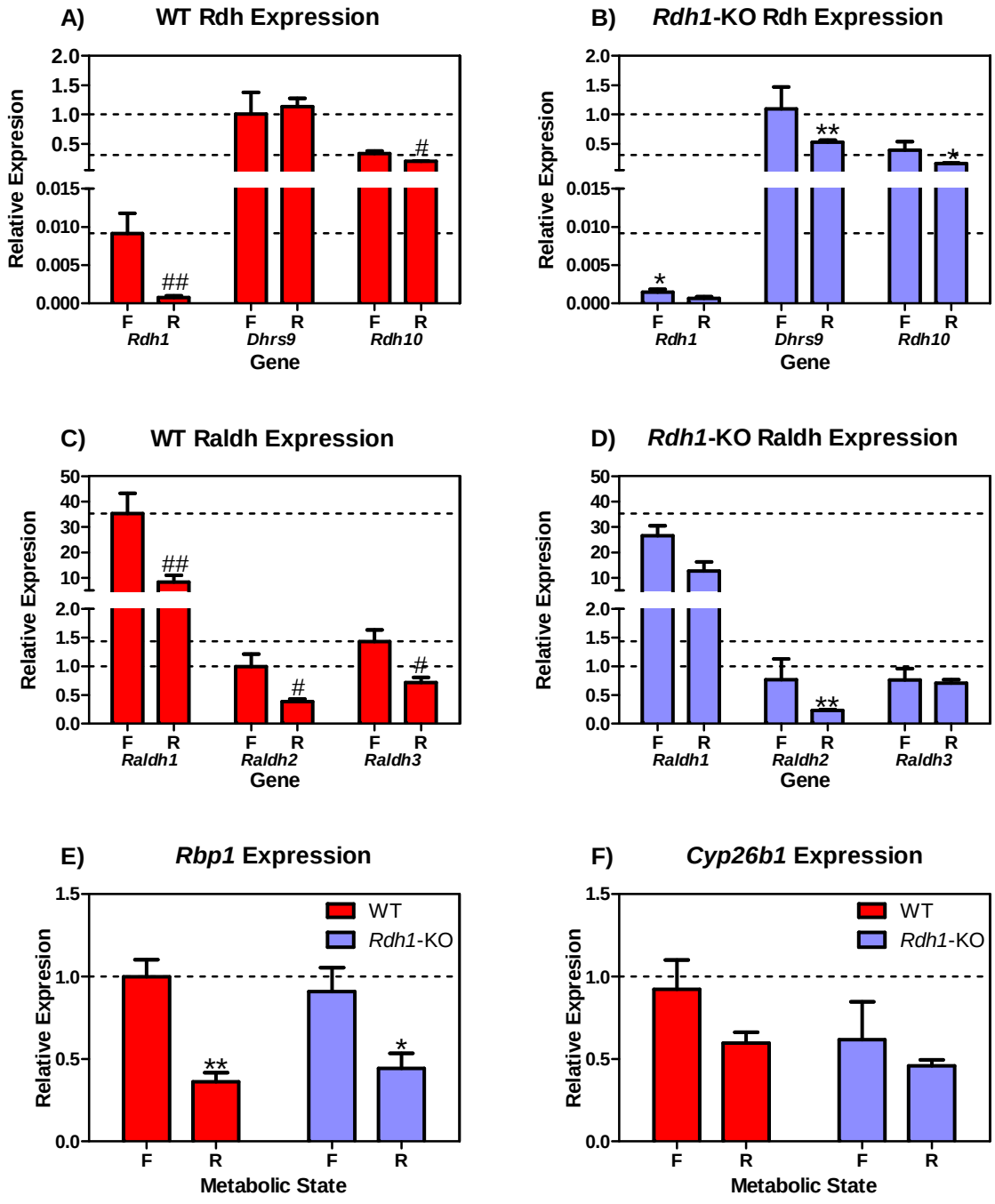

Legend: (See next page.)

Legend: (A) Expression of Rdh in WT BAT (n=3-7) after 16 hours fasting or 6-7 hours refeeding. Tissues from 7.5 week old male mice fed a 93G diet (cohort 12w2). Expression of all genes arbitrarily normalized to fasted *Dhrs9* levels. Dotted lines represent fasted levels of each gene. (B) Expression of Rdh in *Rdh1*-KO BAT (n=3-7) after 16 hours fasting or 6-7 hours refeeding. Tissues from 7.5 week old male mice fed a 93G diet (cohort 12w2). Expression of all genes arbitrarily normalized to fasted WT *Dhrs9* levels. Dotted lines represent fasted WT levels of each gene. By two-way ANOVA, effect of interaction between genotype and refeeding on *Rdh1* ($p \leq 0.05$), effect of genotype on *Rdh1* ($p \leq 0.05$) and effect of refeeding on *Rdh1* ($p \leq 0.01$) and *Rdh10* (all $p \leq 0.05$). (C) Expression of Raldh in WT BAT (n=3-7) after 16 hours fasting or 6-7 hours refeeding. Same mice as (A). Expression of all genes arbitrarily normalized to fasted *Raldh2* levels. Dotted lines represent fasted levels of each gene. (D) Expression of Raldh in *Rdh1*-KO BAT (n=3-7) after 16 hours fasting or 6-7 hours refeeding. Same mice as (B). Expression of all genes arbitrarily normalized to fasted WT *Raldh2* levels. Dotted lines represent fasted WT levels of each gene. By two-way ANOVA, effects of interaction between genotype and refeeding on *Raldh3* ($p \leq 0.05$), effect of genotype on *Raldh3* ($p \leq 0.05$) and effect of refeeding on *Raldh1* ($p \leq 0.05$), *Raldh2* ($p \leq 0.05$) and *Raldh3* ($p \leq 0.05$). (E) Expression of *Rbp1* in WT (n=5-6) and *Rdh1*-KO (n=6) BAT after 16 hours fasting or 6-7 hours refeeding. Same mice as (A) and (B). Expression arbitrarily normalized to fasted WT levels (dotted line). By two-way ANOVA, effect of feeding ($p \leq 0.0001$). (F) Expression of *Cyp26b1* in WT (n=6) and *Rdh1*-KO (n=6) BAT after 16 hours fasting or 6-7 hours refeeding. Same mice as (A) and (B). Expression arbitrarily normalized to fasted WT levels (dotted line). F, fasted; R, refed. WT: red bars. *Rdh1*-KO: blue bars. $**p \leq 0.01$, $*p \leq 0.05$ vs. WT and $\#\#p \leq 0.01$, $\#p \leq 0.05$ vs. Fasted by Student's two-tailed t-test. All values Mean $\pm$ SEM.

Figure 42) Expression of Retinoid Metabolism Genes in PMWAT during Fasting and Refeeding

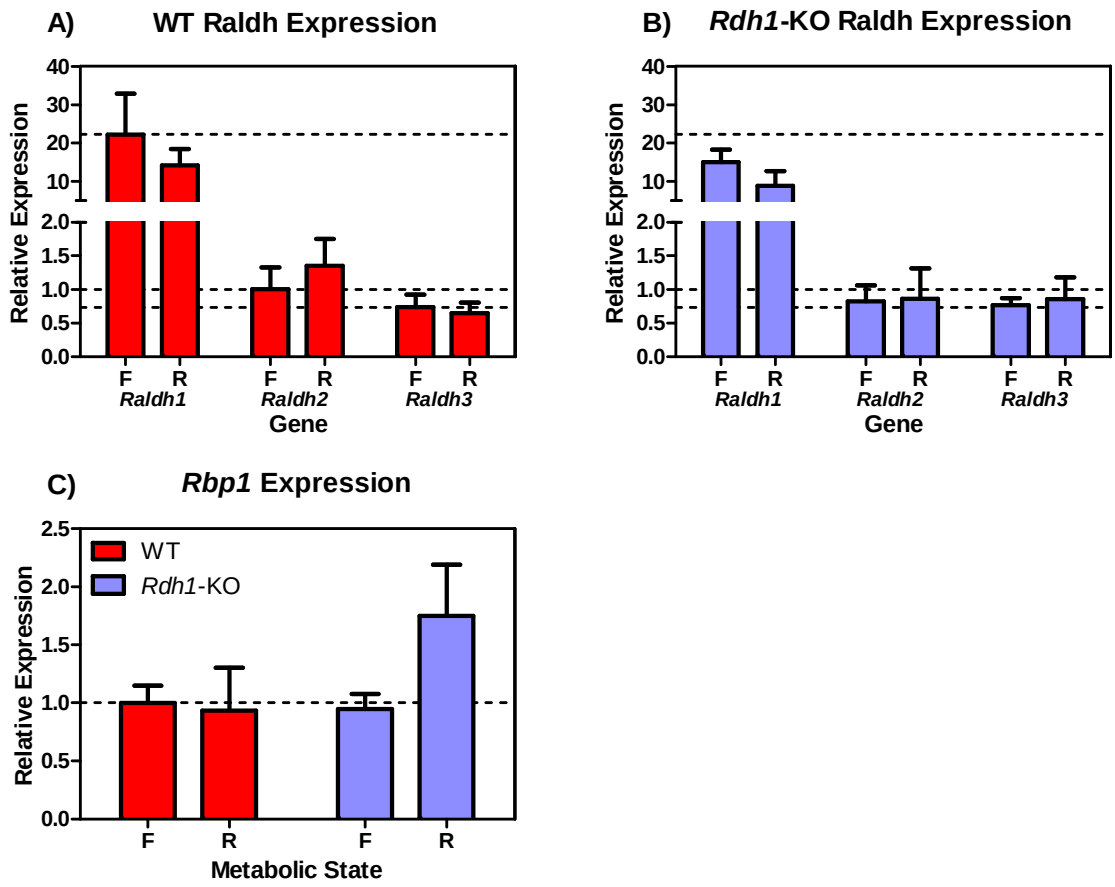

Legend: (A) Expression of Raldh in WT PMWAT (n=5) after 16 hours fasting or 6 hours refeeding. Tissues from 10 week old female mice fed a 93G diet (cohort 12w1). Expression of all genes arbitrarily normalized to fasted *Raldh2* levels. Dotted lines represent fasted levels of each gene. (B) Expression of Raldh in *Rdh1*-KO PMWAT (n=5) after 16 hours fasting or 6 hours refeeding. Tissues from 10 week old male female fed a 93G diet (cohort 12w1). Expression of all genes arbitrarily normalized to fasted WT *Raldh2* levels. Dotted lines represent fasted WT levels of each gene. (C) Expression of *Rbp1* in WT (n=5) and *Rdh1*-KO (n=4-5) PMWAT after 16 hours fasting or 6 hours refeeding. Same mice as (A) and (B). F, fasted; R, refed. WT: red bars. *Rdh1*-KO: blue bars. All values Mean ± SEM.

Figure 43) Expression of Retinoid Metabolism Genes in Female Liver during Fasting and Refeeding

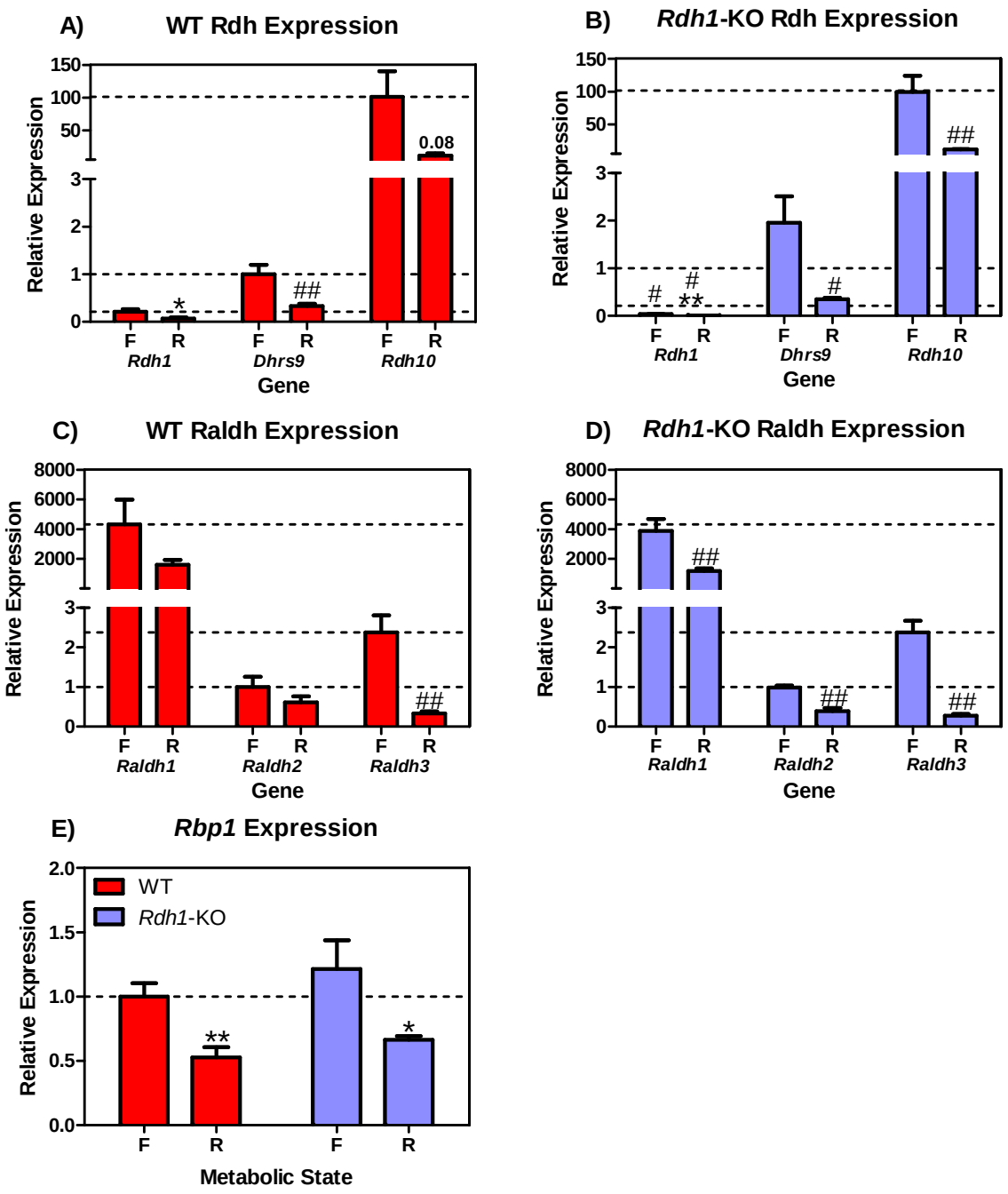

Legend: (See next page.)

Legend: (A) Expression of Rdh in WT liver (n=4-5) after 16 hours fasting or 6 hours refeeding. Tissues from 10 week old female mice fed a 93G diet (cohort 12w1). Expression of all genes arbitrarily normalized to fasted *Dhrs9* levels. Dotted lines represent fasted levels of each gene. (B) Expression of Rdh in *Rdh1*-KO liver (n=4-5) after 16 hours fasting or 6 hours refeeding. Tissues from 10 week old female mice fed a 93G diet (cohort 12w1). Expression of all genes arbitrarily normalized to fasted WT *Dhrs9* levels. Dotted lines represent fasted WT levels of each gene. By two-way ANOVA, effect of interaction between genotype and refeeding on *Rdh1* ($p \leq 0.05$), effect of genotype on *Rdh1* ($p \leq 0.001$) and effect of refeeding on *Rdh1* ($p \leq 0.01$), Dhrs9 ($p \leq 0.01$) and *Rdh10* ($p \leq 0.01$). (C) Expression of Raldh in WT liver (n=5) after 16 hours fasting or 6 hours refeeding. Same mice as (A). Expression of all genes arbitrarily normalized to fasted *Raldh2* levels. Dotted lines represent fasted levels of each gene. (D) Expression of Raldh in *Rdh1*-KO liver (n=5) after 16 hours fasting or 6 hours refeeding. Same mice as (B). Expression of all genes arbitrarily normalized to fasted WT *Raldh2* levels. Dotted lines represent fasted WT levels of each gene. By two-way ANOVA, effect of refeeding on *Raldh1* ($p \leq 0.01$), *Raldh2* ($p \leq 0.01$) and *Raldh3* ($p \leq 0.0001$). (E) Expression of *Rbp1* in WT (n=4-5) and *Rdh1*-KO (n=5) liver after 16 hours fasting or 6 hours refeeding. Same mice as (A) and (B). Expression arbitrarily normalized to fasted WT levels (dotted line). By two-way ANOVA, effect of feeding ($p \leq 0.01$). F, fasted; R, refed. WT: red bars. *Rdh1*-KO: blue bars. $**p \leq 0.01$, $*p \leq 0.05$ vs. WT and $\#\#p \leq 0.01$, $\#p \leq 0.05$ or as indicated vs. Fasted by Student's two-tailed t-test. All values Mean $\pm$ SEM.

Figure 44) Expression of Cyp Genes in Liver during Fasting and Refeeding

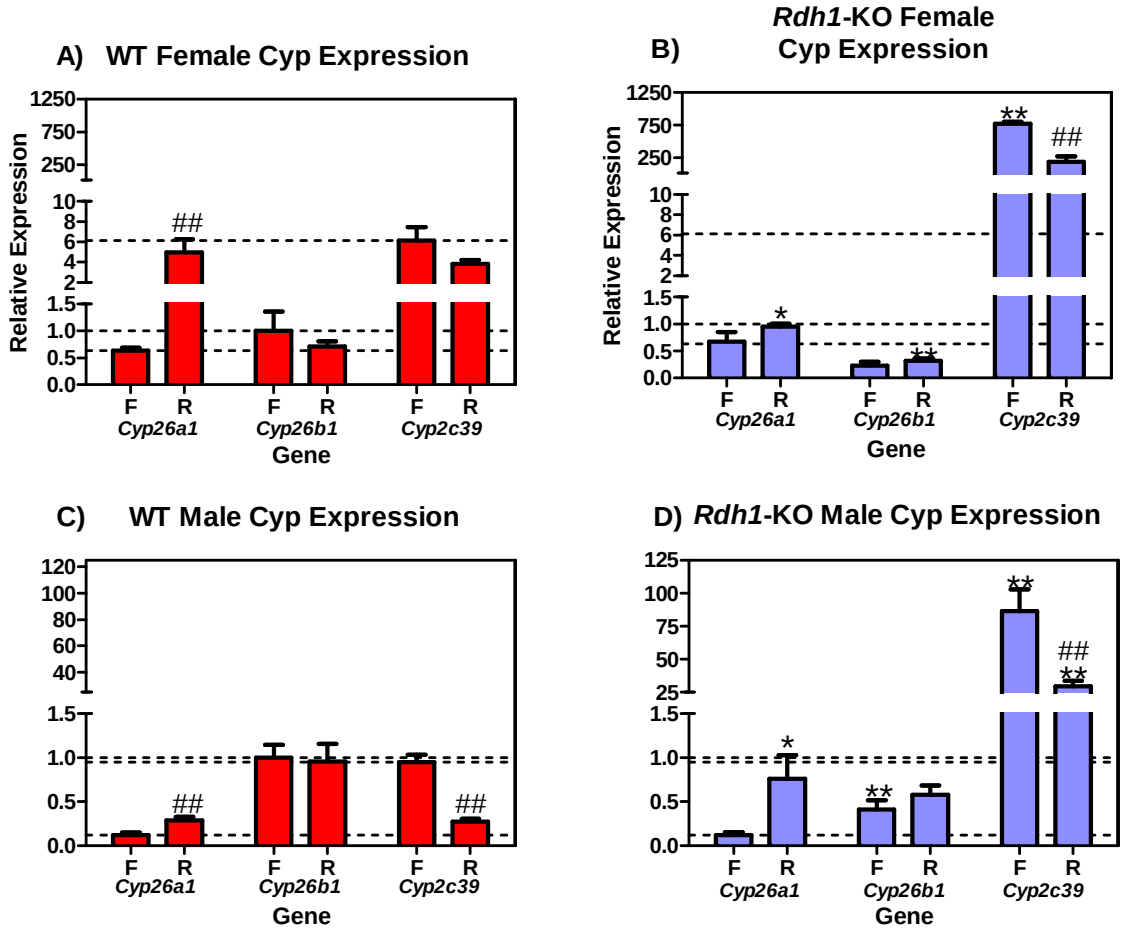

Legend: (See next page.)

Legend: (A) Expression of Cyp in WT liver (n=4-5) after 16 hours fasting or 6 hours refeeding. Tissues from 10 week old female mice fed a 93G diet (cohort 12w1). Expression of all genes arbitrarily normalized to fasted *Cyp26b1* levels. Dotted lines represent fasted levels of each gene. (B) Expression of Cyp in *Rdh1*-KO liver (n=4-5) after 16 hours fasting or 6 hours refeeding. Tissues from 10 week old female mice fed a 93G diet (cohort 12w1). Expression of all genes arbitrarily normalized to fasted WT *Cyp26a1* levels. Dotted lines represent fasted WT levels of each gene. By two-way ANOVA, effect of interaction between genotype and refeeding on *Cyp26a1* ($p \leq 0.01$) and *Cyp2c39* ($p \leq 0.001$), effect of genotype on *Cyp26a1* ($p \leq 0.01$), *Cyp26b1* ($p \leq 0.05$), *Cyp2c39* ($p \leq 0.0001$) and effect of refeeding on *Cyp26a1* ($p \leq 0.01$) and *Cyp2c39* ($p \leq 0.001$). (C) Expression of Cyp in WT liver (n=6) after 16 hours fasting or 6-7 hours refeeding. Tissues from 7.5 week old male mice fed a 93G diet (cohort 12w2). Expression of all genes arbitrarily normalized to fasted *Cyp26b1* levels. Dotted lines represent fasted levels of each gene. (D) Expression of Cyp in *Rdh1*-KO liver (n=6) after 16 hours fasting or 6-7 hours refeeding. Tissues from 7.5 week old female mice fed a 93G diet (cohort 12w2). Expression of all genes arbitrarily normalized to fasted WT *Cyp26a1* levels. Dotted lines represent fasted WT levels of each gene. By two-way ANOVA, effect of interaction between genotype and refeeding on *Cyp2c39* ($p \leq 0.01$), effect of genotype on *Cyp26b1* ($p \leq 0.01$) and *Cyp2c39* ($p \leq 0.0001$) and effect of refeeding on *Cyp26a1* ($p \leq 0.01$) and *Cyp2c39* ($p \leq 0.01$). F, fasted; R, refed. WT: red bars. *Rdh1*-KO: blue bars. **$p \leq 0.01$, *$p \leq 0.05$ vs. WT and ##$p \leq 0.01$, #$p \leq 0.05$ vs. Fasted by Student's two-tailed t-test. All values Mean $\pm$ SEM.

Figure 45) *Raldh1* and *Rbp1* Gene Expression in BAT after 2.5 hours Refeeding

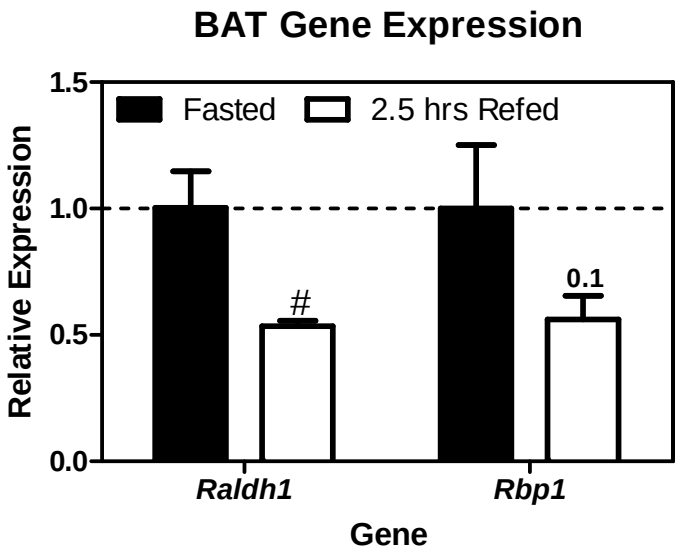

Legend: Gene expression in WT BAT (n=4) after 16 hours fasting or 2.5 hours refeeding. Tissues from 19 week old female mice fed a 93G diet (cohort 12w1). Expression of each gene arbitrarily normalized to fasted levels (dotted line). Fasted: black bars. 2.5 hrs Refed: white bars. #p≤0.05 vs. Fasted by Student's two-tailed t-test. All values Mean ± SEM.

Figure 46) Fasted and Refed Retinoid Metabolism Gene Expression in Chow Fed Mice

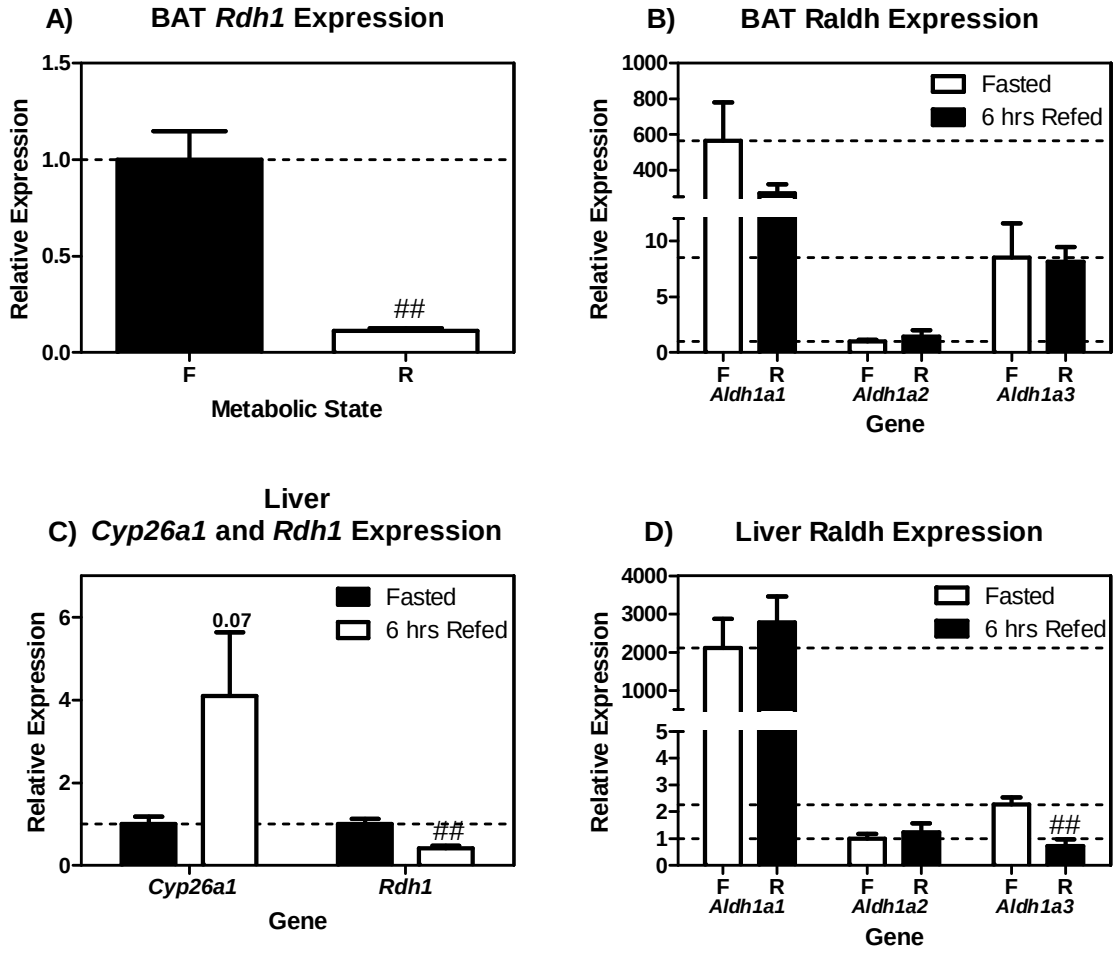

Legend: (A) Expression of *Rdh1* in BAT from 16 hour fasted or 6 hour refed C57BL/6 (n=4-6) male mice age 7.5 weeks and fed a Harlan Chow diet. Expression arbitrarily normalized to fasted level (dotted line) (B) Raldh expression in BAT from 16 hour fasted or 6 hour refed mice in (A). Expression of all genes arbitrarily normalized to fasted *Raldh2* expression. Dotted lines represent the fasted level of each gene. (C) *Cyp26a1* and *Rdh1* expression from 16 hour fasted or 6 hour refed liver of mice in (A). Expression of each gene arbitrarily normalized to fasted level (dotted line). (D) Raldh expression from 16 hour fasted or 6 hour refed liver of mice in (A). Expression of all genes arbitrarily normalized to fasted *Raldh2* expression. Dotted lines represent the fasted level of each gene. F, fasted; R, refed. Fasted: black bars. 2.5 hrs Refed: white bars. ##$p \leq 0.01$, #$p \leq 0.05$ or as indicated vs. Fasted by Student's two-tailed t-test. All values Mean $\pm$ SEM.

Figure 47) Expression of Retinoid Metabolism Genes in HIB-1B Cells in Response to Differentiation and Glucose

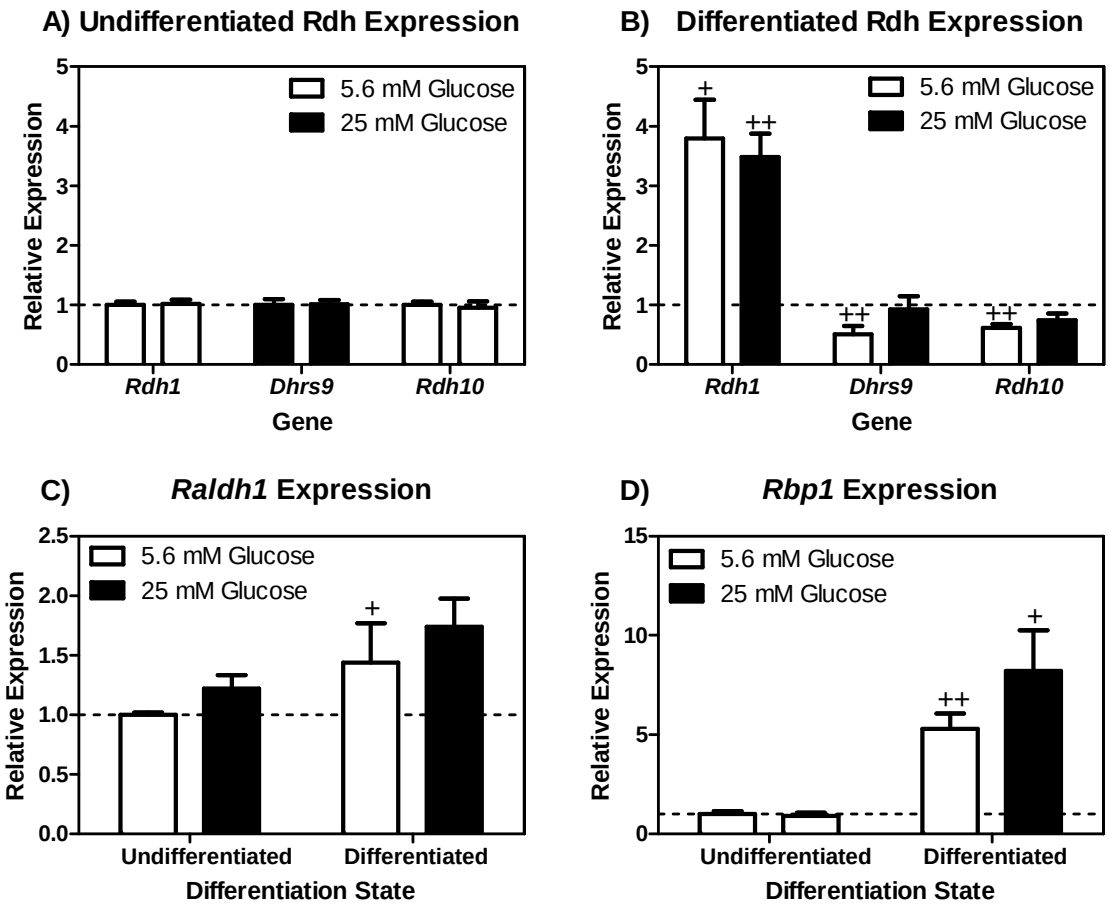

Legend: (A) Expression of Rdh in undifferentiated HIB-1B cells treated with either 5.6 mM (101 mg/dL) or 25 mM (450 mg/dL) glucose for 24 hours. Expression of each gene arbitrarily normalized to 5.6 mM levels (dotted line). (B) Expression of Rdh in differentiated HIB-1B cells treated as in (A). Expression of each gene arbitrarily normalized to 5.6 mM levels in undifferentiated cells (dotted line). By two-way ANOVA, effect of differentiation on *Rdh1* ($p \leq 0.0001$) and *Rdh10* ($p \leq 0.01$). (C) *Raldh1* expression in undifferentiated and differentiated HIB-1B cells treated as in (A). By two-way ANOVA, effect of differentiation ($p \leq 0.05$). (D) *Rbp1* expression in undifferentiated and differentiated HIB-1B cells treated as in (A). By two-way ANOVA, effect of differentiation ($p \leq 0.001$). 5.6 mM Glucose: black bars. 25 mM Glucose: white bars. ++$p \leq 0.01$, +$p \leq 0.05$ vs. Undifferentiated by Student's two-tailed t-test. All values Mean $\pm$ SEM.

Figure 48) Effect of Exogenous 9cRA on Blood Glucose and Insulin Levels

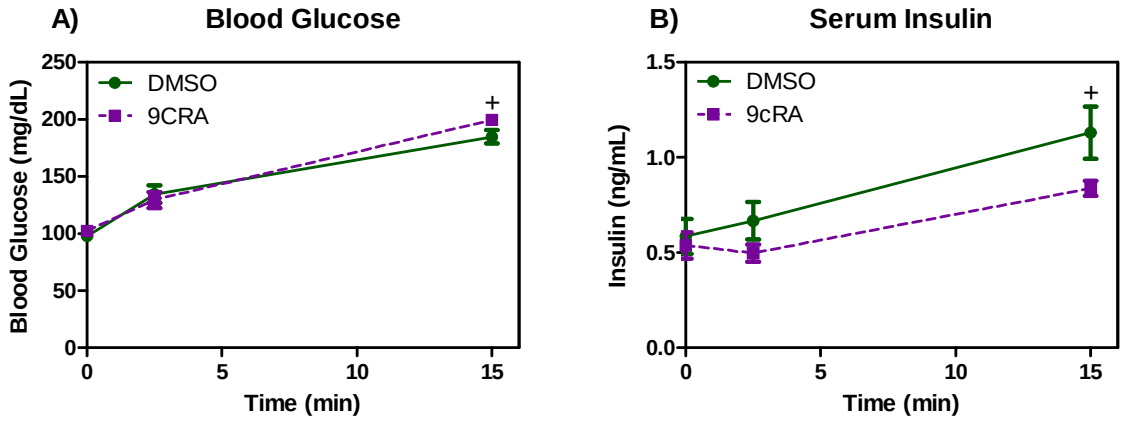

Legend: (A) Blood glucose levels during GTT in DMSO or 9cRA treated C57BL/6 male mice, age 8-12 weeks and fed a Harlan chow diet (n=6-21). (B) Serum insulin levels during GTT in DMSO or 9cRA treated mice from (A) (n=6). DMSO treated: green circles with solid green line. 9cRA treated: purple squares with purple dotted line. +$p \leq 0.05$ vs. DMSO by Student's two-tailed t-test. All values Mean $\pm$ SEM. Adapted from (4).

Figure 49) Metabolic Parameters in *Rbp1*-KO mice

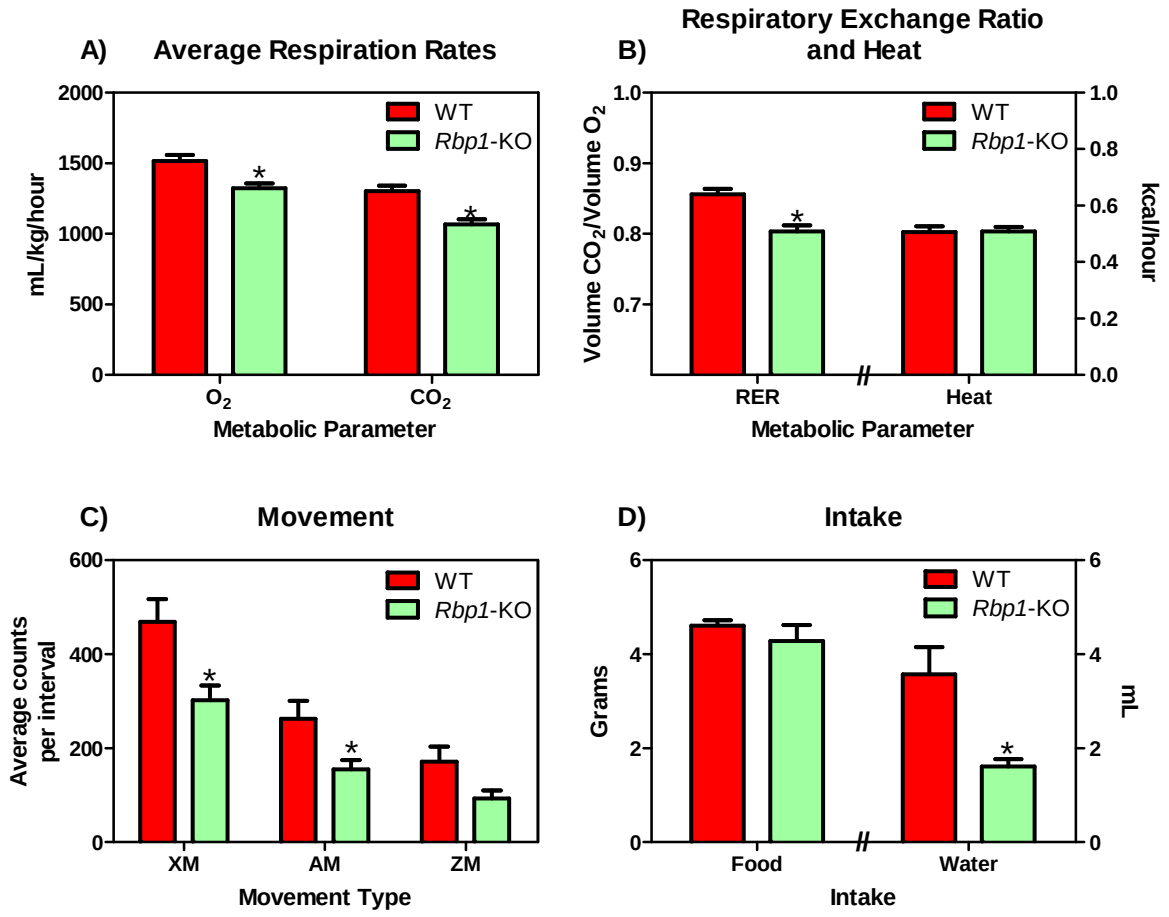

Legend: (A) Average oxygen consumption and carbon dioxide production during 24 hours of *ad lib* feeding in CLAMS for WT (n=8) and *Rbp1*-KO (n=7) male mice fed Harlan Chow, age 17-19 weeks. (B) Average respiratory exchange ratio (RER) and Heat production for mice in (A). (C) Average total horizontal movement (XM), ambulatory movement (AM) and rearing (ZM) movement for mice in (A). (C) Total food and water intake for mice in (A). WT: red bars. *Rbp1*-KO: green bars. *$p \leq 0.05$ vs. WT by Student's two-tailed t-test. All values Mean $\pm$ SEM. Adapted from (71).

Figure 50) Retinoids in Mice Heterozygous for an *Rdh10* Hypomorphic Mutation

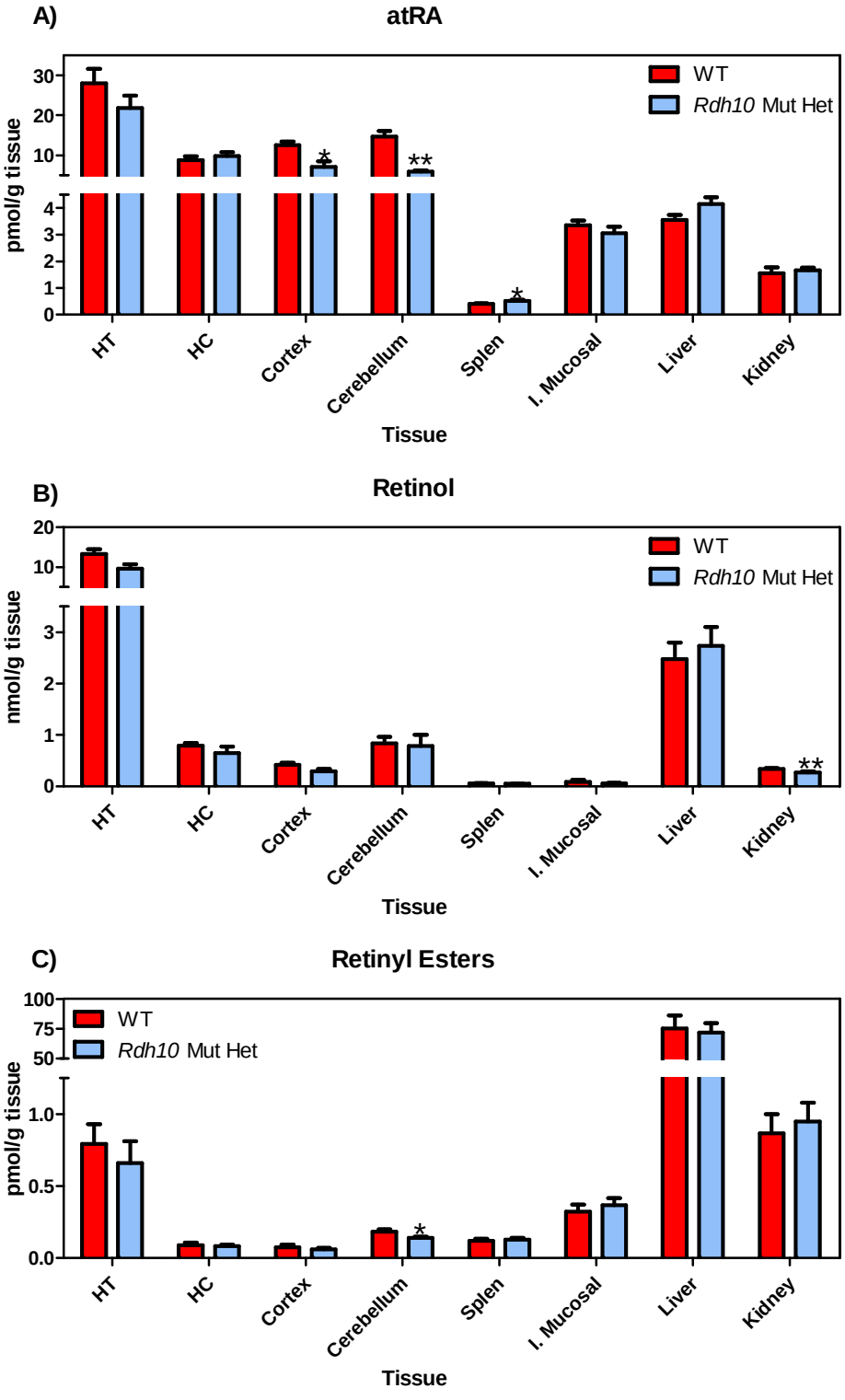

Legend: (See next page.)

Legend: (A) Tissue atRA levels from WT mice (n=4-9) and mice heterozygous for a hypomorphic *Rdh10* mutation (*Rdh10* Mut Het) (n=4-9). All mice 18-19 weeks old and 93G diet-fed. (B) Tissue retinol levels from mice in (A). (C) Tissue retinyl ester levels from mice in (A). HT, hypothalamus; HC, hippocampus; I. Mucosal, intestinal mucosal cells. WT: red bars. *Rdh10* Mut Het: light blue bars. ** $p \leq 0.01$, *$p \leq 0.05$ vs. WT by Student's two-tailed t-test. All values Mean $\pm$ SEM.

Figure 51) Pancreatic Retinoids in CRAD1- and CRAD3-KO Mice

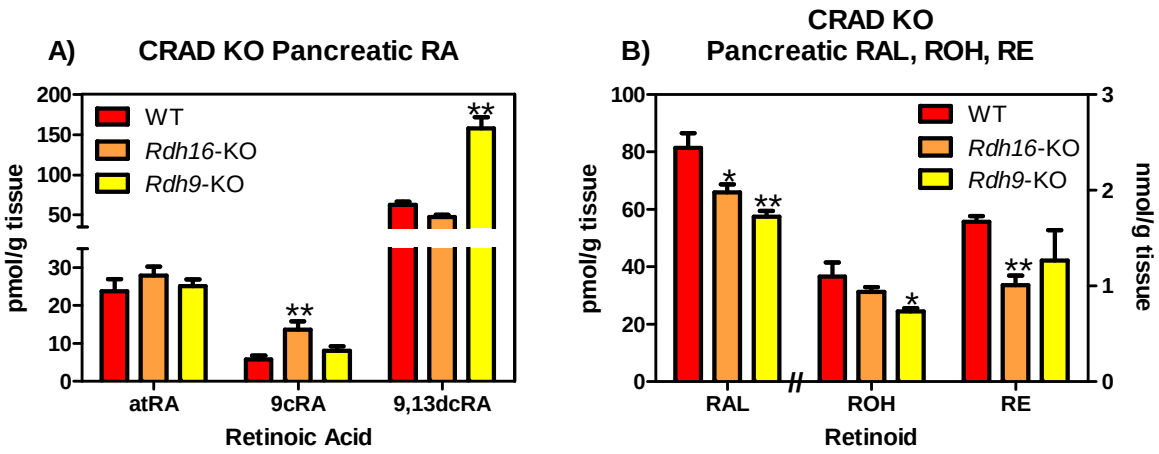

Legend: (A) Pancreatic retinoic acid levels in WT (n=5), *Rdh16*-KO (CRAD1-KO) (n=5) and *Rdh9*-KO (CRAD3-KO) (n=5) male mice fed a Harlan chow, age 30-36 weeks. (B) Pancreatic retinal, retinol and retinyl ester levels in mice from (A). WT: red bars. *Rdh16*-KO: orange bars. *Rdh9*-KO: yellow bars. ** $p \leq 0.01$, * $p \leq 0.05$ vs. WT by Student's two-tailed t-test. All values Mean $\pm$ SEM.

Table 29) Days from Pairing until Birth of Pups in CRAD1-KO Mice

		Male Genotype		
		WT	*Rdh16*-Het	*Rdh16*-KO
Female Genotype	WT	23.3 ± 1.7 days (8)	24.0 ± 2.1 days (8)	24.8 ± 1.6 days (8)
	Rdh16-Het	23.4 ± 0.7 days (8)	25.0 ± 1.7 days (13)	21.7 ± 0.3 days (3)
	Rdh16-KO	25.1 ± 1.9 days (8)	23.0 ± 2.0 days (2)	24.9 ± 2.7 days (7)

Legend: Length of time between pairing and birth of pups for 8-10 week old virgin mating pairs of genotypes indicated. Mice fed Harlan chow. All values Mean ± SEM (number of pairs).

Table 30) Fecundity in CRAD1-KO Mice

		Male Genotype		
		WT	*Rdh16*-Het	*Rdh16*-KO
Female Genotype	WT	7.9 ± 1.0 (8)	7.0 ± 0.8 (8)	7.1 ± 0.9 (7)
	Rdh16-Het	6.0 ± 0.8 (7)	7.0 ± 0.6 (13)	6.0 ± 0.6 (3)
	Rdh16-KO	5.5 ± 1.3 (6)	7.0 ± 0.5 (2)	6.4 ± 2.7 (5)

Legend: For litters surviving until weaning, number of mice per litter born to 8-10 week old virgin mating pairs of genotypes indicated. Mice fed Harlan chow. All values Mean ± SEM (number of litters).

Table 31) Percent Male per Litter in CRAD1-KO Mice

		Male Genotype		
		WT	*Rdh16*-Het	*Rdh16*-KO
Female Genotype	WT	51 ± 9% (8)	59 ± 8% (8)	60 ± 9% (7)
	Rdh16-Het	63 ± 8% (7)	55 ± 6% (13)	60 ± 13% (3)
	Rdh16-KO	44 ± 11% (6)	70 ± 13% (2)	38 ± 12% (5)

Legend: For litters surviving until weaning, percentage of males in litters born to 8-10 week old virgin mating pairs of genotypes indicated. Mice fed Harlan chow. All values Mean ± SEM (number of litters).

Table 32) Parturition Defects in CRAD1-KO Mice

		Male Genotype		
		WT	*Rdh16*-Het	*Rdh16*-KO
Female Genotype	WT	0/8	0/8	1/8
	Rdh16-Het	0/8	0/13	0/3
	Rdh16-KO	0/8	1/3	0/5

Legend: Number of female mortalities during parturition per number of pregnancies in 8-10 week old virgin mating pairs of genotypes indicated. Mice fed Harlan chow.

Table 33) Fertility Rate in CRAD1-KO Mice

		Male Genotype		
		WT	*Rdh16*-Het	*Rdh16*-KO
Female Genotype	WT	8/8	8/8	8/8
	Rdh16-Het	8/9	13/13	3/3
	Rdh1- KO	8/9	3/5	5/5

Legend: Number of successful pregnancies during 28 days of pairing per total 8-10 week old virgin mating pairs of genotypes indicated. Mice fed Harlan chow.

Figure 52) Serum Testosterone and 3-adiol-glucuronide Levels in CRAD1-KO Mice

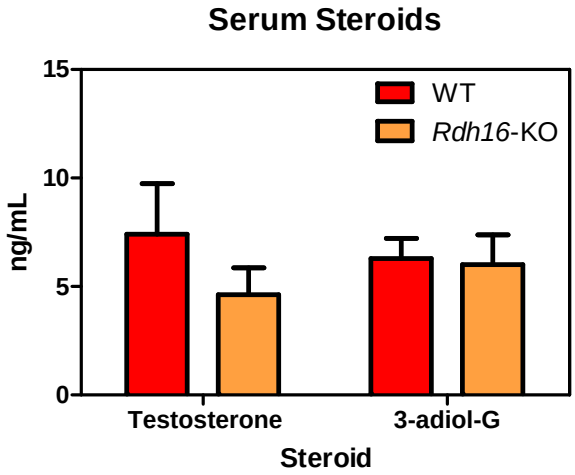

Legend: Serum testosterone and 5α-androstane-3α, 17β-diol glucuronide (3-adiol-G) levels in male, Harlan chow-fed WT (n=9-15) and *Rdh16*-KO (CRAD1-KO) (n=7) mice. WT: red bars. *Rdh16*-KO: orange bars. All values Mean ± SEM.

Figure 53) Semi-quantitative Expression of Steroid Metabolism Genes in CRAD1-KO Mice

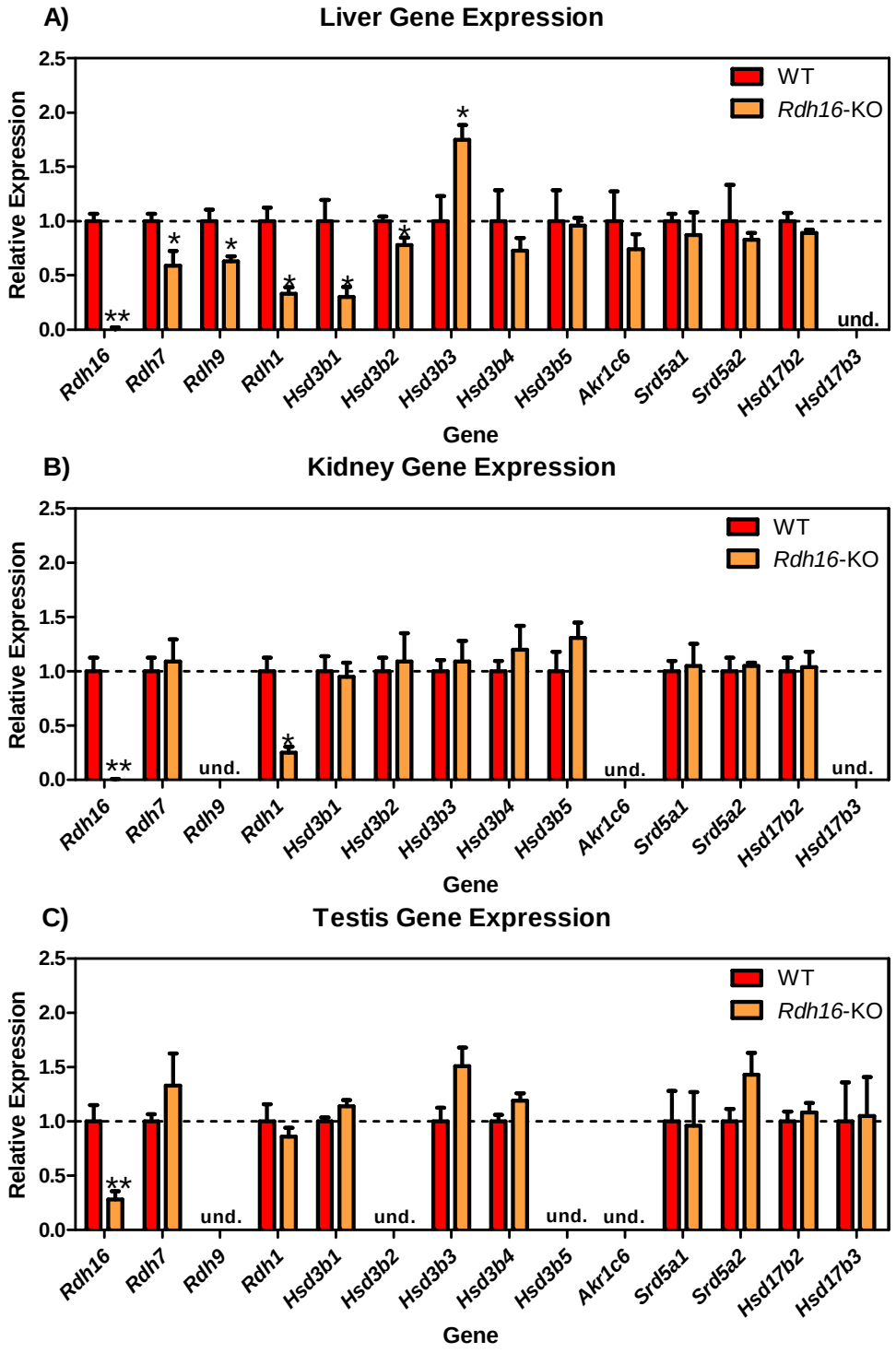

Legend: (See next page.)

Legend: (A) Semi-quantitative gene expression in liver of 35 week old male WT (n=4) and *Rdh16*-KO mice (CRAD1-KO) (n=4). Mice fed Harlan chow. (B) Semi-quantitative gene expression in kidney of mice in (A). (C) Semi-quantitative gene expression in testis of mice in (A). Und.: undetectable under conditions used. **$p \leq 0.01$, *$p \leq 0.05$ vs. WT by Student's two-tailed t-test. All values Mean $\pm$ SEM.

References

1. Napoli, J. L. (2011) *Biochim. Biophys. Acta*. **1821**, 152-167

2. Zhang, M., Chen, W., Smith, S. M., and Napoli, J. L. (2001) *J. Biol. Chem.* **276**, 44083-44090

3. Zhang, M., Hu, P., Krois, C. R., Kane, M. A., and Napoli, J. L. (2007) *FASEB J.* **21**, 2886-2896

4. Kane, M. A., Folias, A. E., Pingitore, A., Perri, M., Obrochta, K. M., Krois, C. R., Cione, E., Ryu, J. Y., and Napoli, J. L. (2010) *Proc. Natl. Acad. Sci. U. S. A.* **107**, 21884-21889

5. Watanabe, M., Houten, S. M., Mataki, C. *et al.* (2006) *Nature* **439**, 484-489

6. Berry, D. C., Jin, H., Majumdar, A., and Noy, N. (2011) *Proc. Natl. Acad. Sci. U. S. A.* **108**, 4340-4345

7. Siegenthaler, J. A., Ashique, A. M., Zarbalis, K. *et al.* (2009) *Cell* **139**, 597-609

8. Ricard, A. (2009) *Mol. Cell. Endocrinol.* **313**, 23-35

9. McCollum, E. V., and Davis, M. (1913) *Journal of Biological Chemistry* **15**, 167-175

10. Hessel, S., Eichinger, A., Isken, A. *et al.* (2007) *J. Biol. Chem.* **282**, 33553-33561

11. Napoli, J. L. (1996) *Clin. Immunol. Immunopathol.* **80**, S52-62

12. Napoli, J. L. (1996) *FASEB J.* **10**, 993-1001

13. Kawaguchi, R., Yu, J., Honda, J., Hu, J., Whitelegge, J., Ping, P., Wiita, P., Bok, D., and Sun, H. (2007) *Science* **315**, 820-825

14. Boerman, M. H., and Napoli, J. L. (1991) *J. Biol. Chem.* **266**, 22273-22278

15. Herr, F. M., and Ong, D. E. (1992) *Biochemistry* **31**, 6748-6755

16. Deltour, L., Foglio, M. H., and Duester, G. (1999) *Dev. Genet.* **25**, 1-10

17. Molotkov, A., Deltour, L., Foglio, M. H., Cuenca, A. E., and Duester, G. (2002) *J. Biol. Chem.* **277**, 13804-13811

18. Molotkov, A., and Duester, G. (2002) *J. Biol. Chem.* **277**, 22553-22557

19. Molotkov, A., Fan, X., Deltour, L., Foglio, M. H., Martras, S., Farres, J., Pares, X., and Duester, G. (2002) *Proc. Natl. Acad. Sci. U. S. A.* **99**, 5337-5342

20. Molotkov, A., Fan, X., and Duester, G. (2002) *Eur. J. Biochem.* **269**, 2607-2612

21. Chai, X., Zhai, Y., and Napoli, J. L. (1996) *Gene* **169**, 219-222

22. Boerman, M. H., and Napoli, J. L. (1995) *Biochemistry* **34**, 7027-7037

23. Chai, X., Boerman, M. H., Zhai, Y., and Napoli, J. L. (1995) *J. Biol. Chem.* **270**, 3900-3904

24. Chai, X., Zhai, Y., Popescu, G., and Napoli, J. L. (1995) *J. Biol. Chem.* **270**, 28408-28412

25. Majumdar, A., Petrescu, A. D., Xiong, Y., and Noy, N. (2011) *J. Biol. Chem.* **286**, 42749-42757

26. Sessler, R. J., and Noy, N. (2005) *Mol. Cell* **18**, 343-353

27. Krust, A., Kastner, P., Petkovich, M., Zelent, A., and Chambon, P. (1989) *Proceedings of the National Academy of Sciences* **86**, 5310-5314

28. Brand, N., Petkovich, M., Krust, A., Chambon, P., de The, H., Marchio, A., Tiollais, P., and Dejean, A. (1988) *Nature* **332**, 850-853

29. Petkovich, M., Brand, N. J., Krust, A., and Chambon, P. (1987) *Nature* **330**, 444-450

30. Leid, M., Kastner, P., Lyons, R., Nakshatri, H., Saunders, M., Zacharewski, T., Chen, J. Y., Staub, A., Garnier, J. M., and Mader, S. (1992) *Cell* **68**, 377-395

31. Kannan-Thulasiraman, P., Seachrist, D. D., Mahabeleshwar, G. H., Jain, M. K., and Noy, N. (2010) *J. Biol. Chem.* **285**, 19106-19115

32. Berry, D. C., and Noy, N. (2009) *Mol. Cell. Biol.* **29**, 3286-3296

33. Schug, T. T., Berry, D. C., Toshkov, I. A., Cheng, L., Nikitin, A. Y., and Noy, N. (2008) *Proc. Natl. Acad. Sci. U. S. A.* **105**, 7546-7551

34. Schug, T. T., Berry, D. C., Shaw, N. S., Travis, S. N., and Noy, N. (2007) *Cell* **129**, 723-733

35. Fiorella, P. D., and Napoli, J. L. (1994) *J. Biol. Chem.* **269**, 10538-10544

36. Fiorella, P. D., and Napoli, J. L. (1991) *J. Biol. Chem.* **266**, 16572-16579

37. Andreola, F., Hayhurst, G. P., Luo, G., Ferguson, S. S., Gonzalez, F. J., Goldstein, J. A., and De Luca, L. M. (2004) *J. Biol. Chem.* **279**, 3434-3438

38. White, J. A., Ramshaw, H., Taimi, M., Stangle, W., Zhang, A., Everingham, S., Creighton, S., Tam, S. P., Jones, G., and Petkovich, M. (2000) *Proc. Natl. Acad. Sci. U. S. A.* **97**, 6403-6408

39. White, J. A., Beckett-Jones, B., Guo, Y. D., Dilworth, F. J., Bonasoro, J., Jones, G., and Petkovich, M. (1997) *J. Biol. Chem.* **272**, 18538-18541

40. Taimi, M., Helvig, C., Wisniewski, J., Ramshaw, H., White, J., Amad, M., Korczak, B., and Petkovich, M. (2004) *J. Biol. Chem.* **279**, 77-85

41. Villarroya, F., Giralt, M., and Iglesias, R. (1999) *Int. J. Obes. Relat. Metab. Disord.* **23**, 1-6

42. Bonet, M. L., Ribot, J., Felipe, F., and Palou, A. (2003) *Cell Mol. Life Sci.* **60**, 1311-1321

43. Palou, A., Pico, C., and Bonet, M. L. (2003) *Forum. Nutr.* **56**, 164-168

44. Bonet, M. L., Oliver, J., Pico, C., Felipe, F., Ribot, J., Cinti, S., and Palou, A. (2000) *J. Endocrinol.* **166**, 511-517

45. Ribot, J., Felipe, F., Bonet, M. L., and Palou, A. (2001) *Obes. Res.* **9**, 500-509

46. Kumar, M. V., Sunvold, G. D., and Scarpace, P. J. (1999) *J. Lipid Res.* **40**, 824-829

47. Jeyakumar, S. M., Vajreswari, A., Sesikeran, B., and Giridharan, N. V. (2005) *J. Mol. Endocrinol.* **35**, 391-398

48. Jeyakumar, S. M., Vajreswari, A., and Giridharan, N. V. (2006) *Obesity (Silver Spring)* **14**, 52-59

49. Felipe, F., Mercader, J., Ribot, J., Palou, A., and Bonet, M. L. (2005) *Biochim. Biophys. Acta* **1740**, 258-265

50. Felipe, F., Bonet, M. L., Ribot, J., and Palou, A. (2004) *Diabetes* **53**, 882-889

51. Gatica, L. V., Vega, V. A., Zirulnik, F., Oliveros, L. B., and Gimenez, M. S. (2006) *J. Vasc. Res.* **43**, 602-610

52. Chan, C. B., and Harper, M. E. (2006) *Curr. Diabetes Rev.* **2**, 271-283

53. Puigserver, P., Vazquez, F., Bonet, M. L., Pico, C., and Palou, A. (1996) *Biochem. J.* **317 (Pt 3)**, 827-833

54. Felipe, F., Bonet, M. L., Ribot, J., and Palou, A. (2003) *Int. J. Obes. Relat. Metab. Disord.* **27**, 60-69

55. Scarpace, P. J., Matheny, M., Moore, R. L., and Kumar, M. V. (2000) *J. Endocrinol.* **164**, 331-337

56. Antras-Ferry, J., Franckhauser, S., Robin, D., Robin, P., Granner, D. K., and Forest, C. (1994) *Biochem. J.* **302 (Pt 3)**, 943-948

57. Pan, C. J., Hoeppner, W., and Chou, J. Y. (1990) *Biochemistry* **29**, 10883-10888

58. Scribner, K. B., Odom, D. P., and McGrane, M. M. (2005) *J. Nutr.* **135**, 2774-2779

59. Lucas, P. C., O'Brien, R. M., Mitchell, J. A., Davis, C. M., Imai, E., Forman, B. M., Samuels, H. H., and Granner, D. K. (1991) *Proc. Natl. Acad. Sci. U. S. A.* **88**, 2184-2188

60. Scott, D. K., Mitchell, J. A., and Granner, D. K. (1996) *J. Biol. Chem.* **271**, 6260-6264

61. Scribner, K. B., Odom, D. P., and McGrane, M. M. (2007) *J. Nutr. Biochem.* **18**, 206-214

62. Ong, D. E. (1984) *Journal of Biological Chemistry* **259**, 1476-1482

63. Ong, D. E., and Chytil, F. (1978) *Journal of Biological Chemistry* **253**, 828-832

64. Vogel, S., Mendelsohn, C. L., Mertz, J. R., Piantedosi, R., Waldburger, C., Gottesman, M. E., and Blaner, W. S. (2001) *Journal of Biological Chemistry* **276**, 1353-1360

65. Levin, M. S., Locke, B., Yang, N. C., Li, E., and Gordon, J. I. (1988) *Journal of Biological Chemistry* **263**, 17715-17723

66. Kane, M. A., Bright, F. V., and Napoli, J. L. (2011) *Biochim. Biophys. Acta* **1810**, 514-518

67. Cowan, S. W., Newcomer, M. E., and Jones, T. A. (1993) *J. Mol. Biol.* **230**, 1225-1246

68. Boerman, M. H., and Napoli, J. L. (1995) *Arch. Biochem. Biophys.* **321**, 434-441

69. Boerman, M. H., and Napoli, J. L. (1996) *J. Biol. Chem.* **271**, 5610-5616

70. Ghyselinck, N. B., Bavik, C., Sapin, V. *et al.* (1999) *EMBO J.* **18**, 4903-4914

71. Kane, M. A., Folias, A. E., Pingitore, A., Perri, M., Krois, C. R., Ryu, J. Y., Cione, E., and Napoli, J. L. (2011) *Mol. Cell. Biol.* **31**, 3277-3285

72. Zizola, C. F., Frey, S. K., Jitngarmkusol, S., Kadereit, B., Yan, N., and Vogel, S. (2010) *Mol. Cell. Biol.* **30**, 3412-3420

73. Wyss, A., Wirtz, G., Woggon, W., Brugger, R., Wyss, M., Friedlein, A., Bachmann, H., and Hunziker, W. (2000) *Biochem. Biophys. Res. Commun.* **271**, 334-336

74. Lei, Z., Chen, W., Zhang, M., and Napoli, J. L. (2003) *Biochemistry* **42**, 4190-4196

75. Ong, D. E., Lucas, P. C., Kakkad, B., and Quick, T. C. (1991) *J. Lipid Res.* **32**, 1521-1527

76. E, X., Zhang, L., Lu, J., Tso, P., Blaner, W. S., Levin, M. S., and Li, E. (2002) *J. Biol. Chem.* **277**, 36617-36623

77. Piantedosi, R., Ghyselinck, N., Blaner, W. S., and Vogel, S. (2005) *J. Biol. Chem.* **280**, 24286-24292

78. Zizola, C. F., Schwartz, G. J., and Vogel, S. (2008) *Am. J. Physiol. Endocrinol. Metab.* **295**, E1358-68

79. Gorry, P., Lufkin, T., Dierich, A., Rochette-Egly, C., Decimo, D., Dolle, P., Mark, M., Durand, B., and Chambon, P. (1994) *Proc. Natl. Acad. Sci. U. S. A.* **91**, 9032-9036

80. de Bruijn, D. R., Oerlemans, F., Hendriks, W., Baats, E., Ploemacher, R., Wieringa, B., and Geurts van Kessel, A. (1994) *Differentiation* **58**, 141-148

81. Gustafson, A. L., Eriksson, U., and Dencker, L. (1999) *Brain Res. Dev. Brain Res.* **114**, 121-126

82. Parenti, R., and Cicirata, F. (2004) *Cerebellum* **3**, 16-20

83. Romand, R., Sapin, V., Ghyselinck, N. B., Avan, P., Le Calvez, S., Dolle, P., Chambon, P., and Mark, M. (2000) *Eur. J. Neurosci.* **12**, 2793-2804

84. Stachurska, E., Loboda, A., Niderla-Bielinska, J., Szperl, M., Juszynski, M., Jozkowicz, A., Dulak, J., and Ratajska, A. (2011) *Acta Biochim. Pol.* **58**, 19-29

85. Chen, A. C., Yu, K., Lane, M. A., and Gudas, L. J. (2003) *Arch. Biochem. Biophys.* **411**, 159-173

86. Fawcett, D., Pasceri, P., Fraser, R., Colbert, M., Rossant, J., and Giguere, V. (1995) *Development* **121**, 671-679

87. Lampron, C., Rochette-Egly, C., Gorry, P., Dolle, P., Mark, M., Lufkin, T., LeMeur, M., and Chambon, P. (1995) *Development* **121**, 539-548

88. Salazar, J., Guardiola, M., Ferre, R. *et al.* (2007) *Clin. Chem. Lab. Med.* **45**, 615-620

89. Berry, D. C., Soltanian, H., and Noy, N. (2010) *J. Biol. Chem.* **285**, 15324-15332

90. Tan, N. S., Shaw, N. S., Vinckenbosch, N., Liu, P., Yasmin, R., Desvergne, B., Wahli, W., and Noy, N. (2002) *Mol. Cell. Biol.* **22**, 5114-5127

91. Graham, T. E., and Kahn, B. B. (2007) *Horm. Metab. Res.* **39**, 717-721

92. Yang, Q., Graham, T. E., Mody, N., Preitner, F., Peroni, O. D., Zabolotny, J. M., Kotani, K., Quadro, L., and Kahn, B. B. (2005) *Nature* **436**, 356-362

93. Niederreither, K., Fraulob, V., Garnier, J. M., Chambon, P., and Dolle, P. (2002) *Mech. Dev.* **110**, 165-171

94. Lin, M., Zhang, M., Abraham, M., Smith, S. M., and Napoli, J. L. (2003) *J. Biol. Chem.* **278**, 9856-9861

95. Sima, A., Parisotto, M., Mader, S., and Bhat, P. V. (2009) *Biochim. Biophys. Acta* **1790**, 1660-1664

96. Niederreither, K., Subbarayan, V., Dolle, P., and Chambon, P. (1999) *Nat. Genet.* **21**, 444-448

97. Martin, M., Gallego-Llamas, J., Ribes, V., Kedinger, M., Niederreither, K., Chambon, P., Dolle, P., and Gradwohl, G. (2005) *Dev. Biol.* **284**, 399-411

98. Ribes, V., Wang, Z., Dolle, P., and Niederreither, K. (2006) *Development* **133**, 351-361

99. Vermot, J., Niederreither, K., Garnier, J. M., Chambon, P., and Dolle, P. (2003) *Proc. Natl. Acad. Sci. U. S. A.* **100**, 1763-1768

100. Dupe, V., Matt, N., Garnier, J. M., Chambon, P., Mark, M., and Ghyselinck, N. B. (2003) *Proc. Natl. Acad. Sci. U. S. A.* **100**, 14036-14041

101. Shimamura, M., Karasawa, H., Sakakibara, S., and Shinagawa, A. (2010) *Biochem. Biophys. Res. Commun.* **401**, 79-84

102. Reichert, B., Yasmeen, R., Jeyakumar, S. M. *et al.* (2011) *Mol. Endocrinol.* **25**, 799-809

103. Fan, X., Molotkov, A., Manabe, S., Donmoyer, C. M., Deltour, L., Foglio, M. H., Cuenca, A. E., Blaner, W. S., Lipton, S. A., and Duester, G. (2003) *Mol. Cell. Biol.* **23**, 4637-4648

104. Ziouzenkova, O., Orasanu, G., Sharlach, M. *et al.* (2007) *Nat. Med.* **13**, 695-702

105. Jette, C., Peterson, P. W., Sandoval, I. T., Manos, E. J., Hadley, E., Ireland, C. M., and Jones, D. A. (2004) *J. Biol. Chem.* **279**, 34397-34405

106. Soref, C. M., Di, Y. P., Hayden, L., Zhao, Y. H., Satre, M. A., and Wu, R. (2001) *J. Biol. Chem.* **276**, 24194-24202

107. Markova, N. G., Pinkas-Sarafova, A., Karaman-Jurukovska, N., Jurukovski, V., and Simon, M. (2003) *Mol. Genet. Metab.* **78**, 119-135

108. Wang, C., Kane, M. A., and Napoli, J. L. (2011) *J. Biol. Chem.* **286**, 6542-6553

109. Wu, B. X., Moiseyev, G., Chen, Y., Rohrer, B., Crouch, R. K., and Ma, J. X. (2004) *Invest. Ophthalmol. Vis. Sci.* **45**, 3857-3862

110. Cammas, L., Romand, R., Fraulob, V., Mura, C., and Dolle, P. (2007) *Dev. Dyn.* **236**, 2899-2908

111. Cunningham, T. J., Chatzi, C., Sandell, L. L., Trainor, P. A., and Duester, G. (2011) *Dev. Dyn.* **240**, 1142-1150

112. Sandell, L. L., Sanderson, B. W., Moiseyev, G., Johnson, T., Mushegian, A., Young, K., Rey, J. P., Ma, J. X., Staehling-Hampton, K., and Trainor, P. A. (2007) *Genes Dev.* **21**, 1113-1124

113. Rhinn, M., Schuhbaur, B., Niederreither, K., and Dolle, P. (2011) *Proc. Natl. Acad. Sci. U. S. A.* **108**, 16687-16692

114. Zhuang, R., Lin, M., and Napoli, J. L. (2002) *Biochemistry* **41**, 3477-3483

115. Su, J., Chai, X., Kahn, B., and Napoli, J. L. (1998) *J. Biol. Chem.* **273**, 17910-17916

116. Hu, P., Zhang, M., and Napoli, J. L. (2007) *Biochim. Biophys. Acta* **1770**, 694-705

117. Shang, E., Lai, K., Packer, A. I., Paik, J., Blaner, W. S., de Morais Vieira, M., Gouras, P., and Wolgemuth, D. J. (2002) *J. Lipid Res.* **43**, 590-597

118. Driessen, C. A., Winkens, H. J., Hoffmann, K. *et al.* (2000) *Mol. Cell. Biol.* **20**, 4275-4287

119. Belyaeva, O. V., and Kedishvili, N. Y. (2006) *Genomics* **88**, 820-830

120. Zhang, M., Thomas, B. C., and Napoli, J. L. (2003) *Gene* **305**, 121-131

121. Zhang, M., Hu, P., and Napoli, J. L. (2004) *J. Biol. Chem.* **279**, 51482-51489

122. Wu, B. X., Chen, Y., Chen, Y., Fan, J., Rohrer, B., Crouch, R. K., and Ma, J. X. (2002) *Invest. Ophthalmol. Vis. Sci.* **43**, 3365-3372

123. Picozzi, P., Marozzi, A., Fornasari, D., Benfante, R., Barisani, D., Meneveri, R., and Ginelli, E. (2003) *FEBS Lett.* **554**, 59-66

124. Reeves, P. G., Nielsen, F. H., and Fahey, G. C.,Jr. (1993) *J. Nutr.* **123**, 1939-1951

125. National Research Council. (1995) *Nutrient requirements of laboratory animals,* 4th Edition Ed., Washington, D.C., USA, National Academy Press.

126. Zarbalis, K., May, S. R., Shen, Y., Ekker, M., Rubenstein, J. L., and Peterson, A. S. (2004) *PLoS Biol.* **2**, E219

127. Chiu, S., Fisler, J. S., Espinal, G. M., Havel, P. J., Stern, J. S., and Warden, C. H. (2004) *Obes. Res.* **12**, 1243-1255

128. Kane, M. A., and Napoli, J. L. (2010) *Methods Mol. Biol.* **652**, 1-54

129. Heikkinen, ,Sami, Argmann, C.,A., Champy, ,Marie-France, and Auwerx, ,Johan.

130. Strawford, A., Antelo, F., Christiansen, M., and Hellerstein, M. K. (2004) *American Journal of Physiology - Endocrinology and Metabolism* **286**, E577-E588

131. Turner, S. M., Murphy, E. J., Neese, R. A., Antelo, F., Thomas, T., Agarwal, A., Go, C., and Hellerstein, M. K. (2003) *American Journal of Physiology - Endocrinology and Metabolism* **285**, E790-E803

132. Lee, W. N., Bassilian, S., Guo, Z., Schoeller, D., Edmond, J., Bergner, E. A., and Byerley, L. O. (1994) *American Journal of Physiology - Endocrinology and Metabolism* **266**, E372-E383

133. Bruss, M. D., Khambatta, C. F., Ruby, M. A., Aggarwal, I., and Hellerstein, M. K. (2010) *Am. J. Physiol. Endocrinol. Metab.* **298**, E108-16

134. Klaus, S., Choy, L., Champigny, O., Cassard-Doulcier, A. M., Ross, S., Spiegelman, B., and Ricquier, D. (1994) *J. Cell. Sci.* **107 (Pt 1)**, 313-319

135. Even, P. C., Mokhtarian, A., and Pele, A. (1994) **18**, 435-447

136. Lowell, B. B., and Spiegelman, B. M. (2000) *Nature* **404**, 652-660

137. Nahmias, C., Blin, N., Elalouf, J. M., Mattei, M. G., Strosberg, A. D., and Emorine, L. J. (1991) *EMBO J.* **10**, 3721-3727

138. Cavaghan, M. K., Ehrmann, D. A., and Polonsky, K. S. (2000) *J. Clin. Invest.* **106**, 329-333

139. McLane, J. (2001) *J. Am. Acad. Dermatol.* **45**, S188-S194

140. Dalmas, E., Clement, K., and Guerre-Millo, M. (2011) *Trends Immunol.* **32**, 307-314

141. Gregor, M. F., and Hotamisligil, G. S. (2011) *Annu. Rev. Immunol.* **29**, 415-445

142. Romanovsky, A. A., Almeida, M. C., Aronoff, D. M., Ivanov, A. I., Konsman, J. P., Steiner, A. A., and Turek, V. F. (2005) *Front. Biosci.* **10**, 2193-2216

143. Seale, P., Kajimura, S., and Spiegelman, B. M. (2009) *Genes Dev.* **23**, 788-797

144. Ahmadian, M., Abbott, M. J., Tang, T. *et al.* (2011) *Cell. Metab.* **13**, 739-748

145. Matsuzaka, T., and Shimano, H. (2009) *J. Mol. Med. (Berl)* **87**, 379-384

146. Penning, T. M. (2010) *Curr. Opin. Endocrinol. Diabetes Obes.* **17**, 233-239

147. Mavalli, M. D., DiGirolamo, D. J., Fan, Y. *et al.* (2010) *J. Clin. Invest.* **120**, 4007-4020

148. Egecioglu, E., Bjursell, M., Ljungberg, A., Dickson, S. L., Kopchick, J. J., Bergstrom, G., Svensson, L., Oscarsson, J., Tornell, J., and Bohlooly-Y, M. (2006) *Am. J. Physiol. Endocrinol. Metab.* **290**, E317-25

149. Bianco, A. C., Maia, A. L., da Silva, W. S., and Christoffolete, M. A. (2005) *Biosci. Rep.* **25**, 191-208

150. Waki, H., and Tontonoz, P. (2007) *Annu. Rev. Pathol.* **2**, 31-56

151. Dubuc, P. U. (1976) *Metabolism* **25**, 1567-1574

152. Trayhurn, P., Thurlby, P. L., and James, W. P. (1977) *Nature* **266**, 60-62

153. Chen, H., Charlat, O., Tartaglia, L. A. *et al.* (1996) *Cell* **84**, 491-495

154. Tartaglia, L. A., Dembski, M., Weng, X. *et al.* (1995) *Cell* **83**, 1263-1271

155. Van Heek, M., Compton, D. S., France, C. F., Tedesco, R. P., Fawzi, A. B., Graziano, M. P., Sybertz, E. J., Strader, C. D., and Davis, H. R.,Jr. (1997) *J. Clin. Invest.* **99**, 385-390

156. Kim, K. H., Lee, K., Moon, Y. S., and Sul, H. S. (2001) *J. Biol. Chem.* **276**, 11252-11256

157. Steppan, C. M., Bailey, S. T., Bhat, S., Brown, E. J., Banerjee, R. R., Wright, C. M., Patel, H. R., Ahima, R. S., and Lazar, M. A. (2001) *Nature* **409**, 307-312

158. Peters, J. M., Lee, S. S., Li, W., Ward, J. M., Gavrilova, O., Everett, C., Reitman, M. L., Hudson, L. D., and Gonzalez, F. J. (2000) *Mol. Cell. Biol.* **20**, 5119-5128

159. Evans, R. M., Barish, G. D., and Wang, Y. X. (2004) *Nat. Med.* **10**, 355-361

160. Shaw, N., Elholm, M., and Noy, N. (2003) *J. Biol. Chem.* **278**, 41589-41592

161. Pelletier, R. M., and Byers, S. W. (1992) *Microsc. Res. Tech.* **20**, 3-33

162. Kim, B. H., Shenoy, A. R., Kumar, P., Das, R., Tiwari, S., and MacMicking, J. D. (2011) *Science* **332**, 717-721

163. Lubeseder-Martellato, C., Guenzi, E., Jorg, A. *et al.* (2002) *Am. J. Pathol.* **161**, 1749-1759

164. Naschberger, E., Werner, T., Vicente, A. B., Guenzi, E., Topolt, K., Leubert, R., Lubeseder-Martellato, C., Nelson, P. J., and Sturzl, M. (2004) *Biochem. J.* **379**, 409-420

165. Wang, C., Zhou, G. L., Vedantam, S., Li, P., and Field, J. (2008) *J. Cell. Sci.* **121**, 2913-2920

166. Bertling, E., Hotulainen, P., Mattila, P. K., Matilainen, T., Salminen, M., and Lappalainen, P. (2004) *Mol. Biol. Cell* **15**, 2324-2334

167. Holmes, R. S. (1994) *Alcohol Alcohol. Suppl.* **2**, 127-130

168. Wu, J., Srinivasan, S. V., Neumann, J. C., and Lingrel, J. B. (2005) *Biochemistry* **44**, 11098-11105

169. Salvatore, D., Bartha, T., and Larsen, P. R. (1998) *J. Biol. Chem.* **273**, 31092-31096

170. Jakobsson, A., Jorgensen, J. A., and Jacobsson, A. (2005) *Am. J. Physiol. Endocrinol. Metab.* **289**, E517-26

171. Shah, G. N., Hewett-Emmett, D., Grubb, J. H., Migas, M. C., Fleming, R. E., Waheed, A., and Sly, W. S. (2000) *Proc. Natl. Acad. Sci. U. S. A.* **97**, 1677-1682

172. Baumann, H., Held, W. A., and Berger, F. G. (1984) *J. Biol. Chem.* **259**, 566-573

173. Chai, X., Zhai, Y., and Napoli, J. L. (1997) *J. Biol. Chem.* **272**, 33125-33131

174. Chen, W. C., Sass, J. O., Seltmann, H., Nau, H., Orfanos, C. E., and Zouboulis, C. C. (2000) *Arch. Dermatol. Res.* **292**, 612-620

175. Horst, R. L., Reinhardt, T. A., Goff, J. P., Nonnecke, B. J., Gambhir, V. K., Fiorella, P. D., and Napoli, J. L. (1995) *Biochemistry* **34**, 1203-1209

176. Horst, R. L., Reinhardt, T. A., Goff, J. P., Koszewski, N. J., and Napoli, J. L. (1995) *Arch. Biochem. Biophys.* **322**, 235-239

177. Casillo, S., and Blackmore, D. K. (1972) *J. Comp. Pathol.* **82**, 477-482

178. Feldmann, H. M., Golozoubova, V., Cannon, B., and Nedergaard, J. (2009) *Cell. Metab.* **9**, 203-209

179. Matsuzaka, T., Shimano, H., Yahagi, N. *et al.* (2007) *Nat. Med.* **13**, 1193-1202